Final Report

National Aeronautics and Space Administration
Planetary Atmospheres Program

on a program of research on the

ORIGIN AND EVOLUTION OF PLANETARY ATMOSPHERES

Contract NAGW-340

July 1, 1982 to April 30, 1992

in the
Lunar and Planetary Laboratory
University of Arizona
Tucson, AZ 85721
(602) 621-4972

John S. Lewis, Principal Investigator

30 May, 1992

Table of Contents

I. ABSTRACT

This report concerns several research tasks related to the origin and evolution of planetary atmospheres and the large-scale distribution of volatile elements in the Solar System.

These tasks and their present status are as follows:

1. We have conducted an analysis of the volatility and condensation behavior of compounds of iron, aluminum, and phosphorus in the atmosphere of Venus in response to published interpretations of the Soviet Venera probe XRF experiment data, to investigate the chemistry of volcanic gases, injection of volatiles by cometary and asteroidal impactors, and reactions in the troposphere.
2. We have completed and are now writing up our research on condensation-accretion modeling of the terrestrial planets.
3. We have laid the groundwork for a detailed study of the effects of water transport in the solar nebula on the bulk composition, oxidation state, and volatile content of preplanetary solids.
4. We have completed an extensive laboratory study of cryovolcanic materials in the outer solar system.
5. We have begun to study the impact erosion and shock alteration of the atmosphere of Mars resulting from cometary and asteroidal bombardment.
6. We have developed a new Monte Carlo model of the cometary and asteroidal bombardment flux on the terrestrial planets, including all relevant chemical and physical processes associated with atmospheric entry and impact, to assess both the hazards posed by this bombardment to life on Earth and the degree of cross-correlation between the various phenomena (NO_x production, explosive yield, crater production, iridium signature, etc.) that characterize this bombardment.

Tasks 2 and 3 are principally aimed at understanding the distribution of volatile elements and the oxidation state of planet-forming solids in the inner Solar System. Tasks 1, 5, and 6 are all targeted on very important geochemical evolutionary processes, largely (but not entirely) aimed at integrating the latest emerging understanding of the chemical, physical, and dynamical properties and population statistics of the Earth-crossing asteroid and comet populations to assess the role of impacts of these bodies in volatile injection, shock-processing, and impact erosion of the atmospheres of the terrestrial planets.

The purpose of these investigations has been to contribute to the developing understanding of both the dynamics of long-term planetary atmosphere evolution and the short-term stability of planetary surface environments.

II. INTRODUCTION

Within the last few years the importance of impacts in shaping the composition and origin of planetary atmospheres has become widely accepted. At the time of accretion, as shown by Ahrens and coworkers, impact devolatilization of infalling volatile-rich asteroidal and cometary bodies must have been extremely efficient. Very early development of atmospheres must have occurred on the terrestrial planets, beginning at a time when only a few percent of the masses of Earth and Venus had accreted.

The presence of an atmosphere during most of the accretionary era can lead, especially on the smaller terrestrial planets, to extensive atmospheric loss by explosive (hydrodynamic) blowoff. As first pointed out by ourselves, and also argued by Cameron and by Ahrens, the blowoff process may very severely deplete the total inventory of volatiles on a planet. G. H. Watkins, using a crude blowoff model, argued that more than 99% of the atmospheric mass of Mars could be lost during the accretion of the last 1% of the mass of Mars. Substantial loss can occur over billions of years even at present impact rates. Thus not only the accretionary era, but also the continuing impact history of a small terrestrial planet, may influence its present abundances of the rare gases and nitrogen. Recent work by Vickery and Melosh provides a strong quantitative basis for modeling of the explosive blowoff process and its application to the atmospheric evolution of Mars.

We first proposed in 1974 that the late infall of cometary carbonaceous asteroidal material on Venus could, even in a conservative estimate, replenish water on Venus at a rate at least equal to the present-day escape rate. The present inventories of hydrogen (water), sulfur, chlorine and fluorine could be entirely provided by later infall, even at the present rate, continuing for billions of years. This suggests that the water abundance on Venus may be in a near steady-state, not declining rapidly from some enormous initial amount. The discovery of a highly enhanced deuterium abundance on Venus by Donahue and coworkers during the Pioneer Venus program has been interpreted by several groups in terms of the unidirectional escape of a massive original supply of water. Strict logic dictates only that the mass of escaped water be at least 100-200 times the present inventory, on the order of 0.1% of a terrestrial ocean, but Donahue and several others have concluded that the original Venus water inventory was at least equivalent to Earth's oceans. All such studies have ignored the very important influence of water added to Venus by cometary and asteroidal infall.

Cameron and Benz, Melosh, and others have argued that giant-impact models (Mars-sized impactors) for the origin of the Moon would have profound consequences for the early atmosphere: almost instantaneous loss of most of the early atmosphere might have occurred. Also, Ahrens has pointed out that the blast wave from much later, smaller surface impacts (kilometer-sized bodies) may remove traces of atmosphere from Earth, and Walker has investigated the effects of the near-cylindrical atmospheric shock propagating from large entering bodies before striking the surface (which is ineffectual at removing atmosphere from bodies with escape velocities of 10 km/s or higher). Whether Earth impacts in the last 4 billion years

can remove significant amounts of atmosphere from Earth or Venus is not yet clear. Ahrens is addressing this problem, and Vickery and Melosh have recently presented criteria for the onset of explosive blowoff by the blast waves from km-size impactors, showing that they can indeed remove atmosphere from Mars, and providing a basis for extension of the theory to Earth.

We suggested in 1982 that, over the last 4 billion years, the most important consequence of cometary and asteroidal impacts on Earth is severe shock heating of large volumes of atmosphere, which produces extremely high concentrations of nitrogen oxides. We have proposed an explicit model to explain not only the scope but also the selectivity of the Cretaceous extinction event as a consequence of the toxicity of NO_x and the destabilization of carbonates in the upper ocean by acid rain. Alvarez has accepted this suggestion as the most probable single mechanism for mass extinction events.

We have, in response to the interesting problems raised by the original accretion of the terrestrial planets and the later impact modification of their atmospheres, concentrated much of our attention on combined condensation-accretion modeling of the terrestrial planets (beginning with Mercury) and on the specific major effects of later impacts on the atmospheric evolution on Venus (volatile addition), Earth (shock chemistry and the subsequent atmospheric and marine geochemistry), Mars (explosive blowoff), and Titan (shock chemistry).

III. RESEARCH ACHIEVEMENTS

We report here, organized according to task, summaries of our recently completed research tasks:

1. Water and Cloud-Forming Condensates on Venus

Achievements: Since our last peer review, we have modeled the time variation of the H and D escape fluxes from Venus in the presence of a stochastic cometary impacat flux. We find that the D enhancement observed on Venus by Pioneer Venus mass spectrometry is found even for model histories in which Venus is formed with no water content. The inference of early oceans on Venus suggested by others as the source of a the D:H enhancement is logically invalid. A very wide range of early conditions, some wet and some dry, can be reconciled with the observations (4, 7, 11).

We have also found that the strange and apparently unphysical altitude profiles found for water vapor by the Venera 11 infrared spectrometer experiment can be explained in part by considering the formation of gaseous carbonic acid near the planetary surface and in part by ascribing much of the 0.94 μm opacity to gaseous sulfuric acid. Further, this model shows hope of reconciling almost all the conflicting evidence regarding the water abundance and its vertical distribution by considering the speciation of water, and by not assuming that the free water

abundance and the total water abundance are the same. A true total abundance of a few tens of ppm for water seems most likely (20). Reprints of this and other recent papers are attached as Appendices.

We have also explored the evidence presented by Krasnopolskii (Icarus 80, 202 (1989)) for the presence of compounds of phosphorus and chlorides of iron and aluminum in the Venus clouds. So far we find no thermodynamic basis for the reported elements and compounds, and propose an explanation of the Venera cloud composition data in terms of an instability in the algorithm used to distinguish chlorine, sulfur and phosphorus in the Soviet XRF data (29).

2. Condensation-Accretion Modeling of the Terrestrial Planets

Achievements: We have carried out a suite of accretion models for the terrestrial planets using a run of mineral chemistry vs. heliocentric distance that is appropriate to conventional Solar Nebula models (28). The accretion probability distributions for the planets are modeled as Gaussians of variable width. We have reported the application of this model to Mercury (5), which presents the most extreme conditions of temperature and proximity to the Sun. These models all underestimate the density (metallic iron content) of Mercury, making it essential to postulate some fractionation mechanism such as heating by the superluminous early Sun, selective accretion due to differences between the physical properties of iron and silicate mineral grains, or large-scale erosion of the crust and upper mantle by giant impact events. For the rest of the terrestrial plant region, generally reasonable densities, oxidation states, and volatile contents are found for intermediate values of the Gaussian half-width (HW). Very broad sampling functions (HW> 0.5 AU) erase the density and composition differences between the terrestrial planets, whereas very narrow sampling functions (HW< 0.1 AU) fail to provide enough volatiles. The paper reporting our results is in preparation (28). Several other papers and reviews relevant to the molecular, mineralogical, and isotopic composition of the Solar System have also been completed (1, 15, 23, 26, 30).

We have recently compiled compositional data on the Earth and interpreted it in terms of condensation-related (volatility-dependent) and differentiation-related processes (especially core formation). This model provides strong constraints on the composition of the core, the bulk composition of the Earth, and the accretion sampling process that formed the Earth (17).

3. Water Vapor Transport in the Solar Nebula

Background: In 1981 JSL had the idea that radial turbulent transport of water in the Solar Nebula would efficiently pump water vapor out past the ice condensation threshold. This would lead to a buildup in the surface density of solids near Jupiter's orbit and to progressive depletion of water across the asteroid belt, with a consequent dramatic enhancement of the stability of reduced materials such as hydrocarbons and enstatite chondrite minerals across the

asteroid belt. The actual work was begun seven years ago as a potential dissertation topic by William Drew, who followed me from MIT to Arizona, but the project was placed on hold after the first year when Drew took a one-year leave of absence. At the end of the second year, Drew elected to withdraw from the University of Arizona and enrolled at Cal Tech, where he went to work for David Stevenson. After another year, Drew left Stevenson's employ to work for Yuk Yung, abandoning the project. A paper by Stevenson and Jonathan Lunine has since appeared, pointing out that turbulent transport of water vapor in the Solar Nebula can lead to efficient outward "cryopumping" of water into the Jupiter formation region, and may be responsible for producing high enough surface densities of solids to actually cause the formation of Jupiter. They did not notice the important role of water depletion in determining the oxidation state and volatile content of preplanetary solids in the terrestrial planet region. Lunine and JSL have discussed this problem at some length, and one of my students, Melinda Hutson, has expressed strong interest in it. She is a reformed meteoriticist with a Master's degree earned working with Bob Dodd at Stony Brook. She has extensive experience with microprobe analysis, and has already begun an analytic study of the most relevant class of meteorites (low-petreologic-grade enstatite chondrites) in the LPL microprobe laboratory.

Larry Lebofsky of the U of A has assisted us in interpreting the multicolor photometry of the asteroid belt and infrared spectra of C, D and P asteroids as powerful means to test this model (8, 10, 12, 18).

One of these tasks deals with the chemical consequences of radial transport of water vapor in the Solar Nebula. Such transport, caused by outward turbulent mixing of water vapor across the water-ice condensation threshold near Jupiter's orbit, establishes a radial gradient in the water vapor content of the terrestrial planet formation region. This occurs, as has been shown by Lunine and Stevenson, even for relatively poorly mixed nebular models of the sort favored by Stevenson. Prinn's reassessment of turbulent mixing in nebular models has shown that radial mixing is much more important than Stevenson's published models suggest, and hence that radial transport of volatiles is even more efficient than previously recognised.

Given rapid radial mixing, ice will accumulate in greater than solar proportions and water vapor will be progressively depleted from the ice condensation threshold inward toward the Sun, with the most severe water depletion found closest to the condensation threshold. Thus the total C:O ratio in the nebula increases outward from the Sun, causing a dramatic radial variation of oxidation state of minerals in the sense opposite to that usually assumed for a compositionally uniform nebula, where the thermodynamic tendency toward progressive oxidation of iron during cooling is dominant. Highly reduced minerals, such as the nitrides, elemental silicon, and unusual sulfides found in the enstatite chondrites, and carbonaceous matter produced by disequilibrating processes in the nebula, both become more stable with increasing distance from the Sun when water transport is allowed. We are pursuing three aspects of this problem: detailed modeling of the geochemical consequences of water transport in the nebula, rough quantitative assessment of the importance of various mechanisms for disequilibration of the nebula, and microprobe analysis of selected meteorites (principally enstatite chondrites) to

test the predictions of this model regarding stable mineral assemblages. Implications of oxygen transport for metal-silicate fractionation during the formation of Mercury are also being investigated.

Melinda Hutson and JSL have begun work on the thermochemistry of the Solar Nebula with proper consideration of water vapor transport. Jonathan Lunine is collaborating with the modeling of water transport, and JSL has prime responsibility for the chemical modeling of mineral stability in the presence of a radial gradient in water vapor concentration. Steffi Engel (presently working for Jon Lunine) is further extending this model to the interpretation of composition of cometary ices (19).

In the context of the same model, we have begun to explore the thermochemistry and petrology of the minerals found in low-petrologic-grade enstatite chondrites. JSL takes the lead in applying the computer model of the nebular chemistry described above to the prediction of the mineralogy of highly reduced condensates formed in the water-depleted portion of the inner Solar System. Melinda Hutson has been carrying out a suite of analyses, principally of enstatite chondrites of low petrologic grade, to test the predictions of the theory, paying special attention to carriers of volatile elements (especially S, N, C and P) and to mineral assemblages that permit calculation of the oxygen fugacity. Because the stability of organic matter is enormously enhanced by reduction of the water abundance, the significance of this model for water transport in the nebula for the formation of the carbonaceous chondrites is also being explored as part of the same program.

Application of the same type of model to the zone of silicate condensation would permit investigation of the relationships between oxygen transport, metal-silicate fractionation, and the origin of Mercury.

4. Laboratory Studies of Low-Temperature Condensates

Background: Voyager 2 observations of tectonic features on the surfaces of the satellites of Saturn and Uranus, as well as observations of the compositions of comet comas, have stimulated new interest in the chemistry and physics of icy solar system condensates (22). It has become abundantly clear that cryovolcanic processes have been important in shaping the surfaces of icy satellites. Outgassing associated with cryovolcanism has also been fundamental in forming the atmospheres of Titan, Triton, and (apparently) Pluto. Thus, to understand these satellite's atmospheres it is important that we also understand the physical chemistry of condensed volatiles in the outer solar system and the nature of cryovolcanic degassing processes.

Achievements: Laboratory work by J.S. Kargel on the equation of state, rheology, and thermal conductivity of ammonia-water liquids has produced data that are of great value in interpreting the behavior of low-temperature "magmas" in the ice-rich satellites of the outer planets (6, 13, 14, 24, 32). The de-gassing history of icy satellites depends on their thermal evolution, and thus, the thermal conductivities of the ices and rock which constitute icy satellites. The conductivities of ice and rock are reasonably well known, but the same is not true of

ammonia hydrate. Our measurements indicate that ammonia dihydrate has a thermal conductivity one-fourth that of water ice for a given temperature. This unexpectedly low conductivity would tend to increase interior temperatures in icy satellites above those modeled based on ammonia-free ice-rock compositions, thus promoting cryovolcanism and degassing.

We have continued the equation-of-state experiments with existing equipment, investigating the effects of adding alkali metal salts, formaldehyde, etc. to the aqueous ammonia liquids. The principal product has been a thorough study of the rheological behavior of "cryomagmas" in ammonia-water-x systems (32). This work has resulted, in collaboration with Bob Strom, in a broad reinterpretation of the eruptive styles and viscous behavior of cryomagmatic activity on the satellites of the Jovian planets. Our laboratory effort was greatly enhanced by the presence of Prof. D.L. Hogenboom, Head of the Department of Physics at Lafayette College, who spent a semester of his sabbatical (Fall 1990) in our lab. He has considerable experience in studying the phase relations in ammonia- and water-rich systems at pressures up to about 2 kb. His work, conducted at no cost to this grant, is being continued in informal collaboration with us since his return to Pennsylvania.

The de-gassing history of icy satellites depends on their thermal evolution, and thus, the thermal conductivities of the ices and rock which constitute icy satellites. The conductivities of ice and rock are reasonably well known, but the same has not been true of ammonia hydrate. Our preliminary measurements indicated that ammonia dihydrate has a thermal conductivity one-fourth that of water ice for a given temperature. This unexpectedly low conductivity would tend to increase interior temperatures in icy satellites above those modelled based on ammonia-free ice-rock compositions, thus, encouraging cryovolcanism and degassing.

Cryovolcanic de-gassing also depends on the solubilities of gases such as N_2 and CH_4 in ammonia-water and other aqueous solutions at low temperatures and high pressures (Kargel and Strom). Limited data have been available in the literature (e.g., CH_4 in water at 273 K) but not for other compositions with more compelling cryovolcanological interest (e.g., CH_4 in ammonia-water at 176 K). We have obtained gas solubility data for ammonia-water solvents over a range of interesting pressures and temperatures.

Cryovolcanic and associated degassing processes also depend on solid-liquid phase relations at elevated pressures typical of the interiors of icy satellites. As part of our collaboration with D.L. Hogenboom we have investigated high-pressure phase equilibria in the ammonia-water system. We have extended this work to the water-magnesium sulfate system, prompted by the great abundance of water-soluble magnesium sulfates in carbonaceous chondrites (33).

5. Impact Erosion and the Evolution of the Martian Atmosphere

Background: It has seemed probable since the 1982 studies by JSL and H. Watkins that impact erosion of the atmosphere of Mars might be the single most important factor in its

evolution (9). Numerical hydrodynamic models of blast waves from cometary and asteroidal impacts have been reported by Vickery and Melosh. They identify a regime of high total energy in which all impactors above a certain velocity (which depends on impactor composition) accelerate most of their own mass and much of the overlying atmosphere to above escape velocity. They apply this model to Mars and find that even relatively small, slow impactors can expel atmospheric and impactor material at speeds above the martian escape velocity. Impactors slightly too small or too slow to cause net blowoff administer severe shocks to the atmosphere and inject cometary and asteroidal volatiles into it.

Ann Vickery and Jay Melosh have been working on the adaptation of their hydrodynamic code to permit simultaneous study of impactor blowoff, atmospheric erosion, and ejection of surface rocks, and my group has considerable experience in modeling the chemical consequences of impact events, including alteration of the chemistry of the retained atmosphere by both shock heating and injection of volatiles by the impactor (3, 7, 11, 27, 31; also LPI Tech. Rept. 86-07 (1986); GSA Special Paper 190, p. 215 (1982); EPSL 22, 239 (1974); Icarus 43, 85 (1980)). This area is ripe for further development.

6. Monte Carlo Modeling of the Impact Histories of the Terrestrial Planets

Achievements: We have constructed and are now testing a Monte Carlo impact model for the Earth in which the known physical, chemical, and dynamical properties of Earth-crossing asteroids and comets, and the compositions and physical properties of the meteorite population that falls on Earth, are all included.

An important aspect of this work is the inclusion of new mass-frequency data on small (roughly 10 to 1000m) near-Earth objects produced by the Spacewatch program at LPL. Their discovery statistics clearly show a rapid upturn in object abundances below 100m diameter. Ten-meter objects are about 100x as common as a linear extrapolation of the Belt asteroid population would predict (D.L. Rabinowitz, Ap. J. submitted, 1992). The new frequency data join smoothly into the classical fireball data for meter-sized objects already established by meteor observers and photographic networks. Since these small bodies carry 10-100x as much mass and energy as has generally been believed, their role in short-term volatile deposition on Venus, atmosphere erosion from Mars, and shock-wave processing of the terrestrial atmosphere is clearly very large.

The purpose of the model to demonstrate a reasonable time-series of impacts for the purpose of cross-correlating the impactor mass, kinetic energy, iridium signature, NO_X and dust production, etc., as well as permitting correlation with cratering and meteorite fall statistics. The phenomena of ablation, deceleration, breakup in the atmosphere, explosive blowoff of material from high-energy impacts [A.M. Vickery and H.J. Melosh, GSA Special Paper 247, 289 (1990)], radiative heating of the ground [I.V. Nemchinov and V.V. Svetsov, Adv. Space Res. 11, 95 (1991); **Effects of Nuclear Weapons** (1977)], skipout into heliocentric orbit, [see L.G. Jacchia, Sky & Tel. 48, 4 (1974); Z. Ceplecha, Bull. Astron. Inst. Czech. 30, 349 (1979); J. Borovicka and Z. Ceplecha, Astron. Ap. 257, 323 (1992)], and capture into eccentric Earth or-

bit are all included in the program. The model clearly demonstrates how the velocity and composition diversity of asteroidal and cometary impactors produces a poor correlation between the various measures of impact severity. In particular, the absence of detectable iridium layers associated with many large impacts is clearly shown (31). The model provides reasonable predictions of the flux of near-horizontal impactors [P.H. Schultz and R.E. Lianza, Nature 355, 234 (1992)]. We have recently begunt to incorporate into the model the injection of volatiles by impactors and the shock production of nitrogen oxides and other species by impact blast waves [2; 3; R.G. Prinn and M.B. Fegley, EPSL 83, 1 (1987); P.J. Crutzen, Nature 330, 108 (1987)]. Neither seems to present any serious problems. We shall then include a Monte Carlo simulation of impacts on a mathematical model of the human population density distribution of the Earth. David Grinspoon has already suggested several ways to improve and extend the existing program, and we will continue to collaborate on its operational use, extending his 1988 PhD Dissertation research done under this grant (11). The program has been written so that the target may be Mercury, Venus, Earth, Mars, or a "custom" planet. It is therefore suitable with little modification to modeling exogenic influences on the evolution of all of the terrestrial planets. We would like to include the effects of tidal waves from oceanic impactors in the hazard assessment, but present understanding of impact tidal wave generation and propagation is probably insufficient to permit this [R. Strelitz, Proc. Lunar Planet. Sci. Conf. 10, 2799 (1979); W.B. McKinnon, GSA Special Paper 190, 129 (1982)].

IV. RECENT RELEVANT PUBLICATIONS

1. D.H. Grinspoon and J.S. Lewis, Deuterium Fractionation in the Pre-solar Nebula: Kinetic Limitations on Surface Catalysis. Icarus, 72, 430 (1987).

2. B.Fegley, Jr., R.G. Prinn, H. Hartman and G.H. Watkins, Chemical Effects of Large Impacts on the Earth's Primitive Atmosphere, Nature 329, 305-308 (1986).

3. T.D. Jones and J.S. Lewis, Estimated Shock Production of N_2 and Organic Matter on Early Titan. Icarus, 72, 381 (1987).

4. D.H. Grinspoon, Was Venus Wet? Deuterium Reconsidered. Science 238, 1702 (1987).

5. J.S. Lewis, Origin and Composition of Mercury. In: Mercury (F. Vilas, C.R. Chapman and M. Matthews, eds.), Univ. of Arizona Press, Tucson, 651 (1988).

6. S.K. Croft, J.I. Lunine and J.S. Kargel, Equation of State of Ammonia-Water Liquid: Derivation and Planetaological Applications. Icarus 73, 279 (1988).

7. D.H. Grinspoon and J.S. Lewis, Cometary Water on Venus: Implication of Stochastic Impacts, Icarus 74, 21 (1988).*

8. T.D. Jones, L.A. Lebofsky and J.S. Lewis, The 3μm Hydrated Silicate Signature on C-Class Asteroids. LPSC XIX (1988).

9. J.S. Lewis, The History of Mars. In: The NASA Mars Conference (D.B. Reiber, ed.), Amer. Astronaut. Soc.Sci. and Technol. Series 71, 23-41 (1988).

10. L.A. Lebofsky, T.D. Jones and F. Herbert, Asteroid Volatile Inventories. In Origin and Evolution of Planetary and Satellite Atmospheres (S.K. Atreya, J.B. Pollack and M.S. Matthews, eds.), Univ. of Arizona Press, 192-229 (1989).

11. D.H. Grinspoon, Large Impact Events and Atmospheric Evolution on the Terrestrial Planets. Ph.D. Dissertation, Department of Planetary Sciences, Univ. of Arizona (1988).

12. T.D. Jones, An Infrared Reflectance Study of Water in Outer Belt Asteroids: Clues to Composition and Origin. Ph.D. Dissertation, Department of Planetary Sciences, Univ. of Arizona (1988).

13. R. Greenberg, S.K. Croft, G. Eplee, B. Janes, J. Kargel, L. Lebofsky, J.I. Lunine, R. Marcialis, J. Melosh, G. Ojakangas, and R. Strom, Miranda. In: Uranus, (J. Bergstralh, ed.), 693-735 (1991).

14. J.S. Lewis, Abundances in Planetary Atmospheres. In: Cosmic Abundances of Matter (C.J. Waddington, ed.), Amer. Inst. Phys., 17-37 (1987).

15. J.S. Lewis, Major Issues in Planetary System Formation: Cosmochemistry. In: The Formation and Evolution of Planetary Systems (H.A. Weaver and L. Danly, eds.), Cambridge University Press, 309-314 (1989).

16. J.Kargel, D. Musselwhite, J.S. Lewis and T. Swindle, Composition of Earth's Inner and Outer Core and Primitive Mantle. In preparation (1990).

17. T.D. Jones, L.A. Lebofsky, J.S. Lewis and M.S. Marley, The Composition and Origin of the C, P and D Asteroids: Water as a Tracer of Thermal Evolution in the Outer Belt. Icarus 88, 172-192 (1990).*

18. S. Engel, J.I. Lunine and J.S. Lewis, Soar Nebula Origin for Volatiles in Comet Halley. Icarus 85, 380 (1990).*

19. J.S. Lewis and D. H. Grinspoon, Vertical Distribution of Water in the Atmosphere of Venues: A Simple Thermochemical Explanation. Science 249, 1273-1275 (1990).*

20. P. Farinella, P. Paolicchi, R.G. Strom, J.S. Kargel, and V. Zappala', The Fate of Hyperion's Fragments. Icarus 83 (1990).

21. B.A. Smith, L.A. Soderblom, and 63 other authors including J.S. Kargel, Voyager 2 at Neptune: Imaging Science Results. Science 246, 1422-1449 (1990).

22. J.S. Lewis, The Origin of the Solar System. In: The Universe and its Origins (S.F. Singer, ed.), Paragon House, N.Y., 113 (1990).

23. J.S. Kargel, S.K. Croft, J.I. Lunine and J.S. Lewis, Rheological Properties of Ammonia-Water Liquids and Crystal-Liquid Slurries: Planetological Applications. Icarus 89, 93-112 (1991).*

24. H. Hartman, M.A. Sweeney, M.A. Kropp, and J.S. Lewis, Carbonaceous Chondrites and the Origin of Life. Origins of Life, in press (1992).

25. J.S. Lewis and Melinda Hutson, Chemistry of the Solar Nebula. In: Chemistry in Space (J.M. Greenberg and V. Pirronello, eds.), Kluwer, Boston, 321-338 (1991).

26. D.H. Grinspoon and C. Sagan, Impact Dust and Climate on the Primordial Earth. In preparation (1991).

27. J.S. Lewis, T.D. Jones and W.H. Farrand, Condensation-

Accretion Models for the Terrestrial Planets, in preparation (1992).

28. J.S. Lewis, Volatility of Compounds of Iron, Aluminum and Phosphorus at the Surface of Venus. In preparation (1992).

29. T.D. Swindle, J.S. Lewis and L.A. McFadden, The Case for Planetary Sample Return Missions, 4:Asteroids. EOS, Vol 72 #44, 282 (1991).

30. J.S. Lewis and D.H. Grinspoon, Cometary and Asteroidal Bombardment of Earth: Monte Carlo Simulation. In preparation (1991).

31. J.S. Kargel, Brine Volcanism and the Interior Structures of Asteroids and Icy Satellites. Icarus, 94, 368 (1991).*

32. D.L. Hogenboom, J.S. Kargel, J.P. Ganasan and J.S. Lewis, The magnesium sulfate-water system at pressures to 4 kilobars. Lunar Planet. Sci. XXII, 581-582 (1991).

33. V.R. Baker, G. Komatsu, T.J. parker, V.C. Gulick, J.S. Kargel and L.S. Lewis, Channels and Valleys on Venus: Preliminary Analysis of Magellan Data. In press (1992).

* Papers 7, 18, 19, 23, and 31 are included as appendices to this report.

V. PERSONNEL

John S. Lewis

Curriculum Vitae

Personal:

Born [redacted].
Married to the former Ruth Margaret [redacted], 1 August 1964.
Six children: John Vandenbergh Lewis, Margaret Lewis Martell, Christopher Franklin Lewis, Katherine Rose Lewis, Elizabeth Adams Lewis, Peter Mandeville Lewis.

Education:

A.B. in Chemistry, Princeton University; 1962; National Merit Scholar.
M.A. in Inorganic Chemistry, Dartmouth College, 1964; Graduate Teaching Assistant.
Ph.D. in Geochemistry and Physical Chemistry, University of California at San Diego, 1968; NDEA Graduate Research Fellow. Dissertation advisor: Harold C. Urey.

Awards and Honors:

Honorary Lecturer, American Astronomical Society Division of Planetary Sciences, 1974.
James B. Macelwane Award, American Geophysical Union, 1976.
NASA Exceptional Scientific Achievement Medal, 1983.

Professional Experience:

Co-Director for Science, NASA/University of Arizona Space Engineering Research Center for Utilization of Local Planetary Resources, 1988-.
Professor of Planetary Sciences, Department of Planetary Sciences and Lunar and Planetary Laboratory, University of Arizona, 1982-
Professor of Planetary Sciences, Department of Earth and Planetary Sciences, Massachusetts Institute of Technology, 1979-1982.
Visiting Associate Professor of Planetary Sciences, Division of Geological and Planetary Sciences, California Institute of Technology, 1/1/74-3/31/74.
Associate Professor of Geochemistry and Chemistry, Department of Earth and Planetary Sciences and Department of Chemistry, Massachusetts Institute of Technology, 1972-79.
Assistant Professor of Geochemistry and Chemistry, Department of Earth and Planetary Sciences and Department of Chemistry, Massachusetts Institute of Technology, 1968-72.

Affiliations:

Member, American Association for the Advancement of Science

Member, NAS/NRC Space Science Board's special panels on Physics of the Outer Planets and on Advanced Exploration of Venus, 1969-70.

Member, JPL Science Advisory Group on exploration of the outer Solar System, 1971-72.

Member, NASA Headquarters Advisory Group on the Outer Planets, 1973.

Member, JPL Mariner Jupiter-Uranus advisory committee, 1974.

Contributing Editor, *Comments on Astrophysics and Space Physics*, 1973-76.

Vice Chairman, Gordon Research Conference on Physics and Chemistry of Space, 1973-75.

Member, Visiting Committee, Dept. of Planetary Sciences and Dept. of Astronomy, Univ. of Arizona, 1973.

Consultant, Venus Science Steering Group, Centre Nationale des Recherches Spatiales, 1974.

Chairman, NASA Uranus Science Advisory Committee, 1974-75.

Chairman, IUGG-AIGA Symposium on the Evolution of Planetary Atmospheres, Grenoble, 1-2 Sept., 1975.

Member, NASA Ames Research Center Advisory Committee on Interstellar Communication, 1975.

Member, NASA Physical Sciences Committee, 1975-78.

Member, NAS/NRC Space Science Board Ad hoc Committee on Biological Contamination of Outer Planets and Satellites, 1975-76.

Co-Investigator, Near-Infrared Mapping Spectrometer, Galileo Jupiter Orbiter, 1977-.

Member, NAS/NRC Space Science Board summer study on Comet and Asteroid Missions, 1978.

Member, NASA Headquarters Planetary Atmospheres Management Operations Working Group, 1979-80.

Associate Editor, *Icarus*, 1980-91.

Member, Space Science Board, 1980-83.

Co-Chairman, Gordon Research Conference on the Origin of Life, 1981-82.

Member, NASA Ames Research Center Advisory Committee on Detection of Extrasolar Planetary Systems, 1983.

Member, IDA Workshop on Defense Applications of Near-Earth Resources, California Space Institute, 1983.

Faculty Fellow, NASA Summer Study on Space Resources, California Space Institute, 1984.

Member, Mars Observer Review Panel, 1985.

Member, NASA Headquarters Planetary Atmospheres Operations Working Group, 1986-89.

Co-Investigator, CRAF Penetrator Probe, 1987-.

Member, Lunar Exploration Science Working Group, NASA, 1988-.

Member, NASA Office of Exploration Science Working Group, 1988-.

Director, American Rocket Company, 1988-.

Vice-President for Research, and Director, ASPERA Corporation, 1989-.

Director, Arizona Space Initiative, 1989-.

Member, Board of Governors, National Space Society, 1990-.

Member, NASA Long Duration Exposure Facility Advisory Committee, 1990-.

Chairman, Conference on the Resources of Near-Earth Space, Tucson, 1991.

Commissioner, Arizona State Space Commission, 1991-.

APPENDICES

Appendix A: *D.H. Grinspoon and J.S. Lewis*, Cometary Water on Venus: Implications of Stochastic Impacts, Icarus 74, 21 (1988).

Appendix B: *T.D. Jones*, L.A. Lebofsky, *J.S. Lewis* and M.S. Marley, The Composition and Origin of the C, P and D Asteroids: Water as a Tracer of Thermal Evolution in the Outer Belt. Icarus 88, 172-192 (1990).

Appendix C: *S. Engel*, J.I. Lunine and *J.S. Lewis*, Solar Nebula Origin for Volatiles in Comet Halley. Icarus 85, 380 (1990).

Appendix D: *J.S. Lewis and D.H. Grinspoon*, Vertical Distribution of Water in the Atmosphere of Venus: A Simple Thermochemical Explanation. Science 249, 1273-1275 (1990).

Appendix E: *J.S. Kargel*, S.K. Croft, J.I. Lunine and *J.S. Lewis*, Rheological Properties of Ammonia-Water Liquids and Crystal-Liquid Slurries: Planetological Applications. Icarus 89, 93-112 (1991).

Appendix F: *J.S. Kargel*, Brine Volcanism and the Interior Structures of Asteroids and Icy Satellites. Icarus, 94, 368 (1991).

Italics designate faculty and students supported under this grant.

ICARUS 74, 21–35 (1988)

Cometary Water on Venus: Implications of Stochastic Impacts[1]

DAVID H. GRINSPOON AND JOHN S. LEWIS

Lunar and Planetary Laboratory, University of Arizona, Tucson, Arizona 85721

Received June 3, 1987; revised September 24, 1987

The short lifetime of water on Venus suggests that the water abundance is in a near steady-state balance between loss by escape and replenishment by infall. In addition, the observed deuterium-to-hydrogen ratio on Venus is consistent with a steady state and does not necessarily imply a past water excess. We present results of a model incorporating a stochastic cometary source and nonthermal escape of hydrogen that produces the observed water abundance and D/H ratio. The stochastic variability of each of these quantities is shown to be large. We conclude that water on Venus is in a quasi-steady state mediated by large comet impacts and that the early history of water on the planet has been obscured by a history of random impacts. © 1988 Academic Press, Inc.

INTRODUCTION

Venus is an exceedingly dry place by terrestrial standards, having a global water inventory five orders of magnitude lower than that on Earth. The aridity of Venus has often been explained as due to the loss of a much greater primordial endowment of water, perhaps up to a full terrestrial ocean, which has been lost due to a runaway greenhouse, UV photolysis, and thermal and nonthermal escape of hydrogen. This model is supported by a deuterium-to-hydrogen ratio 100 times the terrestrial ratio, which is interpreted as a residue left by mass-selective escape of at least 100 times the current water abundance, perhaps a much greater amount depending on the efficiency of deuterium escape (Donahue *et al.* 1982). This scenario has been widely accepted and has diffused into the popular science literature, where it is often presented as a parable of a sister Earth gone astray.

A consideration of the current lifetime of water on Venus casts doubt on this monotonic secular decline in abundance. Dividing the current hydrogen column abundance by the nonthermal escape flux yields a characteristic lifetime on the order of 10^8 years. Either we have arrived just in time to witness the final departure of water from Venus or, much more likely, there is a source of water, and the abundance is in or near steady state. Possible sources include volcanic outgassing (Kumar *et al.* 1983) and cometary impact (Lewis 1974, Grinspoon and Lewis 1986).

Models of planetary formation differ on how much water and bound water should have been incorporated in the original material which accreted to form Venus. It is not known whether there was enough heliocentric mixing of planetesimals in the formation region of the terrestrial planets to give them similar original volatile inventories (Wetherill 1985). The observed variation of density with heliocentric radius among the terrestrial planets would not be produced in an extremely "well-mixed" accretion process. Planet formation may have been a more quiescent process with low eccentricities preventing a large degree of exchange (Greenberg 1987). In this case, the temperature gradient in the nebula would have resulted in a compositional trend

[1] Presented at the Origin and Evolution of Planetary and Satellite Atmospheres Conference, Tucson, AZ, March 1987.

0019-1035/88 $3.00

among the planets which would provide Venus with a much smaller water endowment than Earth (Lewis 1972).

We have pursued an extreme model in which endogenous water sources are neglected, in order to explore and illustrate the possible importance of exogenous water on Venus. The apparent steepness of the size–frequency distribution of comets indicates that the bulk of the mass in the impacting flux may be contained in a relatively small number of massive nuclei. This suggests the possibility of large stochastic variations in water abundance. (The K-T impactor on Earth may have been a 10^{19}-g comet (Lewis *et al.* 1982). This would provide about 50% of the current water abundance on Venus! The mean interval between such impact events appears to be similar to the characteristic lifetime for water on Venus.) Accordingly, we have constructed a model incorporating stochastic impact injection and nonthermal escape of hydrogen, in order to explore the behavior of this interesting system.

WATER ON VENUS

There is a discrepancy between Venera and Pioneer Venus measurements of water abundance, but the favored interpretation is of a surface mixing ratio of 20 ppm rising to a value of 200 ppm at the cloud tops (Young *et al.* 1984). The cause of this gradient is not understood.

The current hydrogen escape flux is dominated by hot O impact (McElroy *et al.* 1982) and charge exchange with hot H^+ (Kumar *et al.* 1983), yielding a total escape flux of 2×10^7 H atoms cm^{-2} sec^{-1}. Assuming that water is the major H-containing species, which appears to be the case, then the column abundance of 0.1 g of H per square centimeter has a lifetime of 10^8 years, quite short compared to the age of Venus.

It is unsatisfactory simply to assume (although it is conceivable) that the present epoch is a unique point in the evolution of the atmosphere of Venus. A much more likely possibility is that Venus is being supplied with water at a rate which balances the nonthermal escape flux. Two potentially large water sources suggest themselves: long-term continuous volcanic outgassing, and impact of volatile rich bodies, among which icy comet nuclei should carry the bulk of the incoming hydrogen.

Although there is good evidence for volcanic activity at some point in the history of Venus (Barsukov *et al.* 1986), the amount of accompanying outgassing is totally unknown. It is not known whether this activity continues at present, although there have been intriguing observations of secular changes in the SO_2 abundance above the clouds (Esposito 1984). Estimates of the time dependence and total extent of outgassing on Venus must be highly dependent on one's preference of models for the origin and geologic evolution of the planet.

Lewis (1974) found that the flux of comets and volatile-rich asteroids could be sufficient to maintain a steady-state abundance of hydrogen on Venus. Estimates of the cometary flux through the inner Solar System have been made based on cratering records, astronomical observations, and dynamical calculations (Weissman 1985, Wetherill and Shoemaker 1982, Ip and Fernandez 1987). Although there is also a large uncertainty in these estimates, this is a known hydrogen source for Venus which may be considered independently of geologic models.

DEUTERIUM ON VENUS

The large deuterium-to-hydrogen ratio in the atmosphere of Venus was established by McElroy *et al.* (1982), who derived a D/H ratio of 1×10^{-2} from the mass 2 ion detection by the Pioneer Venus ion mass spectrometer. Donahue *et al.* (1982) analyzed the PV large probe neutral mass spectrometer measurement of HDO, finding a D/H ratio of $(1.6 \pm 0.2) \times 10^{-2}$. This measurement was regarded as a critical test between theories in which Venus formed in its present dry state and those in which large

amounts of water were lost over the history of the planet.

For computational simplicity it is assumed that the escape flux of hydrogen is close to the diffusion limit, and therefore proportional to the hydrogen abundance, and that the escape of deuterium is likewise proportional to the deuterium abundance multiplied by a factor f, the fractionation factor, which represents the relative inefficiency of deuterium escape due to its larger mass. The differential equations representing the escape of these isotopes have the solution (Hunten 1982, Kasting and Pollack 1983)

$$\left(\frac{D}{H}\right)_1 = \left(\frac{D}{H}\right)_0 \left[\frac{(f_{H_2O})_0}{(f_{H_2O})_1}\right]^{1-f}, \quad (1)$$

where the subscripts 1 and 0 can be taken to mean "present" and "primordial," respectively, and f_{H_2O} is the mixing ratio of water in the atmosphere which we have assumed represents the total hydrogen inventory. It can easily be seen that, using this formalism, the interpretation of a 100-fold deuterium enrichment is that the water abundance has declined by at least a factor of 100, perhaps much greater if f, the deuterium escape efficiency, was significantly larger than zero.

This interpretation depends upon the assumption that there was no concurrent source of hydrogen during the fractionating escape and that the original D/H ratio on Venus was equal to the modern terrestrial ratio. The latter assumption is questionable since the origin of this "standard" is not understood and thus its applicability beyond the Earth is not known (Grinspoon and Lewis 1987). In this model the fractionating nonthermal escape was preceded by a period of hydrodynamic escape of much larger quantities of water, perhaps up to a full terrestrial ocean (Kasting and Pollack 1983). There is little evidence for this hydrodynamic escape phase, beyond the argument that some models of planet formation would have provided Venus with Earthlike quantities of water which then would have escaped in this fashion. An early period of massive hydrodynamic escape has also been invoked by Pepin (1987) to generate the observed mass fractionation of noble gas elements and isotopes.

If, as suggested in the previous section, water on Venus may be in a near steady state, rather than in monotonic decline, then the D/H ratio must be explained in a consistent fashion.

When a time-averaged source term for hydrogen, ϕ, which is equal to the escape flux, is introduced we obtain the solution

$$\frac{D}{H}(t) = \frac{\alpha}{f} - \left[\frac{\alpha}{f} - \left(\frac{D}{H}\right)_0\right] e^{-(\phi f/H)t}, \quad (2)$$

where α is the D/H ratio of the hydrogen source, H is the steady-state hydrogen abundance, and t is the time elapsed.

If we assume that D/H in the hydrogen source is equal to the primordial D/H, an assumption which is perhaps more safe for outgassing than for an external source, then this reduces to Eq. (10) in Krasnopolsky (1985).

Hunten (1982) and Hunten *et al.* (1987) give the solution

$$D/H = \alpha/f \quad (3)$$

for the steady-state case. This is indeed the limiting solution, with the exponential term (representing the decaying signature of the original D/H ratio) disappearing as t goes to infinity. However, it is not obvious that this term can be ignored. The time constant for decay of this exponential term is

$$\tau = H/\phi f. \quad (4)$$

For a hydrogen inventory corresponding to 20 ppm water, an escape flux of 2×10^7 cm^{-2} sec^{-1}, and $f = 0.022$ for charge exchange (Krasnopolsky 1985), we find $\tau = 3.97 \times 10^9$ years. Hunten *et al.* (1987) suggest a weighted fractionation factor, allowing for the relative magnitude and differing fractionation factors of the various escape

mechanisms, of $f = 0.013$. Employing this value in (4) gives us $\tau = 6.71 \times 10^9$ years. Thus the decay time for this term seems to be on the order of the age of the Solar System.

The solar EUV flux was more intense in the past (Zahnle and Walker 1982) and thus it seems likely that the escape flux of H may have been at the diffusion limit, or closer to the limit than at present, for much of the planet's history (Krasnopolsky 1985). This increased flux for a given water abundance would have the effect of lowering τ by an amount proportional to the increase in flux. Uncertainties in estimating the present and past values of ϕ, H, and f make it difficult to determine whether or not the limiting solution of (2), represented by (3), should be reached in 4.5×10^9 years of steady-state evolution of the D/H ratio.

If the source of hydrogen has a terrestrial D/H ratio and the fractionation factor is as modeled by Hunten *et al.* (1987) ($\alpha = 1.6 \times 10^{-4}$, $f = 0.013$), then (3) gives D/H = 1.23×10^{-2}. The average cometary D/H ratio is unknown. Some models of comet formation lead to predictions of enhanced D/H in cometary ices (Vanysek and Vanysek 1985, Ip 1984). Eberhardt *et al.* (1987) used Giotto Neutral Mass Spectrometer measurements to find $0.6 \times 10^{-4} < \mathrm{D/H} < 4.8 \times 10^{-4}$ for Comet Halley. Whether or not this measurement represents the bulk D/H in Comet Halley and whether Halley should contain average cometary D/H are both unknown. Using this range for α in (3) gives a steady-state D/H of 4.6×10^{-3} to 3.7×10^{-2} for Venus, nicely bracketing the observed value. Including the exponential term in (2) with a decay constant on the order of the age of the Solar System lowers these values somewhat, depending on the chosen value for "original" D/H. Yet it is still possible with reasonable assumptions for the unknown parameters α, f, $(\mathrm{D/H})_0$, and H to derive D/H values, employing the steady-state solution, which are consistent with the observations. It is not necessary to postulate any past or "primordial" excess of water on Venus to explain the observed D/H ratio.

THE STOCHASTIC IMPACT INJECTION MODEL

For a power law mass–frequency distribution with a cumulative slope index of less than 2, most of the mass is contained in the largest objects in the distribution. The size distribution of comets appears to be of this nature (Hughes and Daniels 1980, Shoemaker and Wolfe 1982). Thus it seems likely that an exogenous source of hydrogen would be injected in a relatively small number of sudden events rather than as a smooth stream. This should produce large stochastic fluctuations in the water abundance and D/H ratio on Venus. In order to understand better the nature of these fluctuations we constructed a model including a stochastic impacting flux of comet nuclei and nonthermal escape of hydrogen.

There is a large uncertainty in our knowledge of the flux of large bodies through the inner Solar System and the resulting frequencies of impact with the terrestrial planets. Thus any conclusion based on a model including such an impact flux must be robust against large variations in the magnitude of this flux. To treat this uncertainty we defined a baseline flux, which we consider to be the most likely frequency distribution based on the available evidence, and then ran the model with a wide range of modifications to this.

Our baseline flux is an adaptation of the work of Watkins (1983), who, using the results of Dohnanyi (1972), defined the flux of impactors on the Earth in terms of the average time between impact of objects of a given mass or greater as a function of the mass, which for a power law distribution gives a straight line on a plot of log (mass) versus log (time). This flux distribution agrees quite closely with those given by Wetherill and Shoemaker (1982) and Kyte and Wasson (1986). We have modified this flux to include only the cometary impactors and considered the relative probabilities of

impact on Venus and Earth for objects in cometary orbits.

Within the limits of observational uncertainty, it appears that the size distributions of asteroids and comets are similar (Hughes and Daniels 1980, Watkins, 1983). Thus, we represent the flux of comets as a fraction of the total impacting mass, having the same size distribution as the overall flux. In light of the spacecraft observations of the 1986 apparition of Comet Halley, which revealed a lower albedo and larger object than expected, Weissman (1986) now estimates that 50% of the recent terrestrial large impacts are by active cometary nuclei of which approximately one-third are long period and two-thirds are short period. For long-period comets the impact probability on Venus is 77% greater than that on Earth (Weissman 1985). For short-period comets the impact probability is 75% greater on Earth (Basaltic Volcanism Study Project 1981). Thus the cometary flux on the two planets can be considered to be equal within the limits of the other uncertainties involved in the flux estimate.

Based on these considerations we have employed a baseline comet flux which is 50% of the total flux used by Watkins (1983). This distribution is shown in Fig. 1. A pseudo-random-number generator was used to simulate a stochastic flux with this size–frequency distribution. The largest comet in our baseline distribution has a mass of 4.2×10^{19} g, having a characteristic time between impacts of 4.5×10^{9} years. The integrated mass of this flux of comets over the age of the Solar System is 5×10^{20} g. By comparison the mass which Ip and Fernandez (1987) estimated to have been received by Venus from mass loss from the Oort cloud is 6×10^{20} g over this same time period. This is independent of a much larger component of 10^{24} to 10^{25} g which would have been received by Venus in the first few hundred million years of Solar System history due to planetesimals scattered during the formation of Uranus and Neptune (Ip and Fernandez 1987). For a cometary composition of 50% H_2O by mass, an influx of 5×10^{20} g over the age of Venus would be balanced by an average escape flux of 2.5×10^{7} H atoms cm^{-2} sec^{-1}, within 25% of the present escape flux.

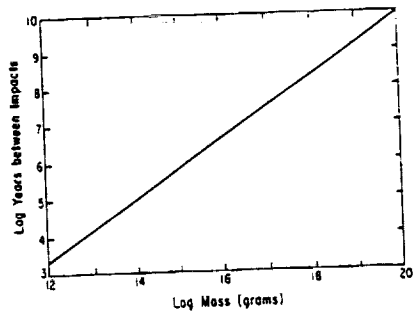

FIG. 1. Estimated comet flux on Venus. The formula for this distribution is $\log_{10}(t) = 0.8333 \ldots \times \log_{10}(M) - 6.699$, for t in years and M in grams.

Kyte and Wasson (1986) have estimated the uncertainty in the terrestrial impact flux as a factor of 4 at the low mass end of the spectrum. For larger masses the uncertainty is at least an order of magnitude, perhaps several. Our baseline flux is conservative in that we have assumed a time-independent flux, remaining at currently estimated impact rates throughout the entire history of Venus. Yet impact rates were surely greater in the past. It is not clear what fraction of the massive early bombardment suffered by the terrestrial planets was due to comets, but dynamical considerations suggest that the rate of comet impact in the early Solar System should have been greater than that at present by many orders of magnitude (Ip and Fernandez 1987). An additional potentially significant source of hydrogen which we have not included is volatile-rich asteroids, particularly that subset of Apollo asteroids that may be extinct cometary nuclei. These objects may have substantial volatile reservoirs in their interiors.

We assume a cometary composition which is 5% hydrogen by mass (Whipple 1984). We further assume that the impacting nuclei are vaporized and that the hydro-

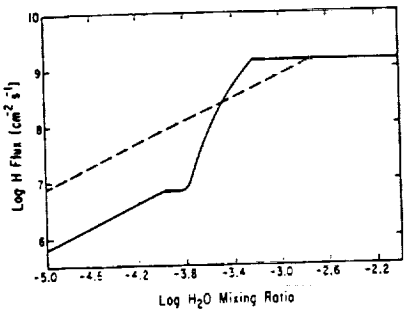

FIG. 2. Hydrogen escape flux adapted from Krasnopolsky (1985). At high f_{H_2O} the cold trap results in an escape flux which is independent of hydrogen abundance. We have extended this function to low f_{H_2O} by assuming a linear relationship. The dashed line is the diffusion-limited flux described in the text.

gen enters the atmosphere and chemically equilibrates, mostly ending up in water molecules. Both Watkins (1983) and Walker (1986) studied impact blowoff of atmospheres and concluded that it is not a significant process for Venus.

The second essential component of this model is the escape flux of hydrogen and deuterium. The function $\phi(f_{H_2O^S})$, which describes the dependence of the hydrogen escape flux on the water mixing ratio at the surface, is quite complex, involving many different escape processes which dominate in different regimes of homopause hydrogen abundance, f_H, and several regimes of differing functional dependence of f_H on $f_{H_2O^S}$. The latter is controlled at present by the sulfuric acid trap and in larger f_{H_2O} regimes by the cold trap. This has been modeled in detail by Kumar *et al.* (1983), Kasting and Pollack (1983), and Krasnopolsky (1985). The results of this modeling are displayed graphically in Fig. 13 of Kumar *et al.* (1983) and Fig. 1b of Krasnopolsky (1985). These results differ somewhat due to different assumptions about the behavior of the sulfuric acid trap and the nature of the cold trap. We have found that these differences are not great enough to affect our results significantly. Our model employs the escape function shown in Krasnopolsky's Fig. 1b. It was necessary to extend this function to regimes of water abundance below the current abundance, where it has not been modeled in detail (since all previous models have assumed a declining water abundance). It was sufficient for our purposes to assume that in this regime the escape flux simply declines in proportion to the water abundance, as the results are not very sensitive to the detailed shape of the escape function in this region. The escape function employed is shown in Fig. 2.

We also performed some runs with escape occurring at the diffusion limit for all water abundances. For this function, also shown in Fig. 2, we used the diffusion-limited flux as a function of homopause hydrogen abundance $\phi = 4 \times 10^{13}$ (f_H) cm^{-2} sec^{-1}, given by Kasting and Pollack (1983). For the sulfuric acid trap function we used the linear function, $f_H = 2 \times 10^{-2}$ $(f_{H_2O^S})$, given by Kumar *et al.* (1983). Krasnopolsky's treatment of this function is more complex, allowing for the dependence of f_H on the H_2O/SO_2 ratio. The use of the resulting nonlinear sulfuric acid trap function explains why the escape function shown in Fig. 2 exceeds the "diffusion-limited" flux at the upper end of the sulfuric acid trap regime, as the latter was derived using the linear assumption.

The horizontal portion of the curve in Fig. 2 represents the cold trap, with an assumed temperature of 170°K, which is the case for the present-day atmosphere (Krasnopolsky 1985). Here the escape flux becomes independent of $f_{H_2O^S}$ until the H_2O mixing ratio rises to ≈10% at the surface, when rapid hydrodynamic escape becomes possible (Kasting and Pollack 1983). The hydrodynamic escape regime is not treated in our model, as the resulting quasi-steady-state water abundances remain well below this value.

The escaping hydrogen was integrated in million-year increments, with the amount of deuterium escaping in each increment equaling the product of the number of escaped H atoms, the instantaneous D/H ratio, and the chosen fractionation factor. In

a more rigorous treatment the fractionation factor would also vary with water abundance as the relative importance of the nonthermal escape processes changed.

The number and mass of impacts were calculated at 50-million-year increments. The cumulative mass of small comets with a characteristic time between impacts of less than 50 million years was included as a constant "low mass trickle" in each increment. For the slope index used, this constituted 34% of the total flux. A simple way to modify this model to include the effect of outgassing would be to increase the value of this parameter, although there is no reason to expect that outgassed and cometary water would have the same D/H. For each 50-million-year increment the water mixing ratio, D/H ratio, cumulative cometary mass, and percentage of water of cometary origin were recorded.

MODEL RESULTS

Figure 3a shows the water abundance as a function of time for five model runs employing an impact flux equal to twice the baseline comet flux. This behavior, spikes of high f_{H_2O} corresponding to large impacts, interspersed with periods of declining water abundance, was typical of runs with a wide range of integrated impact fluxes and with diverse assumptions regarding escape behavior. Figure 3b is a histogram showing percentage of time spent in different bins of water abundance for these same five runs. Figures 4a and 4b show the behavior of the water abundance for a flux depleted by a factor of 2 relative to the baseline flux. As can be seen, the behavior is essentially identical, with the system simply spending a larger percentage of time in the lower water-abundance range. Model runs were performed with the integrated impact flux varied over two orders of magnitude, and still the behavior was similar with the histograms becoming more perturbed (Fig. 5).

The histograms each exhibit a sharp cutoff at the low water-abundance end. This corresponds to the level at which the steady "low mass trickle" for the chosen impact flux just balances the escaping hydrogen flux. The low end cutoff in the histogram for many model runs is higher than the observed 20 ppm water abundance. We do not regard this as problematical, as the uncertainties in this measurement and in many model parameters are large. The model is mainly meant to illustrate the character of the behavior to be expected in this system. In most cases however the system spent a considerable amount of time within the range of uncertainty in the current water abundance, which we consider to be 15–100 ppm.

Figure 6 shows the behavior of the D/H ratio for the same runs displayed in Fig. 5. As expected, the stochastic variation of D/H is large but the net trend is toward larger D/H as the steady state evolves. Figure 7 shows the effect of varying the D/H of the cometary hydrogen and holding all other variables constant. Clearly, the evolution of the D/H ratio is much more sensitive to choices of unknown input parameters than is the f_{H_2O} evolution, which was consistent with observations for a very wide range of assumptions. Although the D/H ratio entered the observed range for some reasonable choices of the input parameters, there were many combinations of total flux, escape function, and cometary D/H for which the planetary D/H remained well below the observed value. For example, an impact flux depleted by a factor of 8 relative to the baseline flux did not produce sufficiently enhanced D/H unless the cometary D/H was a factor of 10 greater than terrestrial. Thus our conclusions about D/H evolution based on this model cannot be as robust as those about f_{H_2O} evolution. These results led us to consider the effect of a time-dependent comet flux on the D/H ratio.

Although the model runs described up to this point have assumed no higher ancient cometary flux, this is counter to both the observational evidence contained in the cratering record of the terrestrial planets

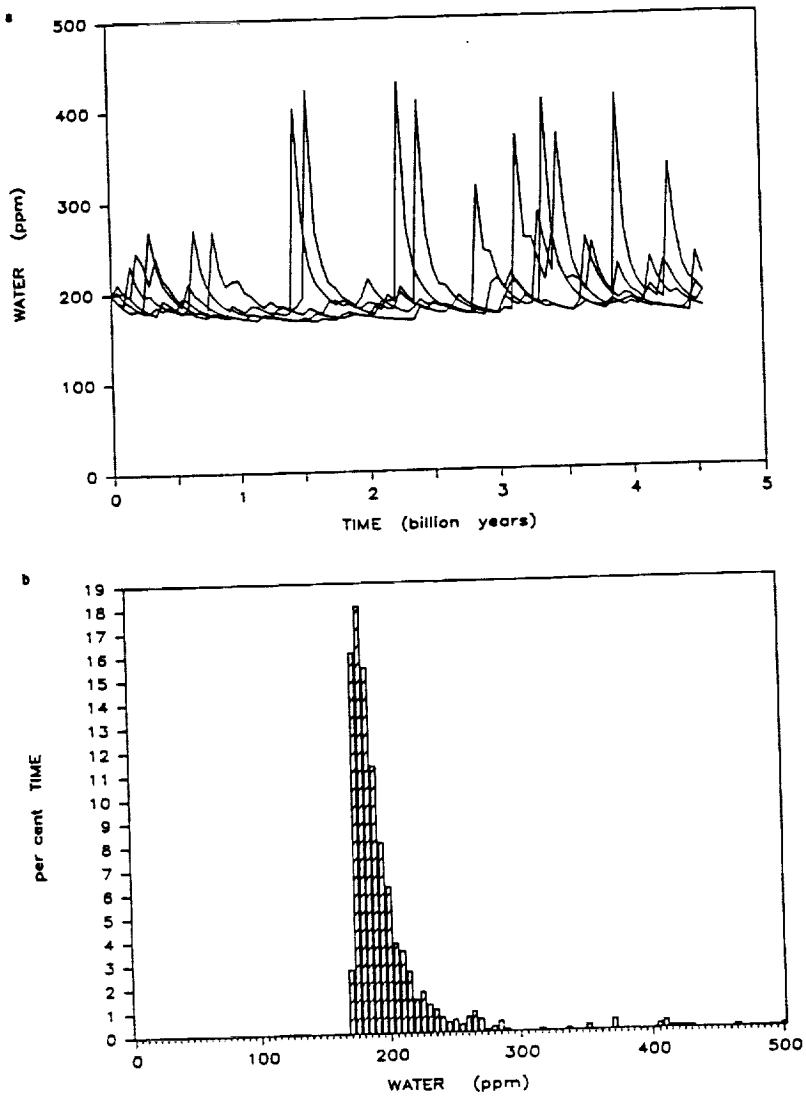

FIG. 3. (a) Five model runs for evolution of water abundance on Venus. These runs employed an impact flux equal to twice the baseline flux shown in Fig. 1. Spikes in water abundance correspond to large comet impacts. (b) Histogram for these five runs showing percentage of time spent in different bins of water abundance.

and the theoretical treatments of outer planet formation and cometary dynamics. We do not wish here to effect a precisely detailed simulation of the time dependence of this flux, but merely to explore the consequences of a past excess in impact rate which mimics to some extent those which have been postulated in the literature. Shoemaker and Wolfe (1982) suggested that the late heavy bombardment of the inner Solar System was due to comets, but Strom (1987) has offered arguments to the contrary based on detailed comparisons of the cratering records of the planets. We simply assume that the proportion of cometary objects in the total impact flux was the same in the past as it is at present.

According to the model of Hartmann

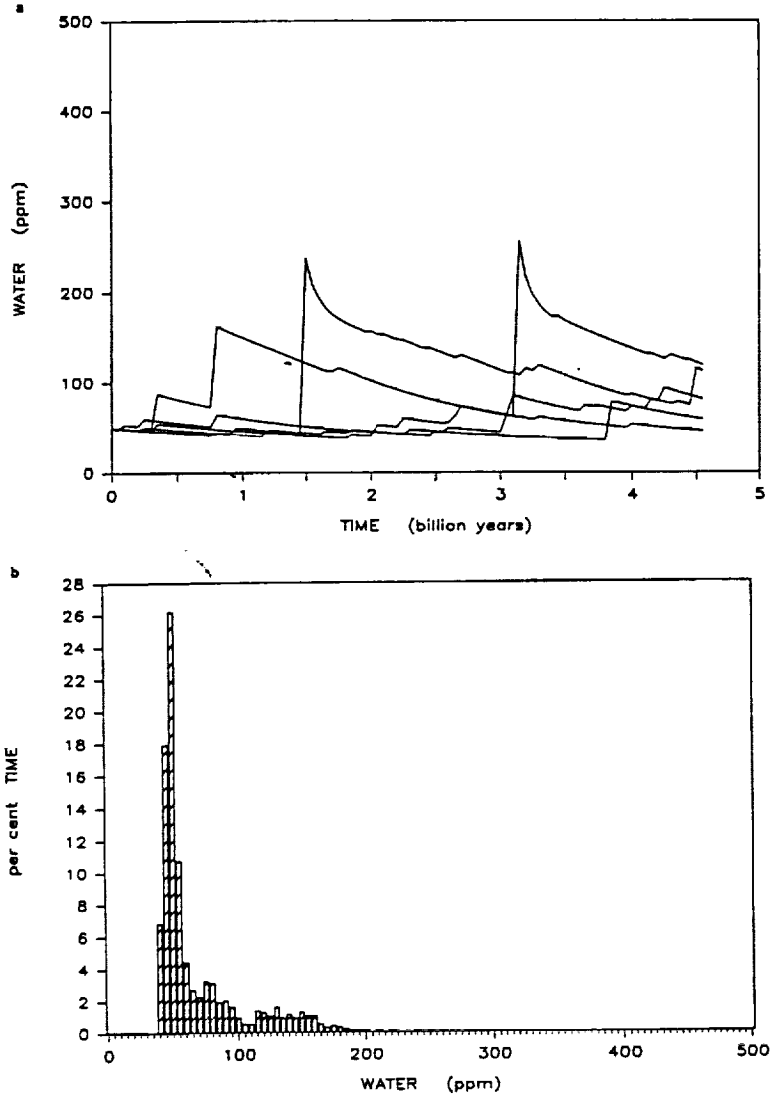

FIG. 4. (a) Results of five runs employing an impact flux depleted by a factor of 4 relative to the runs in Fig. 3. (b) Water abundance histogram for these runs.

(1987), the terrestrial impact flux 4 billion years ago was approximately 10^3 times the current flux, although the earlier, postaccretional flux must surely have been much higher. We modified our model to include an enhancement of the impact rate by 10^3 at $t = -4 \times 10^9$, decreasing with a 150-million-year half-life. This gives a total integrated flux of 2.8×10^{22} g. Compared to the 10^{24} to 10^{25} g which Venus may have received from scattered planetesimals during the formation of Uranus and Neptune (Ip and Fernandez, 1987), this is still a conservative flux estimate. The effect of this time-dependent flux on the evolution of the D/H ratio is shown in Fig. 8. Several more modest time-dependent fluxes were also run. Also shown in Fig. 8 is a run where the baseline flux is depleted by a factor of 4 and the enhancement at $t = -4 \times 10^9$ years is only a

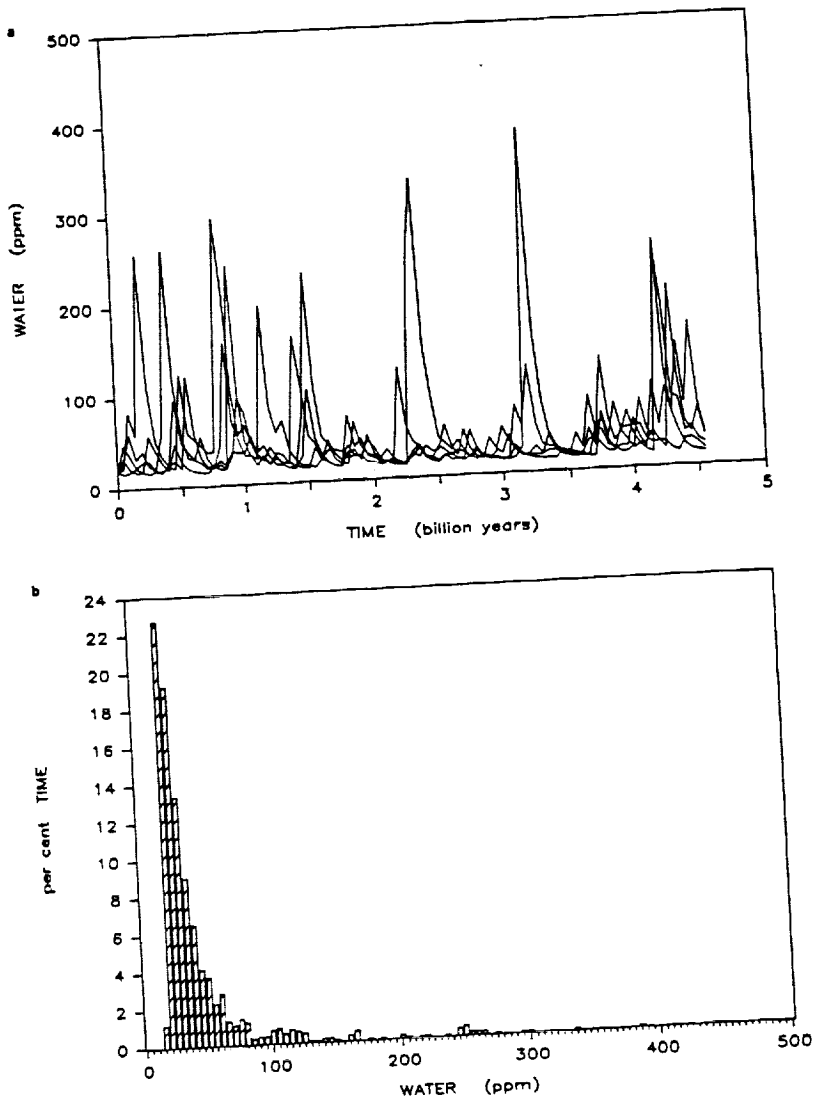

FIG. 5. (a) Five model runs with an impact flux enhanced by a factor of 2 relative to the baseline flux, and with hydrogen escaping at the diffusion limit. (b) Water abundance histogram for these runs.

factor of 500, again decaying with a half-life of 150 million years. The integrated mass of this flux model is 3.3×10^{21} g.

When the effects of such time-dependent fluxes are included, then in nearly every case the current D/H ratio on Venus is exceeded by the model results. In these runs, the large final D/H values are due to a combination of early fractionating water loss and later steady-state evolution. If the steady state were allowed to operate for long enough (several τ) then the final D/H reached would be independent of this early history, but since τ is on the order of the age of the Solar System the resulting D/H ratios are quite enhanced after 4.5 billion years. The water abundance evolution for these time-dependent runs is shown in Fig. 9. This scenario differs from the previously published models of early fractionating wa-

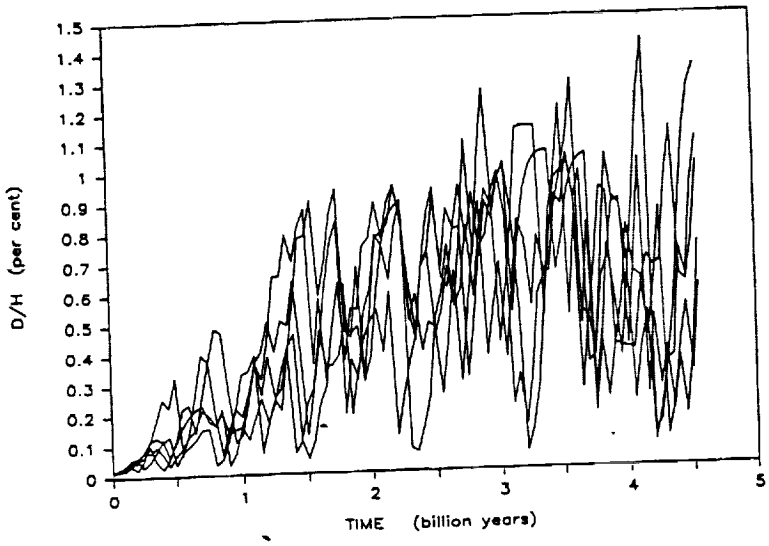

FIG. 6. Evolution of the deuterium-to-hydrogen ratio for the same runs shown in Fig. 5, employing a cometary D/H equal to the terrestrial value of 1.6×10^{-4} and a fractionation factor $f = 0.013$.

ter loss in one important respect: here none of the water excess is endogenous. The large early water abundances are simply the steady-state abundances corresponding to the massive early cometary influxes. The peak water abundances, which are off scale in Fig. 9, are approximately 27,000 and 8000 ppm for the two time-dependent fluxes described above. As the cometary flux declines exponentially to the present-day value, the water abundance declines until the escape flux balances this lower influx.

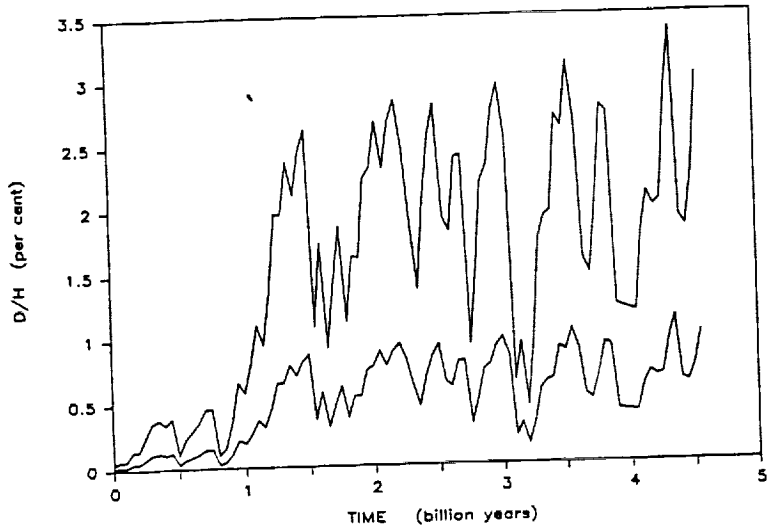

FIG. 7. The effect of cometary D/H on Venus D/H evolution. The lower curve is taken from Fig. 6, employing a terrestrial D/H value. (Note the difference in scale.) The upper curve is the same run, using a cometary D/H value of 4.8×10^{-4}, the observed upper limit for Comet Halley (Eberhardt *et al.* 1987).

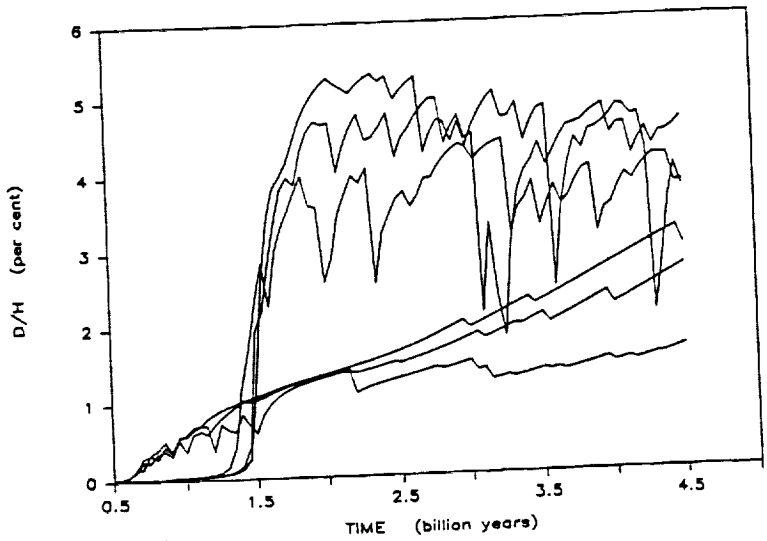

FIG. 8. D/H evolution on Venus for time-dependent comet fluxes. The three upper curves are runs with a flux enhancement of 10^3 at $t = -4.0 \times 10^9$ years, decaying with a half-life of 150 million years. The three lower curves are for a more modest enhancement which is described in the text.

The final results are water abundances which are compatible with the observed abundance on Venus and D/H ratios which are quite enhanced.

DISCUSSION

A consideration of the current lifetime of water on Venus and our model results lead us to conclude that the water abundance on Venus is likely to be in a quasi-steady state, mediated by episodic large comet impacts. Any remnant of an early Earthlike ocean on Venus is obscured by a history of random impacts. Known processes provide an explanation of the observed water abundance and D/H on Venus. There is no need to

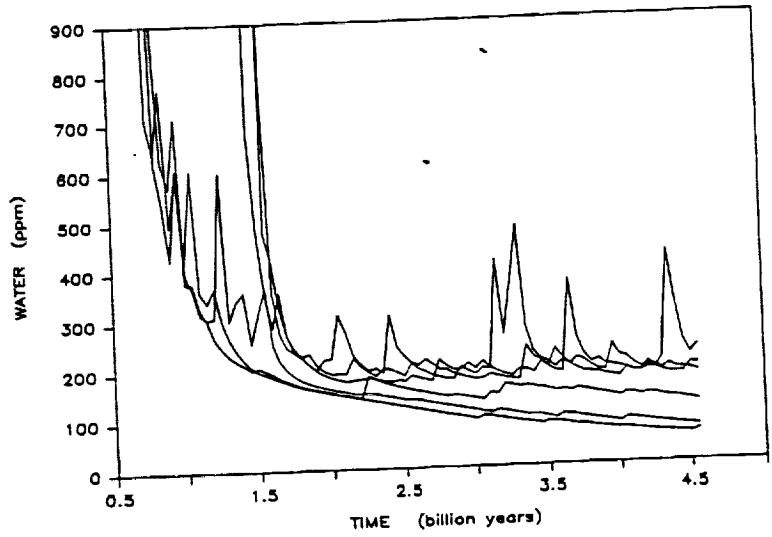

FIG. 9. Water abundance evolution for the same runs shown in Fig. 8. The peak abundances, which are off scale, are discussed in the text.

postulate an unknown source of early water and no evidence that there was one. Outgassing may have contributed as well, but no endogenous source of water is necessary to explain the observations. The water now observed on Venus is quite possibly more than 99% of cometary origin.

The observed deuterium to hydrogen ratio may not be evidence of a "primordial" water excess on Venus. If an early water excess is responsible in part for the current D H, it is likely to have been the steady-state water abundance for an enhanced cometary flux. This ratio is coupled in a complex relationship to the average cometary D/H, the time-integrated cometary flux and any time dependence in the flux, and the actual mass and D/H of any large comets which may have impacted on Venus in the last several hundred million years.

In a similar fashion, the current water abundance on Venus may depend critically on the recent comet impact history of the planet as well as on the average flux and outgassing history. This stochastic variability, as illustrated in Figs. 3 through 5, must add an unavoidable level of uncertainty to any deterministic interpretations of these observations.

It is possible that these stochastic variations in water abundance will be damped by surface-atmosphere buffering reactions of the kind described by Nozette and Lewis (1982). Characterization of the time scale for this buffering is difficult as it depends on such poorly known parameters as diffusion rates through the surface material, particle sizes, and the rates of many heterogeneous reactions which have not been well studied. If there is not significant damping, these oscillations in water abundance may have important implications for the climate history of the planet; water is an important IR absorber which helps to maintain the strong greenhouse.

When a consideration of the likely time dependence of the comet flux is included in the model, then the problem of explaining the current D/H ratio becomes one of explaining why it is so low compared to model results. This could put constraints on the magnitude of any past increase in the cometary flux. However, the attempt to define such constraints will be hampered by the difficulty in determining how the fractionation factor varies with escape flux. The fractionation factor is likely to be higher than at present for enhanced escape fluxes (Krasnopolsky 1985, Kasting *et al.* 1984). This would lower the final D/H for the time-dependent case, possibly reconciling the enhanced values shown in Fig. 8 with the observed values. Chyba (1987) has used scaling arguments to conclude from the lunar impact record that if a small fraction of the late heavy bombardment impact flux was composed of cometary objects then the Earth's oceans could have been fully supplied by cometary water. Under such a scenario Venus should have received similar amounts of water, yet the low D/H may be problematical. A continuous outgassing of juvenile water, as proposed by Kumar *et al.* (1983) and Kasting and Pollack (1983), could help to lower the D/H. As can be seen by examining Eqs. (2) and (4), this would have the effect of lowering the time constant for the steady-state D/H value to be reached. In this case the steady-state value would be that given in Eq. (3) with α being a weighted average of the outgassed and cometary D/H values. Another possible explanation is that Venus has recently (within 10^8 years) suffered a large comet impact which lowered the D/H ratio to the observed value. If the terminal cretaceous event on Earth was caused by a comet shower, rather than by a single large impact, then the water abundance and D/H ratio on Venus should bear the signature of this same catastrophe.

ACKNOWLEDGMENTS

We thank D. M. Hunten and J. F. Kasting for helpful comments on earlier drafts of this paper and C. F. Chyba for providing a preprint of his work. This research was supported by NASA Graduate Student Research Program Fellowship NGT 03-002-803 and NASA Grant NAGW-340.

REFERENCES

BARSUKOV, V. L., *et al.* 1986. The geology and geomorphology of the Venus surface as revealed by the radar images obtained by Veneras 15 and 16. *J. Geophys. Res.* **91,** d378–d398.

Basaltic Volcanism Study Project 1981. *Basaltic Volcanism on the Terrestrial Planets*. Pergamon, Elmsford, NY.

CHYBA, C. F. 1987. The cometary contribution to the oceans of primitive Earth. *Nature*, in press.

DOHNANYI, J. S. 1972. Interplanetary objects in review: Statistics of their masses and dynamics. *Icarus* **17,** 1–48.

DONAHUE, T. M., J. H. HOFFMAN, R. R. HODGES, AND A. J. WATSON 1982. Venus was wet: A measurement of the ratio of deuterium to hydrogen. *Science* **216,** 630–633.

EBERHARDT, P., R. R. HODGES, D. KRAKOWSKY, J. J. BERTHELIER, W. SCHULTE, U. DOLDER, P. LAMMERZAHL, J. H. HOFFMAN, AND J. M. ILLIANO 1987. The D/H and $^{18}O/^{16}O$ isotope ratios in Comet Halley. *Abstr. Lunar Planet. Sci. Conf. XVIII*, 252–253.

ESPOSITO, L. W. 1984. Sulfur dioxide: Episodic injection shows evidence for active Venus volcanism. *Science* **223,** 1072–1074.

GREENBERG, R. 1987. *Planetary Accretion*. Paper given at the Conference on the Origin and Evolution of Planetary and Satellite Atmospheres, Tucson, March 10–14.

GRINSPOON, D. H., AND J. S. LEWIS 1986. Accretion of cometary volatiles on Venus. *Bull. Amer. Astron. Soc.* **18,** 824.

GRINSPOON, D. H., AND J. S. LEWIS 1987. Deuterium fractionation in the pre-solar nebula: Kinetic limitations on surface catalysis. *Icarus* **72,** 430–436.

HARTMANN, W. K. 1987. Moon origin: The impact-trigger hypothesis. In *Origin of the Moon* (W. K. Hartmann, R. J. Phillips, and C. D. Taylor, Eds.). Lunar and Planetary Institute.

HUGHES, D. W., AND P. A. DANIELS 1980. The magnitude distribution of comets. *Mon. Not. R. Astron. Soc.* **191,** 511–520.

HUNTEN, D. M. 1982. Thermal and nonthermal escape mechanisms for terrestrial bodies. *Planet. Space. Sci.* **30,** 773–783.

HUNTEN, D. M., T. DONAHUE, J. F. KASTING, AND J. C. G. WALKER 1987. Escape of atmospheres and loss of water. In *Planetary and Satellite Atmospheres: Origin and Evolution* (S. K. Atreya, J. B. Pollack, and M. S. Matthews, Eds.) Univ. of Arizona Press, Tucson, in press.

IP, W.-H. 1984. Condensation and agglomeration of cometary Ice: The HDO/H_2O ratio as tracer. In *Ices in the Solar System*, pp. 389–396. NATO ASI series, Reidel, Dordrecht.

IP, W.-H., AND J. A. FERNANDEZ 1987. *Exchange of Condensed Matter among the Outer Protoplanets and the Effect on Surface Impact and Atmospheric Accretion*. Paper given at the Conference on the Origin and Evolution of Planetary and Satellite Atmospheres, Tucson, March 10–14.

KASTING, J. F., AND J. B. POLLACK 1983. Loss of water from Venus. 1. Hydrodynamic Escape of Hydrogen. *Icarus* **53,** 479–508.

KASTING, J. F., J. B. POLLACK, AND T. P. ACKERMAN 1984. Response of Earth's atmosphere to increases in solar flux and implications for loss of water from Venus. *Icarus* **57,** 322–334.

KRASNOPOLSKY, V. A. 1985. Total injection of water vapor into the Venus atmosphere. *Icarus* **62,** 221–229.

KUMAR, S., D. M. HUNTEN, AND J. B. POLLACK 1983. Nonthermal escape of hydrogen and deuterium from Venus and implications for loss of water. *Icarus* **55,** 369–389.

KYTE, F. T., AND J. T. WASSON 1986. Accretion rate of extraterrestrial matter: Iridium deposited 33 to 67 million years ago. *Science* **232,** 1225–1229.

LEWIS, J. S. 1972. Low-temperature condensation from the solar nebula. *Icarus* **16,** 241–252.

LEWIS, J. S. 1974. Volatile element influx on Venus from cometary Impacts. *Earth Planet. Sci. Lett.* **22,** 239–244.

LEWIS, J. S., G. H. WATKINS, H. HARTMAN, AND R. G. PRINN 1982. Chemical consequences of major impact events on Earth. *Geol. Soc. Amer.* (Special Paper) **190,** 215.

MCELROY, M. B., M. J. PRATHER, AND J. M. RODRIGUEZ 1982. Escape of hydrogen from Venus. *Science* **215,** 1614.

NOZETTE, S., AND J. S. LEWIS (1982). Venus: Chemical weathering of igneous rocks and buffering of atmospheric composition. *Science* **216,** 181–183.

PEPIN, R. O. 1987. *Atmospheric Composition: Key Similarities and Differences*. Paper given at the Conference on the Origin and Evolution of Planetary and Satellite Atmospheres, Tucson, March 10–14.

SHOEMAKER, E. M., AND R. F. WOLFE 1982. Cratering time scales for the Galilean satellites. In *Satellites of Jupiter* (D. Morrison, Ed.). Univ. of Arizona Press, Tucson.

STROM, R. G. 1987. The Solar System cratering record: Voyager 2 results at Uranus and implications for the origin of impaction objects. *Icarus* **70,** 517–535.

VANYSEK, V., AND P. VANYSEK 1985. Prediction of deuterium abundance in comets. *Icarus* **61,** 57–59.

WALKER, J. C. G. 1986. Impact erosion of planetary atmospheres. *Icarus* **68,** 87–98.

WATKINS, G. H. 1983. *The Consequences of Cometary and Asteroidal Impacts on the Volatile Inventio-*

ries of the Terrestrial Planets. Ph.D. thesis, Massachusetts Institute of Technology.

WEISSMAN, P. R. 1982. Terrestrial impact rates for long and short period comets. *Geol. Sci. Amer.* (Special Paper) **190,** 15.

WEISSMAN, P. R. 1985. Cometary dynamics. *Space Sci. Rev.* **41,** 299–349.

WEISSMAN, P. R. 1986. The mass of the Oort cloud: A post-Halley reassessment. *Bull. Amer. Astron. Soc.* **18,** 799.

WETHERILL, G. W. 1985. Occurrence of giant impacts during the growth of the terrestrial planets. *Science* **228,** 877–879.

WETHERILL, G. W., AND E. M. SHOEMAKER 1982. Collision of astronomically observable bodies with the Earth. *Geol. Sci. Amer.* (Special Paper) **190,** 1.

WHIPPLE, F. L. 1984. Present status of the icy conglomerate model. In *Ices in the Solar System,* Vol. 156, p. 343. NATO ASI series, Reidel, Dordrecht.

YOUNG, L. D. G., A. T. YOUNG, AND L. V. ZASOVA 1984. A new interpretation of the Venera 11 spectra of Venus. I. The 0.94-micron water band. *Icarus* **60,** 138–151.

ZAHNLE, K. J., AND J. C. G. WALKER 1982. The evolution of solar ultraviolet luminosity. *Rev. Geophys. Space Phys.* **20,** 280.

ICARUS 88, 172–192 (1990)

The Composition and Origin of the C, P, and D Asteroids: Water as a Tracer of Thermal Evolution in the Outer Belt

THOMAS D. JONES[1]

NASA Lyndon B. Johnson Space Center, Houston, Texas 77058

LARRY A. LEBOFSKY[1] AND JOHN S. LEWIS

Lunar and Planetary Laboratory, Department of Planetary Sciences, University of Arizona, Tucson, Arizona 85721

AND

MARK S. MARLEY

245-3, NASA Ames Research Center, Moffett Field, California 94035

Received July 3, 1989; revised April 9, 1990

We present results of an extensive laboratory and telescopic investigation of H_2O distribution among the low-albedo, outer belt asteroids (2.5–5.2 AU). The water distribution was determined by surveying asteroids in that region for the 3-μm reflectance absorption of molecular H_2O and structural OH ions; the 3-μm band is the spectral signature of meteorite and asteroid hydrated silicates. The 19 asteroids observed in the survey, augmented by earlier reflectance data, yielded 3-μm band depth measurements that reflect the present outer belt H_2O distribution. Of the 32 C-class asteroids in this sample, 66% have hydrated silicate surfaces, evidence of a mild aqueous alteration episode early in solar system history. The C class is not a primitive asteroid group in the mineralogical sense, but its anhydrous members appear little altered, as do the P and D classes beyond 3.5 AU. In addition to this pronounced hydration state difference between Cs and the more distant Ps and Ds, hydrated silicate abundance declines gradually among the Cs from 2.5–3.5 AU. Coupled with the apparently anhydrous P and D surfaces, this points to an original outer belt asteroid composition of anhydrous silicates, water ice, and complex organic material. Early solar wind induction heating of proto-asteroids declined in intensity with heliocentric distance, and produced the observed radial decrease in hydrated silicate abundance. The mild thermal processing of outer belt asteroids is a continuation of the intense heating and differentiation that occurred sunward of 2.5 AU, and both events are consistent with the induction heating mechanism. Water ice may be preserved in the interiors of P and D objects, and in some larger Cs.

I. INTRODUCTION

Asteroids whose orbits have semimajor axes, **a**, ≥ 2.5 AU are predominantly members of the C, P, and D taxonomic classes. We refer to these as outer belt asteroids since these dark objects dominate the population from near the center of the main belt at 2.5 AU all the way to Jupiter's orbit at 5.2 AU. Spectral observations reveal that some have surfaces dominated by low-temperature, water-bearing minerals. We also infer a substantial organic component from

[1] Visiting Astronomer at the Infrared Telescope Facility which is operated by the University of Hawaii under contract to the National Aeronautics and Space Administration.

0019-1035/90 $3.00

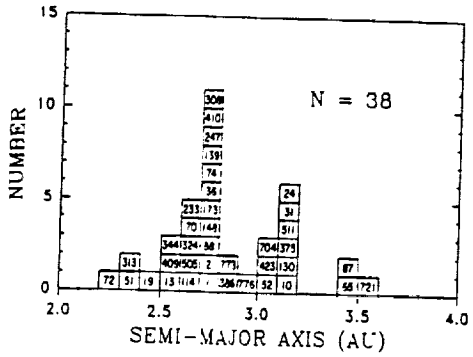

FIG. 1. Spatial distribution of the 38 low-albedo asteroids included in this 3-μm reflectance survey. The sample spans the mid- to outer portion of the main belt, a region dominated by dark asteroids.

th uniformly low albedos. Both traits are typical of relatively unaltered meteorites like the carbonaceous chondrites. If these dark asteroids do retain their original mineralogy, then they should yield direct information on both the solids produced in this portion of the solar nebula, and the early chemical and physical processes operating in the asteroid belt.

This paper discusses the results of a multiyear reflectance survey of low-albedo asteroids, using the 3-μm hydrated silicate absorption to define the H_2O distribution in the outer belt, (see Fig. 1). Hydrated silicates, which are thermodynamically stable at relatively low temperatures ($\leq$500 K), are tracers of early thermal activity on primitive asteroids. The detection of hydrated silicates (via 3-μm spectrometry) on individual asteroids, and their overall outer belt distribution should reveal important characteristics of heat sources that acted on those bodies just after formation.

Previous Work on Low-Albedo Asteroid Composition

This work is part of a larger effort to discover asteroid compositional trends and establish firm links between meteorite classes and likely parent bodies. Such compositional links are important: if remote sensing can reveal an asteroid's present surface mineralogy, via analogy to meteoritic "ground truth," one can establish a tentative "physico-chemical history" for that body (Gaffey 1987). Such an approach will be, of necessity, the only method of establishing individual compositions for large numbers of individual asteroids.

The asteroid belt displays a systematic variation of spectral class with heliocentric distance (Gradie and Tedesco 1982). The S class dominates the inner belt, the Cs the middle and outer part of the main belt, and the Ds the Trojan region. When linked to surface mineralogy by spectrophotometry, the class variation is clear evidence for overlapping "rings" of different asteroid composition at increasing distances from the Sun. If, on the basis of meteorite analogies, one equates the S, C, and D classes, respectively, with volatile-poor silicates, carbonaceous chondrite-like material, and volatile-rich "ultracarbonaceous" material (Gradie and Veverka 1980), the radial structure represents the mineralogical record of belt formation temperatures, or the effects of some radially varying thermal event early in solar system history, or both.

Because of their spectral similarity to the chemically primitive carbonaceous chondrites, the C asteroids have been regarded as substantially unaltered, volatile-rich bodies, darkened by opague organic material that dominates their reflectance properties (Chapman *et al.* 1975). In the outer belt, the P and D classes were thought to be even richer in organics and hydrated clay minerals, unaltered ultracarbonaceous objects formed at low temperatures in the solar nebula (Gradie and Veverka 1980). Mid-IR 3-μm observations of low-albedo asteroids confirmed the presence of surface hydrated silicates on several Cs (Lebofsky 1978). On the basis of this work, Feierberg *et al.* (1985a) suggested that the varying abundance of hydrated silicates among the Cs would be typical of a population of collisional fragments: the Cs were pieces of orginally "wet" (hydrated silicate) parent bod-

ies whose cores had been heated and dehydrated, then shattered. We set out to test this premise in 1986, but our telescopic observations and 3-μm reflectance measurements of carbonaceous chondrites led us to a quite different conclusion, that the variation in hydration state among the dark asteroids reflected different thermal histories controlled by composition and solar distance (Jones *et al.* 1987, 1988a,b, Jones 1988).

Rationale for 3-μm Asteroid Observations

Hydrated silicates are the dominant mineralogical component of carbonaceous chondrite matrix material, or CCMM (Wilkening 1978). Because CCMM is black, and comprises the bulk of CI and CM chondrite matrices, it is thought to be prevalent on the surfaces of primitive outer belt asteroids. Ordinary clays have strong H_2O absorption bands at 1.4 and 1.9 μm in the near-IR. Unfortunately, the reflectance properties of CCMM are dominated at visual/near-IR wavelengths by an opaque, complex organic material known as kerogen. The opaque kerogen lowers the visual albedo and reduces spectral contrast. Shortward of 2.5 μm, organic absorptions effectively overwhelm the relatively weak hydrated silicate overtone and combination bands. Despite the purported abundance of hydrated silicates in the outer belt, visual and near-IR observations have been incapable of identifying them. Only recently have high quality, high resolution reflectance spectra (0.5–0.9 μm) revealed weak Fe^{2+}–Fe^{3+} charge transfer features (indicating phyllosilicates) on several dark asteroids (Vilas and Gaffey 1989). The H_2O and structural hydroxyl absorptions in hydrated silicates at 1.4 and 1.9 μm remain invisible in dark asteroids, due to the presence of organics.

Fortunately, beyond 2.5 μm, the spectral signature of water is sufficiently strong that it dominates the spectrum and allows us to distinguish mineralogical differences typical of the major carbonaceous chondrite classes. The 3-μm hydrated silicate band is a combination of (1) a sharp 2.7-μm fea due to structural OH ions, and (2) a m broader 2.9-μm absorption due to interla H_2O molecules. The wing of the 2.9-μ band overlaps the centers of the 3.1-μm w ter ice feature and the 3.4-μm C-H stret vibration absorption. Since Lebofsky's in tial discovery of a 3-μm band on 1 Cer (Lebofsky 1978), this feature has been t target of increasingly sophisticated obs ing programs, both to determine the exte of hydrated silicate presence in the belt, an to characterize the surface mineralogy individual asteroids (Larson and Veede 1979, Lebofsky 1980, Lebofsky *et al.* 198 Feierberg *et al.* 1981, 1985a, Larson *et a* 1983).

Feierberg *et al.* (1985a) concluded th of the 10 largest C asteroids have a hydr silicate surface component. With hydra silicates apparently a common surface mate rial on the Cs, we decided to establish clearer picture of the H_2O distributior through a broader survey of low-albedo a teroids. In addition, use of a higher spectr resolution would pay dividends in greate characterization of the 3-μm band and poss ble detection of ice and organic absorptic

We obtained higher resolution and spe using the new Cooled Grating Array spe trometer (CGAS) at NASA's Infrared Tel scope Facility (IRTF). (See Tokunaga an Smith [1985] for details). Instead of the sir gle-detector CVF system, the CGAS uses linear 32-detector InSb array to sample th infrared spectrum simultaneously over span of nearly 0.6 μm. CGAS can prod a respectable spectrum faster and at thre times the resolution of a CVF system ($\Delta\lambda \approx 170$, vs 25–50). The improvement i resolution and SNR with CGAS is apparer in spectra of 1 Ceres taken with both instru ments (Figs. 2 and 3). CGAS is ideal for μm surveys of moderately bright asteroid scanning 0.6 μm at a glance, the array ca measure reflectance on both sides of the telluric "water gap," where radiation fro 2.5–2.8 μm is almost totally absorbed b atmospheric H_2O. With such a simultaneou

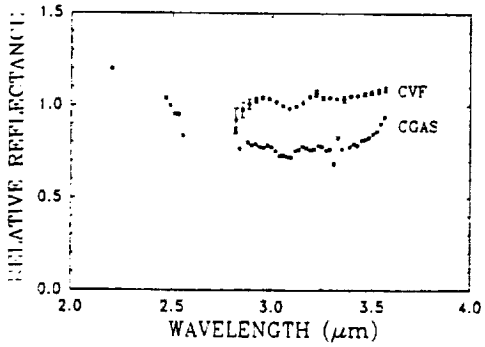

FIG. 2. Spectra of 1 Ceres using the circular variable filter (CVF) photometer and the Cooled Grating Array spectrometer (CGAS) at the NASA IRTF, Mauna Kea. The marked drop in reflectance from 2.2 to 2.8 μm is due to hydroxyl and water of hydration absorptions. Signal loss from 2.5 to 2.8 μm is caused by atmospheric H_2O. Note increase in resolution and spectral range with CGAS. (Spectra are normalized to 1.0 at 2.2 μm (CVF) and 2.5 μm (CGAS), then offset for clarity. CVF spectra have had a calculated thermal component removed. Error bars = 1 σ).

TABLE I

CVF OBSERVATION LOG: NASA INFRARED TELESCOPE FACILITY, MAUNA KEA, HAWAII

Instrument:	RC-2 photometer, CVF		
Observers:	M. A. Feierberg L. A. Lebofsky		
Date	Object	Spectral class[a]	Standard star
02/18/86	511 Davida	C	Hyd 64
	1 Ceres	G	35 Leo
02/19/86	511 Davida	C	Hyd 64
	1 Ceres	G	35 Leo
Instrument:	RC-1 photometer, CVF		
Observers:	L. A. Lebofsky T. D. Jones E. F. Tedesco		
12/08/86	19 Fortuna	G	Hyd 64
	10 Hygiea	C	Hyd 64
	704 Interamnia	F	35 Leo
12/09/86	114 Kassandra	T	Hyd 64
	10 Hygiea	C	Hyd 64
	704 Interamnia	F	35 Leo

[a] The C class includes subclasses B, F, G, and T.

measurement, CGAS yields a far more accurate 3-μm band depth measurement than a sequential CVF scan.

II. CVF and CGAS OBSERVATIONS—1986–88

The observing program goal was to collect 3-μm reflectance data for as large a group of low-albedo asteroids as possible over a span of approximately 2 years. We conducted all observations from the NASA IRTF, on the dates indicated in Tables I and II.

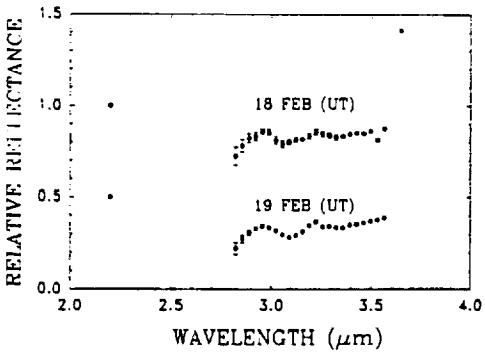

FIG. 3. CVF spectra of 1 Ceres (G class). Reflectance difference between 2.2 μm (K filter) and 2.9 μm is the basis for band depth calculations. The 3.1-μm absorption band is also seen in CGAS spectra, and is probably an H_2O frost feature (Lebofsky 1980).

Table III lists the low-albedo asteroids that have been observed to date at 3 μm. (Piscitelli *et al.* [1988] report CGAS 3-μm observations, but their 3.1–3.6 μm coverage does not include the entire water of hydration band.) With CGAS we were able to cover the brightest of the Cs (and its related subclasses) down to a visual magnitude $\approx$ 12. Unfortunately, members of the P and D classes are usually even fainter, and sky background saturation of the CGAS detectors prevented observations of these interesting groups. To increase the sample size and better characterize the hydrated silicate distribution, we added sensitive CVF observations by Lebofsky (1980) and Feierberg *et al.* (1985a,b).

The data reduction scheme is common to reflectance spectrophotometry (see Lebof-

TABLE II

CGAS OBSERVATION LOG: NASA INFRARED TELESCOPE FACILITY, MAUNA KEA, HAWAII

Date	Object	Spectral class	Standard star
Observers: T. D. Jones, L. A. Lebofsky			
04/21/87	532 Herculina	S	70 Vir
	1 Ceres	G	16 Cyg B
	511 Davida	C	70 Vir
	2 Pallas	B	λ Serp
04/24/87	5 Astraea	S	35 Leo
	511 Davida	C	70 Vir
	18 Melpomene	S	SAO 120107
	2 Pallas	B	SAO 65083
	1 Ceres	G	16 Cyg B
04/25/87	704 Interamnia	F	35 Leo
	16 Psyche	M	35 Leo
	511 Davida	C	70 Vir
	2 Pallas	B	SAO 65083
	1 Ceres	G	16 Cyg B
Observers: T. D. Jones, M. S. Marley			
10/01/87	92 Undina	M	SC 8167
	111 Ate	C	SC 8167
10/02/87	324 Bamberga	CP	Hyd 142
10/03/87	375 Ursula	C	51 Peg
	423 Diotima	C	SAO 147237
	51 Nemausa	CU	K Ceti
	52 Europa	CF	Hyd 142
	13 Egeria	G	Hyd 142
Observers: T. D. Jones, L. A. Lebofsky			
02/01/88	55 Pandora	M	Hyd 106
	13 Egeria	G	Hyd 106
	10 Hygiea	C	35 Leo
02/02/88	313 Chaldaea	C	Hyd 64
	130 Elektra	G	SAO 136389
	505 Cava	FC	35 Leo
02/03/88	55 Pandora	M	Hyd 64
	173 Ino	C	SAO 136389
	409 Aspasia	CX	70 Vir
02/04/88	88 Thisbe	CF	Hyd 64
	324 Bamberga	CP	Hyd 64

sky 1978, 1980, Chapman and Gaffey 1979, Feierberg *et al.* 1985a). We chose standard stars whose spectra were close to solar (Hardorp 1980, 1982): the ratio of asteroid reflectance to solar analog spectrum removes solar absorptions and displays only mineralogical features. The resulting spectra plot relative (i.e., scaled) reflectance vs wavelength; the reflectance is "relative" to that of the standard star, and normalized to 1.0 at 2.2 or 2.5 μm. Spectral quality depended mainly on intrinsic asteroid brightness and viewing geometry; objects near $M_v \approx 12$ proved to be difficult targets. For example, 13 Egeria produced a good spectrum in October 87 (Fig. 4), but by February 88 it had moved away from opposition, and 3-μm band depth measurements became impractical. Note the similar loss of quality for 324 Bamberga in Fig. 4.

The CVF error bars represent the standard deviation (σ) of the brightness at a given wavelength, propagated through the averaging of several complete CVF spectra on the same night. For the CGAS spectra, the 1-σ error bars represent the standard deviation of the mean detector voltage (analagous to brightness) at a given wavelength, similar to the CVF case.

A significant data reduction problem encountered at 3-μm is the removal of asteroid thermal flux. Beyond 3 μm, emitted thermal energy from the asteroid begins to rival reflected sunlight at the telescope. A "standard thermal model" developed by Lebofsky *et al.* (1986) yields an estimate of the emitted/reflected flux ratio at a given wavelength. The emitted flux for main-belt objects is negligible at 3 μm, contributes 5–10% of the signal at 3.4 μm, and dominates beyond 3.5 μm. Removal of the calculated thermal flux does a reasonable job of restoring the spectrum to a normalized reflectance value near 1.0 at 3.5 μm (similar to carbonaceous chondrite spectral behavior), and so we subtracted a calculated thermal component from all CVF spectra (Fig. 5). However, in the case of 511 Davida and 19 Fortuna, the model appears to overcompensate for thermal emission and unrealistically lowers the 3.4-μm reflectance (see Feierberg *et al.* 1985a). Most of the CGAS spectra were free from significant thermal effects at 3 μm, so we chose to leave the CGAS spectra *uncorrected*. (The problem is not severe for most objects in the outer belt, where a lower solar irradiance reduces overall thermal emission and shifts the peak radiation to longer wavelengths.) In the few cases where thermal contributions were important, we did correct the computed 3-μm band depth. To reiterate, the CVF spectra published

TABLE III

ASTEROIDS OBSERVED AT 3 μm

Object	a (AU)	Tholen class	Tedesco[a] class	H_2O	Band depth (%)	Source
1 Ceres	2.768	G	G	Yes	21 ± 1.3	1
2 Pallas	2.773	B	m	Yes	18 1.2	1
10 Hygiea	3.138	C	C	Yes	12 3.7	1
13 Egeria	2.576	G	G	Yes	40 15	1
19 Fortuna	2.442	G	—	Yes	25 6	1
24 Themis	3.129	C	—	Yes	4 ± 2	2
31 Euphrosyne	3.148	C	—	No	0 1	3
36 Atalante	2.749	C	—	Yes	14 1	3
51 Nemausa	2.366	CU	G	Yes	37 15	1
52 Europa	3.095	CF	C	No	0 6	1
65 Cybele	3.428	P	C	No	0 ± 1	3,4
70 Panopaea	2.614	C	C	Yes	35 12	4
72 Feronia	2.266	TDG	—	Yes	8 5	2,4
74 Galatea	2.781	C	—	No	2 5	3
87 Sylvia	3.483	P	PC	No	1 10	2
88 Thisbe	2.769	CF	—	No	0 ± 10	1,4
114 Kassandra	2.678	T	T	No	0 5	1,2
130 Elektra	3.109	G	G	Yes	22 13	1
139 Juewa	2.782	CP	—	No	0 2	3
148 Gallia	2.771	GU	r	No	0 9	1
173 Ino	2.745	C	C	Yes	0 ± 7	1
233 Asterope	2.660	T	T	No	0 2	2
247 Eukrate	2.742	CP	—	No	2 2	3
308 Polyxo	2.749	T	I	Yes	14 2	2
313 Chaldaea	2.376	C	C	Yes	22 15	1
324 Bamberga	2.685	CP	—	Yes	6 ± 1	3
344 Desiderata	2.591	C	C	Yes	18 4	3
375 Ursula	3.134	C	—	Yes	18 14	1
386 Siegena	2.894	C	C	Yes	23 2	3
409 Aspasia	2.577	CX	—	Yes	11 6	1
410 Chloria	2.724	C	C	Yes	24 ± 3	3
423 Diotima	3.069	C	C	No	0 60	1
505 Cava	2.685	FC	—	Yes	5 11	1
511 Davida	3.181	C	C	Yes	12 4	1,3
554 Peraga	2.374	FC	C	No	0	4
704 Interamnia	3.060	F	F	Yes	6 ± 4	1,2
721 Tabora	3.554	D	D	No	0 8	2
773 Irmintraud	2.857	D	D	No	0 6	2
776 Berbericia	2.934	C	—	Yes	23 2	3
			Controls			
4 Vesta	2.362	V	r	No	0 ± 1	4
5 Astraea	2.577	S	S	No	0 6	1
16 Psyche	2.922	M	M	No	2 4	1
18 Melpomene	2.296	S	S	No	0 6	1
55 Pandora	2.761	M	E	Yes	37 22	1
92 Undina	3.205	M	M	Yes	45 12	1
532 Herculina	2.774	S	S	No	0 2	1

Note. Source notes: (1) this work; (2) Feierberg *et al.* 1985b; (3) Feierberg *et al.* 1985a; (4) Lebofsky 1980.
[a] See Tedesco *et al.* 1989

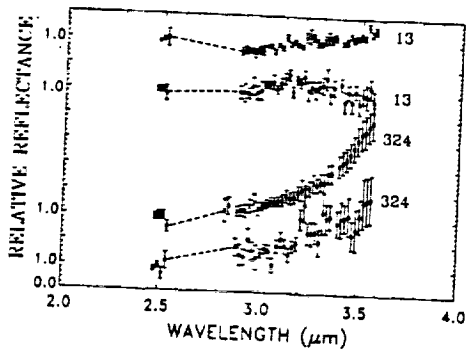

FIG. 4. CGAS spectra of 13 Egeria and 324 Bamberga, showing the deterioration in signal quality due to changes in observing geometry. Errors in band depth measurement become large, and in some cases only a qualitative determination of hydrated silicate presence is possible. Observation are dates listed in Table II.

here have a thermal component removed, the CGAS spectra do not, and the 3-μm band depths listed in Table III are corrected for thermal contributions where appropriate.

The 3-μm H_2O band is a combination of the 2.7-μm structural hydroxyl and 2.9-μm molecular H_2O absorptions. We see it in these spectra as a distinct reflectance drop from 2.5 to 2.9 μm (e.g., Fig. 2). Telluric water vapor obscures the signal from 2.5 to 2.8 μm. The CVF filters precluded coverage between 2.2 and 2.5 μm (Fig. 5), but carbonaceous meteorite spectra are generally flat in this region, so we assumed that the J (1.25 μm), H (1.65), and K (2.2 μm) CVF measurements (only K is shown) define a continuum whose peak reflectance corresponds to the 2.5-μm CGAS value. While most of the CVF spectra lack the S/N and/or resolution ($\lambda/\Delta\lambda \approx 50$) to reveal detailed absorptions, the broad 3-μm band lends itself to easy detection. We define the 3-μm band depth as

$$\text{CVF:} \quad \mathbf{d} = R_{2.2\,\mu m} - R_{2.9\,\mu m}$$
$$\text{CGAS:} \quad \mathbf{d} = R_{2.5\,\mu m} - R_{2.9\,\mu m},$$

where R is the reflectance at the specified wavelength.

In calculating **d**, we excluded data between 2.6 and 2.9 μm, since they are either noisy or unusable there due to telluric H_2O. The same water vapor also obscures the deepest portion of the intense 2.7-μm hydroxyl band; **d** thus underestimates the reflectance drop from 2.7 to 3.0 μm (i.e., the true band depth is $\geq$ **d**). Our calculated 3-μm band depths and associated errors (the latter based on the uncertainty in 2.9-μm reflectance data) appear in Table III.

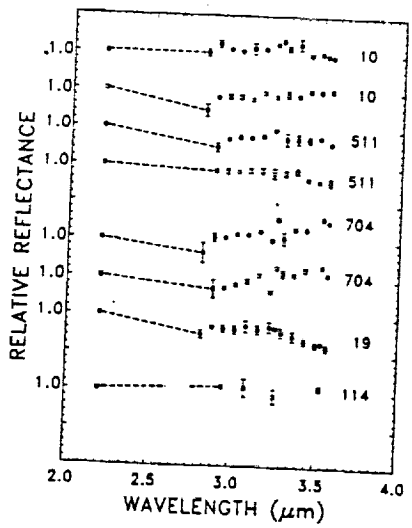

FIG. 5. Circular variable filter spectra of low albedo asteroids. The thermal contribution to the flux at longer wavelengths has been modeled and removed. Gap from 2.5 to 2.8 μm is due to telluric water absorption. See Table I for observation dates.

Selected Asteroid Spectra

The bright asteroids 1 Ceres and 2 Pallas yielded the most detailed 3-μm spectra (Figs. 6 and 7).

1 Ceres (Fig. 6) displays what may be a distinct, optically thin, 3.1-μm water ice absorption superimposed on the long-wavelength wing of the 3-μm band (Lebofsky *et al.* 1981). This feature persists from night to night, but we saw no real structure corresponding to the 3.4-μm organic (C-H stretch) absorption. The declining continuum at 2.5 μm, not seen in carbonaceous chondrite spectra, is peculiar to Ceres. The 3-μm band depth **d** is 0.21 ($\pm$0.01).

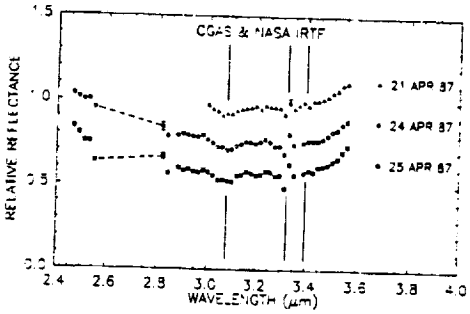

FIG. 6. Cooled Grating Array spectrometer spectra of 1 Ceres taken over several nights in April 1987. Note the prominent 2.5–3.0 μm absorption, probable ice band at 3.1 μm, and the methane artifact at 3.35 μm. We observed no 3.4-μm C-H stretch absorptions. On 21 April we were unable to measure the 2.5-μm continuum. (All CGAS spectra are normalized to 1.0 at 2.5-μm, then offset for clarity. Thermal emission is included, with error bars = 1 σ).

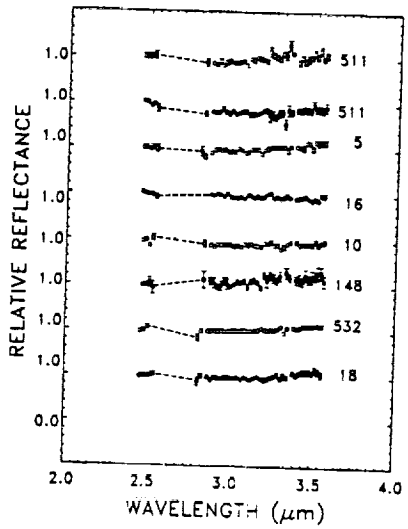

FIG. 8. Seven CGAS spectra of low-albedo asteroids. These asteroids display little or no 3-μm reflectance drop; their surfaces are anhydrous. See Table II for observation dates.

Ceres spectra taken over several nights show remarkable consistency. Rotational variations in the Ceres and Pallas spectra are not significant, because on a given night we averaged spectra over at least one-third of a complete asteroid rotation. (Ceres' period: 9.08 hr; Pallas: 7.88 hr, from Burns and Tedesco [1979]).

Several features in the Ceres CGAS spectra are common to other asteroids:

(1) 3.3-μm methane artifact. Successful averaging of many spectra taken over a wide range of airmass requires an accurate extinction correction for both standard star and asteroid. Limits on the precision of this airmass compensation prevented complete removal of the deep 3.3-μm terrestrial methane absorption, producing a corresponding spike in the asteroid reflectance spectrum.

(2) Thermal emission. Thermal emission is apparent in Ceres CGAS spectra at and beyond 3.5 μm (especially compared with corrected CVF spectra). This thermal component is noticeable to varying degree in other CGAS spectra.

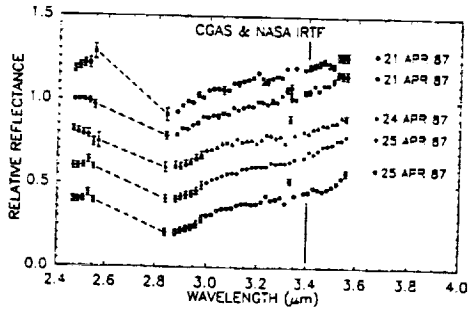

FIG. 7. Cooled Grating Array spectrometer spectra of 2 Pallas taken over several nights in April 1987. Pallas shows a prominent 2.5–3.0 μm absorption, but no ice or organic features.

2 Pallas spectra show similar repeatability (Fig. 7). The spectral shape is similar to that of CM chondrites. The 2.5-μm continuum is more nearly level, no 3.1-μm ice feature is present, and no organic feature is evident at 3.4 μm. Pallas' H_2O band depth **d** is 0.18 ($\pm$0.01).

The high quality Ceres and Pallas CGAS spectra are directly comparable to carbonaceous chondrite reflectance data (Jones 1988; Jones *et al.* 1991, in preparation). Ceres' 3-μm spectrum is unlike that of any carbonaceous chondrite, and only distantly

resembles the CI chondrites. Pallas' spectrum is quite similar to those of CM chondrites, but its H_2O band is not as deep (**d** = 0.18 vs 0.35 for CMs). A possible explanation is that Pallas' surface has a significant anhydrous component mixed with CM-like hydrated silicates (Larson *et al.* 1983, Jones 1988, Jones *et al.* 1990).

Other Asteroids

We observed a number of non-C asteroids to verify that 3-μm bands are not typical of other, anhydrous classes of asteroids. For example, 5 Astraea and 16 Psyche (representing classes S and M, respectively) show no 3-μm reflectance drop (Fig. 8). However, two of the "experimental control" asteroids, 55 Pandora and 92 Undina, did have definite 3-μm absorptions (Fig. 9). Both are M-class, supposedly anhydrous metallic asteroids. With featureless near-IR spectra, neither object was well-categorized under the "TRIAD" Tucson Revised Index of Asteroid Data system (Zellner 1979). The ambiguity arose because visual/near-IR spectra from the C, M, E, and U classes cannot be discriminated without albedo data. Tholen (1984) reclassified both objects as M on the basis of their relatively high albedos. However, the IRAS albedos for 55 and 92 (0.32 and 0.20, respectively) were dependent on assumptions in the thermal model about the surface thermal inertia. If these objects have rocky rather than the assumed dusty surfaces, the resulting higher thermal inertia would lower the emitted thermal flux and the calculated albedo in turn. A lower albedo would be consistent with the observed 3-μm absorptions, more typical of C asteroids. Interestingly, a Soviet polarimetry study of M-class asteroids found anomalous polarization properties for both 55 and 92, and concluded that their surfaces were somehow atypical and/or had a significant silicate component (Lupishko and Belskaya 1989). From our observations, those silicates present are certainly hydrated.

We note here that in our examination of individual asteroid spectra (Figs. 6–12) we found no trace of any 3.4-μm organic ab-

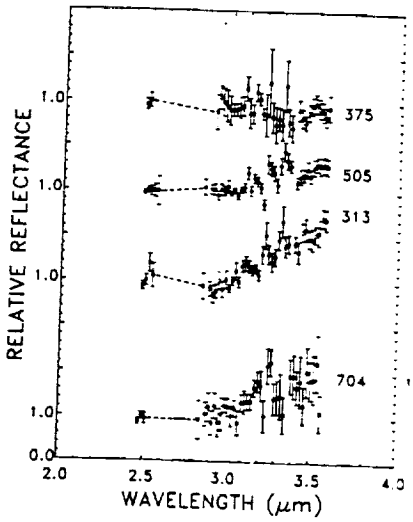

FIG. 10. CGAS spectra of four low-albedo asteroids from 1987 to 1988. See Table II for observation dates. The thermal emission and noisy spectra make band depth estimates uncertain, but determination of hydrated silicate presence is still possible.

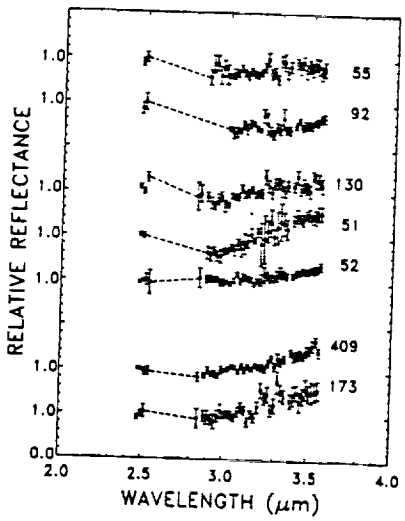

FIG. 9. CGAS spectra of seven low-albedo asteroids, displaying 3-μm absorptions of varying strength. 55 Pandora and 92 Undina are M-class objects that nevertheless have prominent hydrated silicate features. See Table II for observation dates.

sorption. We are thus unable to confirm the direct detection of organic kerogen on any asteroid (Cruikshank and Brown 1987).

III. HYDRATED SILICATE DISTRIBUTION IN THE ASTEROID BELT

We consider a sample of 38 3-μm spectra from low-albedo asteroids, derived from CVF, CGAS, and earlier spectrophotometric data (Lebofsky 1980, Feierberg *et al.* 1985a,b). The measured 3-μm band depths, when compared to asteroid physical and orbital characteristics, offer new insight into the original H_2O distribution in the outer belt.

First, we examined the relationship between asteroid class and the presence of a 3-μm absorption. The sample includes all low-albedo classes: C, P, D, (and the C subclasses G, T, F, and B). Overall, 66% of the C and C subclass objects show a 3-μm absorption diagnostic of hydrated silicates (Fig. 13). The percentage differs for each class (C—68%, G—80%, T—50%, F—66%, and B—100%), but clearly a majority of Cs have hydrated silicate surface components. By contrast, of the seven Ps and Ds in the sample, only one shows a 3-μm band, though 324 Bamberga's feature is very weak. Recent observations by Lebofsky *et al.* (1990) reinforce this contrast: of an additional P and two Ds observed in 1988, none exhibited a 3-μm band. To repeat, only 1 of 10 Ps and Ds observed to date is hydrated. We conclude that low-albedo asteroids fall into two predominant groups, characterized by different hydration states: the carbonaceous chondrite-like Cs, and the ultracarbonaceous Ps and Ds.

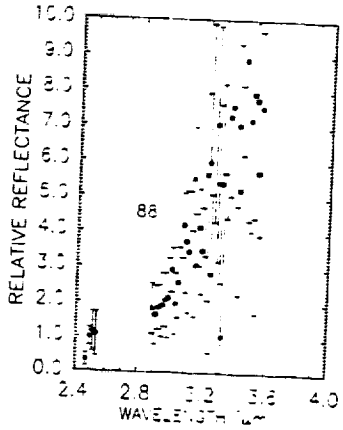

FIG. 12. CGAS spectrum of 88 Thisbe (CF), from Feb. 1988. The rapidly rising thermal component at and beyond 3 μm precludes searches for absorption features other than water of hydration. Removal of the modeled thermal component revealed Thisbe as an anhydrous asteroid.

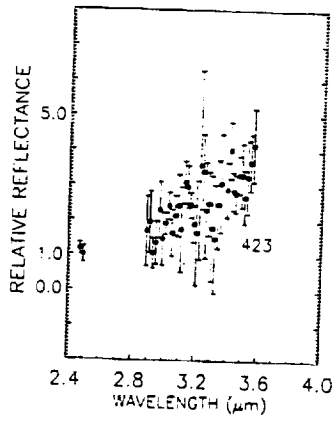

FIG. 11. CGAS spectrum of 423 Diotima (C class), from Oct. 1987. The thermal contribution to the flux at these wavelengths is quite strong, but removal of that component at 2.9 μm still permits a qualitative search for the 3-μm band. Diotoma does not appear to be hydrated.

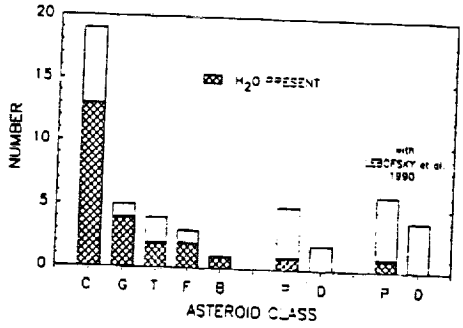

FIG. 13. Observed distribution of the 3-μm hydrated silicate band over the various low-albedo asteroid classes. About two-thirds of the C and C subclasses are hydrated, while the P and D classes are nearly anhydrous. If the Lebofsky *et al.* (1990) observations are included, the contrast is even more striking.

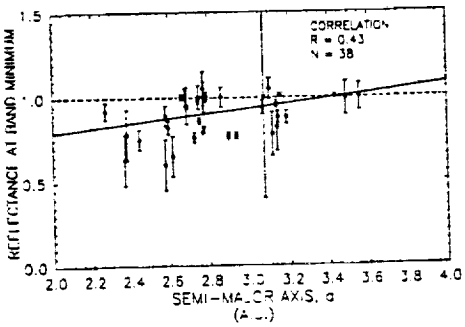

FIG. 14. Observed low-albedo asteroid reflectance at 3-μm vs solar distance. There is a highly significant statistical correlation between increasing reflectance and increasing distance, suggesting that hydrated silicates decline in abundance with distance. Data are from this work, Lebofsky (1980), and Feierberg *et al.* (1985a,b).

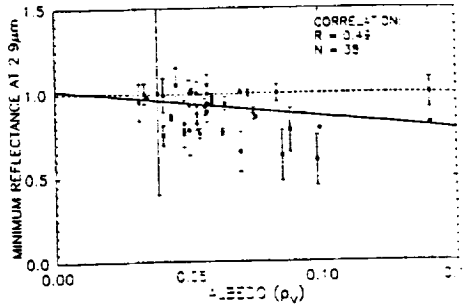

FIG. 15. Observed low-albedo asteroid reflectance at 3-μm vs geometric albedo. Reflectance declines with increasing albedo. The correlation coefficient, R = 0.49, indicates that the positive statistical correlation between albedo and hydrated silicate abundance is highly significant.

A quantitative measure of this class difference can be seen in a comparison of each asteroid's 2.9-μm reflectance value level (or band depth **d**) to orbital semi-major axis (solar distance). Because most Ps and Ds reside beyond 3 AU in the outer belt, a class-wide absence of hydrated silicates there would be recognizable in the form of higher 2.9-μm reflectance values. Figure 14 confirms this trend: in our sample, there are no hydrated asteroids beyond 3.4 AU (the latest 3 Ps and Ds from Lebofsky *et al.* [1990] are all anhydrous and orbit beyond 3.9 AU).

A weighted linear least-squares fit to the sample (Fig. 14) produces a positive slope and a correlation coefficient of $R = 0.43$. For $N = 38$, the probability that an uncorrelated set of data points would yield $R = 0.43$ is <1%; the probability that the data are correlated is >99%. These data indicate a statistically significant decline in hydrated silicates (and surface H_2O content) outward from the C portion of the belt (Jones *et al.* 1988b). They also imply that the supposedly volatile-rich Ps and Ds are the most water-poor objects (spectrally) in the outer belt!

The relationship between solar distance and 2.9-μm reflectance does not appear to be a simple linear one (Fig. 14). The relatively large errors in the reflectance data combine to produce such a poor χ^2 val... that we use the linear model here only to show correlation. A more complicated process must have been at work to create the observed H_2O distribution.

Plots of 3-μm reflectance vs diameter, albedo, eccentricity **e**, and inclination **i** are shown in Figs. 15–18. Band depth appear unrelated to diameter, **e**, and **i**, argui against a collisional origin for the prese population of anhydrous and hydrated aste oids. If, as Feierberg *et al.* (1985a) sug gested, collisions had shattered mildl heated asteroids into fragments of hydrate

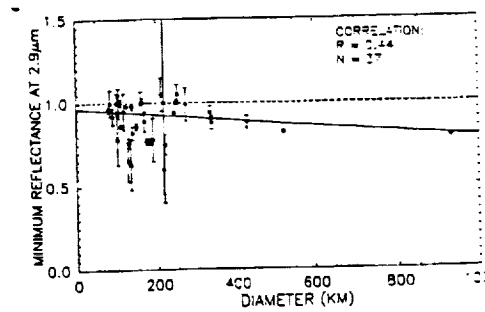

FIG. 16. Observed low-albedo asteroid reflectanc 3-μm vs diameter. Reflectance and diameter also pear strongly correlated, but the linear fit is hea influenced by Pallas and Ceres at diameters >500 k No clear relationship between diameter and hydra silicate abundance can be demonstrated from th data.

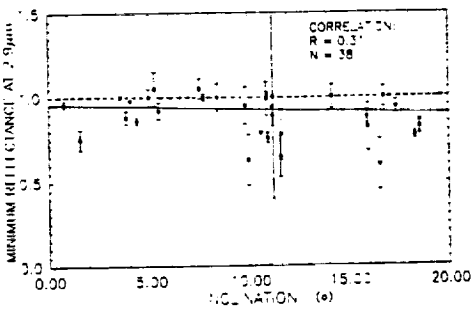

FIG. 17. Observed low-albedo asteroid reflectance at 3-μm vs orbital inclination. The parameters appear statistically uncorrelated. Higher inclinations may be a result of asteroid collisions: the data suggest that collisions are unimportant in controlling hydrated silicate abundance.

mantle and anhydrous core remnants (dehydrated from an original phyllosilicate composition), then the wetter asteroids (the proto-asteroid outer layers) should be in generally more inclined or eccentric orbits. Such a trend is not evident. Further, one anhydrous asteroid, 52 Europa, is 312 km in diameter; it is difficult to imagine the total dehydration of such a large core and the subsequent loss by impact of all hydrated surface components, while still retaining the typical C-class spectrum and low albedo. The hydration state of the outer belt must be largely a function of original composition and thermal evolution rather than collisional history.

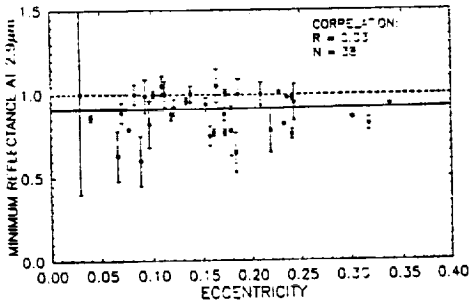

FIG. 18. Observed low-albedo asteroid reflectance at 3-μm vs orbital eccentricity. As in Fig. 17, there is no correlation. Higher eccentricities may be due to collisions as well as gravitational perturbations: these data suggest that collisional history does not control hydrated silicate abundance.

An apparent inverse relationship between 2.9-μm reflectance and albedo supports this conclusion (Fig. 15). Here the probability that these two parameters are correlated ($R = 0.49$, $N = 38$) is $\geq 99\%$. Deeper H_2O bands tend to occur on objects with higher albedo, perhaps due to aqueous emplacement of hydrated salts, carbonates, or sulfates, all light-colored meteoritic phases.

The 3-μm reflectance data help to integrate the low-albedo asteroids into the context of the entire asteroid belt: beyond the differentiated inner belt asteroids (Gaffey 1988), most of the Cs display traces of moderate internal heating and subsequent aqueous alteration. The Ps and Ds, however, despite a supposedly volatile-rich heritage, display no surface H_2O (Lebofsky *et al.* 1990). Our observations support a model for the formation of low-albedo asteroids that explains this seeming paradox.

IV. ORIGINAL OUTER BELT ASTEROID COMPOSITION

The decline in hydrated silicate abundance with increasing heliocentric distance runs counter to the expected volatile enhancement in the "primitive" P and D classes. This paradox must be considered in the context of the original composition these objects probably acquired during accretion from the solar nebula.

A starting point (and only that) for estimating the probable raw materials available for asteroid accretion can be found in the chemical equilibrium condensation models of Lewis (1972) and Grossman and Larimer (1974). In these models proto-asteroids accrete from solid grains condensed under the prevailing nebular conditions in the vicinity of the asteroid belt. In an ideal solar nebula model, condensed solids at all distances equilibrate with the surrounding gas, with conditions near the Sun favoring the closest approach to chemical equilibrium between the two phases. Abundant meteorite evidence suggests that thermodynamic equilib-

rium was not attained in the meteorite (and presumably asteroid) formation zone. (Wood and Chang 1985).

We are interested in particular in the effects of disequilibrium on the production of asteroidal hydrated silicates. These low-temperature minerals are expected products of equilibrium nebular condensation, and are stable against water loss under asteroidal surface conditions. However, the idea of hydrated silicates as "primordial" nebular material has fallen from favor. The present consensus among meteoriticists is that hydrated silicates are of secondary origin (Kerridge and Bunch 1979, McSween 1979, Bunch and Chang 1980, Fredriksson and Kerridge 1988). In addition, there is strong theoretical evidence arguing against a nebular origin for hydrated silicates (Lewis and Prinn 1984, Prinn and Fegley 1987, 1988, Fegley 1988).

The fundamental implication for our work is that asteroidal hydrated silicates, like those in meteorites, must also be alteration products. Two corollaries are readily apparent: (1) There was sufficient water available on parent asteroids to produce hydrated silicates abundant enough to survive impact processing and be detectable today; and (2) an early heat source must have warmed these objects enough to drive an aqueous alteration episode.

Ice as the Asteroidal Water Component

Without hydrated silicates as an accretion feedstock, the C asteroids (and the CI and CM parent bodies) must have originally acquired their present H_2O in the form of ice. Bunch and Chang (1980) discussed the possibility of ice as the original asteroidal water reservoir, but did not propose an explicit origin (see also Nozette and Wilkening 1982). Ice condensation at 3 AU is not an absolute requirement for supplying the C region with water; there was undoubtedly some inward transport of material from Jupiter (5.2 AU) during its formation. (Ice must have condensed at Jupiter's distance to have survived to the present on the Galilean satellites [Lebofsky 1980]). It may have migrated inward via turbulent transport of dust and ice grains (Prinn 1989), scattering of icy Jupiter planetesimals, or via extension of the outer belt accretion (or "feeding") zone toward Jupiter, where ice had already condensed. If accretion were rapid and the material sufficiently icy, significant quantities of ice could be incorporated into early asteroids and protected from sublimation.

Surface ices on asteroids do not have a long life expectancy (Lebofsky 1980). However, any ice incorporated into asteroid interiors during accretion should have survived for the few million years required (at most) for aqueous alteration (DuFresne and Anders 1962, Kerridge and Bunch 1979). Water ice is present today on at least one asteroid—1 Ceres (Lebofsky *et al.* 1981, this work). Given the high equilibrium temperatures of low-albedo asteroids at 3–4 AU (~200 K), only large ones like Ceres, with a generous H_2O inventory, may be able to support surface ices. But near-surface ice may persist if initial sublimation leaves behind a lag deposit similar to those proposed for comets (Brin and Mendis 1979, Houpis and Mendis 1981, Fanale and Salvail 1984). Such a lag deposit would probably make even near-surface ices spectrally invisible.

Low-Albedo Asteroid Composition

Our 3-μm reflectance data draw a picture of hydrated silicate abundance that declines outward through the C, P, and D classes (Jones *et al.* 1988a,b, Jones 1988, this work). Hydrated silicates are conspicuous by their absence on the few observed Ps and Ds (Lebofsky *et al.* 1990). The observations contradict the proposed trend toward primitive compositions (H_2O and organics) in the outer belt (Gradie and Veverka 1980). We resolve this apparent dilemma by proposing that *the hydrated silicate abundance does not reflect a proto-asteroid's original water content, but only the extent to which aqueous alteration occurred there*. The original outer belt asteroid composition was necessarily a mixture of anhydrous silicates, wa-

ter ice, and relic interstellar organic material. The absence of hydrated silicates (on a ', P, or D object) implies either (1) a volatile-poor parent body, or (2) early interior temperatures and pressures too low to support an alteration episode. In the latter case the asteroidal silicates would retain their original anhydrous character, resembling the olivine-rich matrix of the CV chondrites (McSween 1987).

V. NEW SUPPORT FOR ASTEROID ELECTRICAL INDUCTION HEATING

The observed decline in hydrated silicates with heliocentric distance over some 3 AU is inconsistent with ^{26}Al heating. Instead, the range of heating events we observe in the belt seems to fit much more closely with a wide-ranging episode of solar wind induction heating (Sonett *et al.* 1968, Lebofsky *et al.* 1989, Herbert 1989).

The C asteroids as a class do not represent an unaltered mineralogical suite: some two-thirds of our sample have experienced secondary aqueous alteration to some degree. While hydrated and (apparently) anhydrous asteroids are well-mixed inside ≈3 AU, the decline in hydrated silicate abundance with distance seems to be real. Oxygen isotopic evidence from meteoritic hydrated silicates suggests parent bodies achieved temperatures of 0–20°C (Clayton and Mayeda 1984). If we assume hydrated Cs once experienced interior temperatures at least that high, then the hydrated silicate distribution pictured in Fig. 14 corresponds to a crude 300 K isotherm. For example, the fraction of asteroids heated to that temperature is close to unity at 2.5 AU, and near zero in the P region near 3.5 AU. This profile strongly echoes the apparent decline in differentiated asteroids from 2 to 4 AU (Gaffey 1988). The radial dependence common to Gaffey's igneous "isotherm" and our aqueous alteration profile in the C region leave little doubt that the heating intensity also declined with solar distance.

That dependence is a key argument against the action of ^{26}Al as a heat source in the outer belt. The decay of this short-lived radionuclide has been proposed as the cause of both igneous differentiation and mild aqueous alteration on the meteorite parent bodies (Lee 1979). There is no doubt as to its heating potential. For example, if ^{26}Al was present at the concentrations implied by ^{26}Mg excesses in the Allende CV chondrite, it would have melted bodies of radius $\geq \sim 10$ km (Lebofksy *et al.* 1989). That efficiency is a drawback among primitive, low-albedo asteroids, however. Homogeneous distribution of ^{26}Al from 2 to 5 AU would have led to wholesale melting of asteroids with no radial dependence. Both the succession of outer belt asteroid classes (C–P–D) and the decline in hydrated silicate distribution prove that this did not occur.

It is a well-known failing of ^{26}Al that it is most efficient at melting large bodies, yet the two biggest asteroids, Ceres and Pallas, show no evidence of anything beyond low-temperature aqueous alteration. The observed hydrated silicate distribution (Fig. 14) requires even more capricious action by ^{26}Al, because at small scales in the C region both heated and apparently unaltered asteroids are thoroughly mixed. ^{26}Al's heating characteristics are inconsistent with both a general decline in aqueous alteration over a 3 AU span *and* starkly different thermal outcomes on a local scale.

Electrical induction heating (wherein a vigorous early solar wind deposits kinetic energy in a planetary interior via resistance to induced currents) seems to explain both the overall belt compositional structure and our 3-μm hydrated silicate data. Applied to small bodies, this mechanism can account for the igneous differentiation of inner belt asteroids, the apparent decline in hydrated silicate abundance with distance, and the variety of C-class hydration states (Lebofsky *et al.* 1989, Jones *et al.* 1988b, Herbert 1989).

Asteroid induction heating is particularly adept at explaining the production of hydrated and anhydrous surfaces over short distances in the belt. For example, anhy-

TABLE IV

HEAT SOURCE COMPARISON

Observed characteristics	^{26}Al heating	Induction heating
Belt-wide variation (melted vs unaltered)	Yes	Yes
Intensity decline with distance	?	Yes
Small-scale heterogeneity (0.1 AU)	?	Yes
Ineffective at large diameters	No	Yes

drous C asteroid 52 Europa (r = 156 km, albedo < 0.06) has a mean solar distance of 3.1 AU, greater than that of many hydrated asteroids, so it probably formed with at least as much ice as its sunward companions. Collisions were probably incapable of dehydrating 52 Europa while leaving it with a typical C albedo and spectrum. The present anhydrous surface must be a consequence of minimal heating. Could a relatively large asteroid like 52 Europa avoid heating and aqueous alteration, unlike many neighboring Cs?

Such different thermal outcomes are plausible, and stem from the known range of bulk compositions among the carbonaceous chondrites. While similar in bulk chemistry, their measured electrical conductivities span over 6 orders of magnitude (Brecher *et al.* 1975). Similar variation among the C asteroid precursors would have left them wildly different in their susceptibility to electrical induction heating. Some bodies would have been warmed easily, while slight compositional variations would have left a neighboring object cold. Such selectivity would explain qualitatively the variety of hydration states within the C region of the belt. The more general decline in hydrated silicate abundance was probably caused more simply by the reduced intensity of induction heating farther from the Sun.

We compare ^{26}Al and induction heating as suitable asteroid heat sources in Table IV. One can concede that ^{26}Al may have b more abundant in one region of the aster belt, causing widespread heating over, s 1 AU. But it is hard to see how ^{26}Al co produce such different thermal outcon over <0.1 AU (Fig. 14), or cause a grad decline in heating intensity with distan Moreover, ^{26}Al should be most effectiv larger asteroid diameters, a prediction supported by our 3-μm observations (drated silicate abundance is not stron correlated with diameter; Fig. 16). In c trast, electrical induction heating satisfie of the observed characteristics of the m to outer belt heat source (Bell 1986, Jo 1988).

VI. OUTER BELT ASTEROID ORIGIN AND EVOLUTION

Our spectra of outer belt asteroids consistent with their early accretion fr planetesimals made of anhydrous silicat water ice, and organic material. The prop tions of those ingredients varied with he centric distance, with ice and organics m plentiful farther from the Sun. Only the dial dependence of the early induction h ing episode(s) drove the C, P, and D clas down different evolutionary paths: the m erately heated Cs lost nearly all their wa ice, the meltwater supporting the con sion of surface minerals into hydrated s cates. To be complete, our scenario m also explain the anhydrous surfaces of supposedly volatile-rich P and D asteroi which do not exhibit a 3-μm H_2O absorpt (Lebofsky *et al.* 1990).

Why Do the Ps and Ds Appear Dry?

Scenarios that propose mineralogical teration of the Ps and Ds to produce an drous surfaces do not square well with av able evidence. Heating intense enough devolatilize a hydrated silicate object rai a host of objections: externally driven de dration of just the surface would req both an improbable original composit (phyllosilicates) and, because surface la cool most efficiently, an intense heat sou

Neither condition is consistent with the mild modification we see among the Cs. Dehydration by a strong *interior* heat source is even more unlikely, given the great heat sink provided by H_2O and other volatiles (Lewis and Prinn 1984); such a thorough outgassing would also result in extensive spectral and albedo changes. The possibility that organic kerogen is masking the 3-μm H_2O absorption has been proposed, but laboratory results show that suppressing such a strong feature is difficult: adding organic material lowers the albedo to some limiting value ($\approx$ 0.04), but the water band remains visible (Jones 1988, Jones *et al.* 1989, 1991, in preparation). For example, the 3-μm absorption is quite strong in spectra of CI and CM chondrites, despite the intimate mixing of hydrated silicates and organics in the fine-grained matrix. The Ps and Ds must have truly anhydrous surfaces.

Lebofsky *et al.* (1990) specifically discuss the absence of 3-μm features among the Ps and Ds, but a moment spent placing these objects in the context of the other low-albedo asteroids is worthwhile. The most reasonable explanation for the missing H_2O band is incorporation of water in the form of ice (Bunch and Chang 1980). The proto-Ps and Ds may have been loose agglomerations of ice and anhydrous silicates, whose outer layers quickly lost their ice to sublimation or gentle solar insolation, while their interiors never achieved temperatures high enough to drive H_2O vapor or fluid to the surface (Fig. 19). Left unscathed by electrical induction heating in the outer belt, the Ps and Ds lost their near-surface ice to sublimation over billions of years of exposure to vacuum and impacts. A lag deposit of anhydrous silicates and carbonaceous material blanketing the surface, unaltered by liquid water, would explain the lack of a 3-μm band, the low albedos, and reddish near-IR spectra reminiscent of comet nuclei (Hartmann *et al.* 1987). Spectrally, this lag deposit is organic-rich, but H_2O-poor. No observational evidence would preclude the Ps and Ds from retaining some interior ice;

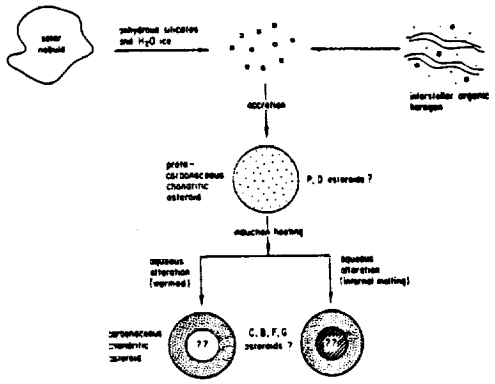

FIG. 19. Proposed scenario for producing low-albedo asteroids. Accretion of ice and anhydrous silicates from the solar nebula, combined with relic interstellar organic kerogen, formed very dark, volatile-rich asteroids, of which the Ps and Ds may be representative. Selective induction heating (dependent on solar distance, electrical conductivity) produces aqueous alteration at the surface and perhaps even melting in the interior, giving rise to the carbonaceous chondrite parent bodies and the present C class. Some Cs are unaffected by heating and may preserve interior ices, along with the Ps and Ds. The P and D classes should preserve nearly unaltered nebular solids and volatiles.

these asteroids would resemble comets in some aspects of structure and composition (Hartmann *et al.* 1987). Judging from the ice/rock ratios of the Galilean satellites, the D asteroids (Trojans in particular) may have had a substantial ($\approx$ 50%) ice component, blurring the distinction between outer belt asteroids and comets.

The Outer Belt Imaged at 3 μm

Our 3-μm reflectance data suggest the following interpretation of the outer asteroid belt (Fig. 20). The proto-asteroids beyond 2.5 AU were composed originally of anhydrous silicates, H_2O ice, and relic interstellar organic material. Electrical induction heating differentiated the inner part of the belt (inside 2.5 AU), while the C region was subjected to mild aqueous alteration. Beyond 3.5 AU, induction heating was largely ineffective, leaving the Ps and Ds unaltered. Those asteroids are the best candidates for preservation of the "primitive" belt composition, including volatiles and the original

anhydrous silicate mineralogy. At the top of Fig. 20 we show how the percentage of "melted" asteroids (differentiated S types) declines with heliocentric distance, declining to near zero beyond 3.5 AU (Gaffey 1988). We show qualitatively how the percentage of aqueously altered Cs also diminishes markedly with distance past 3 AU. Together with Gaffey's 1988 S asteroid work, our 3-μm hydrated silicate observations of low-albedo asteroids strongly support Bell's (1986) explanation for the present radial structure of the belt.

Primitive Asteroids and Carbonaceous Chondrites

The P and D asteroids should represent the belt's least altered mineral assemblages. Meteorites appear not to have sampled the Ps and Ds, but McSween (1987) proposes that the olivine-rich, relatively unaltered CV chondrite matrices are suitable precursors for the hydrated CI/CM chondrites; the same CV material is a good candidate for the P and D anhydrous silicate component as well. Across a span of 2 AU in the belt, we would expect a range of primordial asteroid compositions, with anhydrous Cs, Ps, and Ds all preserving their original mineralogy. We note that Bell *et al.* (1988) nominated 221 Eos (C/S class) as the CV/CO parent body. Its hydration state is unknown, but Eos' semi-major axis ($\approx$ 3 AU) would be consistent with a low-hydrated silicate abundance and an anhydrous, olivine-rich surface.

In contrast, the hydrated C, B, F, G, and T asteroids represent proto-asteroidal material modified by mild induction heating. These classes probably include the parent bodies of the CI and CM chondrites.

Our 3-μm data fit very well into Bell's interpretive framework for the mineralogical evolution of the entire asteroid belt (Bell 1986, Bell *et al.* 1988). He proposed three "superclasses" that relate taxonomy to the observed radial compositional structure. The superclasses (igneous, metamorphic, and primitive) represent the effects of the heliocentrically varying electroinductive heating episode. Igneous types dominate the belt sunward of 2.7 AU, the metamorphic group occupies a narrow zone centered around 3.2 AU, and the primitive class dominates outside 3.4 AU.

We would modify Bell's framework only by noting that P and D mineralogy is definitely not dominated by "clays" (a common assumption prior to the 3-μm survey) and that the Cs are not entirely a primitive class. They *are* chemically primitive, but that label perpetuates the image of carbonaceous chondrites as totally unaltered, when we know that their hydrated silicate mineralogy is secondary.

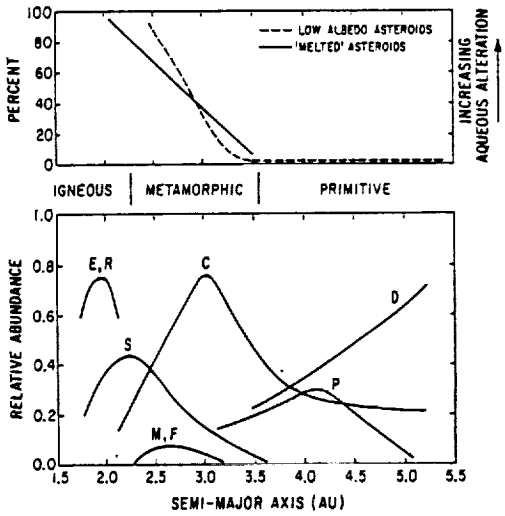

FIG. 20. The 3-μm reflectance of the outer belt asteroids in our survey permits us to trace the hydrated silicate profile, where asteroids were heated to roughly 300 K during the belt-wide heating event. The decline in hydrated silicates with heliocentric distance joins the radial decrease in the abundance of "melted" asteroids in strongly supporting electrical induction heating as the mechanism for early asteroid heating. Differentiated asteroid trend is from Gaffey (1988); the radial succession of asteroid classes is redrawn from Gradie and Tedesco (1982).

VII. FUTURE WORK AND CONCLUSIONS

The unfortunate failure in 1989 of both Soviet *Phobos* spacecraft eliminated near-term prospects for a detailed look at an ob-

ect apparently similar to those observed in our study. Phobos has a visual/near-IR spectrum much like 1 Ceres (Pang *et al.* 1978), and may be a captured main belt fragment; on the basis of the abundance of hydrated Cs in our 3-μm survey, discovery of hydrated silicates on Phobos would not be surprising. Linear crater chains associated with the satellite's parallel grooved fracture planes suggest that it once outgassed water after a major impact (Veverka and Thomas 1979, Hartmann 1980). On the other hand, recent 3-μm observations of Deimos by Bell *et al.* (1989) suggest that it is much less hydrated than the "average" hydrated C spectra we present here. On the basis of 3-μm and shorter wavelength reflectance data, Bell and co-workers conclude that Deimos may be an anhydrous P asteroid fragment from the Cybele region just outside the main belt.

Because of their primitive composition and possible links to comets, a rendezvous with a low-albedo asteroid should be a high NASA priority, particularly in light of the *Phobos* failures. While *Galileo* and later the *CRAF* and *Cassini* missions will return valuable asteroid data, a great deal could be learned cheaply and quickly about low-albedo objects by launching a small, relatively inexpensive spacecraft to a rendezvous with an Earth-crossing C (Cole *et al.* 1990). Ground-based 3-μm spectrophotometry could identify an appropriate hydrated or anhydrous target; a conservative estimate indicates that dozens are more accessible than the lunar surface in terms of the total velocity change required (Lewis and Lewis 1987). The expected compositional and mineralogical data returned would test the thermal evolution scenario presented here, narrow the search for carbonaceous chondrite parent bodies, and enhance any ground-based resource survey of the near-Earth population.

SUMMARY

(1) We obtained 3-μm spectra of 19 low-albedo and 5 S- or M-class asteroids. The IRTF cooled grating array spectrometer proved efficient at recording the 3-μm reflectance of moderately bright, low-albedo asteroids.

(2) We confirmed a 3.1-μm H_2O ice feature in the spectrum of 1 Ceres. However, no 3.4-μm organic features were visible in even the best asteroid spectra. Two M-class objects displayed 3-μm H_2O bands that indicated a hydrated surface component on these "metal" asteroids.

(3) 1 Ceres has no spectral match among the carbonaceous chondrites. Its 3-μm band depth suggests a surface H_2O content of about 5 wt%. The 2 Pallas spectrum closely resembles that of CM chondrites, indicating that Pallas' water content is roughly 2 wt%.

(4) Two-thirds of the C, G, T, F, and B asteroids in the 3-μm sample display a hydrated silicate absorption, indicating that the Cs (and C subclasses) underwent a widespread, though mild, heating and aqueous alteration episode. Only 1 of 10 P and D spectra show even a weak H_2O absorption, indicating a major difference in the hydration states of the C and P/D classes. The latter appear to have escaped extensive heating and aqueous alteration.

(5) Hydrated silicates gradually decline in abundance through the C region of the outer belt, disappearing entirely among the P and D classes. The presence of hydrated silicates correlates positively with albedo, but is unrelated to eccentricity, inclination, or diameter. The water distribution among the C, P, and D classes is consistent with an original composition of anhydrous silicates, water ice, and complex organic kerogen. Complex carbon compounds and H_2O were probably more abundant in the outer belt.

(6) The declining abundance of hydrated silicates with heliocentric distance, the variety of C asteroid hydration states at near-identical solar distances, and mild warming of even large asteroids is consistent with electrical induction heating just after asteroid formation. Anhydrous Cs are not dehydrated core fragments, but primitive bodies that escaped induction heating.

(7) The volatile inventory of the outer belt

was dominated by water ice. The inferred composition of the Ps and Ds suggests that they may still retain interior ices.

ACKNOWLEDGMENTS

This manuscript is a distillation of the results of my thesis work at the University of Arizona, completed in 1988. I thank all those who encouraged and supported this work, most importantly my wife Elizabeth. Not far behind, of course, were my advisors and colleagues John S. Lewis and Larry A. Lebofsky. Others helped at every turn: Jack Salisbury, Mark Marley, Bill Boynton, Scottie Cantrell, Lon Hood, Chuck Sonett, Alan Tokunaga, Kris Sellgren, Craig Foltz, and Jeff Bell. This work would have been impossible but for the constant help and encouragement of my friends and colleagues at the Lunar and Planetary Laboratory, University of Arizona. This work was supported by NASA Grants NSG-7144 and NAGW-1146.

REFERENCES

BELL, J. F. 1986. Mineralogical evolution of the asteroid belt. *Proc. Lunar Sci. Conf.* **17,** 985–986.

BELL, J. F., P. D. OWENSBY, AND B. R. HAWKE 1988. The 52-color asteroid survey: Final results and interpretation. *Lunar Planet. Sci. XIX,* 57–58.

BELL, J. F., J. R. PISCITELLI, AND L. A. LEBOFSKY 1989. Deimos: Hydration state from infrared spectroscopy. *Lunar Planet. Sci. XX,* 58–59.

BRECHER, A., P. L. BRIGGS, AND G. SIMMONS 1975. The low-temperature electrical properties of carbonaceous meteorites. *Earth Planet. Sci. Lett.* **28,** 37–45.

BRIN, G. D., AND D. A. MENDIS 1979. Dust release and mantle development in comets. *Astrophys. J.* **229,** 402–408.

BUNCH, T. E., AND S. CHANG 1980. Carbonaceous chondrite phyllosilicates and light element geochemistry as indicators of parent body processes and surface conditions. *GCA* **44,** 1543–1577.

BURNS, J. A., AND E. F. TEDESCO 1979. Asteroid light curves: results for rotations and shapes. In *Asteroids* (T. Gehrels, Ed.), pp. 494–527. Univ. of Arizona Press, Tucson.

CHAPMAN, C. R., D. MORRISON, AND B. ZELLNER 1975. Surface properties of asteroids: A synthesis of polarimetry, radiometry, and spectrophotometry. *Icarus* **25,** 104–130.

CHAPMAN, C. R., AND M. J. GAFFEY 1979. Reflectance spectra for 277 asteroids. In *Asteroids* (T. Gehrels, Ed.), pp. 655–687. Univ. of Arizona Press, Tucson.

CLAYTON, R. N., AND T. K. MAYEDA 1984. The oxygen isotope record in Murchison and other carbonaceous chondrites. *Earth Planet. Sci. Lett.* **67,** 151–161.

COLE, K. J., H. FEINGOLD, J. MCADAMS, M. L. STANCATI, AND J. R. FRENCH 1990. A planetary small missions program using small spacecraft. *Lunar Planet. Sci. XXI,* 212–213.

CRUIKSHANK, D. P., AND R. H. BROWN 1987. Organic matter on asteroid 130 Elektra. *Science* **238,** 183–184.

DUFRESNE, E. R., AND E. ANDERS 1962. On the chemical evolution of the carbonaceous chondrites. *GCA* **26,** 1085–1114.

FANALE, F. P., AND J. R. SALVAIL 1984. An idealized short-period comet model: Surface insolation, H_2O flux, dust flux, and mantle development. *Icarus* 60, 476–511.

FEGLEY, M. B., JR. 1988. Cosmoschemical trends of volatile elements in the solar system. In *LPI Technical Report 88-04: Workshop on the Origins of Solar Systems.* (J. A. Nuth and P. Sylvester, Eds.), pp. 51–60. Lunar and Planetary Institute, Houston.

FEIERBERG, M. A., L. A. LEBOFSKY, AND H. P. LARSON 1981. Spectroscopic evidence for aqueous alteration products on the surface of low albedo asteroids. *GCA* **95,** 971–981.

FEIERBERG, M. A., L. A. LEBOFSKY, AND D. J. THOLEN 1985a. The nature of C-class asteroids from 3-μm spectrophotometry. *Icarus* **63,** 183–191.

FEIERBERG, M. A., L. A. LEBOFSKY, AND D. J. THOLEN 1985b. Are T, P, and D asteroids really ultraprimitive? *Bull. Amer. Astron. Soc.* **17,** 730.

FREDRIKSSON, K., AND J. F. KERRIDGE 1988. Carbonates and sulfates in CI chondrites: Formation by aqueous activity on the parent body. *Meteoritics* **23,** 35–44.

GAFFEY, M. J 1987. Instrumental requirements and observational strategies for spectrophotometric data acquisition during a CRAF-type asteroid flyby. *Lunar Planet. Sci. XVII* 308–309.

GAFFEY, M. J. 1988. Thermal history of the asteroid belt: Implications for accretion of the terrestrial planets. *Lunar Planet. Sci. XIX* 369–370.

GRADIE, J. C., AND J. VEVERKA 1980. The composition of the Trojan asteroids. *Nature* **283,** 840–842.

GRADIE, J. C., AND E. F. TEDESCO 1982. Compositional structure of the asteroid belt. *Science* **216,** 1405–1407.

GROSSMAN, L., AND J. W. LARIMER 1974. Early chemical history of the solar system. *Rev. Geophys. Space Physics* **12,** 71–101.

HARDORP, J. 1980. The sun among the stars. III. Energy distributions of 16 northern G-type stars and the solar flux calibration. *Astron. Astrophys.* **91,** 221–232.

HARDORP, J. 1982. The sun among the stars. V. A second search for solar spectral analogs. *Astron. Astrophys.* **105,** 120–132.

HARTMANN, W. K. 1980. Surface evolution of two-component stone/ice bodies in the Jupiter region. *Icarus* **44,** 441–453.

HARTMANN, W. K., D. J. THOLEN, AND D. P. CRUIKSHANK 1987. The relationship of active comets, "extinct" comets, and dark asteroids. *Icarus* **69,** 33–50.

HERBERT, F. 1989. Primordial solar wind heating of planetesimals and asteroids. *Icarus* **78**, 402–410.

HERBERT, F., AND C. P. SONETT 1979. Electromagnetic heating of minor planets in the early solar system. *Icarus* **40**, 484–496.

HERBERT, F., AND C. P. SONETT 1980. Electromagnetic inductive heating of the asteroids and moon as evidence bearing on the primordial solar wind. In *Proc. Conf. Ancient Sun* (R. O. Pepin, J. Eddy, and R. B. Merrill, Eds.), pp. 563–576.

HOUPIS, H. L. F., AND D. A. MENDIS 1981. On the dust zoning of rapidly rotating cometary nuclei. *Astrophys. J.* **251**, 409–414.

JONES, T. D. 1988. An infrared reflectance study of water in outer belt asteroids: Clues to composition and origin. PhD dissertation. University of Arizona, Tucson.

JONES, T. D., L. A. LEBOFSKY, AND J. S. LEWIS 1987. Mid-IR reflectance spectra of C-class asteroids: New results from the NASA IRTF. *Bull. Amer. Astron. Soc.* 19, 841.

ONES, T. D., L. A. LEBOFSKY, AND J. S. LEWIS 1988a. The 3-μm hydrated silicate signature on C class asteroids: Implications for origins of outer belt objects. *Lunar Planet. Sci. XIX* 567–568.

JONES, T. D., L. A. LEBOFSKY, AND J. S. LEWIS 1988b. Observational evidence for solar wind induction heating of low albedo asteroids. *Meteoritics* **23**, 277.

JONES, T. D., L. A. LEBOFSKY, AND J. S. LEWIS 1989. Mid-IR reflectance spectra of carbonaceous chondrites: Application to low-albedo asteroids. *Meteoritics* **24**, 282.

JONES, T. D., L. A. LEBOFSKY, AND J. S. LEWIS 1991. Mid-IR reflectance spectra of carbonaceous chondrites: Applications to low-albedo asteroid surfaces. In preparation.

KERRIDGE, J. F., AND T. E. BUNCH 1979. Aqueous activity on asteroids: Evidence from carbonaceous meteorites. In *Asteroids* (T. Gehrels, Ed.), pp. 745–764. Univ. of Arizona Press, Tucson.

LARSON, H. P., AND G. J. VEEDER 1979. Infrared spectral reflectances of asteroid surfaces. In *Asteroids* (T. Gehrels, Ed.), pp. 724–744. Univ. of Arizona Press, Tucson.

LARSON, H. P., M. A. FEIERBERG, AND L. A. LEBOFSKY 1983. The composition of asteroid 2 Pallas and its relation to primitive meteorites. *Icarus* **56**, 398–408.

LEBOFSKY, L. A. 1978. Asteroid 1 Ceres: Evidence for water of hydration. *Mon. Not. R. Astron. Soc.* **182**, 17–21.

LEBOFSKY, L. A. 1980. Infrared reflectance spectra of asteroids: A search for water of hydration. *Astron. J.* **85**, 573–585.

LEBOFSKY, L. A., M. A. FEIERBERG, A. T. TOKUNAGA, H. P. LARSON, AND J. R. JOHNSON 1981. The 1.7- to 4.2-μm spectrum of asteroid 1 Ceres: Evidence for structural water in clay minerals. *Icarus* **48**, 453–459.

LEBOFSKY, L. A., M. V. SYKES, E. F. TEDESCO, G. J. VEEDER, D. L. MATSON, R. H. BROWN, J. C. GRADIE, M. A. FEIERBERG, AND R. J. RUDY 1986. A refined "standard" thermal model for asteroids based on observations of 1 Ceres and 2 Pallas. *Icarus* **68**, 239–251.

LEBOFSKY, L. A., T. D. JONES, AND F. HERBERT 1989. Asteroid volatile inventories. In *Origin and Evolution of Planetary and Satellite Atmospheres*. (S. K. Atreya, J. B. Pollack, and M. S. Matthews, Eds.), pp. 192–229. Univ. of Arizona Press, Tucson.

LEBOFSKY, L. A., T. D. JONES, P. D. OWENSBY, M. A. FEIERBERG, AND G. J. CONSOLMAGNO 1990. The nature of low-albedo asteroids from 3-μm multicolor photometry. *Icarus* **83**, 16–26.

LEE, T. New isotopic clues to solar system formation 1979. *Rev. Geophys. Space Phys.* **17**, 1591–1611.

LEWIS, J. S. 1972. Low temperature condensation from the solar nebula. *Icarus* **16**, 241–252.

LEWIS, J. S., AND R. G. PRINN 1984. *Planets and Their Atmospheres*. Academic Press, Orlando.

LEWIS, J. S., AND R. A. LEWIS 1987. *Space Resources: Breaking the Bonds of Earth*. Columbia University Press, New York.

LUPISHKO, D. F., AND I. N. BELSKAYA 1989. On the surface composition of the M-type asteroids. *Icarus* **78**, 395–401.

MCSWEEN, H. Y., JR. 1979. Are carbonaceous chondrites primitive or processed? A review. *Rev. Geophys. Space Phys.* **17**, 1059–1078.

MCSWEEN, H. Y., JR. 1987. Aqueous alteration in carbonaceous chondrites: Mass balance constraints on matrix mineralogy. *GCA* **51**, 2469–2477.

NOZETTE, S., AND L. L. WILKENING 1982. Evidence for aqueous alteration in a carbonaceous xenolith from the Plainview (H5) chondrite. *GCA* **46**, 557–563.

PANG, K. D., J. B. POLLACK, J. VEVERKA, A. L. LANE, AND J. M. AJELLO 1978. The composition of Phobos: Evidence for carbonaceous chondrite surface from spectral analysis. *Science* **199**, 64–66.

PISCITELLI, J. R., D. P. CRUIKSHANK, R. H. BROWN, A. T. TOKUNAGA, AND J. F. BELL. The search for solid macromolecular carbon on asteroids. *Bull. Amer. Astron. Soc.* **20**, 864.

PRINN, R. G. 1989. On neglect of nonlinear momentum terms in solar nebular accretion disk models. *Astrophys. J.* **348**, 725–729.

PRINN, R. G., AND B. FEGLEY, JR. 1987. The atmospheres of Venus, Earth, and Mars: A critical comparison. *Annu. Rev. Earth Planet. Sci.* **15**, 171–212.

PRINN, R. G., AND B. FEGLEY, JR. 1988. Solar nebula chemistry: Origin of planetary, satellite and cometary volatiles. In *Origin and Evolution of Planetary and Satellite Atmospheres* (S. Atreya, J. Pollack, and

M. Matthews, Eds.), pp. 78–136. Univ. of Arizona Press, Tucson.

SONETT, C. P., D. S. COLBURN, AND K. SCHWARTZ 1968. Electrical heating of meteorite parent bodies and planets by dynamo induction from a pre-main sequence T Tauri "solar wind." *Nature* **219,** 924–926.

SONETT, C. P., AND R. T. REYNOLDS 1979. Primordial heating of asteroid parent bodies. In *Asteroids* (T. Gehrels, Ed.), pp. 822–848. Univ. of Arizona Press, Tucson.

TEDESCO, E. F., J. G. WILLIAMS, D. L. MATSON, J. C. GRADIE, G. J. VEEDER, AND L. A. LEBOFSKY 1989. A three-parameter asteroid taxonomy. *Astron. J.* **97,** 586–606.

THOLEN, D. J. 1984. *Asteroid Taxonomy from Cluster Analysis of Photometry*. PhD dissertation, Univ. of Arizona, Tucson.

TOKUNAGA, A. T., AND R. G. SMITH 1985. A faint object spectrometer for the infrared. *Astrop Space Sci.* **118,** 471–472.

VEVERKA, J., AND P. THOMAS. 1979. Phobos Deimos: A preview of what asteroids look like *Asteroids* (T. Gehrels, Ed.), pp. 628–651. Univ Arizona Press, Tucson.

VILAS, F., AND M. J. GAFFEY 1989. Phyllosilicate sorption features in main-belt and outer-belt aster reflectance spectra. *Science* **246,** 790–792.

WILKENING, L. L. 1978. Carbonaceous chondritic n terial in the solar system. *Die Naturwissenschaf* **65,** 73–79.

WOOD, J. A., AND S. CHANG 1985. *The Cosmic Hi of the Biogenic Elements and Compounds*. N. SP-476. NASA, Washington, D.C.

ZELLNER, B. 1979. The Tucson revised index of aste oid data. In *Asteroids* (T. Gehrels, Ed), p 1011–1013. Univ. of Arizona Press. Tucson.

ICARUS 85, 380–393 (1990)

Solar Nebula Origin for Volatile Gases in Halley's Comet[1]

STEFFI ENGEL, JONATHAN I. LUNINE, AND JOHN S. LEWIS

Lunar and Planetary Laboratory, University of Arizona, Tucson, Arizona 85721

Received July 11, 1989; revised December 28, 1989

Modeling of physical and chemical processes in solar nebula environments is applied to the present data base on the composition of gases in Halley's comet to infer the conditions under which that comet formed. Key molecular ratios—CH_4 to CO, CO_2 to CO, and NH_3 to N_2—are compared to predictions of solar nebula models. Nebular thermochemistry is quantified for a range of solar elemental compositions corresponding to varying degrees of depletion of water in the inner part of the nebula. The edge of the chemically active region is fixed by rates of chemical reactions in the presence of grains. The mixing of molecules from chemically active regions to the outer nebula is parameterized using recent studies of this process. The incorporation of volatile molecules into water ice by clathration and absorption is then applied to yield predicted ratios of volatile species for comparison with the data. We find that, assuming chemistry in the inner nebula is catalyzed by reactions on grains, the abundances of the volatile carbon species CH_4, CO, and CO_2 in Halley could have been supplied by the solar nebula. The NH_3 abundance in Halley is, however, too high to have been derived from the nebula; an alternative source must be invoked. We suggest that the surrounding giant molecular cloud is a possible source for ammonia. This requires that nebular mixing not be 100% efficient. We also consider the heating and processing of grains entering the nebula by gas drag.

INTRODUCTION

The origin of the solar system is now recognized as part of the larger issue of the phenomenon of star formation in the Galaxy. Consequently, the chemistry of the disk which was to become the planets (that is, the solar nebula) must have been intimately tied up in the chemistry of the surrounding giant molecular cloud which was the likely supply for the nebular gas and dust. While meteorites are regarded as primarily products of solar nebula processes, comets are variously considered to be pristine remanants of interstellar processes, molecular cloud material partially altered in the solar nebula, or products entirely of solar nebula condensation and chemistry. Given the diversity of materials thought or known to be contained in comets, ranging from highly refractory silicates through organics of moderate volatility to ices and gases of high volatility, the middle view must be the appropriate one: comets contain records of processes stretching from those in the molecular cloud (and perhaps even prior epochs), through infall and entry into the solar nebula, to the solar nebula itself.

To understand the history of comet formation, distinct epochs must be isolated by selecting materials within a fixed range of volatility which may say something about a particular set of events in one (or a small subset of) primordial environments. The most volatile species in comets, namely the small molecules with low polarizability (methane, carbon monoxide, noble gases), likely reflect the final stages of chemistry and physics occurring in the solar nebula.

[1] Contribution 89-32, Theoretical Astrophysics Program, University of Arizona.

0019-1035/90 $3.00

TABLE I

ABUNDANCES IN COMET HALLEY USED IN THIS STUDY[a]

CO	0.05–0.1
N_2	<0.05
CH_4	0.01–0.04
NH_3	0.003–0.01
CO_2	0.02–0.04
H_2CO	0.01–0.1
HCN	0.001

[a] Molecular abundances are mole fractions relative to water. Inequality indicates an upper limit (nondetection).

although some of these materials may have had their origin in the surrounding molecular cloud. The comprehensive ground- and space-based observations of Halley's comet in 1985 and 1986 provided the first opportunity to assemble an inventory of gases contained in comets, and interpretation of this inventory in terms of cometary formation environments is now appropriate. Table I from Lunine (1989) lists the abundances of key molecular species in Halley's comet relative to water. The table is generally consistent with that in Weaver (1989). The interpretation of the ground-based and spacecraft data is an involved and controversial process; the aforementioned papers discuss the inventory in terms of observational uncertainties in some detail. We therefore do not repeat the discussion here; original references for the data can also be found in those two papers.

In the present effort we consider a range of processes in the solar nebula which may have determined the budget of volatile gases in the outer solar system. The model is tuned to, and compared with, the budget of gases shown in Table I. While we find that many of the carbon-based molecules have abundances which can be fitted by a plausible solar nebula model (with certain modifications and caveats), other species, such as formaldehyde and ammonia, decidedly cannot. They indicate that the chemical history of at least a subset of volatiles stretches beyond the solar nebula to other sources. We consider these sources toward the end of the paper.

Prinn and Fegley (1989) were the first to consider the gas budget of Halley in terms of solar nebula models. They concluded that substantial mixing of material from the vicinity of giant planets was required to explain the data. Why then the present analysis? The new features of this study include (1) consideration of the partitioning of gases between the nebula and ice phases, which alters the inventory of gases trapped in the ice, and hence the comet, compared to what was in the nebula; (2) a model for the thermochemistry of molecular species in the chemically active zone of the nebula, which considers the elemental carbon-to-oxygen ratio to be a varible, based on the model of diffusive redistribution of water by Stevenson and Lunine (1988); (3) consideration of different efficiencies of mixing of gases in the solar nebula, which affects the degree of chemical coupling between the outer and inner regions of the nebula; and (4) calculation of the thermal history of icy grains falling into the solar nebula and subjected to drag heating.

In what follows we assume that the composition of Comet Halley is reflective at least in part of the physical and chemical processes associated with the origin of the solar system and planets. A different viewpoint has been put forth, that Halley is genetically completely unrelated to the solar system but was captured well after the epoch of planetary formation. Support for this model has come in the form of a nonterrestrial $^{13}C/^{12}C$ ratio (Wyckoff *et al.*, 1989). While we acknowledge the possibility that Halley is an "oddball" (the prevailing view is that most comets could not have been captured in this fashion), we also point out that understanding of the carbon isotope data is far from complete. Until and unless this issue is resolved, we make the assumption that formation of Halley was coeval and colocated with that of the solar system.

Further observations of other comets and the upcoming CRAF mission may help resolve this critical issue.

Section 2 describes the modeling of nebular physical and chemical processes; section 3 gives the model results. Section 4 describes the implications of the results for the ability of solar nebula models to explain cometary compositions: this section also describes models of the heating of grains falling into the nebula. Section 5 concludes the paper with prospects for future measurements and their impact on theory.

2. NEBULAR PHYSICAL AND CHEMICAL PROCESSES

A. *Thermochemical Calculations*

In the inner portion of the nebular disk, temperatures are sufficiently high that a suite of reactions interchanging CH_4 with CO and CO_2, and NH_3 with N_2, proceed at rates such that equilibrium is reached on time scales much shorter than the lifetime of the nebular disk. Because temperatures fall with increasing radial distance from the proto-Sun, there must exist a region, for each suite of reactions, at which the time to achieve equilibrium among molecular species becomes comparable to the lifetime of the nebula (or, more stringently, the time scale for dynamic mixing). This region fixes the ratios of the molecular species *for any parcels of gas mixed outward from that region* (i.e., transported to lower temperature regions). This concept was first quantified for the nebula by Lewis and Prinn (1980) and Prinn and Fegley (1981). Provided nebular mixing is sufficiently vigorous that there is significant interchange of gas between the cold outer nebula and the hot, chemically active inner nebula, this "quench zone" will fix the inventory of gas-phase molecular species in the entire solar nebula. Prinn and Fegley (1989) argue that thermochemistry of this sort predominates over chemistry driven by other energetic processes, such as lightning and nebular flares. We therefore assume here that thermochemistry is the primary determinant of the molecular inventory in the inner portion of the solar nebula.

To model the gas-phase chemistry occurring in the inner disk, we constructed a comprehensive chemical model which computes equilibrium among 50 molecular species of the elements H, O, C, N, and S. Thermodynamic data were taken from the JANAF tables (1971). Equilibrium was evaluated along a hydrogen–helium adiabat such that a temperature T of 2000°K occurs at 10^{-2} bar total pressure and 600°K at 10^{-4} bar. Based on the nebular model of Cameron (1978), 680°K occurs at 1 AU from the proto-Sun. Recent models (reviewed in Wood and Morfill 1988) indicate that such a temperature profile does *not* reproduce well the radial temperature profile in a nebula with varying opacity due to grains, different mechanisms of angular momentum transport, etc. However, the model results are not sensitive to variations of pressure at a given temperature over a couple of orders of magnitude. Our application of the results to Halley is sensitive to the temperature as a function of radial distance from the Sun, through the models of mixing of gas to the outer part of the nebula. The reader will see in Section 3 that it is straightforward to assess the effect of such uncertainties.

For a given set of elemental abundances, and a fixed temperature and total pressure in a given region, the partial pressures for the various molecular species are calculated iteratively. The results are shown in Fig. 1. The temperatures correspond to the adiabat described above. Consistent with the results of Lewis and Prinn (1980) and Prinn and Fegley (1981), CO and N_2 dominate at higher temperature, and CH_4 and N_2 at lower temperature. The water abundance is tightly coupled to the abundance of CO, especially for the O/C = 1 case. The CO_2 abundance is a strong function of the elemental abundance as well. The nitrogen-bearing species, while sensitive to temperature, are not sensitive to the oxygen abundance expressed by the oxygen-to-carbon ratio.

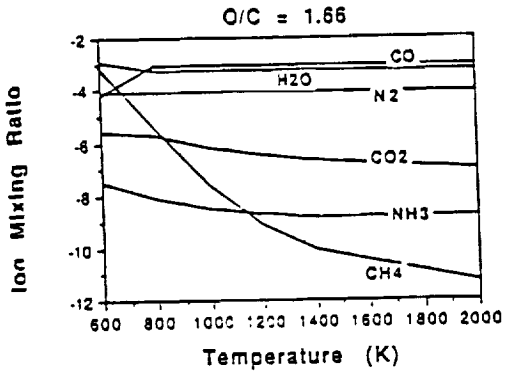

FIG. 1. Calculated equilibrium abundances for volatile species of interest in this paper along a H–He adiabat are shown. The O/C ratio was assumed to be solar.

B. Reaction Kinetics and the Quench Temperature

A continuing uncertainty which plagues the modeling of solar system chemistry concerns reaction rates. In particular, limitations in understanding the gas-phase reactions which interconvert CO and CH_4 have been well documented (SPASE 1989). We accept the rates used by previous authors [reviewed very recently by Prinn and Fegley (1989)]. The numbers we give below refer to a nebular lifetime (or most sluggish mixing time) of 10^{13} sec, based upon astrophysical evidence on the lifetime of disks around young stars (Strom *et al.* 1989). In the gas phase, the CO–CH_4 reaction system quenches at 1470°K, the N_2–NH_3 interconversion at 1600°K, and CO–CO_2 at 830°K. Reference to Fig. 1 then gives the abundance ratios at those temperatures.

Anticipating the discussion in Section 3, these temperatures are so high that very little CH_4 or NH_3 is expected anywhere in the solar nebula, except in the high-pressure nebulas surrounding the giant planets, which are highly reducing environments. This has been noted by Prinn and Fegley (1989), in connection with their analysis of Halley's comet. However, the presence of a significant population of refractory grains in the inner nebula opens the possibility of catalyzed reactions, as first noted by Lewis and Prinn (1980) and Prinn and Fegley (1981). These reactions effectively lower the quench temperature, provided they occur.

There are currently no experimental data at the proper temperatures and hydrogen pressures to determine directly the catalyzed rates of reaction. Vannice (1975) comes closest, with high (but not solar) ratios of hydrogen to CO. The dominant product of the catalysis is C_1 hydrocarbons, with smaller amounts of higher hydrocarbons. On the basis of those experiments, Prinn and Fegley (1989) calculate a quench temperature of 520°K. Similarly, they calculate a quench temperature for iron-catalyzed conversion of N_2 to NH_3 of 480°K (terminated in this case by formation of iron oxides in the nebula). Figure 1 shows that while N_2 still dominates over other nitrogen-bearing species, the lower quench temperature produces a CH_4-dominated carbon inventory.

Prinn and Fegley (1989) have pointed out that the conditions under which effective grain catalysis may occur are not well understood. They propose that if grain surfaces are not relatively pure (that is, become coated with carbonaceous or sulfur-bearing material) the catalysis becomes highly inefficient. They also propose that production of heavy-organic material is a more probable outcome than that of methane. While the experimental data do not exist to answer this question definitively one way or the other, we note that the available data do show positive results in the CO–CH_4 conversion, but that the issue of what constitutes an effective catalysis surface remains open. Our model results for methane are predicated on efficient catalysis, and the reader is reminded of this in later sections.

C. Diffusive Redistribution of Water Vapor

The decision to let the O-to-C ratio vary rests on the realization that nebular transport processes may act to produce strong

regional variations in elemental abundances in the solar nebula. Evidence for this is present in chondrites (Rubin *et al.* 1988), although much of this effect may be due to dust in the nebula and possibly environments other than the nebula itself. Stevenson and Lunine (1988) modeled the effect of transport and condensation processes on water. Under the assumption that viscous processes transport mass and angular momentum, the water distribution through the nebula as a function of time was tracked. The condensation boundary in the region 3 to 5 AU acts as a "cold finger," to actively and continually remove water from the gas phase. Consequently, the profile of nebular water vapor may be strongly altered on a time scale comparable to the evolution of the disk itself. In the later stages of the nebula, when material is not being resupplied from the surrounding molecular cloud, the inner part of the disk could be strongly depleted of water, and hence have an average oxygen-to-carbon ratio of unity. The cosmochemical implications of this for inner solar nebula bodies is potentially important but complicated, as the water depletion may vary both spatially and temporally [see the discussion following Fegley and Prinn (1989)]. Figure 2 shows equilibrium abundances of molecules for the case in which O/C = 1. Methane is now much more abundant at a given temperature than for the solar case, and carbon dioxide is depleted. The nitrogen species are not affected.

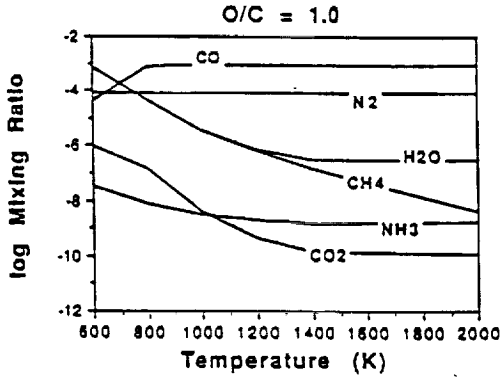

FIG. 2. As in Fig. 1, but the O/C ratio is unity. Oxygen is depleted due to the removal of water vapor to the water condensation boundary. CH_4 is more abundant than in the solar case and CO and H_2O are depleted.

D. Nebular Mixing

The calculations considered above focus on active chemistry in the hot inner part of the disk, inward of 1 AU [for hot models of the nebula, such as those of Boss (1988), active thermal chemistry could occur as far out as 3 AU]. If such chemistry affected the abundances in Halley, which probably formed no closer in than 15–20 AU [see the review on cometary origins by Weissman (1985)], radial mixing of material from the outer and inner portions of the disk would have had to occur. Traditionally, studies of nebular thermal chemistry as in Lewis and Prinn (1980) have assumed that the inner and outer parts of the disk were fully mixed over the lifetime of the nebula, and hence the molecular composition was determined entirely by that at the radial quench zone.

Good models relating the transport of nebular angular momentum to the mixing of trace species do not yet exist; the problem probably requires treatment by three-dimensional hydrodynamic codes. Stevenson (1989) considered a semianalytical model of a viscous accretion disk. By linearizing the stress term associated with angular momentum transport, it is possible to solve the continuity equations for the viscous disk. Stevenson assumes $D = k\nu$, where D is the diffusion coefficient for mass transport and ν is the eddy viscosity (diffusion coefficient for angular momentum transport). He argues that numerical models place the proportionality constant k between 1 and 3, which severely limits the degree of radial mixing in the nebula. Approximately, the mixing ratio of a species produced at radial distance R_p has a mixing ratio at R diluted by the factor $(R_p/R)^{3/2k}$. For a chemical quench zone at 1 AU and a comet formation region at roughly 20 AU, the mixing ratio is diluted by 100 for $k = 1$ and by 5 for $k = 3$. What is occurring physically is that because the

eddy and mass diffusion coefficients are assumed proportional, the total amount of mass mixing over the nebular lifetime (defined by the redistribution of a significant fraction of the disk angular momentum) is fixed. A higher mass diffusion coefficient is accompanied by a higher angular momentum diffusion coefficient and hence shorter nebular lifetime.

Prinn (1989) argues that because the eddy stress terms are quadratically nonlinear, a linearized solution does not capture all of the processes involved in mixing. He points out that natural systems exhibit nonlinear acceleration processes which may produce an effective k of 10 or higher. For a k of 10, a trace species mixing ratio at 20 AU is over 60% that at 1 AU where it is assumed formed. In this concept the inner and outer portions of the nebula are nearly fully mixed.

As noted above, the resolution of this problem requires a three-dimensional, hydrodynamic investigation of various nebular models, in which angular momentum and mass are transported not only by viscous (local) processes but also by waves. Here we consider three cases in which material is mixed from 1 AU out to the region 15 to 20 AU, corresponding to 100%, 10%, and 1% mixing. From the scaling given above the reader can select others.

E. Trapping of Volatile Molecular Species in Water Ice

The spacecraft and ground-based investigations of Halley did not give information as to how the various parent molecules were locked into the nucleus originally. Direct condensation is unlikely for methane and more volatile molecules based on solar nebula temperature–pressure profiles. In the interstellar cloud, attachment of molecules such as N_2 and CO to grains, followed by hydrogenation to form H_2O, CH_4, and NH_3, has been suggested (Blake *et al.* 1987). We show below that such grains probably evaporated upon entry into the solar nebula. The most likely mechanism in the solar nebula for getting very volatile species into comets is trapping of gases in water ice, either by adsorption or by clathration. Trapping on media other than water ice is possible, but in the outer solar nebula the abundance of water is such, and its ability to trap species great enough, that we assert it to be most important in this process.

Highly uncertain is the dominant mode of trapping. Physical adsorption will occur on icy surfaces, but for anything but very small ice grains (i.e., less than 0.1 μm), the amount of gases trapped on surfaces is small, not enough to explain the ratio of volatile species to water ice of over 10% seen in Table I. Volumetrically significant adsorption (caused either by codeposition of water vapor and volatiles or by exposure of fresh ice to the gas) can trap sufficient volatiles, provided the water ice is amorphous (Mayer and Pletzer 1986). Clathrate formation is, roughly speaking, a three-dimensional adsorption process which involves reorientation of the ice crystal structure to produce large voids, capable of trapping volatile species such as methane and nitrogen. The ratio of trapped species to ice is about 13%, consistent with the Halley data, but requires physical exposure of all of the ice to the gas, since diffusion is very slow (Lunine and Stevenson 1985).

Codeposition is an unlikely way to trap volatiles in the nebula, in spite of it being a favorite for laboratory simulation (Bar-Nun and Kleinfeld 1989). Reference to condensation plots shows that water ice condenses, for most solar nebula models, at temperatures around 140–160°K, well above the temperature (roughly 50°K) at which clathrate formation or significant adsorption of volatiles would occur. Trapping of gases in amorphous ice runs into the difficulty that condensation temperatures for water ice in the nebula are well above 130°K, which is generally recognized as that required to make amorphous ice from the vapor (Hobbs 1974). Note that amorphous ice cannot be made by cooling crystalline ice. Nonetheless, some amorphous ice may have sur-

vived entry into the nebula and we do not dismiss its presence in primordial comets.

Clathrate formation, while thermodynamically plausible, requires good exposure of the ice to the gas (as does volumetrically significant adsorption). We can think of only one plausible process by which fresh ice may be exposed to trap gas: relatively slow collisions among planetesimals to expose fresh ice. Lunine and Stevenson (1985) considered this process, and while the numbers are marginal, they do not by any means rule out this possibility. We adopt as a working hypothesis that the volatiles in Comet Halley were trapped in water ice in the form of clathrate hydrates.

Lunine (1989) considered the chemical fractionation processes which occurred during trapping to alter the abundances of molecules from those in the nebular gas. We briefly sketch the argument here, considering the species methane, carbon dioxide, carbon monoxide, nitrogen, and ammonia. In the carbon species, methane incorporates into clathrate much more readily than does carbon monoxide; at low temperatures carbon dioxide thermodynamically prefers to form dry ice but some will be trapped in the clathrate. We expect a lower CO-to-CH_4 ratio in the clathrate than in the nebula. How much lower depends upon the availability of cage sites for trapping, and hence on the amount of ice exposed to the nebular gas. In the case of a small number of available cage sites, and hence extreme competition, the CO/CH_4 value is depleted in the clathrate by a factor of 10^6 or more. The CH_4 and CO abundances relative to water ice in Halley given in Table I constrain for us the amount of ice exposed to the gas: it must be nearly the maximum possible. Assuming a gaseous nebula in which most of the carbon is in the form of CO, with CH_4 secondary, essentially all of the nebular methane is trapped, while only a fraction of the carbon monoxide can be accommodated. Under such conditions, the CO/CH_4 value is depleted in the clathrate by a more modest factor, 10 to 100.

Bar-Nun and Kleinfeld (1989) find a similar CO depletion factor for their experiments involving codeposition of amorphous ice with CO–CH_4 gas mixtures. While their experimental situation is rather complex, the results imply that (a) the amorphous ice is able to trap amounts of CH_4 and CO comparable to clathrate, and (b) the molecular interactions between the trapped molecules and water ice are similar in clathrate and amorphous ice, which is not unexpected.

Since carbon dioxide is able to condense out as dry ice for the abundances predicted by Fig. 1 and plausible quench temperatures, we assume here that essentially all of the carbon dioxide in the region of Comet Halley's formation was available for incorporation into the nucleus. Therefore, the CO-to-CO_2 ratio in Halley is predicted to be 10 to 100 times less that in the nebula, again because a significant fraction of the CO does not make it into the clathrate.

Turning to the nitrogen species, we find a slightly more complex situation. Because ammonia attaches to water in the form of hydrogen-bonded ammonia hydrates, its abundance in the ice is decoupled from the molecular nitrogen which only weakly incorporates into clathrate hydrate. The only constraint on the N_2-to-NH_3 ratio in the Halley formation zone is the measured ratio of ammonia to water. If it were 15% in Halley, then arguably the NH_3-to-N_2 ratio in the nebula would be infinite, i.e., all of the elemental nitrogen was locked up as ammonia. (This assumes, of course, solar elemental N-to-O abundance and condensation of all of the water and ammonia.) The abundance of ammonia of roughly 0.1% in Halley constrains the nebular N_2-to-NH_3 ratio to be roughly 10 to 100.

F. Postformation Processing

We have not attempted to model the chemical evolution of species in the nucleus after formation. While temperatures of most comets stored in the Oort cloud remain low [less than 30K (Stern and Shull 1988)], slow diffusion of species within the ice over time

or during earlier encounters with the Sun, cannot be ruled out. The nucleus of Halley below the thermal wave is at approximately 25°K based on observations of the spin temperature in water (Mumma *et al.* 1989). It is possible that the molecular inventory observed in Comet Halley has been somewhat modified by postformation processes, but not to a great extent given the very low internal temperature.

3. MODEL RESULTS

We use the nebular chemistry model described above to predict the ratios of key molecular species in the region of formation of Comet Halley. We assume that Halley formed at roughly 20 AU from the Sun; recent support for the agglomeration of at least the short-period comets in this region was presented by Duncan (1989); whether this is relevant to Halley is problematic. We also assume that the chemically active zone in the nebula extends out to roughly 1 AU from the Sun. We then compute CO/CH_4, CO/CO_2, and N_2/NH_3 at 20 AU as a function of the elemental O-to-C ratio in the chemically active zone, assuming that heterogeneous catalysis on grains was effective in reducing the quench temperature to below 800°K. Three mixing efficiencies are considered, corresponding to full mixing of outer and inner nebular gas, 10% mixing, and 1% mixing. The outer solar nebula is assumed to start with a gaseous inventory of CO and N_2; any CH_4, NH_3, and CO_2 are supplied by inner nebula chemistry. We revisit this assumption after presenting our results.

Figures 3, 4, and 5 show the results. Because we desire to compare nebular gas-phase abundances, we do not compare our model directly with the Halley data. Rather, we apply the fractionation corrections discussed in Section 2E to the Halley data. Thus, the Halley CO/CH_4, CO/CO_2, and N_2/NH_3 ratios are all increased by a factor of 10 to 100 over the values in Table I. The range in the figures is actually larger to ac-

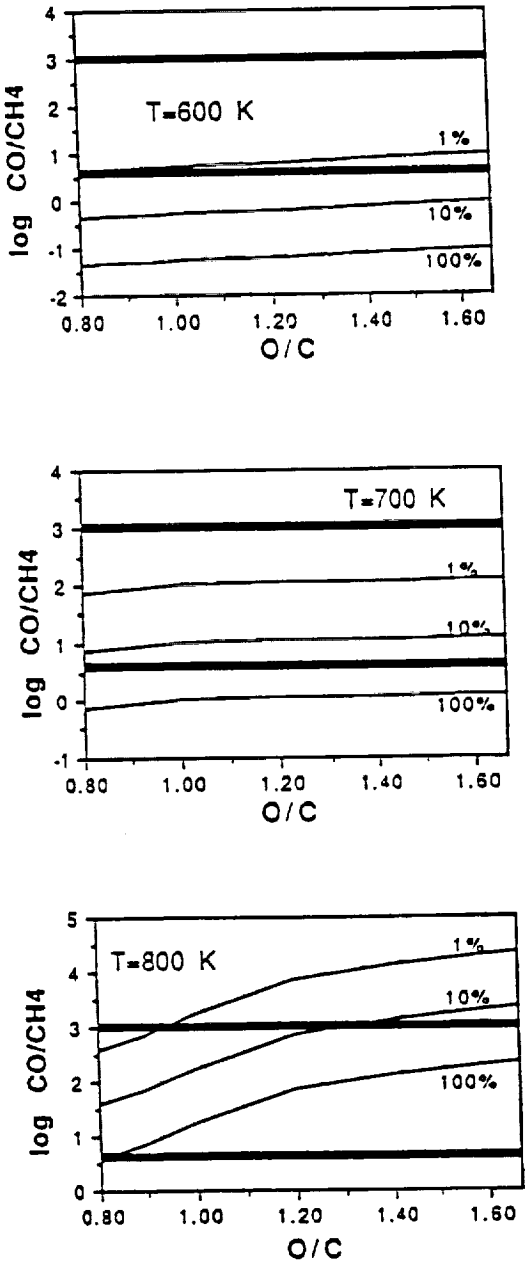

FIG. 3. For three different quench temperatures, CO/CH_4 abundance is plotted versus O/C ratio. The thick lines are the Halley data corrected for fractionation effects, like clathration and adsorption, and uncertainties in the measurements. The thin lines represent the values from our calculations assuming different degrees of mixing into the outer solar nebula. It can be seen that the amount of CH_4 found in Comet Halley is consistent with an inner solar nebula origin for quench temperatures of 600 to 800°K and for a range of nebular mixing efficiencies and elemental O/C values.

count for uncertainties in the measured values themselves. Results for three different quench temperatures are shown.

Figure 3 indicates that the Halley data are consistent with methane manufactured in the solar nebula at quench temperatures of 600 to 800°K for a range of nebular mixing efficiencies and elemental O/C values. These quench temperatures are all appropriate for catalyzed reactions on grain surfaces; if gas-phase chemistry only were operative insufficient methane (by orders of magnitude) would be available to fit the Halley data. Figure 4 paints a similar picture for CO_2; although gas-phase reactions can occur with quench temperatures as low as 830°K without catalysis, it appears that lower temperatures (and hence reactions on grains) are required to reproduce the Halley abundance. Note that to fit both the Halley CO/CH_4 and CO/CO_2 ratios for a given inner nebula elemental abundance and nebula mixing efficiencies, somewhat different quench temperatures are required in Figs. 3 and 4. This is not surprising, since the reaction schemes (and hence rates) are different, so that for a fixed nebular lifetime or mixing time, different quench temperatures for CO–CH_4 and CO–CO_2 would be expected.

Figure 5 shows the result for N_2/NH_3 for the 100% nebular mixing case, which yields the most NH_3 in the outer nebula. Clearly, insufficient ammonia is produced to account for the Halley observations. Quench temperatures below any reasonable range would be required to fit the Halley data. It is interesting to note that Marconi and Mendis (1988) argue that the Halley results are actually consistent with zero ammonia, when variations in the solar UV flux (which is required for the data reduction) are considered. However, the corroborating data of Wyckoff *et al.* (1989) appear to place the ammonia abundance on a firm footing.

New elemental abundances determined by Anders and Grevesse (1989) change the O-to-C ratio significantly, from 1.66 to 2.36. Running our chemical model for O-to-C ratios higher than those given in the figures results in an increase in the H_2O and CO_2 abundances while the CH_4 and CO abundances decrease. Because CO decreases slightly less rapidly than CH_4, the predicted

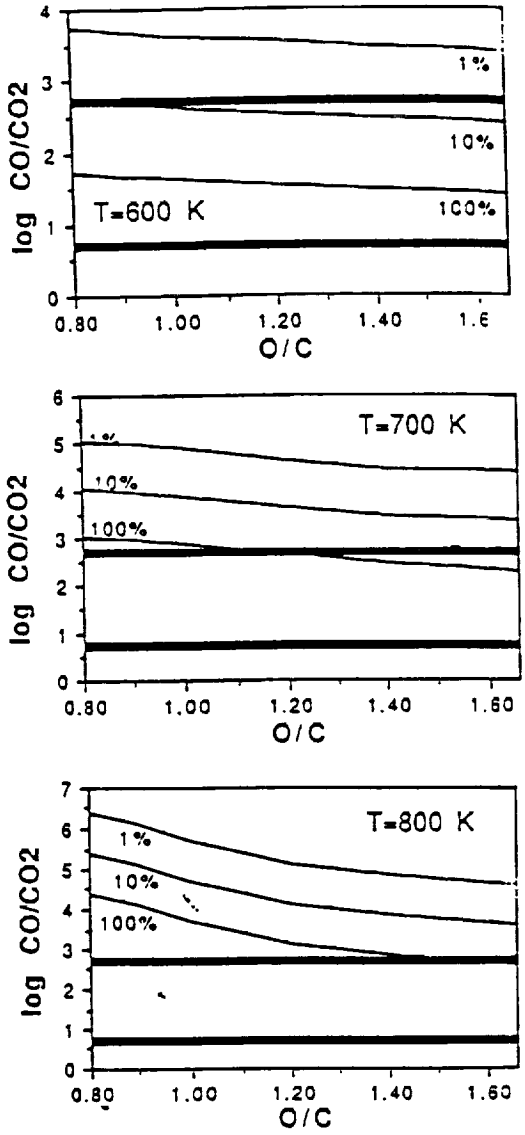

FIG. 4. Fracionated Halley values and data from our own model were calculated in the same way as described in Fig. 3. A solar origin for CO_2 in Comet Halley requires quench temperatures slightly lower than those for CH_4.

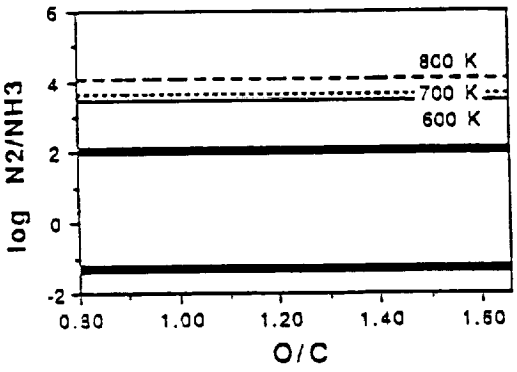

FIG. 5. Distribution of nitrogen between N_2 and NH_3 is independent of the O/C ratio.

CO/CH_4 value would increase for a given quench temperature. However the CO/CO_2 number decreases significantly. The reader can see these tendencies in Figs. 3 and 4. For the lower initial O/C of 1.66 two different quench temperatures for CO–CH_4 and CO–CO_2 interconversion were required to fit the Halley data. For O/C greater than 1.66, the quench temperatures for these two reaction schemes begin to approach each other. Otherwise, our conclusions are not qualitatively affected by the new abundance determination.

In summary, the Halley CO/CH_4 and CO/CO_2 ratios are reproduced by a nebular chemical model in which heterogeneous catalysis occurs efficiently and gases are trapped in water ice which eventually forms Halley's nucleus. The model NH_3 abundance is orders of magnitude below that seen in Halley, however.

4. IMPLICATIONS

A. Solar Nebula Origin for Volatiles in Halley

The results presented above indicate that the abundances of the carbon-bearing species CO, CO_2, and CH_4 can be accounted for by more or less traditional models of solar nebula chemistry involving equilibrium chemistry in the inner disk, quenching, and transport of gas parcels outward to the region at which Halley formed. The workability of this model hinges, however, on several assumptions or assertions:

1. Halley formed in the Uranus/Neptune region, and not at several hundred AU (this can be relaxed if nebular radial mixing is assumed to be very efficient: but see below).
2. Catalysis of chemical reactions on grains in the inner nebula was an efficient and widespread process.
3. Gases were incorporated into Halley by being trapped in water ice which favored incorporation of CH_4 over CO. CO_2 was incorporated with high efficiency largely as dry ice.

Note that constraints on nebular mixing or the radial distance of the quench zone are not very tight: Figs. 3 and 4 show that a range of mixing efficiencies could be played off against quench zone location. Likewise the results do not place firm constraints on the inner nebula elemental abundances.

The inability to explain Halley's ammonia abundance with this model forces us to consider alternatives. We favor the hypothesis that the ammonia in Halley was derived largely from the surrounding giant molecular cloud. Chemical models and observations of giant molecular clouds (Blake *et al.* 1987) suggest that NH_3 may be abundant. The amounts of methane and carbon dioxide in such clouds are not known. Inability to detect methane, even with tight observational constraints, implies that either (a) CH_4 is locked up in grains or (b) CO vastly dominates over CH_4.

To argue that Halley incorporated interstellar ammonia requires that nebular mixing be less than 100% efficient, otherwise essentially all of the ammonia which found its way into the nebula would have been cycled to high-temperature regions and recycled outward as molecular nitrogen. The recent evidence that formaldehyde is present in Halley (Mumma and Reuter 1989) tends to argue in favor of this hypothesis,

since that molecule is not expected to form in abundance in solar nebula chemical processes. Moreover, there is evidence from the Mumma and Reuter data of compositional heterogeneity across the nucleus of Halley.

We therefore postulate the following situation: The nebula is radially mixed only to a limited extent. CH_4 and CO_2 are manufactured in the inner part of the disk, transported outward past the quench zone to the region of comet formation, and trapped in ice grains which went to form the nucleus of Halley. Along with this gas was incorporated some relatively pristine giant molecular cloud material, containing NH_3, which was incorporated into Halley either in separate grains or through the gas phase. We cannot rule out the possibility that some CH_4 was also present in the unprocessed molecular cloud gas. Our results indicate to us that Halley is a hybrid, containing giant molecular cloud gas *partially* reprocessed in the inner solar nebula.

Prinn and Fegley (1989) have proposed that the reduced gases in Comet Halley are the result of chemistry occurring in the gaseous subnebulas surrounding Jupiter and Saturn, followed by sweep-up of this material (in gaseous or solid form) by solar orbiting objects. As noted by the authors, the dynamics of such processes needs to be quantified. We offer the present model for Halley's volatiles as an alternative hypothesis.

B. Drag Heating or Grains Entering the Solar Nebula

It is of interest to assess whether icy grains falling into the solar nebula from the surrounding molecular cloud could have found their way unaltered to the nucleus of Halley. Several processes may modify grains during infall: (1) grain–grain collisions, (2) accretion shock heating at the nebular boundary, and (3) drag heating of grains. We explore the third process here.

The calculations are based on a paper by Wood (1984), in which drag heating was proposed as a possible means of forming chondrules. Here we use the formalism for heating of icy grains, and add a term for sublimation of water ice. Heat gained by aerodynamic drag will be lost by radiation and sublimation; the energy balance for the grain can be described as

$$\frac{\partial T_p}{\partial t} = \frac{4\pi r_p^2}{mc}\left[\frac{\alpha\rho_g v^3}{8} - \varepsilon\sigma(T_p^4 - T_0^4) - LP_s\sqrt{\frac{\mu_g}{2\pi kT}}\right]$$

where the sublimation rate of ice is given by

$$\frac{\partial m}{\partial t} = P_s\sqrt{\frac{\mu_g}{2\pi kT}}\,4\pi r_p^2$$

T_p, r_p, v, m, and c are particle temperature, radius, velocity, mass, and specific heat; μ_g and ρ_g are the gas molecular mass and density (the latter set here to a value of 10^{-11} g/cm^3). T_0 is the background radiation temperature (10°K); L and P_s are the latent heat of sublimation and the vapor pressure. Finally α, ε, σ, and k are the accommodation coefficient (set to 0.5), the thermal emissivity, the Stephan–Boltzmann constant, and the Boltzmann constant. The equations are solved iteratively with the temperature T_p as the independent variable. After each time step the sublimed mass was subtracted from the original mass and the new particle radius and velocity were calculated. The radiative properties of a particle depend strongly on the particle size through the emissivity. For a 1-mm particle (probably larger than most interstellar grains) an emissivity of 0.75 was assumed (Wood 1984); for r_p = 50 nm, ε = 0.01 (Greenberg 1978). Thus small particles are poor radiators and hence sublime more rapidly than larger particles.

Particles falling onto the accretion disk have infall velocities dependent on their final radial distance from the disk center. A final orbital distance of 15–20 AU corresponds to an infall velocity of 6 km/sec, whereas 1 km/sec corresponds to several thousand AU. These velocities are conser-

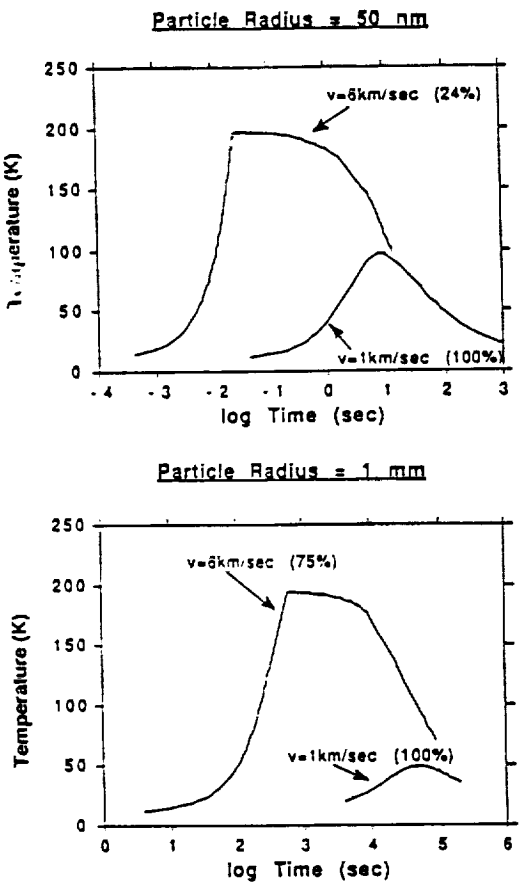

FIG. 6. For two different particle velocities, the heating characteristics of these particles during infall onto the accretion disk are shown.

vative, in the sense that they assume zero initial velocity contributed by random motions (or energetic processes) within the molecular cloud itself. Figure 6 shows the temperature rise versus time for the two different particle sizes given above. For each size, curves corresponding to the two infall velocities 1 and 6 km/sec are shown. The amount of mass remaining after heating and sublimation is shown for each curve, expressed as a percentage of the original mass of the particle.

The results indicate that while significant release of volatiles accompanies drag heating of infalling particles, some mass survives in both the large- and small-particle cases. However, peak temperatures are high enough that molecules loosely bound to the interstellar grains would be released into the gas phase. Sublimation moderates the temperature rise to a great degree, such that some amorphous ice could have survived entry into the solar nebula. Other mechanisms for heating infalling grains, such as accretion shock, have yet to be explored.

5. CONCLUSIONS AND PROSPECTS

A model of equilibrium chemistry in the solar nebula was combined with considerations of nebular mixing, elemental abundance variation, and fractionation effects associated with trapping of gases in water ice to predict the inventory of major carbon- and nitrogen-bearing molecules at 20 AU, assumed here to be roughly the region within which Halley formed. For a range of nebular mixing efficiencies and elemental O-to-C ratios, the Halley data on the CO, CO_2, and CH_4 abundances could be reproduced fairly well. However, the predicted NH_3 abundance falls far short of that inferred for Halley. We adopt the alternative hypothesis that the ammonia is preserved from the giant molecular cloud within which the solar nebula is embedded. Infall of grains and consequent drag heating are sufficient to release volatile gases into the nebula, as well as sublime much of the water; however, remnants of interstellar grains, including amorphous ice, could have in part survived.

The comparison with Halley data is to a large extent stymied by uncertainties in the true parent molecule abundances in that comet and the lack of knowledge of the manner by which the volatile gases were trapped in the nucleus. It is also unclear how typical the composition of Halley may be. Perhaps not unexpectedly, significant developments in ground-based observations of comets accompanied the International Halley Watch program and associated spacecraft flybys. It is hoped that in the next few years these techniques will be brought to bear on a number of comets to assemble a good sample of inventories of water, ammonia, methane,

carbon monoxide, formaldehyde, and other volatile species accessible to remote studies.

The next breakthrough in nucleus studies may have to await the Comet Rendezvous Asteroid Flyby Mission (CRAF). The CRAF penetrator will carry a suite of instruments designed to determine the ice structure and the manner in which volatiles are trapped in a subsurface nucleus sample. An extensive inventory of parent molecules will be accumulated. Other experiments on the Mariner Mark II spacecraft will involve detailed chemical studies of the dust particles emitted from the nucleus. These types of observations are required to tightly constrain the type of modeling attempted here. It is to be hoped that the calculations presented above give at least a flavor of the kinds of information which could be derived on cometary formation from the CRAF mission, and others such as the Rosetta comet nucleus sample return, to follow.

ACKNOWLEDGMENTS

Ronald Prinn, Michael Mumma, Harold Weaver, Bruce Fegley, Akiva Bar-Nun, William Irvine, and Alan Stern provided very helpful comments on this work. Our effort is supported in part by NASA Grant NAGW-1039 from the Planetary Atmospheres Program and the Geology and Geophysics Program.

REFERENCES

ANDERS, E., AND N. GREVESSE 1989. Abundances of the elements: Meteoritic and solar. *Geochim Cosmochim. Acta* 53, 197–214.

BAR-NUN, A., AND I. KLEINFELD 1989. On the temperature and gas composition in the region of comet formation. *Icarus* 80, 243–253.

BLAKE, G. A., E. C. SUTTON, C. R. MASSON, AND T. G. PHILLIPS 1987. Molecular abundances in OMC-1: The chemical composition of interstellar molecular clouds and the influence of massive star formation. *Astrophys. J.* 315, 621–645.

BOSS, A. P. 1988. Angular momentum transport by gravitational torques in the early solar nebula. *Lunar Planet. Sci. XIX*. 122–123.

CAMERON, A. G. W. 1978. The primitive solar accretion disk and the formation of the planets. In *The Origin of the Solar System* (S. F. Dermott, Ed.), pp. 49–75. Wiley, New York.

DUNCAN, M. 1989. The origins of short- and long-period comets. *Bull. Amer. Astron. Soc.* 21, 781.

FEGLEY, B., JR., AND R. G. PRINN 1989. Solar nebula chemistry: Implications for volatiles in the solar system. In *The Formation and Evolution of Planetary Systems* (H. A. Weaver, L. Danly, and F. Paresce, Eds.). Cambridge Univ. Press, London/New York. pages 171–211.

GREENBERG, J. M. 1978. In *Cosmic Dust* (J. A. M. McDonnell, Ed.), p. 187. Wiley, Chichester.

HOBBS, P. V. 1974. *Ice Physics*. Oxford Univ. Press (Clarendon), London.

JANAF Thermochemical Tables, 2nd ed. 1971. National Standard Reference Data Service, U.S. National Bureau of Standards, No. 37.

LEWIS, J. S., AND R. G. PRINN 1980. Kinetic inhibition of CO and N_2 reduction in the solar nebula. *Astrophys. J.* 238, 357–364.

LUNINE, J. I. 1989. Primitive bodies: Molecular abundances in Comet Halley as probes of cometary formation environments. In *The Formation and Evolution of Planetary Systems* (H. A. Weaver, L. Danly, and F. Paresce, Eds.), pp. 213–242. Cambridge Univ. Press, London/New York.

LUNINE, J. I., AND D. J. STEVENSON 1985. Thermodynamics of clathrate hydrate at low and high pressures with application to the outer solar system. *Astrophys. J. Suppl.* 58, 493–531.

MARCONI, M. L., AND D. A. MENDIS 1988. On the ammonia abundance in the coma of Halley's comet. *Astrophys. J.* 330, 513–517.

MAYER, E., AND R. PLETZER 1986. Astrophysical implications of amorphous ice: A microporous solid. *Nature* 319, 298–301.

MUMMA, M. J., W. E. BLASS, H. A. WEAVER, AND H. P. LARSON 1989. Measurements of the *ortho–para* ratio and nucleus spin temperature of water vapor in comets Halley and Wilson (1986L) and implications for their origin and evolution. In *The Formation and Evolution of Planetary Systems* Conference Abstract Book.

MUMMA, M. J., AND D. C. RELTER 1989. On the identification of formaldehyde in Halley's comet. *Astrophys. J.*, in press.

PRINN, R. G. 1990. On neglect of non-linear momentum terms in solar nebula accretion disk models. *Astrophys. J.* 348, 725–729.

PRINN, R. G., AND M. B. FEGLEY 1981. Kinetic inhibition of CO and N_2 reduction in circumplanetary nebulae: Implication for satellite composition. *Astrophys. J.* 249, 308–317.

PRINN, R. G., AND B. FEGLEY, JR. 1989. Solar nebula chemistry: Origin of planetary, satellite and cometary volatiles. In *Origin and Evolution of Planetary and Satellite Atmospheres* (S. K. Atreya, J. B. Pollack, and M. S. Matthews, Eds.). Univ. of Arizona Press, Tucson, pp. 78–136.

RUBIN, A. E., B. FEGLEY, AND R. BRETT 1988. Oxidation state in chondrites. In *Meteorites and the Early Solar System* (J. F. Kerridge and M. S. Matthews, Eds.), pp. 488–511. Univ. of Arizona Press, Tucson.

S[illegible]SE 1989. *Laboratory Research for Planetary Atmospheres*. NASA Planetary Atmospheres Program Office.

STERN, S. A., AND J. M. SHULL 1988. The influence of supernovae and passing stars on comets in the Oort cloud. *Nature* 332, 407–411.

STEVENSON, D. J. 1990. Chemical heterogeneity and imperfect mixing in the solar nebula. *Astrophys. J.* 348, 730–737.

STEVENSON, D. J., AND J. I. LUNINE 1988. Rapid formation of Jupiter by diffusive redistribution of water vapor in the solar nebula. *Icarus* 75, 146–155.

S[illegible]OM, S. E., S. EDWARDS, AND K. M. STROM 1989. Constraints on the properties and environment of primitive solar nebulae from the astrophysical record provided by young stellar objects. In *The Formation and Evolution of Planetary Systems* (H. A. Weaver, L. Danly, and F. Paresce, Eds.). Cambridge Univ. Press, London/New York, pp. 91–109.

VANNICE, M. A. 1975. The catalytic synthesis of hydrocarbons from H_2/CO mixtures over the group VIII metals. *J. Catal.* 37, 449–461.

WEAVER, H. A. 1989. The volatile composition of comets. *Highlights Astron.*, in press.

WEISSMAN, P. R. 1985. The origin of comets: Implications for planetary formation. In *Protostars and Planets II* (D. C. Black and M. S. Matthews, Eds.). pp. 895–919. Univ. of Arizona Press, Tucson.

WOOD, J. A. 1984. On the formation of meteoritic chondrules by aerodynamic drag heating in the solar nebula. *Earth Planet. Sci. Lett.* 70, 11–26.

WOOD, J. A., AND G. E. MORFILL 1988. A reivew of solar nebula models. In *Meteorities and the Early Solar System* (J. F. Kerridge and M. S. Matthews, Eds.), pp. 329–347. Univ. Arizona Press, Tucson.

WYCKOFF, S., L. LINDHOLM, P. A. WEHINGER, B. A. PETERSON, J.-M. ZUCCONI, AND M. C. FESTOU 1989. The $^{12}C/^{13}C$ abundance ratio in Comet Halley. *Astrophys. J.* 339, 488–500.

Reports

Vertical Distribution of Water in the Atmosphere of Venus: A Simple Thermochemical Explanation

JOHN S. LEWIS AND DAVID H. GRINSPOON*

Several lines of evidence concerning the vertical abundance profile of water in the atmosphere of Venus lead to strikingly unusual distributions (the water vapor abundance decreases sharply in the immediate vicinity of the surface) or to serious conflicts in the profiles (different infrared bands suggest water abundances that are discrepant by a factor of 2.5 to 10). These data sets can be reconciled if (i) water molecules associate with carbon dioxide and sulfur trioxide to make gaseous carbonic acid and sulfuric acid in the lower atmosphere, and (ii) the discrepant 0.94-micrometer water measurements are due to gaseous sulfuric acid, requiring it to be a somewhat stronger absorber than water vapor in this wavelength region. A mean total water abundance of 50 ± 20 parts per million and a near-surface free water vapor abundance of 10 ± 4 parts per million are derived.

THE SURFACE TEMPERATURE OF VENUS is roughly 750 K, far too high for the presence of liquid water: any water present would at once boil away and exist as water vapor in the atmosphere. But it is also well established that the atmosphere of Venus is extremely dry: whereas heating Earth to the temperature of Venus would produce a very wet atmosphere with a surface partial pressure of water vapor of about 300 atm, typical estimates of the water partial pressure on Venus are near 3×10^{-3} atm, fully 10^{-5} as much. But almost as interesting as the extraordinary aridity of Venus is the serious disagreement among the results of the several experiments that have attempted to measure the water abundance below the clouds. This problem is reviewed in detail by von Zahn *et al.* (*1*).

Very high water concentrations of several thousand parts per million were reported as a result of the Pioneer Venus gas chromatograph (PVGC) experiment (*2*), whereas all other direct measurements of the water content lie in the range from 20 to 200 ppm. The PVGC experimenters pointed out, however, that their high value could be caused by the slow evaporation of sulfuric acid (H_2SO_4) droplets ingested during passage through the clouds. Another, less direct, measurement was carried out by the infrared net flux radiometers on the four Pioneer Venus (PV IR) entry probes (*3*). The absolute fluxes measured below the clouds were much too large to be reasonable and increased with depth. Large corrections were applied to the data on the basis of a proposed error source, but even the corrected data show many cases in which the flux increases with depth. The results for the four probes were found to be extremely discordant, suggesting water-mixing ratios from 10 to over 1000 ppm. For these reasons, we shall attempt no quantitative explanation of the PVGC or PV IR radiometer data.

The most sensitive measurements bearing on the water abundance in the lower atmosphere of Venus, infrared spectra returned by the Soviet Venera 11 entry probe (*4*), cover a spectral region (0.7 to 1.25 μm) within which one weak (0.82 μm) and two strong (0.94 and 1.13 μm) water bands are found. The intensity of transmitted sunlight was measured from an altitude of over 61 km down to the planetary surface. Below an altitude of about 44 km, just below the base of the H_2SO_4 cloud layer, we would normally expect the mole fraction of water vapor to be independent of altitude. Preliminary interpretation of these bands (*4*), however, showed clearly that such homogeneous models did only a poor job of explaining the data. Models in which the water mole fraction increased with altitude, from about 20 ppm at the surface to about 200 ppm at the cloud base, gave an improved but not convincing fit. The water vapor profiles that fitted the 0.94-μm data best had the unfortunate property that they seemed quite unphysical. In a search for "hydrogen-hiding" reactions with other known or suspected atmospheric constituents (C, N, O, S, F, Cl, As, Sb, and P compounds), no explanation for such a strange water distribution could be found.

A much more thorough interpretation of the Venera 11 data (*5*) refined the dilemma. It was found that (i) if it was assumed that all the opacity in the Venera 11 spectral region was due to carbon dioxide (CO_2) and H_2O, the data for the 0.94-μm band required a vertical variation in the water abundance from about 20 ppm at the surface to a peak value of about 200 ppm near the cloud base at 44 km, with the abundance dropping off again above the clouds to below 30 ppm near 60 km (Fig. 1); (ii) the 0.84- and 1.13-μm bands, although not analyzable with the same precision, were compatible with average water abundances of about 20 ppm, an amount insufficient to provide even half the equivalent width of the 0.94-μm band. This result clearly implied a contribution from an absorber other than water in the 0.94-μm band, but no such species could be identified: however, the correlation of the gaseous absorption maximum with the cloud base suggested the possibility of a gaseous absorber formed by evaporation of H_2SO_4 cloud droplets (*5*). If, rather unreasonably, we ignore the estimate of 20 ppm given by the 0.84- and 1.13-μm bands and attribute all of the 0.94-μm opacity to water vapor, then the average water abundance (integrated over the altitude range from 0 to 70 km) would be 43 ppm. A lower limit on the water abundance would be set by attributing the excess (discordant) opacity in the 0.94-μm band near an altitude of 44 km to some other species besides water. Then the altitude-averaged water abundance required to explain the rest of the 0.94-μm opacity is near 24 ppm.

We have developed a model of the chemical behavior of water on Venus (*6*), based on laboratory data for the thermodynamics of the gas-phase reaction

$$H_2O + SO_3 = H_2SO_4 \qquad (1)$$

on the vapor pressure of H_2SO_4 (*7*, *8*), and on the stability of the gaseous carbonic acid (H_2CO_3) molecule,

$$H_2O + CO_2 = H_2CO_3 \qquad (2)$$

which has recently been characterized (*9*). We use a standard enthalpy change of $\Delta H^0_{298} = -22.7$ kcal mol^{-1} and an entropy change of $\Delta S^0 = -34.42$ cal mol^{-1} K^{-1} for reaction 1 (*6*), and $\Delta H^0_{298} = 6$ kcal mol^{-1} and $\Delta S^0 = 2$ cal mol^{-1} K^{-1} for reaction 2 (*10*).

Venus atmospheric models were calculated for water-mixing ratios ranging from 20

Lunar and Planetary Laboratory, University of Arizona, Tucson, AZ 85721.

*Present address: National Aeronautics and Space Administration, Ames Research Center, MS 245-3, Moffett Field, CA 94035

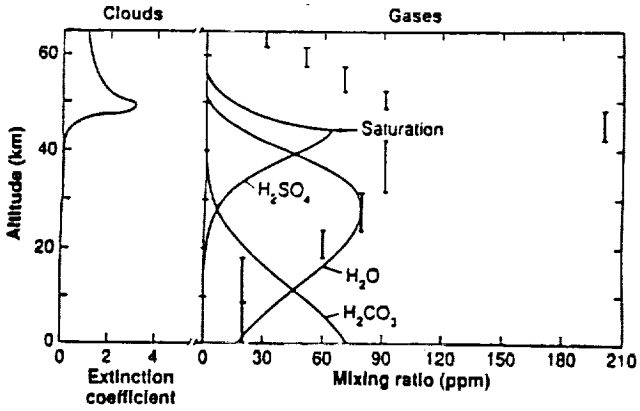

Fig. 1. Vertical distribution of water on Venus inferred from the Venera 11 and 12 infrared scanning photometer for a ten-layer model atmosphere (*5*). The Venera data (*4*, *5*) show a wide variation from layer to layer, with a striking minimum at the surface and a strong "spike" near an altitude of 45 km. Calculated profiles of the gases H_2CO_3, H_2O, and H_2SO_4 are shown (assuming a total of 90 ppm water) for the model described in the text. The smoothed cloud density is given for reference on the left side of the diagram (*20*).

to 200 ppm. In our first models we made the simplifying assumption that in the vicinity of the clouds the abundances of both water and sulfur trioxide (SO_3) were derived from the evaporation and dissociation of H_2SO_4 and hence were equal (an excess of water is more probable). The results of such a calculation for a water abundance of 90 ppm are shown in Fig. 1.

Several generalizations emerge from this and other calculated models. First, the depletion of water vapor near the ground can be ascribed to the formation of gaseous H_2CO_3. Second, SO_3 and water vapor have negligible affinity near the surface, and thus H_2SO_4 vapor reaches 1 ppm only near an altitude of 21 km. Third, gaseous H_2SO_4 is extremely stable in the vicinity of the cloud base, reaching 63 ppm (versus 27 ppm for water vapor) near 44 km. The anomalous (excess) 0.94-μm absorption peak corresponds almost perfectly with the calculated profile of gaseous H_2SO_4. This finding strongly suggests that H_2SO_4 vapor, or some other gas derived directly from it, is responsible for the very high spike in the 0.94-μm absorption. Fourth, the column-average free water vapor abundance for this model is 36 ppm, compared to the assumed total water abundance of 90 ppm: 60% of the total water is bound to CO_2 or SO_3 (principally the former). The percentage of free water is model-independent because the equilibrium expressions for reaction 2 gives a H_2O:H_2CO_3 ratio that is independent of the total water abundance. Therefore, the lower limit on free water set above by omitting the 45-km "spike" then suggests a minimum total water abundance of 24/0.6 = 40 ppm, and the free water abundance of 20 ppm deduced from the 0.82- and 1.13-μm bands implies a total water abundance of 20/0.6 = 33 ppm. Precisely at the surface, fully 80% of the total water is bound to CO_2. All these results are extremely insensitive to plausible errors in the thermodynamic data used (*11*). Finally, the falloff of the water abundance above the clouds is governed by the vapor pressure of water over concentrated H_2SO_4, as has been long accepted (*1*), and no new modeling of this familiar phenomenon was attempted.

The altitude at which H_2SO_4 saturates to make constant-boiling (98% by weight) H_2SO_4 droplets is a sensitive function of the gaseous H_2SO_4 abundance. Steffes (*8*) has shown from vapor pressure arguments that 15 to 30 ppm H_2SO_4 would not only provide saturation above altitudes of 46 to 48 km, but that this amount of H_2SO_4 vapor would also account for the microwave absorption seen in spacecraft occultation experiments.

In light of the present model, it is interesting to reexamine the other sources of data on the water abundance below the Venus clouds. Figure 2 summarizes the results from the Venera 11 and 12 mass spectrometers (*12*), the Venera 12 gas chromatograph (*13*), the Pioneer Venus Large Probe Mass Spectrometer (LMS) (*14*), and, for comparison, the Venera 11 and 12 infrared photometer data for the same altitudes (*4*, *5*). Our model suggests that the striking discordance between these experimental results is due to the complex and unexpected altitude-dependent speciation of water. Our model predicts that there should be an altitude interval (19 to 35 km) within which at least 70% of the total water is in the form of free H_2O vapor. It is satisfying to find that the data from these six experiments are concordant within (and only within) this altitude interval. We therefore use the four reported detections of water in this region, plus the lower limits discussed above, to estimate a total water content in the range from 30 to 70 ppm.

At the surface the nominal percentage of total water bound in gaseous H_2CO_3 is 80%. Allowing an uncertainty of a factor of 3 in the equilibrium constant for reaction 2 [in accord with the estimates of gaseous H_2CO_3 abundance given in (*9*)], the fraction of total water bound as H_2CO_3 at the surface of Venus must lie in the range 80^{+13}_{-20}%. The correct water partial pressure to use in equilibrium treatments of the chemical interaction of atmospheric gases with crustal minerals is then 10^{+10}_{-5} ppm. Discussions with Donahue (*15*) have revealed that the Pioneer Venus LMS experiment did not provide direct evidence for the $H_2CO_3^+$ ion near the surface of Venus, but the speciation of gaseous H_2CO_3 in the LMS inlet system and ionization region is quite unknown. The abundance of free hydrogen seen by the LMS varies rapidly and (apparently) inexplicably with altitude in the same altitude range where we predict abundant H_2CO_3 vapor. These data remain unpublished.

We conclude that the 0.94-μm band measures opacity due not only to CO_2 and water vapor but also to some other cloud-related species such as gaseous H_2SO_4. The general trends evident in the Venera 11 infrared data, including both the complex altitude dependence of opacity and the impossibility of reconciling the 0.84- and 1.13-μm data with free water abundances much larger than 20 ppm, are all readily comprehensible when formation of gaseous H_2SO_4 and H_2CO_3 is considered. Laboratory study of the near-infrared absorption spectrum of

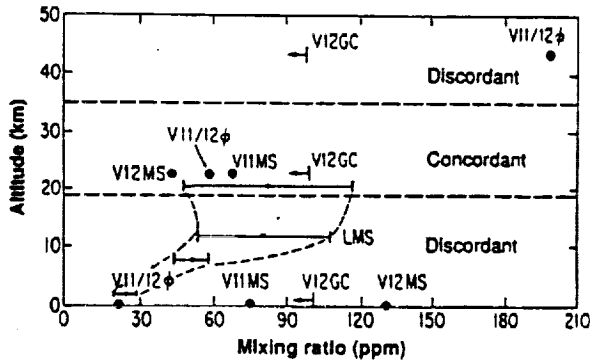

Fig. 2. Comparison of water abundance determinations for the atmosphere of Venus beneath the main cloud layer. The Venera 11 (V11) and Venera 12 (V12) entry probe experiments that provided these data are the infrared photometer (φ) (*4*, *5*), the mass spectrometer (MS) (*12*), and the gas chromatograph (GC) (*13*) experiments. The Pioneer Venus LMS data are given with the original authors' error bars (*14*). Because of the unanticipated complexity of the speciation of water, these experiments yielded highly discordant results. However, the region from 19 to 35 km, where free water vapor dominates and complexes are minor, yielded concordant estimates of the water abundance.

H_2SO_4 vapor and related compounds could permit a quantitative interpretation of the Venus spectrum, and is strongly encouraged. The near-surface association of CO_2 and water vapor is a direct result of our acceptance of the data of Terlouw *et al.* (*9*). It is critically important that the equilibrium behavior of this system be confirmed by further experiments. One can also directly test this model by using Venus water profiles to be measured by the Near Infrared Mapping Spectrometer experiment on the Galileo spacecraft (*16*). Further, the conditions of temperature and pressure and the high CO_2 and water vapor abundances conducive to extensive gaseous H_2CO_3 formation are closely similar to those hypothesized for early Earth. An improved understanding of the thermochemical and optical properties of this species may permit substantial improvement of these models.

REFERENCES AND NOTES

1. U. von Zahn, S. Kumar, H. Niemann, R. Prinn, in *Venus*, D. M. Hunten, L. Colin, T. M. Donahue, V. I. Moroz, Eds. (Univ. of Arizona Press, Tucson, 1983), pp. 299–430.
2. V. I. Oyama *et al.*, *J. Geophys. Res.* **85**, 7891 (1980).
3. H. E. Revercomb, L. A. Sromovsky, V. E. Suomi, *Icarus* **61**, 521 (1985).
4. V. I. Moroz, N. A. Parfent'ev, N. F. San'ko, *Cosmic Res. (U.S.S.R.)* **17**, 601 (1979).
5. L. D. G. Young, A. T. Young, L. V. Zasova, *Icarus* **60**, 138 (1984).
6. J. L. Gmitro and T. Vermeulen, *Am. Inst. Chem. Eng. J.* **10**, 740 (1964).
7. G. P. Ayers, R. W. Gillett, J. L. Gras, *Geophys. Res. Lett.* **7**, 433 (1980).
8. P. G. Steffes, *Icarus* **64**, 576 (1985).
9. J. K. Terlouw, C. B. Lebrilla, H. Schwartz, *Angew. Chem. Int. Ed. Engl.* **26**, 354 (1987).
10. Terlouw *et al.* (*9*) found in the mass spectrum of NH_4HCO_3 vapor (at 120 K) a peak for H_2CO_3 with a peak area somewhat less than 1% of that for CO_2. Vapor pressure data on NH_4HCO_3 (*17*) give a Gibbs free energy of vaporization to NH_3, H_2O, and CO_2 of −4600 cal mol^{-1} at 120 K. Because of the very large theoretical activation energy of at least 40 kcal mol^{-1} for dissociation of gaseous H_2CO_3 into water vapor and CO_2 (*18*), we assume that the CO_2:H_2CO_3 ratio was fixed at about 5×10^{-3} in the evaporation chamber rather than in the mass spectrometer. In combination with a $\Delta H^\circ_{f_{298}}$ of −146.1 kcal mol^{-1} for formation of H_2CO_3 from the elements (*9*) and a $\Delta H^\circ_{f_{298}}$ of −152.1 kcal mol^{-1} for gaseous CO_2 plus H_2O from the JANAF tables (*19*), we deduce an enthalpy change at 400 K of 6 kcal mol^{-1} and an entropy change of 2 cal mol^{-1} K^{-1} for reaction 2.
11. As a sensitivity test, we calculated a large number of models without using laboratory thermodynamic data on H_2CO_3 and H_2SO_4 vapors. Instead, grids of enthalpy and entropy values for both reactions were systematically explored to see which values could give a satisfactory fit to the Venus water profile. We found that the ranges of best-fit thermodynamic properties required to fit the Venus observations were extremely close to the published laboratory data.
12. V. G. Istomin, K. V. Grechev, V. A. Kochnev, *Space Res.* **20**, 215 (1980).
13. B. G. Gel'man *et al.*, *ibid.*, p. 219.
14. J. H. Hoffman, R. R. Hodges, Jr., T. M. Donahue, M. B. McElroy, *J. Geophys. Res.* **85**, 7882 (1980).
15. T. M. Donahue, personal communications.
16. J. B. Pollack, personal communication.
17. W. K. Hutchison, *J. Chem. Soc.* **1931**, 410 (1931); T. Stobiecki, A. Baranski, Z. Kowalski, *Chem. Stosow.* **1**, 81 (1957).
18. See, for example, M. T. Nguyen and T.-K. Ha, *J. Am. Chem. Soc.* **106**, 599 (1984).
19. *JANAF* (Joint Army–Navy–Air Force) *Thermochemical Tables* (Dow Chemical Company, Midland, MI, 1973).
20. L. W. Esposito, R. G. Knollenberg, M. Ya. Marov, O. B. Toon, R. P. Turco, in *Venus*, D. M. Hunten, L. Colin, T. M. Donahue, V. I. Moroz, Eds. (Univ. of Arizona Press, Tucson, 1983), pp. 484–564.

21. We thank K. Vemulapalli, D. M. Hunten, A. T. Young, and J. Kasting for helpful discussions.

4 December 1989; accepted 16 May 1990

Negative Pressure-Temperature Slopes for Reactions Forming $MgSiO_3$ Perovskite from Calorimetry

E. Ito, M. Akaogi, L. Topor, A. Navrotsky

A new and sensitive differential drop solution calorimetric technique was developed for very small samples. A single experiment using one 5.18-milligram sample of perovskite, synthesized at 25 gigapascals and 1873 Kelvin, gave 110.1 ± 4.1 kilojoules per mole for the enthalpy of the ilmenite-perovskite transition in $MgSiO_3$. The thermodynamics of the reaction of $MgSiO_3$ (ilmenite) to $MgSiO_3$ (perovskite) and of Mg_2SiO_4 (spinel) to $MgSiO_3$ (perovskite) and MgO (periclase) were assessed. Despite uncertainties in heat capacity and molar volume at high pressure and temperature, both reactions clearly have negative pressure-temperature slopes, −0.005 ± 0.002 and −0.004 ± 0.002 gigapascals per Kelvin, respectively. The latter may be insufficiently negative to preclude whole-mantle convection.

$MgSiO_3$-RICH PEROVSKITE IS thought to dominate the earth's lower mantle (*1*). Knowing its stability is crucial for understanding the seismic discontinuity near 650 km and for predicting lower mantle properties. The pressure-temperature (P-T) slope (dP/dT) of reactions forming perovskite may help determine whether the mantle is compositionally layered or whether whole mantle convection can occur; a strongly negative slope would inhibit convection across the boundary (*2*, *3*). The nature of convection has important implications for the evolution of the earth, its heat budget, and the coupling of convection in the core to processes in the mantle and crust.

Ito and Yamada (*4*) first demonstrated that for the transformations of $MgSiO_3$ ilmenite to perovskite and of Mg_2SiO_4 spinel to perovskite and periclase, have negative slopes ($dP/dT < 0$) and that both reactions occur at similar pressures and temperatures. Ito and Takahashi (*5*) refined these observations. They concluded that the pronounced sharpness of the 650-km discontinuity can be reasonably interpreted as the dissociation of silicate spinel into perovskite plus magnesiowustite. Although their data suggest that dP/dT is negative, pressure and temperature determinations in multianvil devices still have considerable uncertainties, and phase boundary reversals are difficult. Thus, the slope of the perovskite-forming reaction has remained somewhat uncertain. Because of the importance of this slope in considerations of whole mantle convection, it is desirable to determine dP/dT by a different and independent method, in order to test whether the phase synthesis runs were indeed close to equilibrium, to confirm that the slope is negative, and to obtain a reliable value for dP/dT.

High-temperature oxide melt solution calorimetry (*6*) offers a means of obtaining thermochemical data for high-pressure silicates (*7–9*). However, in order to apply this technique to the very small amounts of $MgSiO_3$ perovskite obtainable by synthesis at 25 GPa in a multianvil apparatus, its sensitivity had to be improved. In this report, we describe a new differential drop-solution technique and report a calorimetric determination, using 5 mg of perovskite, of the enthalpy difference between $MgSiO_3$ pyroxene and perovskite. Combination with earlier thermodynamic data (*7–10*) allows calculation of the stability fields of $MgSiO_3$ perovskite and comparison with high-pressure studies.

E. Ito, Institute for Study of the Earth's Interior, Okayama University, Misasa, Tottoriken, 682 02, Japan.
M. Akaogi, Department of Chemistry, Gakushuin University, Tokyo 171, Japan.
L. Topor and A. Navrotsky, Department of Geological and Geophysical Sciences, Princeton University, Princeton, NJ 08544.

ICARUS 89, 93–112 (1991)

Rheological Properties of Ammonia–Water Liquids and Crystal–Liquid Slurries: Planetological Applications

J. S. KARGEL, S. K. CROFT, J. I. LUNINE, AND J. S. LEWIS

Lunar and Planetary Laboratory, University of Arizona, Tucson, Arizona 85721

Received April 25, 1990; revised August 24, 1990

The viscosities of aqueous mixtures plausibly representing a range of cryovolcanic substances seen on the icy satellites have been measured in the laboratory or obtained from literature sources. These viscosities range from 10^{-2} poise (pure water) to 10^{2} poises (ammonia–water peritectic) to about 10^{5} poises (ammonia–water–methanol peritectic). The viscosities of the liquid mixtures examined in this work are much greater than would be expected based on the assumption that the end member molecules are noninteractive. This observation supports others based on molar volumes and vapor pressure relations indicating that strong molecular interactive forces exist and have an important bearing on the physical properties of the mixtures. With supercooling and/or partial crystallization, these substances may attain viscosities several orders of magnitude greater than those given above. The rheological effects of partial crystallization parallel the same effects in silicate lavas, so it is reasonable to interpret cryovolcanic morphologies on the icy satellites in the same ways that we interpret remotely observed silicate volcanic morphologies on the Earth and terrestrial planets, after accounting for differences in surface gravities and lava densities, and allowing for uncertainties in surface slopes and extrusion rates. Given the wide range of viscosities for simple aqueous mixtures, and the rheological effects of realistic thermal states, the characteristics of observed cryovolcanic flows and resurfaced plains on the icy satellites can be understood within the framework of conventional magmatic processes working on exotic icy substances.

1. INTRODUCTION

The reconnaissance of the Voyager spacecraft through the outer solar system revealed an unexpected diversity and intensity of internally driven modifications to the surfaces of icy satellites. Pre-Voyager theoretical arguments suggested that some of the icy satellites might have been volcanically ("cryovolcanically") active at some point, where the "lava" was water or some cryogenic liquid such as ammonia–water (Lewis 1972, Consolmagno and Lewis 1978). Voyager's observations have confirmed these early suspicions, but have further indicated that cryovolcanic processes are complex and varied and have combined with tectonic and other processes to produce a bewildering variety of bizarre landscapes, each unique in its own expression.

Our present understanding of icy satellites does not lend itself to a good predictive understanding of the geological styles of icy satellites. The genesis of the many distinctive landforms and landscapes must, however, relate in some way to important intersatellite variable parameters including satellite radius, surface gravity, rock : ice ratio, heat source, and ice composition. Ice and cryolava compositions and composition-dependent rheologies are likely to be of particular importance for satellites with histories of cryovolcanism. However, our present knowledge of solid–liquid phase equilibria and other physicochemical properties of volatile assemblages relevant to cryovolcanism lags at least 60 years behind our equivalent knowledge of silicate properties relevant to terrestrial igneous processes.

This report is the second from our group attempting to redress some important deficiencies. In an earlier paper we presented the equations of state for ammonia–water liquids (Croft *et al.* 1988). Here, we present rheological data for ammonia–water liquids and partially crystallized slurries and apply these data to matters pertaining to cryovolcanism. We extend our report to include ammonia–water–methanol liquids, taking methanol to be representative of many possible ammonia–water-soluble chemical components likely to be present in minor or trace amounts in icy satellites. (Other likely components include $(NH_4)_2S$, NH_4CN, $(CH_2)_6N_4$, NaCl, NH_4Cl, $(NH_4)_2SO_4$, amino acids, and many others; Kargel 1988, 1990.) We also summarize data from the literature for other substances so as to provide an overview of the extreme rheological range of plausible cryovolcanic agents.

Previous work on the viscosities of superliquidus ammonia–water liquids include two reports from the Russian literature (Pleskov and Igamberdyev 1939, Pinevich 1948) and, more recently, an abstract by McKinnon and Meadows (1984). The Russian workers were concerned with viscosities at temperatures above 200 K, although McKin-

0019-1035/91 $3.00

non and Meadows extrapolated their data down in temperature and through composition to the ammonia–water eutectic and estimated viscosities similar to those reported here from direct measurements.

2. EXPERIMENTAL

The rheologies of ammonia–water and ammonia–water–methanol liquids and liquid–crystal slurries were investigated using the falling sphere and rotating disk methods.

2.1 Rotational Viscometry

These measurements were obtained with an HB Model Brookfield viscometer. This instrument measures the resistance encountered by cylindrical and disk-like spindles rotating in a viscous medium contained in a coaxial cylindrical vessel. All of the measurements reported here were made with Brookfield's largest spindle ("HB1"). This spindle is classified as a disk spindle, although it actually is a short cylinder, 5.6 cm in diameter, 2.3 cm high, and mounted on a coaxial cylindrical shaft 0.3 cm in diameter. The geometry is rather complex, so the conversion from rotation rates and applied torque to absolute viscosities is by the manufacturer's calibration rather than from first principles.

Viscosity was measured as functions of temperature, composition, strain rate, and degree of partial crystallization (Table I). Measurements at three or more different spindle rotation rates for each composition and temperature allowed departures from Newtonian viscous behavior to be detected and quantified (Newtonian behavior was observed in all samples except for some partially crystallized slurries, as described below). For a consistent and simple presentation, all viscosities reported in Table I were either obtained with the spindle rotating at 20 revolutions per minute, or were reduced to 20 rpm using a power-law extrapolation or interpolation of data obtained at other rotation rates; to complete the rheological description of non-Newtonian slurries the power-law exponent, n, is also given in Table I (these details are irrelevant when the substance rheology is Newtonian, in which case $n = 1$ and the viscosity alone is sufficient to describe the rheology).

The range of reliable viscosities obtained with this instrument is from about 1 to 10^3 poises (10 poise = 1 Pa-sec). Instrumental precision may, in principle, approach 1% at full scale torque. In practice, measurements were repeatable to about ±3% to ±15%, 8% being most typical. These larger figures include the fact that torque was most typically not at full scale, and include uncertainties in the temperature and composition of the liquid (see below) as well as other experimental sources of error.

Each run used about 1400 ml of solution contained in a closed and insulated cylindrical polyethylene vessel with

TABLE I
Ammonia–Water Viscosities Obtained by Rotational Viscometry

Composition (wt.% NH_3)	Temperature (K)	% Crystallization	Viscosity (poise)	Power law exponent, n
12.4	254.05	5	2.0	1.6
12.4	252.95	9	2.4	1.4
12.4	249.95	16	8.0	1.8
12.4	248.95	18	7.6	1.9
12.4	245.55	26	10.1	1.5
14.0	251.15	2	1.0	1.9
14.0	249.75	6	1.4	2.1
14.0	244.95	18	3.0	1.8
14.0	244.15	19	4.0	2.1
18.1	240.05	5	9.2	1.7
18.1	238.95	7	12.0	2.1
18.1	233.35	12	22.0	2.2
18.1	231.45	17	44.0	1.9
18.1	227.55	21	63	1.8
18.1	221.15	25	77	2.2
21.6	226.95	6	2.6	2.1
21.6	224.55	8	3.6	2.1
21.6	220.45	13	4.6	2.2
21.6	213.45	18	15.4	2.4
21.6	199.55	25	51	1.9
25.2	214.75	3	2.6	1.6
25.2	211.65	5	6.2	1.8
25.2	206.15	9	12.4	1.6
25.2	199.35	13	17.0	1.3
26.7	209.65	0	1.2	1.0
26.7	204.35	5	6.6	1.4
26.7	195.65	10	15.0	1.2
28.4	207.85	0	1.2	—
28.4	202.85	0	2.0	1.0
28.4	199.85	1	2.8	1.0
28.4	196.65	3	5.3	1.1
28.4	191.45	6	13.6	1.2
28.4	184.65	10	40.0	1.2
28.4	183.75	10	40.0	1.2
29.4	209.15	0	1.0	—
29.4	205.75	0	1.4	—
29.4	205.45	0	1.3	—
29.4	202.85	0	1.8	—
29.4	202.55	0	1.8	—
29.4	198.95	0	3.0	—
29.4	198.05	0	3.2	1.0
29.4	197.55	0	3.3	1.0
29.4	197.35	0	4.0	—
29.4	196.35	0	4.2	1.0
29.4	195.75	0	4.8	1.0
29.4	193.05	2	7.2	1.0
29.4	192.15	2	8.2	1.0
29.4	190.35	4	10.6	1.0
29.4	188.65	5	16.0	1.0
29.4	188.05	5	16.5	1.0
29.4	184.45	6	40.0	1.0
29.4	183.55	7	54	1.0
29.4	182.05	8	68	1.0
29.4	177.65	9	102	1.0
29.4	176.25	10	116	1.0
29.4	175.75	10	166	1.0
29.6	195.75	0	4.2	1.1
29.6	185.75	5	25.3	1.0

TABLE I—*Continued*

Composition (wt.% NH_3)	Temperature (K)	% Crystallization	Viscosity (poise)	Power law exponent, n
29.6	181.05	8	61	1.1
29.6	176.15	—	488	1.0
33.0	202.25	0	1.7	—
33.0	190.15	0	6.6	1.0
33.0	185.15	0	13.9	1.0
33.0	180.75	0	22.4	1.1
33.0	175.85	—	97	1.0
33.0	176.25	—	78	1.0
33.0	176.15	—	93	1.0
35.5	204.55	0	1.3	—
35.5	200.25	0	1.9	—
35.5	195.85	0	3.2	—
35.5	190.25	0	6.2	1.0
35.5	183.95	0	14.0	1.0
35.5	183.15	0	15.0	1.0
35.5	182.25	0	17.4	1.0
35.5	180.45	0	24.8	1.0
35.5	179.15	0	29.4	1.1
35.5	177.95	0	32.6	1.0
35.5	177.65	0	39.4	—
35.5	176.45	0	35.6	1.0
35.5	175.55	0	43.2	1.0
35.5	173.85	0	50	1.1
35.5	176.45	0	40.0	—
35.5	173.45	0	70	1.0
35.5	171.55	0	74	1.0
42.0	203.35	0	1.2	1.0
42.0	198.45	0	1.9	1.1
42.0	194.25	0	2.9	1.0
42.0	189.45	0	5.3	1.1
42.0	188.75	0	6.4	1.0
49.1	199.35	0	1.2	1.0
49.1	196.75	0	1.6	1.0
49.1	194.85	0	1.8	1.0
57.0	190.65	0	1.1	—
57.0	187.95	0	1.6	1.0

Note. All viscosities were obtained with the HB1 spindle operating at or reduced to 20 rpm. A dashed entry under the crystallization column indicates that partial crystallization occurred at an invariant point preventing use of the lever rule to calculate % crystallization. A dashed entry in the power law exponent column indicates that the data needed to calculate n were not obtained.

a 12.2-cm internal diameter. This vessel was slowly cooled in liquid nitrogen, and was opened for short periods of time to stir and thermally homogenize the liquid, to make viscosity and temperature measurements, and to observe crystallization. The total duration of each run was typically 15 hr, with a mean cooling time on the order of 2–4 K per hour.

Temperature was measured with chromel–alumel thermocouples and platinum resistance thermometers; these instruments were calibrated at the freezing points of water, methanol, and acetone, the sublimation point of carbon dioxide, and the boiling points of nitrogen and water (the latter three temperatures corrected to take into account the laboratory air pressure). The accuracy of the temperature measurements was about ±0.2 K. However, it was difficult to thermally homogenize the more viscous, low-temperature mixtures; this increased the effective temperature error to as much as ±0.5 K for measurements below about 185 K, and ±0.8 K for measurements below 170 K.

2.2. *Falling Sphere Method*

The classical analytical approximation of Stokes gives the viscosity, μ, of a viscous medium if the settling rate of a solid sphere is measured

$$\mu = 2\Delta\rho a^2 g/9U, \tag{1}$$

where $\Delta\rho$ is the density of the solid sphere minus that of the liquid, a is the radius of the sphere, g is the gravitational acceleration, and U is the terminal velocity of the sphere. Equation (1) is a very good approximation if the flow around the sphere is a very slow creeping motion where the Reynolds Number, Re, is much less than 1. Re is given by

$$\mathrm{Re} = 2a\rho_f U/\mu, \tag{2}$$

where ρ_f is the density of the fluid. Various theoretical treatments have offered analytical corrections to the Stokes equation for non-creeping flow at Re of order 1 and higher, although none of these solutions closely reflects reality. Therefore, it is the usual practice to apply empirical corrections. The present data have been reduced according to the empirical correction factors of Le Clair *et al.* (1970). Because the correction factors are Re-dependent and Re is μ-dependent, and μ is not initially known, it was necessary to apply an iterative routine starting with the Stokes approximation to converge on the true, corrected values of Re, the correction factor, and the true, corrected viscosity.

The Stokes Eq. (1) and empirical Re-correction factors apply only in an infinite fluid medium. Rigid boundaries, in this case those of the container, retard the motion of the sinking sphere, so wall corrections must also be applied. The wall effect was accounted for based on the work of Fidleris and Whitmore (1961).

To extend viscosity measurements over many orders of magnitude spheres of various sizes and densities were utilized. These included Cr-steel, glass, nylon, and ultra-high molecular weight polyethylene spheres ranging from 0.6 to 1.3 cm in diameter. Plastics were utilized in the runs at high temperatures in order to minimize the density contrast of the sphere relative to the liquid. Steel and glass were selected to maximize the density contrast for runs

at low temperatures where the liquid became extremely viscous. The temperature-dependent densities of these materials were determined to within ± 0.0004 g cm^{-3}. Small air bubbles sometimes were entrained in the liquid or adhered to the spheres; in some instances this problem may have contributed significant error to measured viscosities.

It was important to thermally equilibrate the sphere with the liquid before measuring its descent rate, both to achieve the correct density contrast with the liquid, and to avoid having the sphere disturb the temperature and viscosity of the sample adjacent to the sphere.

Large hemispherically headed steel bolts, normally used on railroad ties and in wooden bridges, were used in place of spheres to obtain two semi-quantitative viscosity estimates of order 10^6 poises. The effective density of the bolt heads was calculated as the mass of the bolt divided by the volume of a sphere with equivalent cross-sectional area.

The uncertainty in the liquid temperature caused by thermal heterogeneity effectively limited the precision of viscosities measured in excess of about 100 poises. The uncertainties in the density contrasts between the plastic spheres and the viscous media, and the combination of large and somewhat uncertain empirical corrections for the wall effect and finite Re limited the precision of viscosities below about 1 poise. Hence, the falling sphere method yielded its best results between 1 and 100 poises, the same viscosity-temperature-composition region where most rotational viscometric data were obtained. In general, the quality of the falling sphere data is not as good as the quality of the rotational viscometry except near 1 poise. However, the falling sphere method yielded useful results over a broader viscosity range, from 10^{-2} to 10^6 poises.

2.3. Liquid Preparation

The compositional range for the ammonia–water liquids investigated in this study is from about 12.6 to 56.0 wt% NH_3. Ammonia–water solutions with compositions ranging up to 29.9 wt.% NH_3 were prepared by diluting analytical reagent grade ammonium hydroxide (Mallinckrodt, 3 ppm total impurities) with distilled water (maximum 1 ppm impurities). Ammonium hydroxide was precooled to about 260 K to reduce ammonia vapor loss during transfer from the bottle. The composition of the ammonia–water reagent was determined by two independent methods: measurement of the liquid's specific gravity (Croft *et al.* 1988) and measurement of its liquidus temperature.

Solutions with NH_3 contents greater than 29.9% were prepared by mixing ammonium hydroxide solution with anhydrous liquid ammonia (Matheson, maximum 100 ppm total impurities, mostly water); since mixing was done at ambient pressure it was necessary to mix these solutions at low temperatures to prevent boiling. Ammonia was cooled by the Joule–Thompson effect to the normal boiling point (240 K) upon extrusion from the high-pressure cylinder. Ammonia and ammonia–water reagent were then cooled to the freezing point of pure ammonia (196 K) prior to mixing. The quantities of the liquids used in preparing the solutions were measured volumetrically, and their masses were determined using the temperature–composition–density relationship of Croft *et al.* (1988). Determinations of the liquidus temperature before and after experimental runs indicated that ammonia vapor loss and atmospheric water vapor condensation over the course of each run amounted to a reduction of the ammonia concentration from the initial value by about 0.1–0.3%, absolute. The uncertainty in the initial compositions is $\pm 0.2\%$ NH_3. Therefore, one may take $\pm 0.4\%$ as the uncertainty in the liquid composition for a given viscosity measurement. Ammonia–water–methanol liquids were prepared in the same general fashion, using analytical reagent methanol (Mallinckrodt, maximum 0.07% impurities).

3. RESULTS

3.1. Ammonia–Water Liquids above the Liquidus

Figure 1 and Table I show temperature-dependent viscosities of ammonia-water solutions obtained by rotational viscosity. Figure 2 and Table II show the viscosities obtained by the falling sphere method. Figure 2 also shows a curve, discussed below, fit to all superliquidus data obtained in this study (including rotational viscometry) and a fit to the data of Pinevich (1948), both curves for 30% NH_3 solution.

Temperature–composition–viscosity fit. Least-squares numerical fitting procedures (Bevington 1969) were applied to the viscosity measurements to obtain interpolation equations. The basic form of the fitting equation adopted is:

$$\mu = \exp\{A + B/T\}, \tag{3}$$

where μ is the viscosity, T is temperature, and A and B are material constants. The form of Eq. (3) is the one commonly adopted to express viscosity data for both liquids and gases (Touloukian *et al.* 1975), and has both theoretical and empirical support. Effectively, $\exp\{A\}$ is a reference viscosity at very high temperatures and B is an "activation temperature" related to an activation energy. Both A and B vary with ammonia content of ammonia–water liquids, thus in our fit, A and B are represented by polynomial expressions in the mass fraction, X, of ammonia in the mixtures. Both earlier work (McKinnon

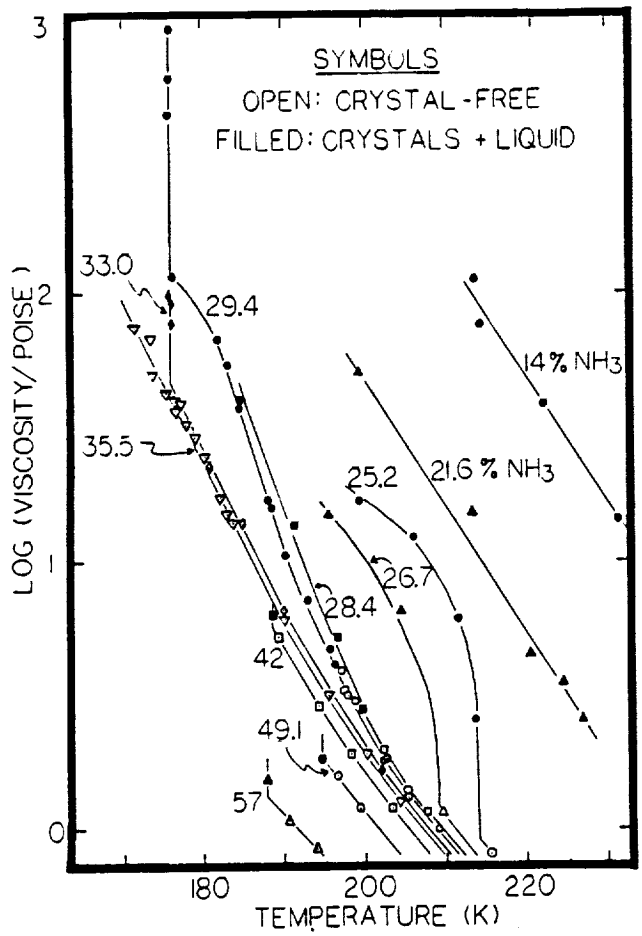

FIG. 1. Effective viscosities of ammonia–water liquids and slurries obtained by rotational viscometry using Brookfield's largest spindle operated at 20 rpm.

and Meadows 1984, Kargel 1987) and our initial attempts to fit both the high-temperature data (Pinevich 1948, Pleskov and Igamberdyev 1939) and our data (Tables I and II) indicated that B was a function of temperature also. Attempts to fit the values of B as a smooth function of temperature were unsuccessful. Measurements bracketing the apparent transition near 240 K indicated a sharp, rather than a gradual transition (Fig. 2). Therefore, two separate fits were made: one to data above 240 K (including the mixed NH_3–H_2O data of Pinevich 1948, and Pleskov and Igamberdyev 1939; pure H_2O data of Haar *et al.* 1984; and pure NH_3 data of Alei and Litchman 1972), and a second to data below 240 K (Tables I and II and supercooled H_2O data from Weast and Selby 1967). The least-squares numerical fits are

$$A = -10.8143 + 0.711062\,X - 22.4943\,X^2 + 41.8343\,X^3 - 18.5149\,X^4 \quad (4a)$$

$$B = 1819.86 + 250.822\,X + 6505.25\,X^2 - 14923.4\,X^3 + 7141.46\,X^4 \quad (4b)$$

for $T > 240$ K, and

$$A = -13.8628 - 68.7617\,X + 230.083\,X^2 - 249.897\,X^3 \quad (5a)$$

$$B = 2701.73 + 14973.3\,X - 46174.5\,X^2 + 45967.6\,X^3 \quad (5b)$$

for $T < 240$ K. RMS deviations from Eq. (4) for the data used in the fit are about 5%. RMS deviations from Eq. (5) for the viscometer data (Table I) used in the fit is about 10%. Deviations of the Stokes Flow data (Table II) from Eq. (5) is about 15%.

Isovisces computed from Eqs. (3), (4), and (5) are shown in Fig. 3. The computed transition curve between the two solutions is also shown. As with density and bulk modulus (Croft *et al.* 1988), viscosities of ammonia–water liquids show an anomalous maximum near the eutectic composition (see below). Approximate mean activation temperatures are about 2050 K for $T > 240$ K, and about 4200 K for $T < 240$ K. The corresponding activation energies are, respectively, about 17 kJ/mole and 35 kJ/mole, which agree reasonably well with the results of McKinnon and Meadows (1984). Further discussion of this transition is given in Section 4.1.

3.2. *SuperCooled Ammonia–Water Liquids*

The ability to chill liquids below their normal freezing points without crystallization is a common metastable phenomenon (supercooling). The experimentalist must use some measure of patience to prevent significant supercooling of liquids close in composition to the ammonia–water peritectic. In fact, Rupert (1909), in the earliest determination of the complete solid–liquid phase diagram of the ammonia–water system, extrapolated supercooled "liquidus" data from higher temperatures leading to the erroneous conclusion that a eutectic occurred in this system near 158 K, 17 K below the actual value. Several subsequent determinations also erred on the low side.

The correct eutectic composition and temperature (35.4 wt.% NH_3, 175.4 K) and the existence of ammonia dihydrate and of the ammonia–water peritectic (32.6% NH_3, 176.2 K) were first established by Rollet and Vuillard (1956). The early errors, due to strong metastability in the ammonia–water system, have caused a fair amount of confusion in the planetary science community as to the actual minimum melting temperature, with published temperatures of 170, 173, 175, and 176 K. For primitive, previously undifferentiated ammonia–water ices, the actual temperature of melting at low pressures is the peritec-

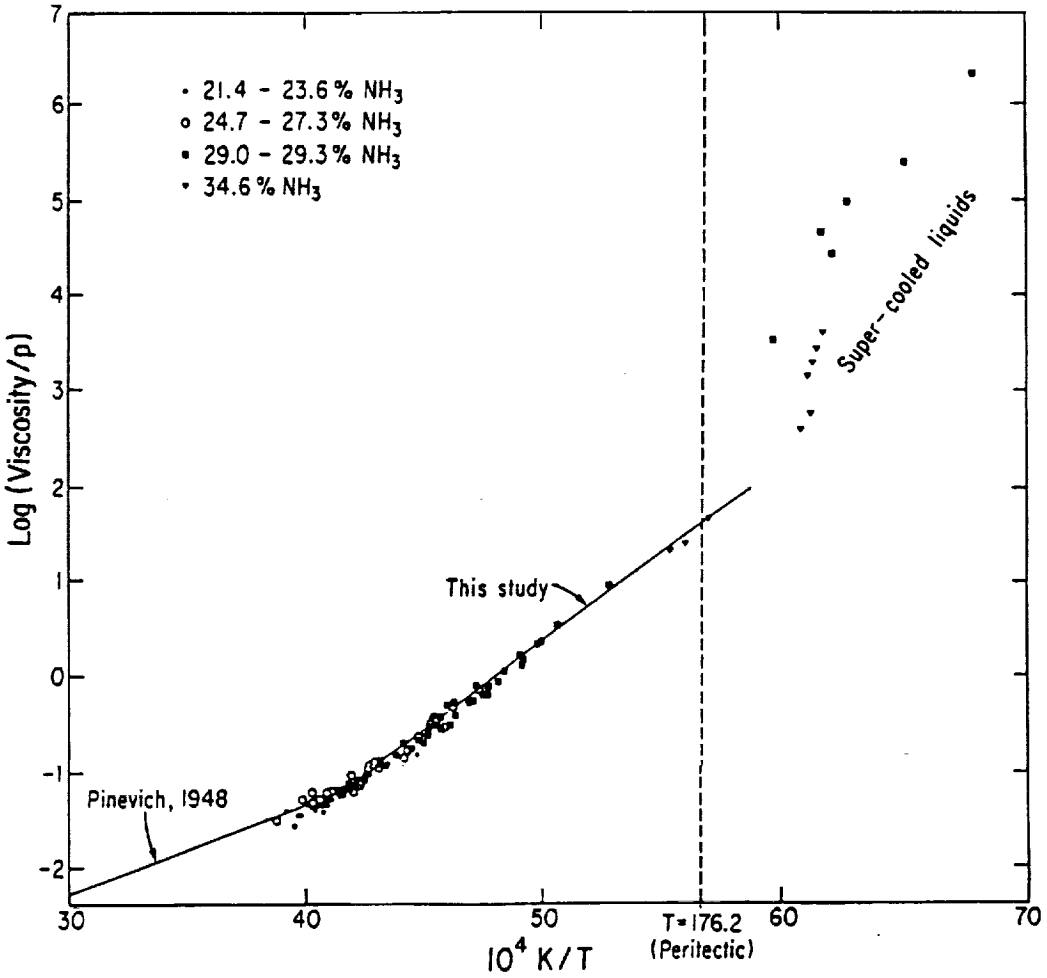

FIG. 2. Viscosities of ammonia–water liquids obtained by the falling sphere method. Curves represent all data obtained by both methods in this study and data of Pinevich (1948).

tic, 176.2 K, rather than the eutectic as is commonly stated. The supercooling phenomenon continues to frustrate many experimentalists when crystallization is desired. However, under certain circumstances supercooling may occur in natural cryovolcanic settings and may be an important factor governing the rheologies of these cryolavas.

Figures 1 and 2 show the viscosities of supercooled ammonia–water liquids near the peritectic in composition. It is possible to maintain ammonia–water liquids several K below the normal freezing point for several hours as long as they are not too vigorously stirred and as long as ice nucleii are not introduced by atmospheric condensation or from moist thermocouple probes or viscometer spindles. It was, therefore, very easy to get good viscosity measurements by either viscometric technique for slightly supercooled liquids.

The more highly supercooled mixtures become highly viscous and thermally inhomogeneous, requiring energetic manual mixing, long thermal equilibration times, or small sample sizes in order to obtain more thermally homogeneous mixtures. Invariably, vigorous manual mixing triggers crystal nucleation within a few minutes, often before the liquid can be thermally homogenized. Sometimes crystallization may be triggered merely by inserting a thermocouple probe or dropping a steel sphere into the liquid. The great difficulty encountered in trying to stir and otherwise manipulate these mixtures severely limited the number and quality of viscosity determinations for highly supercooled mixtures and made them impossible to study by rotational viscometry. The measured viscosities for the strongly supercooled mixtures (Fig. 2 and Table II) were all obtained by the descending sphere method using liquids lacking any observable signs of crystallization. The greatest uncertainty in these measurements is the temperature, which typically varied by 1 K

TABLE II
Viscosities of Ammonia–Water Mixtures Obtained by the Descending Sphere Method

Composition (wt.% NH_3)	Temperature (K)	Stokes viscosity (poises)	Corrected viscosity (poises)
21.4	238.6	0.121	0.069
21.4	239.6	0.117	0.065
21.4	240.0	0.120	0.067
21.4	240.7	0.122	0.069
21.4	241.5	0.144	0.060
21.4	241.5	0.110	0.057
21.4	243.5	0.105	0.052
21.4	244.5	0.098	0.046
21.4	245.6	0.095	0.044
21.4	248.7	0.092	0.042
21.4	251.6	0.085	0.035
21.4	251.7	0.085	0.035
21.4	255.2	0.081	0.038
23.2	234.1	0.162	0.097
23.2	235.3	0.161	0.095
23.2	236.8	0.149	0.084
23.2	237.3	0.136	0.069
23.2	238.0	0.140	0.073
23.2	238.4	0.132	0.065
23.2	240.5	0.124	0.058
23.2	244.6	0.118	0.050
23.2	245.6	0.102	0.038
23.2	247.0	0.110	0.045
23.2	247.6	0.104	0.040
23.6	223.6	0.210	0.146
23.6	230.0	0.180	0.117
23.6	234.1	0.160	0.097
23.6	239.7	0.130	0.065
23.6	249.6	0.112	0.046
23.6	253.3	0.089	0.027
24.7	250.6	0.124	0.052
24.7	244.6	0.134	0.062
24.7	238.0	0.134	0.063
24.7	233.0	0.195	0.121
24.7	225.9	0.241	0.164
24.7	223.4	0.505	0.233
24.7	220.8	0.636	0.334
24.7	219.8	0.665	0.345
25.0	217.8	0.392	0.305
25.0	219.6	0.387	0.295
25.0	234.1	0.183	0.111
25.0	236.4	0.147	0.074
25.0	238.8	0.143	0.070
25.0	248.3	0.120	0.048
25.0	257.9	0.101	0.031
27.3	211.1	1.19	0.715
27.3	216.3	0.866	0.477
27.3	220.1	0.716	0.370
27.3	222.9	0.317	0.225
27.3	226.6	0.220	0.138
27.3	232.0	0.199	0.114
27.3	236.2	0.163	0.080
27.3	238.2	0.179	0.094
27.3	241.3	0.138	0.058
27.3	243.4	0.145	0.063
27.3	246.3	0.134	0.052
27.3	248.3	0.145	0.062
29.0	159.9		102,000 S
29.0	161.5		29,400 S
29.0	162.5		49,500 S
29.0	167.9		3,570 S
29.0	199.9	3.38	2.29
29.0	203.5	1.58	1.31
29.0	206.7	1.35	1.11
29.0	209.3	1.29	0.784
29.0	209.6	0.811	0.658
29.0	210.6	1.11	0.652
29.0	211.9	1.01	0.813
29.0	212.7	0.673	0.538
29.0	213.2	0.660	0.527
29.0	215.8	0.514	0.400
29.0	216.3	0.936	0.530
29.0	217.2	0.409	0.309
29.0	217.5	0.407	0.300
29.0	217.6	0.915	0.497
29.0	219.9	0.449	0.344
29.0	220.1	0.420	0.314
29.0	220.4	0.416	0.315
29.0	221.4	0.331	0.243
29.0	222.5	0.285	0.196
29.0	223.2	0.304	0.221
29.0	225.7	0.254	0.165
29.0	226.8	0.294	0.201
29.0	228.3	0.229	0.146
29.0	232.0	0.216	0.125
29.0	235.9	0.171	0.083
29.0	239.2	0.164	0.075
29.0	241.5	0.155	0.066
29.3	147.7	4,070,000	2,300,000 S
29.3	154.2	481,000	270,000 S
29.3	189.3	9.07	7.89
29.3	197.3	3.72	3.23
29.3	200.1	2.22	1.92
29.3	203.2	1.49	1.28
29.3	203.8	1.70	1.13
29.3	207.7	0.887	0.74
34.6	163.9		1,490 S
34.6	163.3		2,060 S
34.6	162.9		2,850 S
34.6	162.2		4,300 S
34.6	180.6		20.4
34.6	178.6	34.5	24.3
34.6	175.6	68.3	48.0
34.6	164.6	614	412 S
34.6	163.6	893	600 S
34.6	175.8	1025	688 17% crystals
40.4	193.9		5.92
40.4	193.4		5.93
40.4	192.9		5.73

TABLE II—*Continued*

Note. S, supercooled without crystallization. Corrected viscosities have been corrected for the wall effect and finite Reynolds number. The magnitude of the corrections can be assessed by comparison with the Stokes viscosities which have not been corrected.

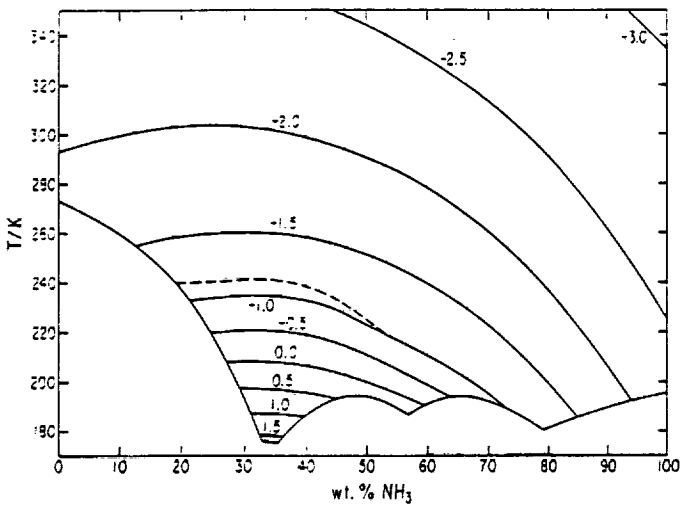

FIG. 3. Temperature–composition–$\log_{10}$ viscosity fit for ammonia–water liquids. Dashed curve shows the transition temperature where the activation energy changes.

through the sample. Considering the sharp temperature dependence of the viscosities in this thermal regime, this introduces a considerable uncertainty in the viscosities for any given temperature.

Figure 2 shows that the viscosities of strongly supercooled ammonia–water liquids exhibit far more powerful compositional and temperature dependencies than do the superliquidus mixtures. This behavior is explained in terms of glass formation in Section 4.1.

3.3. *Partially Crystallized Ammonia–Water Slurries*

Complex rheologies. In contrast to the relatively simply Newtonian viscous behavior of the crystal-free liquids discussed above, partially crystallized slurries are generally characterized by an extremely complex rheology. Even 1 or 2% partial crystallization may introduce a rich variety of rheological phenomena, including hysteresis effects and, most importantly, strain-rate-dependent (shear stress dependent) effective viscosities. The complex rheological behavior of the slurries makes it difficult to exactly reproduce the measured viscosities. For example, the strain rate dependence ensures that the same geometry and shear rate of a viscometric measurement must be reproduced exactly in order to reproduce the same results.

The thermal history also affects the viscosity of ammonia–water slurries. The effective viscosities of well-stirred slurries maintained at constant temperature generally decrease slowly, some tens of percent, over periods of about 10 hr. Part of this phenomenon is probably thixotropy (shear thinning) and is common for particle suspensions in liquids. However, thinning also occurs to some extent for mixtures which are left undisturbed at some constant temperature below the liquidus, and for mixtures which are slightly warmed after cooling without otherwise disturbing them. Such "time-thinning" is probably related to the slow recrystallization of suspended ice, which may initially tend to have dendritic (snowflake-like) forms characteristic of quenched crystals; more compact euhedral and resorbed forms may physically interact less extensively than quenched crystals, for a given crystal packing fraction, therefore yielding lower effective viscosities. To maintain as self-consistent a data set as possible, the effective viscosities of slurries reported in Table I were measured while cooling the mixtures at more or less steady rates.

Simple models of complex rheologies. The rheological behaviors of crystal–liquid suspensions are commonly approximated as "Newtonian" viscous substances, as "power-law" ("pseudo-plastic") substances, or as "Bingham plastics," the latter two comprising common types of non-Newtonian substances. These are sometimes useful approximations to the rheological behavior of naturally occurring slurries (e.g., mud and lava flows), although they often apply only over limited ranges of deformation rates and applied shear stresses.

A Newtonian substance is characterized by a linear dependence of strain rate, $\dot{\varepsilon}$, on applied shear stress, σ, and by the lack of a yield strength. Its viscosity, μ, is defined simply as

$$\mu = \sigma/\dot{\varepsilon}. \tag{6}$$

A Bingham plastic is also characterized by a linear dependence of the strain rate on the applied shear stress, but unlike the Newtonian substance, it also displays a finite yield strength. A Newtonian-like effective viscosity, μ_{eff}, can still be described for a Bingham plastic using Eq. (6), although this effective viscosity varies with the applied shear stress (unlike Newtonian substances). The Bingham viscosity, μ_B, is a constant (for constant temperature) given by

$$\mu_B = (\sigma - Y)/\dot{\varepsilon}, \tag{7}$$

where Y is the yield stress. When $Y \ll \sigma$ a Bingham plastic appears to behave essentially as a Newtonian fluid. When $\sigma < Y$ then no permanent plastic deformation occurs and the substance appears to be an elastic solid.

A pseudoplastic substance lacks a yield strength, and the strain rate has a power-law dependence on the applied shear stress

$$\dot{\varepsilon} = Ae^{-Q/RT}\sigma^n, \tag{8}$$

where A is a constant for a given temperature, Q is the activation energy for viscous flow, and R is the gas constant. The exponential term gives the temperature dependence of the strain rate, and n gives the power-law dependence of the strain rate on the applied shear stress (Newtonian and Bingham substances may have similar temperature dependencies). A value of $n = 1$ signifies Newtonian viscous behavior. As the effective viscosity is simply $\sigma/\dot{e}$ (which is constant only in the special case when $n = 1$), we may rewrite Eq. (8) in terms of the effective viscosity,

$$\mu_{\text{eff}} = \sigma^{1-n} e^{Q/RT}/A. \tag{9}$$

Equations (7) and (9) indicate that the effective viscosities of Bingham and power-law substances are functions of the applied shear stress, and in each case give higher effective viscosities as the shear stress and strain rate are decreased. On a graph of strain rate vs shear stress a Newtonian liquid plots as a straight line passing through the origin, a Bingham plastic plots as a straight line with some positive intercept on the shear stress axis, and a power-law substance plots as a curve passing through the origin. In each case the effective viscosity is given by the slope of a straight line passing through the origin and the point of interest on a diagram of stress vs strain rate.

Newtonian character of peritectic slurries. Fortunately, the slurries with the greatest planetological interest (those close in composition to the peritectic) do not exhibit the most troublesome of rheological phenomena (the strain-rate dependence of effective viscosities), so we shall discuss these first.

It is useful to define a relative viscosity, μ_r

$$\mu_r = \mu_s/\mu_l, \tag{10}$$

where μ_s is the viscosity of the slurry, and μ_l is the viscosity of the intergranular liquid phase in the absence of suspended crystals.

Equation (10) has broad relevance only if the slurry is Newtonian. This requirement is satisfied by slurries containing 29% or more NH_3 (at least for the ranges of crystallization and shear rates examined in this work). Figure 4 shows the dependence of μ_r on the percentage of crystals, ϕ, in ammonia–water slurries. ϕ was estimated either by the petrological "lever rule" when there was a reasonably close approach to equilibrium crystallization and when the temperature remained above the peritectic, or by the temperature rise associated with the latent heat released by partial crystallization of supercooled mixtures. μ_s was measured, while μ_l was calculated for the equilibrium liquidus composition at the temperature of the slurry. Like terrestrial lavas, the rheology of ammonia–water liquids is extremely sensitive to its thermal state. Further discussion of this matter is saved for Section 4.2.

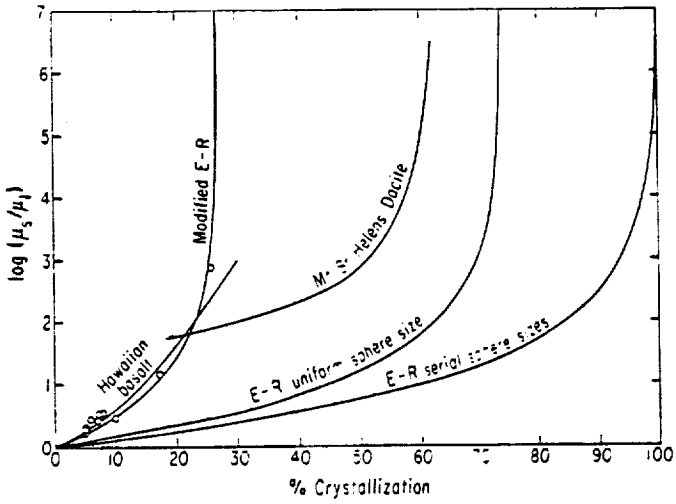

FIG. 4. Dependence of relative viscosity on degree of crystallization. Open circles are ammonia–water slurries. Silicate lava curves are from McBirney and Murase (1984). Theoretical Einstein–Roscoe (E–R) formulations are for uniform solid spheres suspended in a viscous liquid ($C = 1.35$), and for a serial sphere size distribution ($C = 1$), and modified to approximately fit the ammonia–water slurry data ($C = 3.7$).

Figure 5a shows a stress-strain plot for a near-peritectic mixture at various degrees of partial crystallization. No significant departures from ideal Newtonian behavior are discernable. The data can be fit with a power-law where $n = 1$ (the Newtonian condition). A yield strength was not evident for peritectic and near-peritectic mixtures. However, Murase *et al.* (1985) observed an apparent yield strength for Mt. St. Helens dacite only after 70% crystallization. We have not examined slurries with anywhere near this quantity of crystals.

Power-law behavior of water-rich slurries. As the water content of ammonia–water slurries increases from the peritectic their rheologies increasingly depart from Newtonian, with the apparent viscosity describable to a first approximation with a power-law dependence on the strain rate (applied shear stress). Ammonia–water compositions considerably more water-rich than the peritectic were difficult to work with at high degrees of crystallization owing to their strongly non-Newtonian, "slushy" character. At lower degrees of partial crystallization these slurries had a "creamier" consistency and their rheologies were readily studied with the rotational method. The lever rule can be applied to water-rich samples to precisely determine the extent of crystallization as long as the temperature of the slurry remains above the peritectic point.

Figure 5b shows representative stress–strain rate plots obtained for a relatively water-rich mixture at various

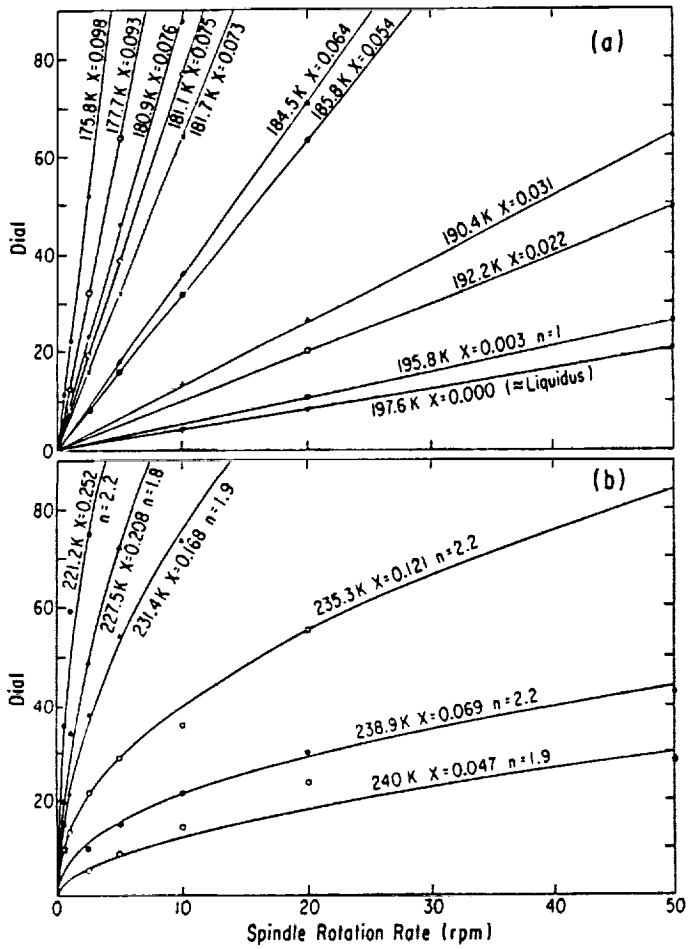

FIG. 5. Strain rate (proportional to spindle rotation rate) vs shear stress (proportional to dial reading). (a) Newtonian behavior of slurries containing 29.4–29.6% NH_3. (b) Power-law pseudo-plastic behavior of slurries containing 18.1% NH_3. X indicates fraction of crystals. n indicates power-law index (equation 8 and Table I).

degrees of partial crystallization. These slurries obey a simple power-law relation to a reasonable approximation. The Bingham approximation completely fails to characterize ammonia–water slurries, at least for the ranges of crystal contents and shear rates investigated here.

Figures 1 and 4 show that abrupt surges in the effective viscosities of water-rich ammonia–water mixtures occur as these substances partially crystallize below their liquidi. Supercooled liquids do not display this phenomenon. This surge in effective viscosity corresponds to the onset of non-Newtonian ($n > 1$) rheological behavior. Figure 6 shows the dependence of the exponent n (from Eqs. (8) and (9)) on the degree of crystallization for several compositions. The exponent n was calculated based on viscosity measurements made at several different spindle rotation rates.

Non-Newtonian power-law viscosities characterize the more water-rich slurries, with n ranging up to about 2. It was surprising to find that n attains its full value with only a few percent crystals, and either levels off or even decreases slightly as the degree of crystallization increases (the effective viscosity, however, certainly does continue to rise sharply as crystallization ensues). This behavior could be a hysteresis effect as described above, where the first few percent of quenched crystals gradually take on more compact, euhedral forms after several hours of slow cooling, thereby minimizing interactions with the liquid and with other crystals.

Although this work does not support a Bingham rheology for ammonia–water slurries, it is possible that such a rheology would be found at a lower range of strain rates or at higher crystal contents than investigated here. Qualitative observations may support this speculation; a stick-slip type of behavior was found for the more water-rich slurries where the ice crystal content exceeded about 25%. That is, the spindle was found to stick and surge in an unpredictable type of rotation. Although this made rheological measurements unreliable, it may indicate that a yield strength was being attained. Alternatively, stick-slip behavior may have been indicating that the spindle was simply cutting a hole in the highly viscous (pseudo-plastic) medium, causing the spindle to surge through free space, followed by the collapse of the sticky material onto the spindle. Or, if the modified Einstein–Roscoe formulation discussed in Section 4.2 is approximately correct, then small heterogeneities in the amount of crystals

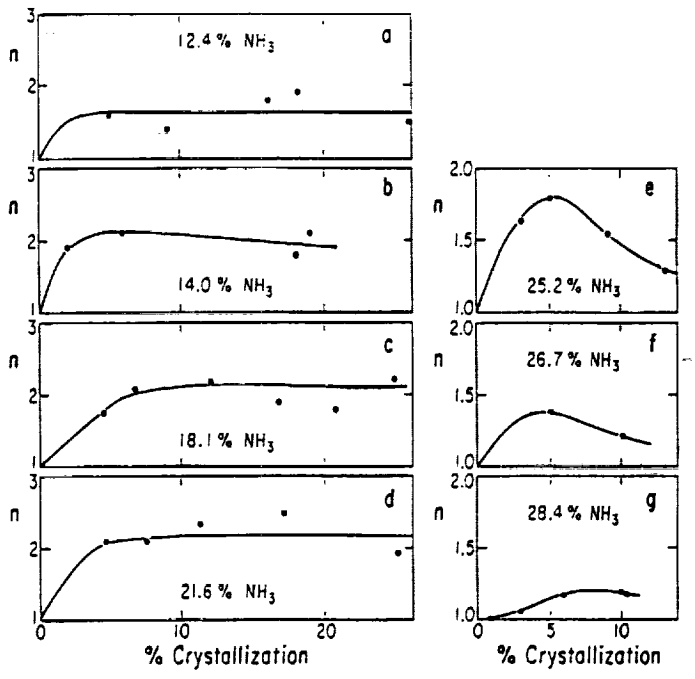

FIG. 6. Strain rate dependence of μ_{eff}, expressed as the power-law exponent n, as a function of the degree of crystallization.

could cause radical local variations in effective viscosity (lumpiness).

3.4. *Ammonia–Water–Methanol Liquids*

Methanol (CH_3OH) is one of the simplest and most abundant organic molecules in interstellar space (Irvine *et al.* 1985) and is readily produced in large quantities by ion bombardments and ultraviolet irradiations of carbon-bearing water ice (Khare *et al.* 1989, Roessler and Nebeling 1988). Methanol and many other molecules may possibly constitute minor or trace components of icy satellites. Since the electric dipole moment of methanol (1.70 D) is similar to the dipole moments of water (1.85 D) and ammonia (1.47 D), we would expect *a priori* that methanol would interact with ammonia–water in extensive liquid solution. Hence, if they are present in at least minor quantities (even hundredths or tenths of 1%) in icy satellites, methanol and other strongly polar substances may contribute to the volcanological complexity and geomorphic diversity of icy satellites (Kargel 1990). This work explores some of the rheological implications when just this one of the many plausible minor components is added to the ammonia–water system.

Kargel (1990) mapped out the liquidus surface of the ternary system H_2O–NH_3–CH_3OH in composition–temperature space at 1 atm. (Fig. 7). The detailed structure of this system, particularly near the methanol corner and near the thermal minima, are known only in approximate form, owing to the difficulty encountered in crystallizing and manipulating these highly viscous mixtures at such low temperatures. The ternary equivalent of the ammonia–water peritectic has been bracketed in temperature–composition space by melting experiments (giving the peritectic temperature) and by extrapolations of the liquidus temperature–composition curves (giving the peritectic composition, and less reliably, the peritectic temperature). The peritectic liquid appears to contain about 33% CH_3OH, 23% NH_3, and 44% H_2O by mass, and apparently freezes near 153 K (all values have large uncertainties at this point).

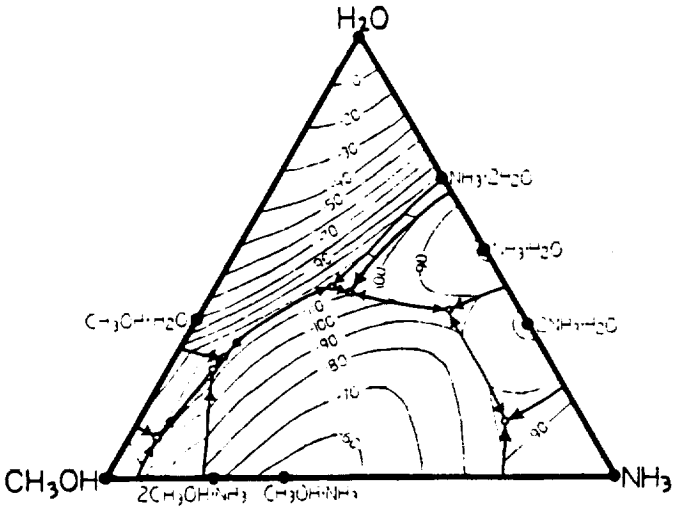

FIG. 7. Liquidus surface of the system H_2O–NH_3–CH_3OH (from Kargel 1990). Isotherms in °C. Arrows on cotectics indicate the direction of liquid migration upon cooling.

TABLE III
Viscosities of Ammonia–Water–Methanol Liquids (by Rotational Viscometry)

Liquid compositions (weight fractions)			Temperature	Viscosity	A	B
H_2O	NH_3	CH_3OH	(K)	(poises)	(Equation (3))	
0.486	0.207	0.307	186.1	26	−34.78	7108.2
			177.4	266		
			167.6	1820		
0.215	0.092	0.693	187.5	1.8	−28.44	5390.6
			179.7	4.3		
			171.1	14.8		
			164.1	75		
			158.0	388		
0.241	0.000	0.759	178.3	2.2	−21.29	3936.9
			168.1	8.4		
0.379	0.090	0.531	198.1	2.7	−31.17	6328.6
			189.9	6.8		
			184.1	20.0		
			177.9	103		
0.442	0.227	0.331	210.7	1.0	−29.80	6188.8
			202.9	2.3		
			201.5	2.9		
			201.2	2.2		
			200.2	3.5		
			198.3	4.6		
			195.8	5.8		
			192.9	7.8		
			192.8	9.0		
			190.7	12.6		
			189.0	17.1		
			185.8	23.6		
			182.0	54		
			177.7	122		
			174.3	320		
			172.2	370		
			170.2	1040		
			165.1	3260		

Table III and Fig. 8 show the viscosities of ammonia–water–methanol liquid mixtures. Some of these mixtures became extremely bubbly at the lower temperatures, and it is possible that the bubbles affected some viscosity measurements. Pure methanol and ammonia end members are less viscous than liquid water for a given temperature. The ternary mixtures, however, are considerably more viscous than simple noninteractive mixing would

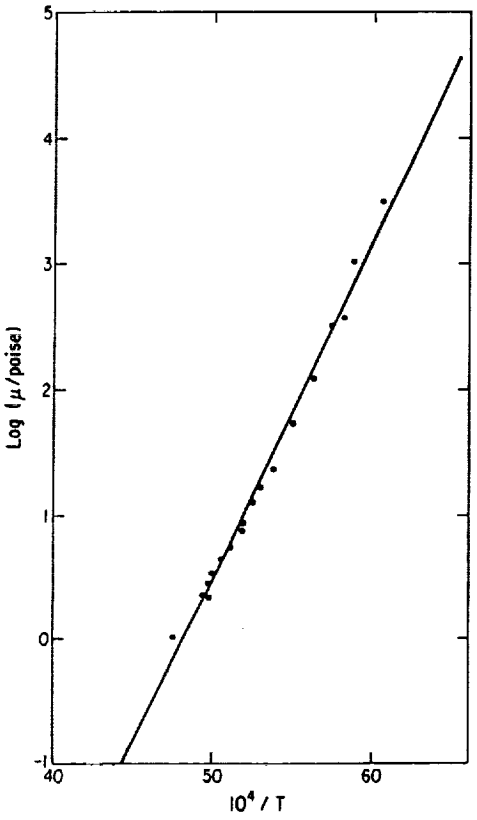

FIG. 8. Viscosities of ammonia–water–methanol liquid (near ternary peritectic) as a function of temperature, obtained by rotational viscometry.

suggest. Hence, powerful molecular interactions among the three components are indicated by the viscosity data.

This inference is supported by the molar volumes of ternary mixtures, which indicate highly nonideal solution behavior and closer intermolecular spacings than in any one of the pure liquids or any of the binary liquid mixtures. For example, the density of a liquid close in comparison to the ternary peritectic ($H_2O:NH_3:CH_3OH$ = 0.470 : 0.201 : 0.329 by mass) is 0.8706 g cm^{-3} at 298 K. This is 6% denser than is calculated based on the densities of the three pure end members and the assumption of noninteractive mixing. It is also 2% denser than calculated from the densities of pure methanol added to ammonia–water liquid assuming no interaction between the methanol and the ammonia–water. Croft *et al.* (1988) had earlier shown that ammonia and water interact strongly in solution. We infer from these density data that methanol interacts strongly with water and ammonia molecules, although less strongly (gram for gram) than the ammonia–water interaction.

The ammonia–water–methanol peritectic mixture has an extraordinarily high extrapolated viscosity near the freezing point, about 4×10^4 poises, three orders of magnitude greater than the viscosity of ammonia–water peritectic liquid (which is itself 3 to 4 orders more viscous than either pure water or pure ammonia at their freezing points). This viscosity estimate is a factor of several uncertain because of the uncertain temperature of the peritectic and because of uncertainties in the extrapolation of the data (a nonlinear fit in Fig. 8 would result in a greater viscosity at the peritectic and reduced rms deviation). The extremely high viscosity of the ternary peritectic compared to the ammonia–water binary peritectic is primarily due to the large additional freezing-point depression imposed by methanol. Ternary molecular interactive forces appear to be secondarily responsible. Just a few percent partial crystallization or a few degrees of supercooling make this mixture impossible to manipulate.

3.5. Comparisons of Planetologically Important Liquids and Ices

Figure 9 shows the viscosities of liquid water, ammonia–water, ammonia–water–methanol, water–magnesium sulfate (Kargel, 1990), and methane–nitrogen (Touloukian *et al.* 1975) mixtures at their respective eutectic and peritectic freezing points. Figure 9 also compares these viscosities to those of common silicate lavas at their liquidus temperatures. The silicate lavas are certainly not plausible volcanic agents on the icy satellites, but are included in Fig. 9 to provide a geologically familiar frame of reference. All of the viscosities shown in Fig. 9 are for crystal-free liquids. Volcanologically realistic amounts of supercooling and partial crystallization can increase these viscosities by many orders of magnitude, as shown in the sections above. Therefore, the viscosities in Fig. 9 are best utilized simply to show the approximate relative differences in the viscosities of the different types of lavas

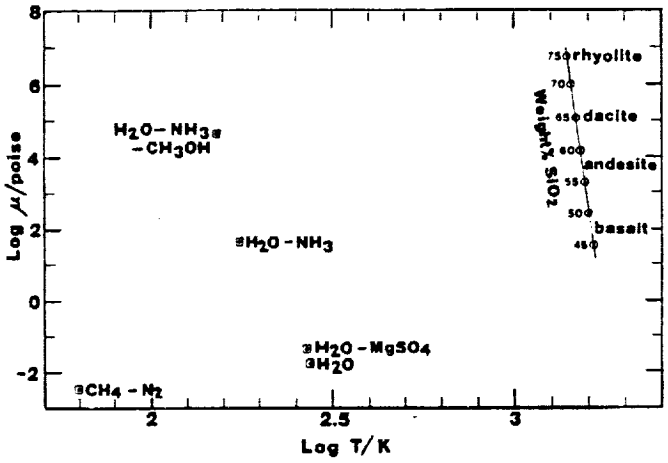

FIG. 9. Viscosities of cryogenic and silicate liquid mixtures. All data are for crystal-free mixtures. Silicates are at their respective liquidi; cryogenic liquids are at their respective eutectic and peritectic points.

FIG. 10. Lab samples of aqueous liquids and slurries of possible cryovolcanic importance. (a) H_2O–NH_3 liquid near the peritectic composition, T = 176 K, 6% ice crystals, ≈100 poises. (b) Supercooled H_2O–NH_3 liquid also containing a few percent ice crystals, T = 160 K, ≈10^4 poises. (c) H_2O–NH_3–CH_3OH peritectic liquid, T = 163 K (about 10 K above peritectic temperature), ≈10^4 poises.

and cryogenic substances. Assuming that superheating of cryolavas above the liquidus is minor or absent (this is true of silicate lavas), then the liquidus viscosities in Fig. 9 correspond to lower limits on the actual eruptive viscosities.

Figures 10a–10c qualitatively illustrate the viscosities of some cryovolcanologically plausible ammonia–water liquids in various thermal states. The ammonia–water–methanol liquid (Fig. 10c) could not be manipulated near its freezing point due to its highly viscous nature, so the experimenter had to settle for a photograph of the sample taken about 10 K above its peritectic temperature.

As seen from Fig. 9 ammonia–water and ammonia–water–methanol peritectic liquids have about the same viscosities as basaltic and dacitic lavas, respectively, and are many orders of magnitude more viscous than pure water, salt brines, or methane–nitrogen mixtures at their respective freezing points.

4. THEORETICAL INTERPRETATIONS AND PLANETOLOGICAL APPLICATIONS

4.1. Theoretical Interpretation of Ammonia–Water Liquid Rheology

Viscosity vs composition. Liquid water is a highly structured phase which, at temperatures well above the freezing point, exhibits some long-range order consistent with the crystal structure of hexagonal ice I (Eisenberg and Kauzmann 1969). Likewise, ammonia, also hydrogen-bonded, exhibits structure in the liquid. It is of interest to understand whether the mixed liquid is ordered, and what the nature of that ordering is. Viscosity data can contribute in this area. In the present section, we interpret the viscosity data as indicating very strongly that the liquid is a mixture of water molecules and ammonia–hydrate and dihydrate molecules, rather than simply free water and ammonia molecules. We also show weak evidence for further structure in the liquid: the following section of viscosity versus temperature provides a more compelling argument for additional structure in the liquid.

In an ideal solution, the viscosities of the two end members characterize the viscosity of the mixture according to the equation (Hummel and Arndt 1985)

$$\log \mu_{mix} = x \log \mu_y + (1 - x) \log \mu_z, \qquad (11)$$

where μ_y is the viscosity of component y, and x is its mole fraction. In turn, the viscosity of each individual component at temperature T is given by Eq. (3) which can also be written as

$$\mu = \exp\left(A + \frac{B_\gamma}{TS}\right), \qquad (12)$$

where S is the configurational entropy of component x, and A, B_γ are constants (compare with Eq. 3). In the case that the solution is not ideal, an additional term is added to Eq. (11) which expresses the contribution of the entropy of mixing of the solution. The notion that the viscosity may be expressed solely in terms of entropy corresponds to the view that material transport in liquids depends on the number of configurations attainable by the system, and that the energy required to shift from one configuration to another is not the rate-limiting step of the transport process. Such a view works well for certain

silicate melts such as plagioclase, even down to the glass temperature (Hummel and Arndt 1985). We adopt this view for our preliminary analysis of the viscosity–composition data and find that it provides a useful perspective.

We assume first that the ammonia–water liquid, above any of the eutectic, peritectic, or congruent melting points, is an ideal mixture of ammonia and water molecules. We then use the fits to the viscosity data given in the previous section to compare the viscosity as a function of composition to that predicted by the ideal mixing equation, with the viscosities of pure water and pure ammonia defining the end members. We use the fits to the data rather than the data themselves because the trends are easier to see using the fits; the goodness-of-fit is thoroughly described above and the reader should refer to this section again before drawing any conclusions.

Figure 11a shows the result of this analysis at 280 K. The solid line is the viscosity; the dashed line is that predicted from ideal mixing. The dashed curve is up to 65% lower in magnitude than the solid line. Discrepancies above the 10 to 20% level are significant, as is the disagreement in the sign of the slope for ammonia mole fractions less that 25%. The direction of the discrepancy is toward a negative entropy of mixing; i.e., the real liquid has fewer configurations available to it than the ideal mixing would predict; hence, the real viscosity is higher than the ideal.

The simplest approach to introducing a restriction in the number of available configurations is to assume that the liquid is composed not of water and ammonia molecules in any configuration, but instead that the molecules are restricted to hydrogen-bonded clusters according to composition. These clusters plausibly correspond to the stoichiometric, solid ammonia hydrate compounds. Thus between mole fractions of 0 and 33% the end member liquid components are H_2O and $2H_2O.NH_3$; between 33 and 50% the end members are $2H_2O.NH_3$ and $H_2O.NH_3$.

Figures 11b and 11c show the results of using the ideal mixing model with the endmember components indicated above. In some sense, the improved agreement is almost a trivial one in that we are taking smaller compositional slices of the viscosity curve in constructing the dashed line, and hence a better fit is to be expected. However, the great improvement in the fit, and the consistency in the sign of the slope, suggest that the result should be regarded as significant. The dashed curve fits the solid curve to within 6% in both the water–dihydrate, and dihydrate–monohydrate regions (Figs. 11b and 11c, respectively). This is much better than the scatter in the data and hence, to within the accuracy of the viscosity data, these dashed, "ideal" curves represent the viscosity data from 0 to 50% ammonia at 280 K. One is tempted to argue that the systematic, small negative residual entropy of mixing suggests additional structure in the liquid, but more accurate data are required to test this assertion.

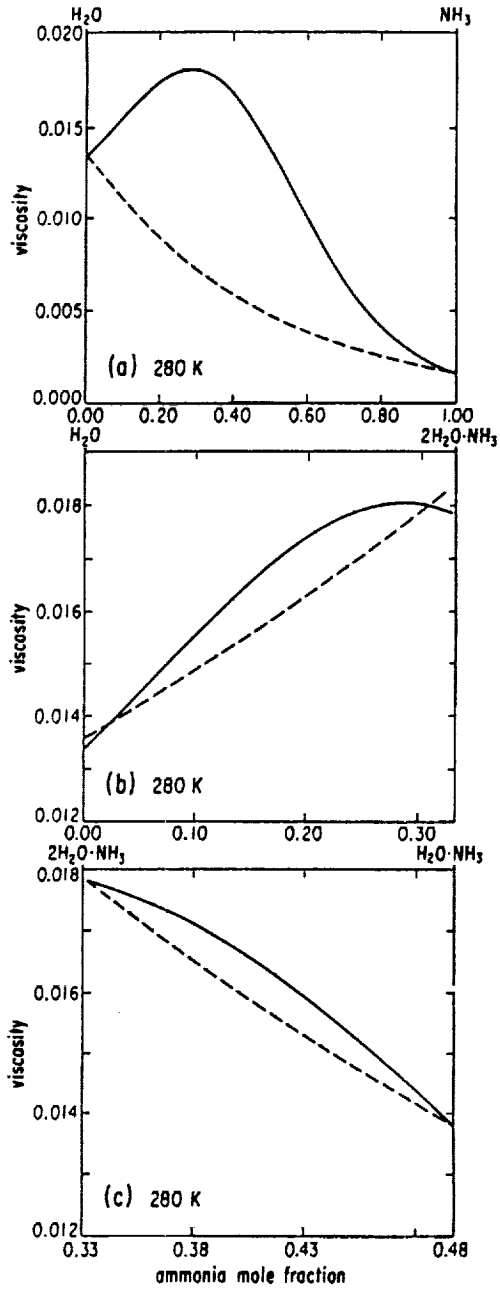

FIG. 11. Viscosity (in poises) versus ammonia mole fraction at 280 K, shown by the solid lines based on fits described in the text. The dashed line in (a) is a model viscosity based on ideal solution of individual ammonia and water molecules. The dashed line in (b) and (c) is a model viscosity based on ideal solution, in which the endmembers represent the compositions of the congruent melting points (or equivalently, the solid hydrates).

We have performed the same test at 220 K, the lowest temperature at which sufficient data are available to make accurate comparisons, and reach the same conclusion. The end member water–ammonia model provides a poor fit to the viscosity data (discrepancies of up to 90%); using

the congruent compositions as end members reduces the errors to 17% or less at 220 K. Note that in this case, we have had to extrapolate the pure water viscosity to well-below the freezing point which undoubtedly introduces additional errors at this low temperature.

The conclusion we draw from Fig. 11 is that the viscosity of the ammonia–water system, well into the liquid regime, can be interpreted in terms of a liquid structure composed of clusters of molecules corresponding to the composition of the solid hydrates (or equivalently the congruently melting end members). Thus from 0 to 33% ammonia, free ammonia molecules do not exist; instead the smallest ammonia unit in the liquid is $2H_2O.NH_3$. From 33 to 50%, the smallest units in the liquid are dihydrate and monohydrate "molecules." Evidence for any additional structure in the liquid which limits accessible configurations is slim or nonexistent. To search for such additional order, higher precision in the data at low temperatures is required. However, additional evidence for order is provided in the following subsection, which treats the dependence of viscosity on temperature.

Viscosity vs temperature. We fitted the viscosity data (for 33% ammonia liquid) with the expression:

$$\mu \propto \exp(B/T) \tag{13}$$

While in the previous section we argued that the viscosity is given as a function of composition by a composite expression involving at least two terms, we are only interesting here in fixed composition and variable temperature. In effect, we are assigning B to be an "activation energy" (normalized by the gas constant) in the sense of a simple Newtonian fluid, and asking what is its variation with temperature. No more significance than this should be attached to the fit.

The data show two interesting characteristics when fitted to Eq. (13). First, there is a significant change in activation energy at around 240 K, wherein below 240 K $B = 4200$, and above 240 K $B = 2050$ as described in Section 3.1. In both temperature regions B is nearly constant with temperature. Below 176 K, the subcooled liquid has a value of B which increases steeply with decreasing temperature below the peritectic, presaging the onset of glass formation at some lower temperature. The change in activation energy near 240 K suggests a structural change in the liquid involving a loss of attainable configurations at temperatures below the transition. Unfortunately, with the present data, we cannot constrain well the width (in temperature) of the transition; however, we are confident that the data show a discrete rather than gradual change in the liquid structure. The effect is reminiscent of the changes in physical properties which water undergoes as it approaches its freezing point, in which significant long-range order becomes rather established with decreasing temperature (Eisenberg and Kauzmann 1969).

It therefore appears that, in addition to the formation of single-unit hydrate clusters in the liquid over a large range of temperature, some long-range order involving many clusters becomes established at temperatures approaching the congruent melting point of the hydrates. Further investigation of this effect requires higher precision in the viscosity data.

Likewise, the onset of the glass transition is suggested by the peritectic-composition data below 176 K. In this regime the viscosity can be described by an equation which takes account of incipient glass formation at a temperature T_g

$$\mu \propto \exp\left(\frac{+D}{T - T_g}\right), \tag{14}$$

where D is a constant. Preliminary calculations were performed to estimate a glass temperature based on the viscosity data and are in fair agreement with the observed value, measured by Van Kasteren, of 120 K. However, the scatter in the viscosity data permits acceptable fits producing glass temperatures up to 140 K. Therefore, more precise data are required before we can assert with certainty that we are seeing the onset of glass formation in the peritectic liquid.

4.2. *Volcanological Implications of Slurry Rheology*

Figures 1 and 4 illustrate an important rheological consequence of partial crystallization. The sharp increase in viscosities starting with the onset of crystallization is very similar to that observed for silicate lavas, particularly basalt. However, it is likely that relative viscosities of lavas in general depend not just on the crystal fraction but probably also on the size distribution and form of the crystals. Obviously, skeletal, dendritic, and rodlike crystals would interact differently (more extensively) than spherical or other equant crystals would. Delicate skeletal and rod-like crystallites form when liquid water is quenched (Hobbs 1974) and when water vapor condenses rapidly below the frost point (forming snow and frost). Slow crystallization or recrystallization after rapid precipitation in lavas and glacial ice causes larger, more equant crystal forms to develop so as to minimize the surface area and associated free energy. We expect that a similar behavior would occur in ammonia–water and other aqueous slurries and that this would have rheological effects. Consistent with this idea, we have observed that the viscosity of ammonia–water slurries is somewhat dependent on its thermal history (Section 3.3).

Having expressed our concern that the viscosity of a

particular composition probably depends on much more than just its temperature and crystal content, we can still state with surety that the slurries we examined behaved rheologically very much like silicate lavas. This is not a trivial observation since it is by no means obvious that hydrogen-bonded aqueous mixtures should behave similarly to silicate lavas. The fact that these substances do exhibit similar rheological behavior, at least under the conditions we examined, implies that it is reasonable to interpret cryovolcanic morphologies on the basis of experience gained with terrestrial and extraterrestrial silicate lava flows.

The relative viscosities of ammonia–water slurries and of silicate lavas are much greater than predicted based on Einstein–Roscoe approximations assuming spherical particles (Graham *et al.* 1964). A mere 25% crystallization can increase the viscosities of ammonia–water and silicate slurries by *three orders of magnitude* relative to the homogeneous liquid phase. This increase can be modeled (see "modified E–R" curve in Fig. 4) by a modified form of the Einstein–Roscoe formulation

$$\mu_r = \mu_l(1 - C\phi)^{-2.5}, \qquad (15)$$

where the coefficient C is assigned a value of 3.7 (this compares to $C = 1.35$ for uniform spheres traveling in aggregates). C physically represents the increased effectiveness of highly aspherical crystals and crystal aggregates in blocking much of the liquid volume from participating in the deformation of the slurry.

According to Eq. (15), $C = 3.7$ means that a slurry would behave as a solid when ϕ attains a value near 30% crystals (compared to about 70% crystals for uniform spheres where $C = 1.35$, and 100% crystals for a serial distribution of sphere sizes where $C = 1$). Possibly this is the critical crystal fraction when a basalt or ammonia–water slurry attains a yield strength, or at least appears to have one. Below this critical crystal fraction, where all of our measurements were made, we observed a Newtonian rheology for near-peritectic slurries, and a power-law rheology for water-rich slurries (Section 3.3).

Even in the total absence of a yield strength the effective cessation of motion of a cooling flow could be quite abrupt, occurring when the chilled flow front and margins crystallize the critical volume fraction of solids. When this happens the viscosity of the chilled crust of the flow increases sharply, even as the less crystallized interior slurry maintains a relatively low viscosity. This effect could be approximated with a Bingham rheology involving a yield strength. However, on the basis of our experiments and the data of others (e.g., Shaw 1969, and Murase *et al.* 1985), we suspect that the commonly utilized Bingham model is simply a convenient way to approximate thermally and rheologically heterogenous flows having power-law rheologies. The final dimensions of lava flows depend on the dynamical problem of the characteristics of the eruptive event, the viscous run-out of the flow, and the cooling behavior of the flow margins. Any true yield strength probably does not appear until the final moments when the lava flow has already virtually attained its final shape. This could explain the widely observed correlation between lava viscosity (and composition) and apparent yield strength (McBirney and Murase 1984, Murase *et al.* 1985, Fink and Zimbelman 1986, Moore and Ackerman 1989). Nevertheless, the yield strength concept is widely used among volcanologists, and we feel that it does provide useful results.

4.3. Cryolava Rheology and Comparative Planetology

Surface gravity is probably one of the more important variable parameters affecting the evolution and appearance of planets and satellites. Of present concern are the effects that intersatellite variations in surface gravity may impose on the dimensions and morphologies of cryovolcanic flows. Variations in lava viscosity affect lava flow morphology opposite to variations in the product of lava density and surface gravity. This is evident, for example, in problems dealing with Newtonian flow down an inclined plane or channel flow (Turcotte and Schubert 1982). Since simple rheological models of lava flows often seem to give incorrect results (evidently because the dynamical rheological structures of lava flows are not simple!), we find it easiest and safest to perform a first-order gravity scaling of cryogenic liquids so as to arrive at a gravity-scaled rheological analog among terrestrial lavas. Based on simple flow models we define a "mobility index" = $\log_{10}(\rho g/\mu)$. Liquids with the same mobility index should, to a reasonable approximation, behave in rheologically similar ways.

Figure 12 shows the mobility indices of silicate and cryogenic liquids plotted against surface gravity. Obviously our choice of plotting parameters ensures that there will be a positive correlation with a slope of unity. The purpose of this figure is simply to provide a visual guide for rheological gravity scaling.

For example, from Fig. 12 we see that liquid water and salt brines on Ganymede would be about 10 times "runnier" than the most fluid lavas (komatiite) on Earth, thus probably producing submeter flow thicknesses on Ganymede. Mixtures of nondipolar molecules such as methane and nitrogen on Triton would be even more fluid. Ammonia–water on Enceladus should be roughly comparable to andesite on Earth, perhaps producing flows on the order of a few tens of meters thick on low slopes. Ammonia–water–methanol on Miranda or Ariel should behave like rhyolite on Earth, producing flows up to several hundred meters thick on low slopes.

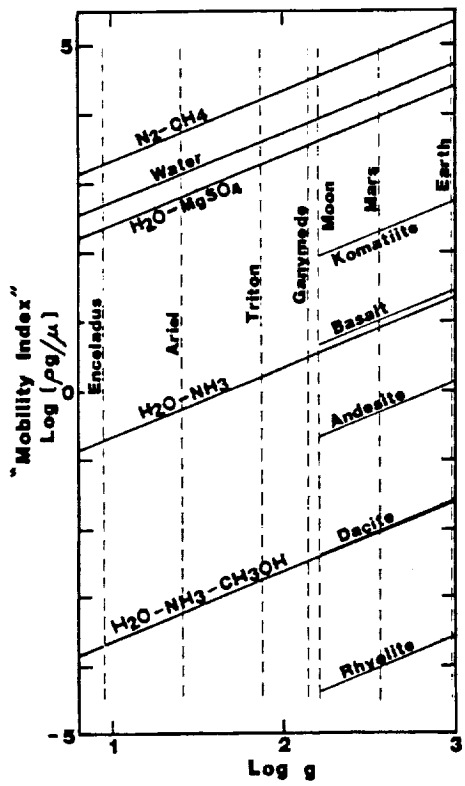

FIG. 12. Gravity-scaling of viscosities of volcanic and cryovolcanic liquids. In each case the viscosity at the freezing point (liquidus) and in the absence of suspended crystals is represented. Data for volatile mixtures are the eutectic and peritectic compositions. Silicate lava viscosities are from the first author's compilation of experimental data for natural and synthetic rock compositions, and the temperatures for which these viscosities apply are the eutectic temperatures in synthetic water-free multicomponent mixtures approximating natural rock compositions (Morse 1980).

Another important aspect illustrated by Fig. 12 is that while intersatellite variations in surface gravity may be an important variable factor controlling surface morphologies, cryolava compositions are far more important if these compositions vary significantly through the outer Solar System.

4.4. Observed Cryovolcanic Morphologies

The observed morphologies of volcanic deposits on the terrestrial planets have been used to place crude constraints on the magma rheologies (e.g., Pieri and Baloga 1986, Dragoni *et al.* 1986, Fink and Bridges 1990, and references therein). The techniques are admittedly imperfect, but seem to give reasonable results. Not all of the techniques can be applied to flows on the icy satellites because not all of the morphologic features found on terrestrial flows are seen on the ice flows, probably because of the generally poor resolution (order 1–10 km) of available images of icy satellite cryovolcanic deposits. A few techniques are useful, however. Fink (1980) presented a theory from which the internal viscosity of a volcanic flow can be estimated from the amplitude and wavelength of drag folds (corda or festoons) on the flow surface, when present. Hulme (1974) presented a method of estimating the yield strength of a flow from the height and curvature of the flow's convex or lobate edge. Since effective yield strengths seem to correlate with viscosities, the latter gives a qualitative estimate of viscosities as well. Assuming that these techniques can be applied to deposits on the icy satellites, the observed morphologies imply a broad range of effective viscosities at the time of emplacement for deposits on various satellites.

The coronal deposits on the Uranian satellite Miranda are interpreted as cryovolcanic flows (Croft 1987, 1988) with lobate edges hundreds of meters thick and surface ripples with amplitudes of hundreds of meters and wavelengths of a few kilometers. Assuming the ripples are corda, internal viscosities of 10^8–10^9 poise are obtained. The lobate deposit dimensions imply yield stresses of 0.01–0.1 bar. Both measurements are consistent with each other and imply rheologies comparable to terrestrial andesites. On Ariel, there are long linear and lobate flows with convex edges on the order of a kilometer high, implying yield strengths on the order of a bar. No corda are visible, but comparison with the inferred yield strength indicate probable viscosities in the range of 10^{10} poise. These high viscosities imply that the erupted substances on Miranda and Ariel were composed of some low-melting-temperature aqueous mixture, probably involving several chemical components and perhaps a high degree of crystallinity. High as they are, these viscosity estimates are orders of magnitude below the 10^{16} poises obtained by Jankowski and Squyres (1988) for the flows on Ariel. Straightforwardly interpreted viscosities of this order would suggest that the flows were erupted as solid ice (as the title of their paper indicates) rather than as volcanic slurries. However, Jankowski and Squyres pointed out that their viscosities are upper limits, and considered alternatives to solid ice including ice mobilized by interstitial cryogenic liquids. Jankowski and Squyres' models assumed a homogeneous and purely viscous rheology, and did not adequately consider the critically important rheological effects of the chilled crust of the flows on their mobility. Following Greenberg *et al.* (1990) and Schenk (1989), who suggested that a 4–6 order-of-magnitude crust correction factor must be applied to the results of simple flow models, we consider (on the basis of Jankowski and Squyres' uncorrected results) that eruptive viscosities on the order of 10^{10}–10^{12} poises are more likely for Ariel, and an order of magnitude less for Miranda, in rough agreement with the results based on corda and yield strengths.

Neptune's large satellite Triton has both flat deposits

with no discernable lobate edges and thick, lobate flows and ridges. The former are apparently low-viscosity deposits, possibly like those on Enceladus and Tethys, whereas the latter are high viscosity deposits with rheologies comparable to the stiff flows on Ariel and Miranda (Kargel and Strom 1990).

Several Saturnian satellites show evidence of resurfacing. Most spectacular are the broad, smooth plains of Enceladus. These plains are nearly featureless at the best image resolutions (2 km per line-pair), except where they are interrupted by arcuate and linear ridges (Squyres *et al.* 1983, Pozio and Kargel 1989). The lack of obvious flow margins and fronts in these plains, coupled with the very low surface gravity of Enceladus, indicates that the cryovolcanic liquids must have possessed much lower viscosities than the substances which formed the lobate deposits on the Uranian and Neptunian satellites. However, considering the limitations of image resolution, substances as viscous as ammonia–water are allowed.

Another large cryovolcanic plain is found on Tethys to the east of Ithaca Chasma. The plain is recognizable in contrast to the rugged cratered terrain due to its flat surface and somewhat lower crater density. The western boundary of the plain with the cratered terrain is very irregular (Moore and Ahern 1983) and suggests flooding of the rugged upland to a constant topographic level. There is no visible raised edge to the plains deposit, again suggesting a relatively low viscosity at the time of emplacement.

Another style of cryovolcanism is seen on Ganymede, the largest of the icy satellites. Its surface consists of moderately cratered dark plains and light, grooved, smooth materials. The light materials were early recognized to be cryovolcanic deposits on the basis of age, stratigraphy, and embayment relationships (e.g., Lucchitta 1980, Head *et al.* 1981, Parmentier *et al.* 1982). The rougher dark plains were later recognized to consist of a complex of darker cryovolcanic flows based again on embayment patterns, age relationships, and albedo variations (Casacchia and Strom 1984, Croft 1985, 1986). The edges of the light deposits are generally defined by tectonic structures. In the few cases where embayment relations are not tectonically disturbed, there is little or no evidence for a raised edge where topographic variations on the order of 100 m would easily be seen. The boundaries of albedo patches within the dark terrain (which presumably represent individual flows or distinct groups of flows) range from relatively sharp to quite diffuse. The highest resolution images show little or no vertical definition to the edges of the albedo patches or to the smooth dark patches within the dark terrain (interpreted as local flooding by Casacchia and Strom 1984), again where topographic variations of 100 m would be visible. The thinness of the flows and the general lack of definable flow edges indicate low viscosity flows with maximum yield stresses of 0.01–0.1 bar, and probably much less. The flows may have been emplaced as liquid water, slush, or brine with viscosities of 10^{-2} poise, although ammonia–water cannot be ruled out based on the available data. Observations by Galileo will place firmer bounds on the rheology and composition.

The cryovolcanic surfaces seen on the icy satellites vary enormously in their morphologies, and accordingly we infer a great range in their rheological properties at the times of eruption. These properties are nonetheless within the range of viscosities for likely cryomagma compositions. In particular, the higher inferred viscosities on the icy satellites can easily be reached by partially crystallized cryogenic binary materials such as ammonia–water or by cryogenic ternary mixtures, while very water-rich substances, salt brines, or ice-free ammonia–water can explain the lower inferred viscosities. A direct correspondence between composition and morphology is not justifiable, because the inferred differences in rheology may be (and probably are) due to differences in eruption temperatures and crystallinity of the cryomagmas as well as differences in composition. In addition, pressure is an important variable affecting liquid compositions and cryovolcanic rheologies (Cynn *et al.* 1989; Hogenboom and Kargel, 1990), although we have not explicitly considered such effects to date. Beyond these uncertainties, we find it intriguing that the more fluid cryolavas were erupted on the satellites of Jupiter and Saturn, while the more viscous cryolavas were erupted on the satellites of Uranus and Neptune.

5. SUMMARY

Cryovolcanic deposits have been observed on many of the icy satellites. We have gathered relevant viscosity data from the literature and have performed new viscosity measurements on a number of theoretically plausible cryomagma compositions. The compositions included binary and ternary mixtures of water, ammonia, and methanol, both as liquids and as partially crystallized slushes. The viscosities of one-component liquids are orders of magnitude too fluid to account for many of the flows, particularly those any with discernable thickness. Binary mixtures of liquid water and ammonia have substantially higher viscosities, up to 100 poise, enough to account for many of the observed flows. The thickest observed flows require the much higher viscosities that are only reached in our experiments by ternary mixtures or partially congealed binary mixtures. Collectively, these materials can account for all observable flows; thus, we find no justification for postulating solid-state extrusion.

These experiments point out the importance of mixtures of simple compounds that provide a difference in temperature between the solidus and liquidus in allowing the complex behavior of real extrusive materials, whether on the

terrestrial planets or on the icy satellites. Our experiments are still only an initial foray into the complexity of materials and material properties that almost certainly exists on the icy satellites, complexity that must be taken into account as more detailed models of their structure and history are constructed.

ACKNOWLEDGMENTS

We thank Robert Strom for many constructive discussions related to this work. Special thanks to Jay Melosh who kindly loaned us his Brookfield viscometer. J.I.L. acknowledges support from NASA Grant NAGW-1039; S.K.C. and J.S.K. from NSG-7146; and J.S.K. and J.S.L. from NHGW-340.

REFERENCES

ALEI, JR., M., AND W. M. LITCHMAN 1972. Density and viscosity of liquid ND_3. *J. Chem. Phys.* **57**, 4106–4110.

BEVINGTON, P.R. 1969. *Data Reduction and Error Analysis for the Physical Sciences*. McGraw-Hill, New York.

CASACCHIA, R., AND R. G. STROM 1984. Geologic evolution of Galileo Regio, Ganymede. *Proc. Lunar Planet. Sci. Conf. 14, part 2, J. Geophys. Res. (Suppl.)* **89**, B419–B428.

CONSOLMAGNO, G. J., AND J. S. LEWIS 1978. The Evolution of Icy Satellite Interiors and Surfaces. *Icarus* **34**, 280–293.

CROFT, S. K. 1985. A new scenario for differentiation of Ganymede and Callisto. *Lunar Planet. Sci. XVI*, 152–153.

CROFT, S. K. 1986. Ganymede and Callisto: Toward a new synthesis. *Rep. Planet. Geol. Geophys.—1895*. NASA TM 88383, 57–59.

CROFT, S. K. 1987. Miranda geology and tectonics: A non-catastrophic interpretation. *Lunar Planet. Sci. XVIII*, 207–208.

CROFT, S. K. 1988. Miranda's Inverness Corona interpreted as a cryovolcanic complex. *Lunar Planet. Sci. XIX*, 225–226.

CROFT, S. K., J. I. LUNINE, AND J. S. KARGEL. 1988. Equation of state of ammonia–water liquid: Derivation and planetological application. *Icarus* **73**, 279–293.

CYNN, H.-C., S. BOONE, A. KOUMVAKALIS, M. NICOL, AND D. J. STEVENSON 1989. Phase diagram for ammonia–water mixtures at high pressure: Implications for icy satellites. *Proc. Lunar Planet. Sci. Conf., 19th*, pp. 433–441.

DRAGONI, M., M. BONAFEDA, AND E. BOSCHI 1986. Downslope flow models of a bingham liquid: Implications for lava flows. *J. Volcanol. Geotherm. Res.* **30**, 305–325.

EISENBERG, D., AND W. KAUZMANN 1969. *The Structure and Properties of Water*. Oxford Univ. Press, New York.

FIDLERIS, V., AND R. L. WHITMORE 1961. Experimental determination of the wall effect for spheres falling axially in cylindrical vessels. *Brit. J. Appl. Phys.* **12**, 490–494.

FINK, J. 1980. Surface folding and viscosity of rhyolite flows. *J. Volcanol. Geothermal Res.* **8**, 250–254.

FINK, J., AND N. BRIDGES 1990. Predicting extra-terrestrial lava flow morphology. *Lunar Planet. Sci. XXI*, 363–364.

FINK, J. H., AND J. R. ZIMBELMAN 1986. Rheology of the 1983 Royal Gardens basalt flows, Kilauea Volcano, Hawaii. *Bull. Volcanol.* **48**, 87–96.

GRAHAM, A. L., R. D. STEELE, AND R. B. BIRD 1964. Particle clusters in concentrated suspensions. 3. Prediction of suspension viscosity. *Ind. Eng. Chem. Fundam.* **23**, 420–425.

GREENBERG, R., S. CROFT, D. JANES, J. KARGEL, L. LEBOFSKY, J. LUNINE, R. MARCIALIS, H. MELOSH, G. OJAKANGAS, AND R. STROM 1991. Miranda, in *Uranus* (J. Bergstralh and M. S. Matthews, Eds.). Univ. of Arizona Press, Tucson. In press.

HAAR, L., J. S. GALLAGER, AND G. S. KELL 1984. *NBS/NRC Steam Tables*. Hemisphere Pub. Corp. New York.

HEAD, J. W., M. L. ALLISON, E. M. PARMENTIER, AND S. W. SQUYRES 1981. High-albedo terrain on Ganymede: Origin as flooded graben. *Lunar Planet. Sci. XII*, 418–420.

HOBBS, P. V. 1974. *Ice Physics*. Oxford Univ. Press.

HOGENBOOK, D. L., AND J. S. KARGEL 1990. Ammonia–water densities and phase relations to four kilobars. *Lunar Planet. Sci. XXI*, 522–523. [Abstract]

HULME, G. 1974. The interpretation of lava flow morphology. *Geophys. J. R. Astron. Soc.* **39**, 361–383.

HUMMEL, W., AND J. ARNDT 1985. Variation of viscosity with temperature and composition in the plagioclase system. *Contrib. Mineral. Petrol.* **90**, 83–92.

IRVINE, W. M., F. P. SCHLOERB, A. HJALMARSON, AND E. HERBST 1985. The chemical state of dense interstellar clouds: An overview. In *Protostars and Planets II*. (D. E. Black and M. S. Matthews, Eds.), pp. 579–620. Univ. of Arizona Press, Tucson.

JANKOWSKI, D. G., AND S. W. SQUYRES 1988. Solid-state ice volcanism on the satellites of Uranus. *Science* **241**, 1322.

KARGEL, J. S. 198?. Density and Viscosity Measurements of NH_3–H_2O Liquids. *Lun. Planet. Sci. XVIII*, 475–476. [Abstract]

KARGEL, J. S. 1988. Liquidus phase relations and liquid properties in the system H_2O–NH_3–CO_2–H_2CO. *Lun. Planet. Sci. XX*, 583–584. [Abstract]

KARGEL, J., AND R. STROM 1990. Cryovolcanism on Triton. *Lun. Planet. Sci. XXI*, 599–600. [Abstract]

KARGEL, J. S. 1990. *Cryomagmatism in the Outer Solar System*. Ph.D. dissertation. Univ. of Arizona, Tucson, 309 pages.

KHARE, B. N., W. R. THOMPSON, B. G. J. P. T. MURRAY, C. F. CHYBA, C. SAGAN, AND E. T. ARAKAWA 1989. Solid organic residues produced by irradiation of hydrocarbon-containing H_2O and H_2O/NH_3 ices: Infrared spectroscopy and astronomical implications. *Icarus* **79**, 350–361.

LE CLAIR, B. P., A. E .HAMIELEC, AND H. R. PRUPPACHER 1970. A numerical study of the drag on a sphere at low and intermediate reynolds numbers. *J. Atmos. Sci.* **27**, 308–315.

LEWIS, J. S. 1972. Low temperature condensation from the solar nebula. *Icarus* **16**, 241–252.

LUCCHITTA, B. K. 1980. Grooved terrain on Ganymede. *Icarus* **44**, 481–501.

MCBIRNEY, A. R., AND T. MURASE 1984. Rheological properties of magmas. *Annu. Rev. Earth Planet. Sci. 1984*, 337–357.

MCKINNON, W. B., AND M. MEADOWS 1984. Rheological measurements of ammonia–water melt. *Bull. Amer. Astron. Soc.* **16**, 686. [Abstract]

MOORE, H. J., AND J. A. ACKERMAN 1989. Martian and terrestrial lava flows. *Lun. Planet. Sci. XX*, 711–712. [Abstract]

MOORE, J. M., AND J. L. AHERN 1983. The geology of Tethys. *Proc. Lunar Planet. Sci. Conf. 13th, Part 2, J. Geophys. Res. Suppl.* **88**, A577–A584.

MORSE, S. A. 1980. *Basalts and Phase Diagrams*. Springer-Verlag, New York.

MURASE, T., A. R. MCBIRNEY, AND W. G. MELSON 1985. Viscosity of the dome of Mount St. Helens. *J. Volcanol. Geotherm. Res.* **24**, 193–204.

PARMENTIER, E. M., S. W. SQUYRES, J. W. HEAD, AND M. L. ALLISON 1982. The tectonics of Ganymede. *Nature* **295**, 290–293.

PIERI, D., AND S. M. BALOGA 1986. Eruption rate, area, and length relationships for some Hawaiian lava flows. *J. Volcanol. Geotherm. Res.* **30**, 29–45.

PINEVICH, G. 1948. Viscosity of ammonia–water solutions and of liquid ammonia. *Kholodil. Tekh.* 20(3), 30–37. [In Russian]

PLESKOV, V. A., AND I. IGAMBERDYEV 1939. Viscosity of mixtures of ammonia and water at 20°C. *J. Phys. Chem. (USSR)* **13**, 701–702.

POZIO, S., AND J. S. KARGEL 1989. The tectonic and igneous evolution of Enceladus. *Lunar Planet. Sci. XX*. 864–865.

ROESSLER, K., AND B. NEBELING 1988. High energy and radiation chemistry in space. *Lunar Planet. Sci. XIX*, 994–995. [Abstract]

ROLLET, A. P., AND G. VUILLARD 1956. Sur un novel hydrate de l'ammoniac. *C.R. Acad. Sci. Paris* **243**, 383–386.

RUPERT, F. F. 1909. The solid hydrates of ammonia. *J. Amer. Chem. Soc.* **31**, 866–868.

SCHENK, P. 1989. Fluid volcanism on Miranda and Ariel. *Lunar Planet. Sci. XX*, 958–959. [Abstract]

SHAW, H. R. 1969. Rheology of basalt in the melting range. *J. Petrol.* **10**, 510–535.

SQUYRES, S. W., R. T. REYNOLDS, P. M. CASSEN, AND S. J. PEALE 1983. The evolution of Enceladus. *Icarus* **53**, 319–331.

TOULOUKIAN, Y. S., S. C. SAXENA, AND P. HESTERMANS 1975. Viscosity of liquids and liquid mixtures. In *Thermophysical Properties of Matter*. Vol. 11. Viscosity, pp. 33–46. Plenum, New York.

TURCOTTE, D. L., AND G. SCHUBERT 1982. *Geodynamics: Applications of Continuum Physics to Geological Problems*. Wiley, New York.

VAN KASTEREN, P. H. G. 1973. The crystallization behavior and caloric properties of water/ammonia mixtures between 70 and 300 K. *Bull. Inst. Froid. Annexe* **4**, 81–87.

WEAST, R. C., AND S. M. SELBY 1967. *Handbook of Chemistry and Physics*, 48th ed., Chemical Rubber Co., Cleveland.

ICARUS 94, 368–390 (1991)

Brine Volcanism and the Interior Structures of Asteroids and Icy Satellites

JEFFREY S. KARGEL

Lunar and Planetary Laboratory, University of Arizona, Tucson, Arizona 85721

Received January 28, 1991; revised September 6, 1991

Cryovolcanism is among the foremost processes responsible for modifying the surfaces of icy satellites. Volcanic brine petrogenesis in ammonia-deficient satellites should mainly involve eutectic melting in relevant salt–water systems. Carbonaceous chondrites provide useful insights into the compositions of salts and aqueously altered rock in icy satellites and asteroids. C1 chondrites contain about one-fifth by mass of salts in various states of hydration. Many aspects of the petrogenesis and physical volcanology of icy satellite brines should be well described in the system H_2O–$MgSO_4$–Na_2SO_4. Minor components include sulfates of K, Ni, Mn, and Ca. Chondrites also contain abundant carbonates, but these are probably not very important in brine magmatism due to their low solubilities under expected conditions. Chlorides are also unimportant under most circumstances because of the low cosmic abundance ratio of Cl/S. Soluble salts may have profound effects on the geology and structure of icy satellites and asteroids. In some models late episodes of water volcanism are facilitated by high buoyant forces due to the relatively high densities of sulfate-rich mantle and crustal layers. In other models early hypersaline brine volcanism quickly yields to plutonic magmatism due to low crustal densities. Europa probably has a layered crust composed of anhydrous Mg–Na sulfates near the base and a frozen or partially molten eutectic mixture of ice and hydrated Mg and Na sulfates near the surface. Ganymede may have a crust about 300 km thick composed of a 10 : 1 ratio of ice : mirabilite, and a mantle 500 km thick composed of 50% ice phases plus 50% hydrated Mg and Na sulfates.

1. INTRODUCTION

Many icy satellites have dynamic geologic histories including episodes of widespread cryovolcanism and extensive internal chemical differentiation. Cryovolcanism, first predicted by Lewis (1971), is among the most important processes documented by the Voyager project. Most volcanic plains on icy satellites apparently were extruded as aqueous solutions formed by partial melting. The compositions of aqueous "lavas" are likely to fall into two broad classes: relatively high-temperature salt–water solutions and truly cryogenic mixtures of ammonia, water, and other substances. This work is devoted to a sentation of the properties and probable composit of ammonia-free salt–water solutions, and on selec planetological applications of these data.

Aqueous brines rather than ammonia–water liqu would have been generated wherever ammonia was sent or deficient, and temperatures in the satellite's asteroid's interior attained the eutectic melting poin a relevant salt–water mixture. NH_3 would be abse regions of the Solar System where temperatures in solar or circumplanetary nebula remained too warm ammonia hydrates to condense; where nebular nitrog was entirely in the form of N_2 rather than NH_3 (Prinn a Fegley 1988); where some NH_3 condensed but the amou was stoichiometrically deficient with respect to high reactive substances such as CO_2 (yielding ammonium c bonate) and H_2CO (yielding hexamethylenetetramin (Kargel 1990); or where prior melt extraction episo had left the interior barren of ammonia hydrate and wi excess water ice and soluble salts. One or more of the situations could have prevailed for any given satellite asteroid, to the best of our knowledge. However, NH free brine volcanism is most likely to have occurred o large asteroids and the icy Galilean satellites of Jupite temperatures in the nebula where these objects forme probably exceeded those required for ammonia hydrat condensation (Lewis 1974, Cameron 1978, Prinn and Fegley 1981).

Salt–water cryomagmatism may occur by either of tw paths, depending on whether salts were initially present If the rock component resembled type C1 or C2 carbona ceous chondrites then it would initially have containe abundant water-soluble substances. If, however, thes objects and their precursor material had never seen aque ous chemistry prior to or during accretion then these ob jects would have consisted of ice intermixed with rock resembling C3 or ordinary chondrites; as internal temperatures attained or approached the melting point of ice aqueous reactions would have driven the assemblage to-

0019-1035/91 $3.00

ward equilibrium, possibly yielding hydrated phyllosilicates and soluble salts. Thus, regardless of whether salts were initially present, partial melting probably would yield brines rather than pure water. The composition and salinity of a particular brine would depend on the oxidation state of sulfur in the rock, solution pH, and other factors.

This contribution will: (1) constrain the probable compositions of brines generated in chondritic asteroids and icy satellites; (2) present an objective rationale simplifying these compositions to a minimum of components; (3) examine some physical properties of simple salt–water mixtures; and (4) discuss possible planetological consequences of salt–water magmatism.

This paper is restricted to physical chemistry data appropriate to 1 atm due to a paucity of relevant data taken at elevated pressures. The planetological applications at this juncture are exploratory and qualitative. The author and co-workers have recently initiated experimental studies of high-pressure phase equilibria in salt–water systems necessary for more quantitatively realistic planetological applications (Hogenboom *et al.* 1991).

Previous publications from this laboratory related to cryovolcanism have dealt mainly with the densities and viscosities of ammonia–water liquids (Croft *et al.* 1988, Kargel *et al.* 1991). A review of published and original physical chemistry data for a broad range of plausible crovolcanic liquids and general applications to the geology of icy satellites were presented in the author's dissertation (Kargel 1990).

The compositions of volcanic brines may vary within broad limits. These compositions dictate the temperatures of partial melting and the likelihood that melting can occur in convecting satellites. These compositions also determine the quantities of brine and the thicknesses of salty crusts and mantles that might form, the surface compositions of icy satellites, the physical properties of erupted brines, and the morphologic characteristics of landforms and landscapes produced by brine volcanism.

2. IMPLICATIONS OF CHONDRITE SALTS FOR EXTRATERRESTRIAL BRINE COMPOSITIONS

Aqueous alteration of carbonaceous chondrites. Carbonaceous chondrites offer valuable insights into the nature of low-temperature water–rock chemical interactions in chondritic asteroids, and the composition of water-soluble material produced during such alteration events. Aqueous alteration in carbonaceous chondrites is shown by a great abundance of aqueously precipitated salts, of secondary phyllosilicates including montmorillonite, saponite, chlorite, and serpentine, of certain sulfides and hydroxides including tochilinite and brucite, and of spherulitic magnetite (DuFresne and Anders 1962, Bostrom and Fredriksson 1964, Kerridge *et al.* 1979, Zolensky and McSween 1988, Bunch and Chang 1980, Barber 1985, Keller and Buseck 1990). In a general sense, most salts and alteration products in chondrites are similar to the phases produced by chemical weathering, diagenesis, and low-grade metamorphism of common terrestrial rocks. Since primary phases in chondrites are also generally similar to terrestrial crustal phases, including olivine, pyroxenes, feldspars, and sulfides, one reasonably infers that many of the aqueous reactions in carbonaceous chondrite parent bodies were probably similar to common terrestrial weathering and low-grade metamorphic reactions involving combinations of oxidation, carbonation, hydrolysis, and hydration.

Formation of secondary epsomite, magnetite, and serpentine can be represented by a composite reaction involving the oxidation of troilite and hydrolysis of forsterite in an aqueous medium:

$$12Mg_2SiO_4 + 6FeS + 54H_2O + 13O_2 \rightarrow 6[Mg_3Si_2O_5(OH)_4] + 6[MgSO_4 \cdot 7H_2O] + 2Fe_3O_4 \quad (1)$$

Planetologists commonly assume that the rock in icy satellites closely resembles carbonaceous chondrites chemically and mineralogically. Quite incompatibly, another common assumption is that the rocky fraction of icy satellites does not participate in low-temperature magmatic processes except as a stable inert component of the residuum of partial melting. While few would argue that the first assumption is unlikely, the second assumption, that rock is inert, is generally invalid. Either the rock contains abundant water-soluble salts if it resembles type 1 or 2 carbonaceous chondrites, or, if it more closely resembles type 3 carbonaceous chondrites or unequilibrated ordinary chondrites, then the rock contains unstable anhydrous minerals that normally would break down and yield soluble components upon reaction with water. As shown in Fig. 1a, the quantities of soluble matter present in extensively altered type C1 chondrites and less altered C2 chondrites are considerable. Commensurate with these abundances are the effects that the salts would have on the igneous and geological evolution of differentiated icy satellites and asteroids.

Theoretical modeling of cryomagma generation and evolution in salty icy satellites and asteroids is much more complex than in the simplistic salt-free case, since the number of chemical components, and free parameters, becomes very large. However, several factors justify consideration of simplified chemical systems.

Salts dominated by $MgSO_4$. Salts in C1 and C2 chondrites are dominated by metal sulfates (Fig. 1b), particularly the hydrated magnesium sulfate, epsomite ($MgSO_4 \cdot 7H_2O$). Other important salt components include sulfates

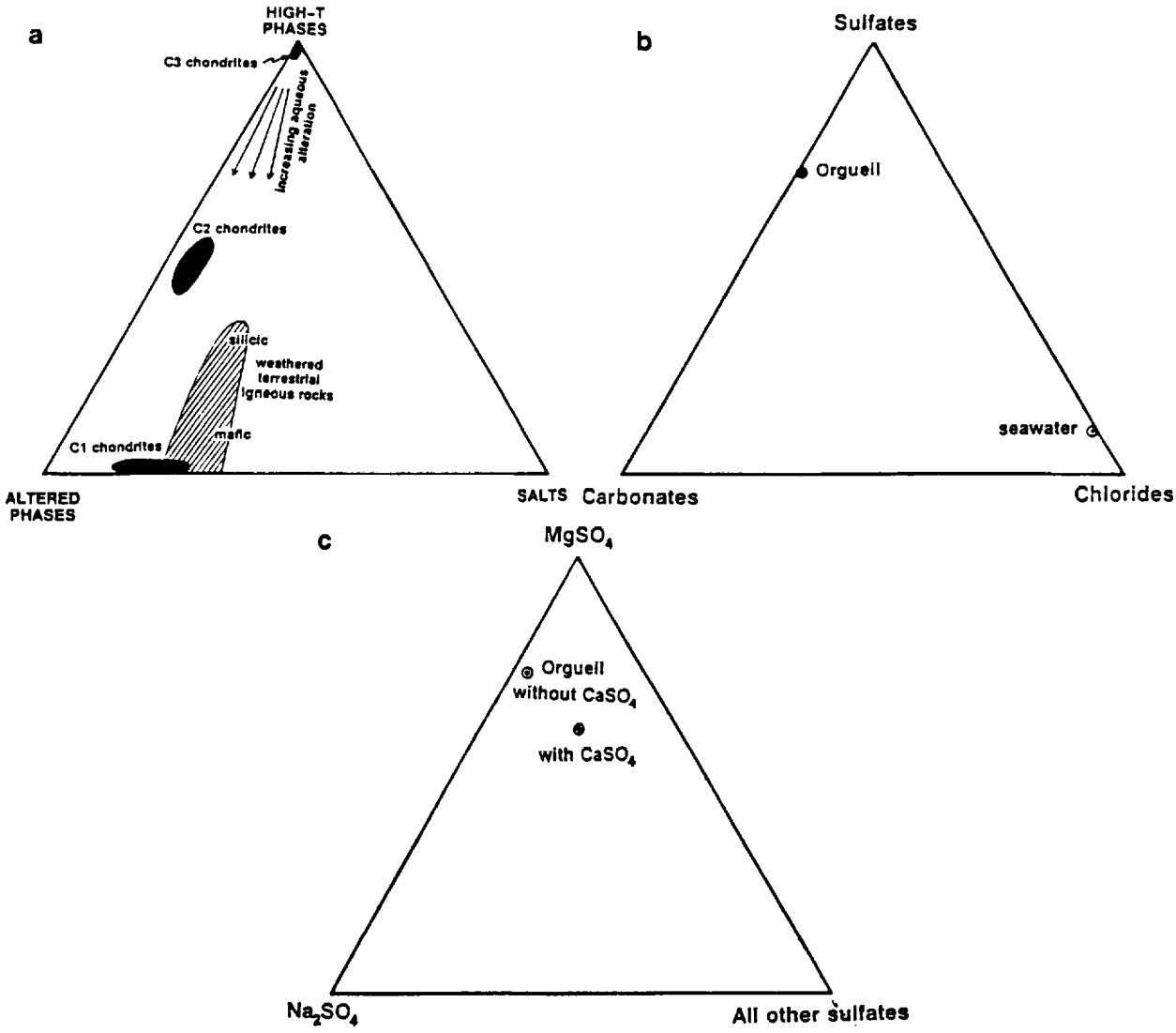

FIG. 1. Compositions of chondritic meteorites (derived from Fredriksson and Kerridge 1988, Burgess *et al.* 1991, and Dodd 1981). (a) Relativ mass proportions of salts (dehydrated sulfates and carbonates), aqueously altered rock components (mostly phyllosilicates and hydroxides), ar unaltered anhydrous minerals (including olivine, pyroxene, sulfides, and metal). (b) Relative mass proportions of sulfates, carbonates, and chloride (assuming all chlorine occurs as chlorides). Evaporated seawater for reference. (c) Relative mass proportions of magnesium sulfate, sodium sulfat and all other sulfates combined. The composition of all highly soluble material, ignoring the chlorides, is given by the point "without $CaSO_4$" i (c).

of Ca and Na (Fig. 1c), and carbonates of Ca, Mg, and Fe. Minor components include sulfates of Ni, Mn, and K. Chlorides have not been widely reported in chondrites, a fact attributed to a cosmic abundance ratio Cl/S ~ 0.01, and, according to one reviewer, possibly also reflecting the relative stability of Cl-rich chlorapatite and sodalite during low-temperature aqueous alteration. $MgCO_3$ and $BaSO_4$ have been reported from interplanetary dust particles. (Reitmeijer 1990, Richardson 1978, Bostrom and Fredriksson 1964, DuFresne and Anders 1962, Nagy and Andersen 1964, Fredriksson and Kerridge 1988, Burgess *et al.* 1991).

The relatively large fraction of sulfates, especially mag nesium sulfate, and the exceedingly low abundance o chlorine in chondrite salts contrast sharply with most ter restrial brines and evaporite deposits (Fig. 1b). Terrestria salts are most often dominated by NaCl and are relatively deficient in $MgSO_4$. This distinction is easily explained The Earth's continental upper crust, from which mos terrestrial brines ultimately derive their solutes, has bee greatly enriched in Na and depleted in Mg by multistage igneous fractionations, and was derived from a mantl that had previously seen severe chalcophile elemen depletions apparently related to core formation. Na is

factor of 6 *less* abundant and magnesium a factor of 7 *more* abundant in C1 chondrites relative to the average continental upper crust (Anders and Grevesse 1989, Taylor and McLennan 1985). Sulfur, 40% of which is oxidized in the form of sulfates in the C1 chondrite Orgueil (Fredriksson and Kerridge 1988), is well over an order of magnitude more abundant in chondrites than in the Earth's upper crust, while the condritic abundance of chlorine is similar to its abundance in the upper crust.

One could usefully consider scenarios where SO_4 or Mg are unimportant in chondritic brines, or where Fe^{+2} is as abundant as magnesium. For example, chemically reducing conditions during aqueous alteration could stabilize S in the form of relatively insoluble metal sulfides. Reducing conditions could also allow high concentrations of dissolved Fe^{+2}; in view of the chondritic ratio Fe/Mg ~ 2 (Anders and Grevesse 1989), dissolved Fe^{+2} easily could be as important as Mg under these conditions. Strongly alkaline conditions, perhaps caused by a high NH_3 content, could sharply curtail hydrolysis, thus slowing the rates at which major cations enter solution; furthermore, sufficiently alkaline conditions would stabilize Fe and Mg in the form of solid Fe- and Mg-hydroxides (Brookins 1988), preventing significant concentrations of these metals in aqueous solution. Strongly acidic conditions could favor significant solution of carbonates. While these are not a priori unlikely situations, the author maintains a more conservative approach is assuming the prevalence of conditions and mineralogies represented by available aqueously altered cosmic material (i.e., carbonaceous chondrites). Thus, a substantial fraction (40%) of S is in the form of sulfate, particularly highly soluble $MgSO_4$ and Na_2SO_4; carbonates and $CaSO_4$ are nearly insoluble; and the abundances of dissolved Cl^- and Fe^{+2} are negligible.

Over one-fifth of the mass of the C1 chondrite Orgueil consists of salts in various states of hydration (Fig. 1). Calculated entirely on an anhydrous basis, salts constitute 14.6% by mass of this meteorite, of which about two-thirds of the salts (by mass) are highly water soluble under normal conditions. $MgSO_4$, constituting nearly three-fourths of the highly water-soluble fraction, is clearly the single most important salt in chondritic brines, followed by Na_2SO_4.

Minor and weakly soluble salt components. $MgSO_4$ and Na_2SO_4 together account for 97% of the highly water-soluble fraction of Orgueil. The remaining 3% consists primarily of the sulfates of K, Mn, and Ni. As shown in Fig. 1b Ca–Mg–Fe carbonates are important solid components of chondrites, but are normally nearly insoluble, and could not normally constitute important components of magmatic brines. The same is true, to a slightly smaller degree, of $CaSO_4$. The high abundance of carbonates and gypsum in carbonaceous chondrites is a result of localized and essentially isochemical aqueous alteration and *in situ* chemical reprecipitation. Therefore, these phases would remain with the solid rocky residue during anatexis and melt removal. Brine magmatism, as considered in this report, is a fundamentally different process in that it involves open-system transport of highly soluble components, resulting in gross chemical fractionations on large spatial scales.

3. PHASE EQUILIBRIA

Aqueous binary sulfates. Figure 2 shows solid–liquid phase equilibria in binary aqueous systems involving $MgSO_4$, Na_2SO_4, $CaSO_4$, K_2SO_4, $MnSO_4$, and $NiSO_4$, all at 1 atm pressure. These binaries include all the major and minor sulfate components reported in carbonaceous chondrites, listed in order of abundance (Fredriksson and Kerridge 1988). The system H_2O–$MgSO_4$ is by far the single most important of these binaries. Under unexpected conditions, not examined in this work, aqueous $FeSO_4$ or $(NH_4)_2SO_4$ could also be important components, and might yield very different types of petrological evolution than considered below.

The phase equilibria shown in Fig. 2 probably should remain valid, as a first approximation, to pressures up to 2 kbars, since none of the substances are extremely volatile or unusually compressible. Higher pressures should progressively introduce qualitative changes, particularly solid-state phase changes. Kargel (1990), drawing on published data, showed that solid–liquid equilibria in the system H_2O–NaCl remain qualitatively unchanged, except for the stable ice polymorph, under pressures ranging from 1 atm to 12 kbars. The system H_2O–$MgSO_4$ currently is being studied experimentally under pressures up to 4 kbars; early results (Hogenboom *et al.* 1991) indicate no major surprises. However, subtle pressure-dependent aspects may have significant planetological consequences. These results will be presented elsewhere.

Metastable magmatic phenomena often occur in nature, particularly in quenched lavas. Supercooling, glass formation, and precipitation of metastable sulfate solids occur regularly under laboratory conditions, and indeed are avoidable only with considerable patience. Metastable phenomena, analogous to those which occur in the laboratory and in silicate volcanic flows, are especially likely during rapid solidification of the surfaces of aqueous sulfate flows. Persistence of these metastable phases over geologically lengthy periods is possible, a speculation supported by the occurrence of metastable magnesium and calcium sulfate minerals in terrestrial evaporite deposits. More often, terrestrial evaporite minerals revert to their stable forms when held at normal temperatures for a few hours or days (the surfaces of icy satellites are not "nor-

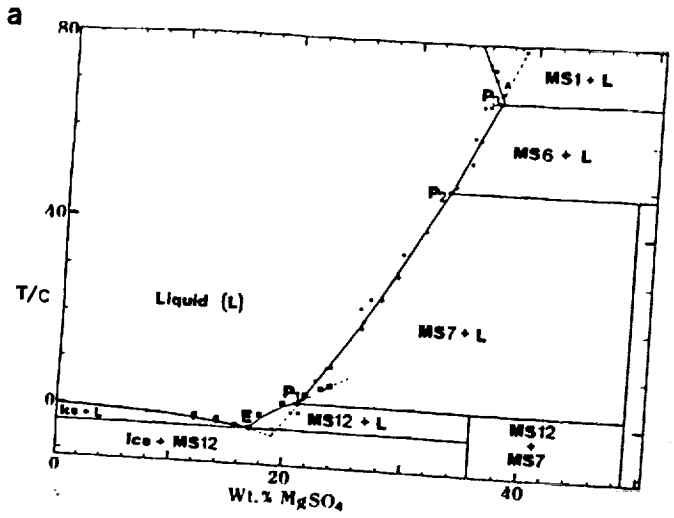
a
MS1 + L
MS6 + L
MS7 + L
MS12 + L
MS12 + MS7
Liquid (L)
Ice + L
Ice + MS12
T/C
Wt.% MgSO4

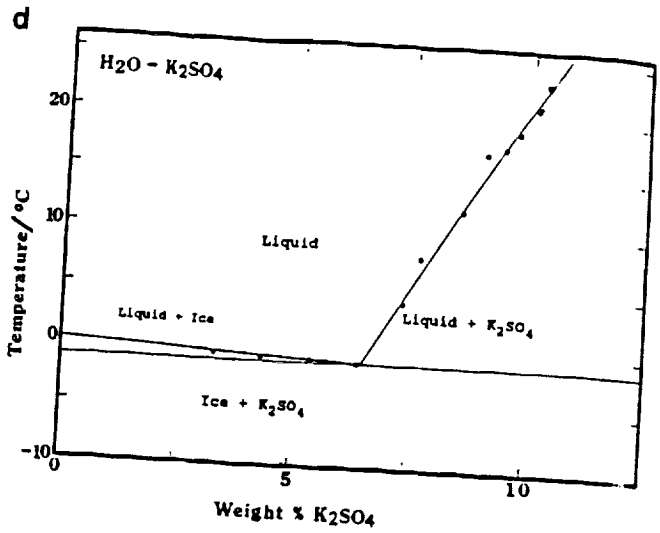
d
H2O - K2SO4
Liquid
Liquid + Ice
Liquid + K2SO4
Ice + K2SO4
Temperature/°C
Weight % K2SO4

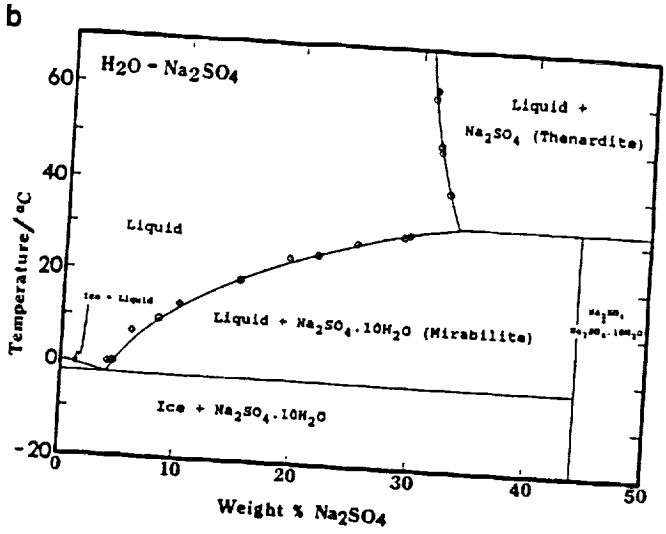
b
H2O - Na2SO4
Liquid
Liquid + Na2SO4 (Thenardite)
Liquid + Na2SO4·10H2O (Mirabilite)
Ice + Na2SO4·10H2O
Temperature/°C
Weight % Na2SO4

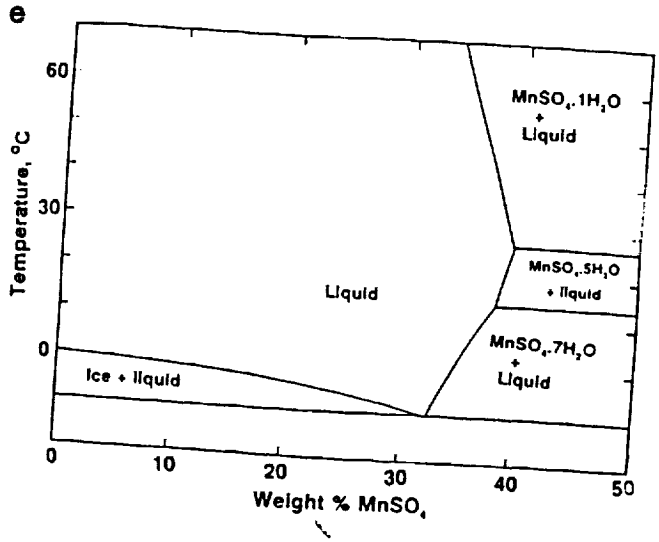
e
MnSO4·1H2O + Liquid
Liquid
MnSO4·5H2O + liquid
MnSO4·7H2O + Liquid
Ice + liquid
Temperature, °C
Weight % MnSO4

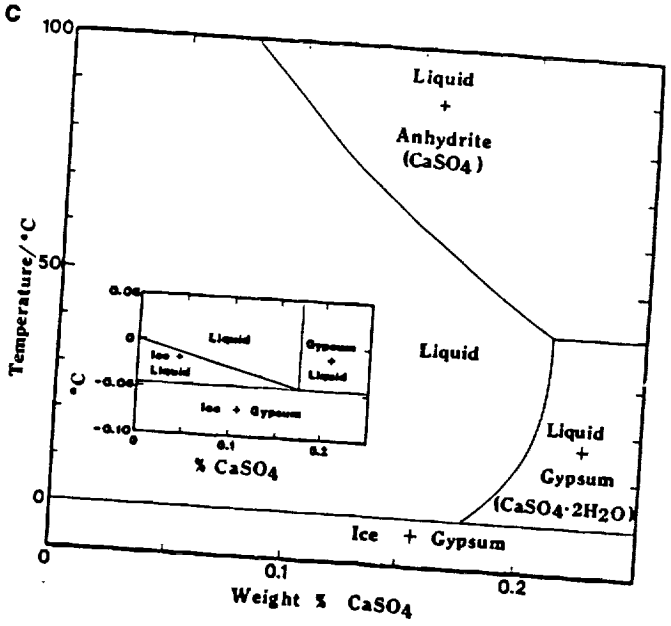
c
Liquid + Anhydrite (CaSO4)
Liquid
Liquid + Gypsum (CaSO4·2H2O)
Ice + Gypsum
Temperature/°C
Weight % CaSO4

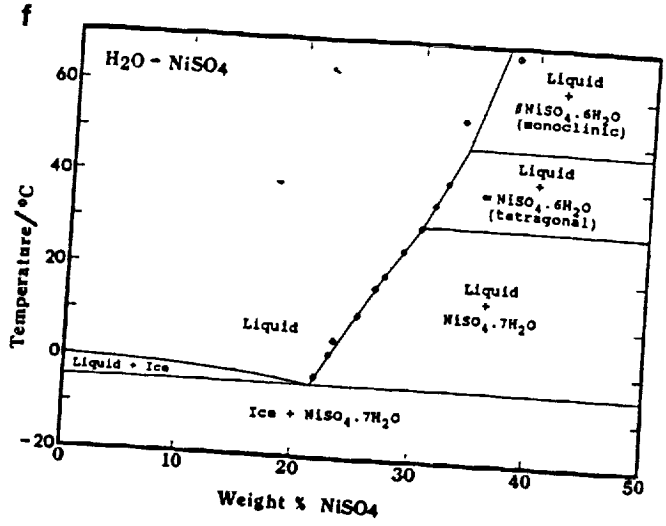
f
H2O - NiSO4
Liquid + NiSO4·6H2O (monoclinic)
Liquid + NiSO4·6H2O (tetragonal)
Liquid
Liquid + NiSO4·7H2O
Liquid + Ice
Ice + NiSO4·7H2O
Temperature/°C
Weight % NiSO4

mal," however). Solidification of the interiors of extraterrestrial aqueous sulfate flows would likely occur over sufficiently long intervals (hours to days) that equilibrium solid assemblages probably would be produced. More importantly, melting processes in asteroid and satellite interiors would occur over very lengthy periods and major departures from equilibrium are unlikely. Thus, despite the likelihood that flow surfaces would be metastable (an aspect with possible spectroscopic significance), most magmatic phenomena probably would involve essentially equilibrium processes.

The recognition that $MgSO_4$ is probably the most important solute in extraterrestrial volcanic brines invites examination of multicomponent phase equilibria when other chondrite sulfate components are added to aqueous $MgSO_4$. These ternary phase equilibria are illustrated in Fig. 3 and are discussed below.

System H_2O–$MgSO_4$–Na_2SO_4. Nearly all Na in Orgueil is in the form of Na_2SO_4, the second most abundant sulfate component in Orgueil after $MgSO_4$. It is fruitful to consider phase equilibria of these components together in aqueous solution (Fig. 3a). This system includes 97% of the highly water-soluble material in Orgueil (Fredriksson and Kerridge 1988).

Solid solution between magnesium and sodium sulfates is negligible. This system exhibits a large number of hydrous and anhydrous phases, including several stoichiometric double salts. Epsomite ($MgSO_4 \cdot 7H_2O$), hexahydrite ($MgSO_4 \cdot 6H_2O$), kieserite ($MgSO_4 \cdot 1H_2O$), and bloedite ($MgSO_4 \cdot Na_2SO_4 \cdot 4H_2O$) apparently occur in carbonaceous chondrites. A eutectic liquid (81% H_2O, 16% $MgSO_4$, 2.8% Na_2SO_4 by mass) coexists near -5°C with water ice, mirabilite ($Na_2SO_4 \cdot 10H_2O$), and $MgSO_4 \cdot 12H_2O$. Melting and crystallization sequences of ice-free and ice-rich model assemblages are modeled and discussed in a planetological context in Section 5.

System H_2O–$MgSO_4$–$CaSO_4$. The high abundance of $CaSO_4$ in carbonaceous chondrites (Fig. 1c) seems at first to suggest that this also may be an important component in cryomagmatic brines. However, $CaSO_4$ is sparingly soluble in water (Fig. 2c), indicating a very limited capacity of chondritic brines to transport $CaSO_4$. This contrasts with the Earth's hydrologic cycle where enormous quantities (water : rock ratios $\sim 10^3$–10^4) of dilute, unsaturated solutions of $CaSO_4$ and other salts are transported to the sea or inland basins; evaporative concentration results in extensive precipitation of gypsum and anhydrite in basins distant from the points where the solutes originated. Anatexis and magma migration in icy satellites and asteroids occur just once or a few times, involving water : rock ratios $\sim$ 1. This quantity of brine can dissolve only an insignificant fraction of the gypsum present in carbonaceous chondrites. Large amounts of $CaSO_4$ are formed by aqueous activity in icy satellites and asteroids, but nearly all is precipitated *in situ*.

Figure 3b shows the solubility curve exhibited by gypsum in magnesium sulfate solutions. This type of solubility curve is shared by other multicomponent aqueous sulfate solutions and is explained by nonideal solution properties and ionic complexing (Cameron and Bell 1905, Harkins and Paine 1919). The ternary eutectic liquid contains about 17% $MgSO_4$ (essentially the same as in the binary system H_2O–$MgSO_4$) and only 0.06% $CaSO_4$. Clearly this result warrants neglecting $CaSO_4$ as a soluble component for most purposes.

System H_2O–$MgSO_4$–K_2SO_4. As with Na, nearly all K in Orgueil is in the form of sulfate. The potential importance of K_2SO_4 is sharply limited by the low cosmic abundance of K. K_2SO_4 constitutes 0.13% of Orgueil and less than 2% of the total sulfates (Fredriksson and Kerridge 1988). However, K is even less abundant in Earth than in Orgueil. Even so, terrestrial silicate igneous fractionations yield major quantities of potassic phases in the continental crust, a fact with many important geological consequences. One cannot rule out analogous complex igneous fractionations in aqueous sulfate systems in differentiated satellites and asteroids.

The system H_2O–$MgSO_4$–K_2SO_4 (Fig. 3c) is somewhat similar to the system H_2O–$MgSO_4$–Na_2SO_4, as one might anticipate from the geochemical similarities of K and Na; the most notable distinction is that K_2SO_4 lacks a hydrated equivalent of mirabilite. Among the similarities, solid solution between Mg and K sulfates is negligible, and a series of double salts occurs. One of these, schoenite ($K_2SO_4 \cdot MgSO_4 \cdot 6H_2O$), coexists with ice, $MgSO_4 \cdot 12H_2O$, and the ternary eutectic liquid. In asteroids and icy satellites, however, K_2SO_4 probably occurs in solid solution, substituting for Na_2SO_4 in various salts.

System H_2O–$MgSO_4$-$MnSO_4$. $MnSO_4$ constitutes less than 1% of the highly soluble fraction of Orgueil and only 0.06% of the whole meteorite. Even so, $MnSO_4$ is worth considering as a minor component. Figure 3d illustrates phase equilibria in this system. Solid phases exhibit substantial but incomplete solid solution, reflecting the identi-

FIG. 2. Phase equilibria in binary aqueous sulfate systems at 1 atm. (a) H_2O–$MgSO_4$. (b) H_2O–Na_2SO_4. (c) H_2O–$CaSO_4$. (d) H_2O–K_2SO_4. (e) H_2O–$MnSO_4$. (f) H_2O–$NiSO_4$. Data sources: Loewell (1855), Etard (1894), Cottrell (1900), Cameron and Bell (1905), van Klooster (1917), Mulder and Smith *et al.* tabulated in Archibald and Gale (1924), Tantzov (1924), Robson (1927). Smits *et al.* (1928), Posnjak (1938), Bodaleva and Lepeshkov (1956), Novikova (1957), 1989 CRC Handbook of Chemistry and Physics, Kargel (1990).

C-2

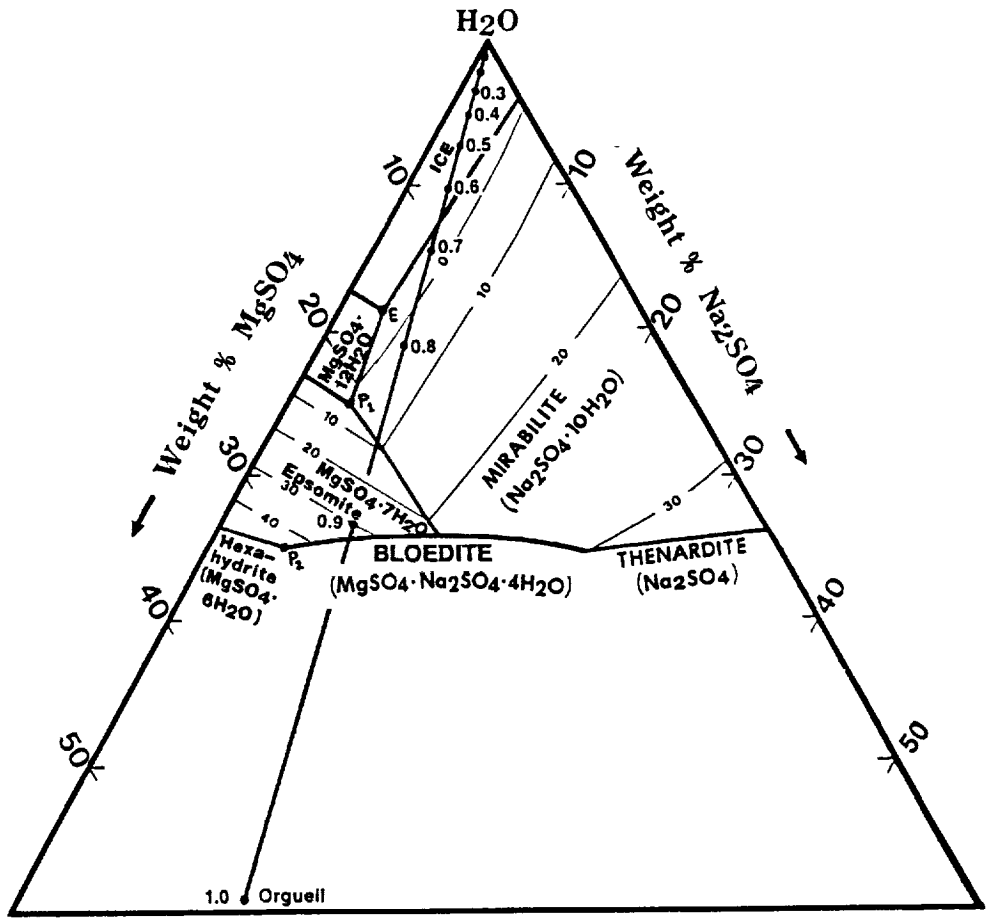

FIG. 3. Ternary aqueous phase equilibria involving third components added to the system H_2O–$MgSO_4$. (a) H_2O–$MgSO_4$–Na_2SO_4. (b) H_2O–$MgSO_4$–$CaSO_4$. (c) H_2O–$MgSO_4$–K_2SO_4. (d) H_2O–$MgSO_4$–$MnSO_4$. (e) H_2O–$MgSO_4$–$NiSO_4$. Data sources: Binary phase diagrams and sources listed in Fig. 2 caption: Levi (1923), Blasdale (1927), Starrs and Storch (1930), Starrs and Clarke (1930), Benrath and Blankenstein (1934), Benrath and Neumann (1939), Soboleva (1960).

cal valence states of Mg and Mn and their roughly similar ionic radii. Among the hepta- and hexahydrates, the solid phases have higher contents of Mg, lower concentrations of Mn, and higher Mg/Mn ratios than coexisting liquids. In silicate petrological vernacular, Mn is moderately incompatible.

System H_2O–$MgSO_4$–$NiSO_4$. The chondritic ratio Ni/Mg ~ 0.12 (Anders and Grevesse 1989), nearly two orders of magnitude greater than in Earth's upper crust (Taylor and McLennan 1985), allowing the possibility that Ni could be an important constituent of cryovolcanic brines. Indeed, Mg–Ni–Na sulfates in Orgueil include up to 28% $NiSO_4$, although on average $NiSO_4$ is minor (Fredriksson and Kerridge 1988). Figure 2f shows binary phase relations of aqueous $NiSO_4$. Comparison with the H_2O–$MgSO_4$ system shows that sulfate solubility curves and the series of hydrated solids are very similar, except that $NiSO_4$ hexahydrate forms crystallographically distinct monoclinic and tetragonal polymorphs, whereas $MgSO_4$ forms only the monoclinic variety. The apparent lack of a Ni counterpart to $MgSO_4 \cdot 12H_2O$ might reflect kinetic problems in forming Ni dodecahydrate, rather than its lack of existence, as Mg dodecahydrate is also more difficult to form than heptahydrate.

The hydrates of $MgSO_4$ and $NiSO_4$ form complete solid solutions, analogous to the behavior of Mg and Ni in silicates. This is not unexpected since the valence states of Ni and Mg are the same and their ionic radii are nearly identical. The literature sources used in the construction of Fig. 3e did not find Mg dodecahydrate, so the three-phase cotectic between ice and sulfate involves the heptahydrate. This cotectic is a simple thermal trough running almost isothermally across the phase diagram from one binary to the other. The stability field of tetragonal $NiSO_4 \cdot 6H_2O$ terminates at a peritectic upon the addition of just 4% $MgSO_4$ to the binary H_2O–$NiSO_4$ eutectic liquid. Therefore, except for this small tetragonal hexahydrate field occurring only for very Ni-rich compositions, the aqueous $MgSO_4$ and $NiSO_4$ systems, and ternary mixtures of them, are isomorphic.

Two sets of representative three-phase triangles in Fig

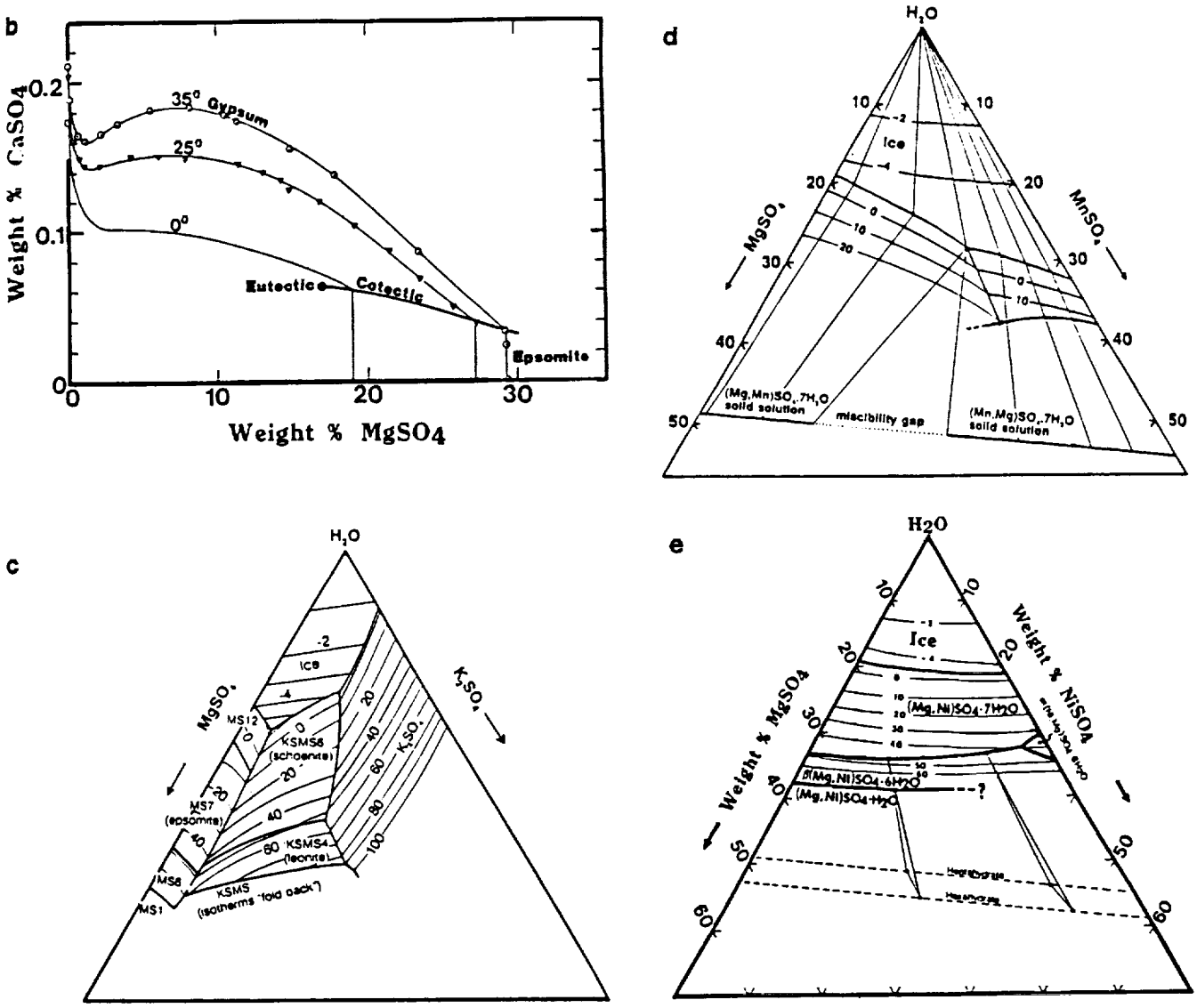

FIG. 3—*Continued*

3e connect the compositions of solid sulfates with their equilibrium liquids on the sulfate–ice cotectic. These data indicate that the partitioning behavior of Ni and Mg among the sulfates and liquid are very similar and of order unity, in accordance with these metals' chemical similarity. In other words, the ternary phase equilibria are insensitive to the Mg/Ni ratio of the solution. Hence, one may treat ternary mixtures in this system as pseudobinary mixtures, with little sacrifice in accuracy, by combining $MgSO_4$ + $NiSO_4$ on a molar basis into a single component. Therefore, the chondrite salt vein compositions reported by Fredriksson and Kerridge (1988), which strictly must be described with no less than four major components (H_2O and sulfates of Mg, Ni, and Na), can be reduced to three components. Examined in more detail, the Ni/Mg ratios of solid solutions are always greater than in the coexisting liquid, so Ni can be considered a compatible element.

Synthesis. The physical chemistry of carbonaceous chondrite-equilibrated sulfate brines may be roughly approximated in the system H_2O–$MgSO_4$ (Fig. 2a), and more accurately in the ternary system H_2O–$MgSO_4$–Na_2SO_4 (Fig. 3a). Minor sulfate components (sulfates of Ni, Mn, and K) usually would not have major effects on the liquid's physical properties and major phase equilibria. However, it is possible to make a rough accounting for these components as long as their concentrations are low. With little loss in accuracy one may sum K_2SO_4 and Na_2SO_4 into a single component and $MgSO_4$, $NiSO_4$, and $MnSO_4$ into another component. However, as terrestrial experience shows very well, complex igneous fractionations can cause initially minor components to become major ones in strongly differentiated materials. In this event, quaternary and higher-order chemical systems may be required for a more accurate accounting.

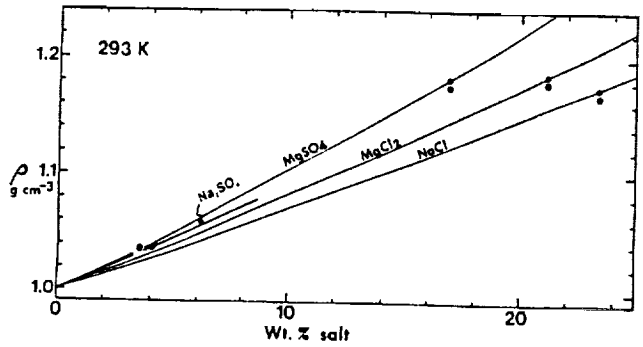

FIG. 4. Densities of aqueous salt solutions as functions of concentration. Eutectics denoted by solid circles. Sources in text.

$CaSO_4$ and the carbonates of Ca, Mg, and Fe are sparingly soluble under a broad range of environmental conditions. While these salts are important constituents of carbonaceous chondrites, they were formed by largely *in situ* processes of solution and precipitation, and would not have constituted an important fraction of the ionic load in chondritic hypersaline brines.

The chondritic ratio of Cl/S ~ 0.01, sharply limiting the potential volumes of low-temperature chloride brines. Taking Ganymede as an example, eutectic melting at −52°C in the system $MgCl_2$–$CaCl_2$–H_2O, involving all the chlorine present, could yield 0.22 mass percent of eutectic brine, equivalent to 0.37 vol% of Ganymede (assuming Ganymede contains 60% by mass of chondritic rock containing 698 ppm Cl). Although this is not a large quantity, it is capable of forming a crust 3 km thick if completely extruded. If nothing else is capable of melting, perhaps because convective adiabats are cooler than the melting points of aqueous sulfates, then chloride brine volcanism could dominate surface geology and composition.

One reviewer suggested that low-temperature petrologic evolution of ice-bearing systems containing both chlorides and sulfates could be very complex. Alternatively, as another reviewer suggested, chlorine could remain immobilized in stable, nearly insoluble phases such as chlorapatite and sodalite until temperatures in the range of hundreds of degrees Celsius are attained. In the latter case, late-stage eruptions of hydrothermal chloride brines may occur during dehydration of phyllosilicates.

4. DENSITIES AND VISCOSITIES OF BRINES

Densities. Published sources give the densities of aqueous salt solutions as functions of composition and temperature (CRC Handbook of chemistry and Physics, Fabuss *et al.* 1966, Korosi and Fabuss 1968, Chen *et al.* 1980). The data collectively cover concentrations up to the aqueous salt eutectics, and extend over a wide range of temperatures above 293 K. Figure 4 gives the densities of planetologically important aqueous salts as functions of concentration for 293 K and 1 bar. These data can be extrapolated and interpolated over data gaps to obtain the eutectic liquid densities at the eutectic temperatures. The eutectic liquid in the system H_2O–$MgSO_4$ (17 wt% $MgSO_4$) at the eutectic temperature (−3.9°C) has a density of about 1.186 g cm^{-3}.

The densities of frozen eutectic mixtures of ice and salts are also of planetological interest, particularly in the systems involving H_2O, $MgSO_4$, and Na_2SO_4. The densities of most solid sulfate phases of interest have been published (CRC Handbook), but the density of $MgSO_4 \cdot 12H_2O$ has not. A preliminary measurement of this density, 1.51 ± 0.01 g cm^{-3}, was presented orally by Hogenboom *et al.* (1991). The densities of solid magnesium and sodium sulfates are shown graphically as a function of water content in Fig. 5; to the level of precision presented in this diagram these densities are not significantly temperature-dependent.

Figure 6 summarizes the densities of selected liquids and solids of cryovolcanic interest. All liquids in Fig. 6 are buoyant with respect to rock–ice mixtures, thus encouraging early aqueous volcanism.

A frozen eutectic mixture of 47% ice and 53% $MgSO_4 \cdot 12H_2O$ has a density of about 1.126 g cm^{-3}, about 5% lower than the density of the coexisting liquid. A frozen eutectic mixture in the system H_2O-$MgSO_4$-Na_2SO_4 has a density ~1.133 g cm^{-3}. Thus, the solid floats on the liquid, presenting the same buoyancy "problem" as occurs for water and ice. Once a thick volcanic crust forms subsequent volcanism is inhibited by the negative buoyancy of the late-arriving liquids relative to that of the solid crust (Croft 1985). Adapting the suggestion of Croft *et al.* (1988) for ammonia–water magmatism, early

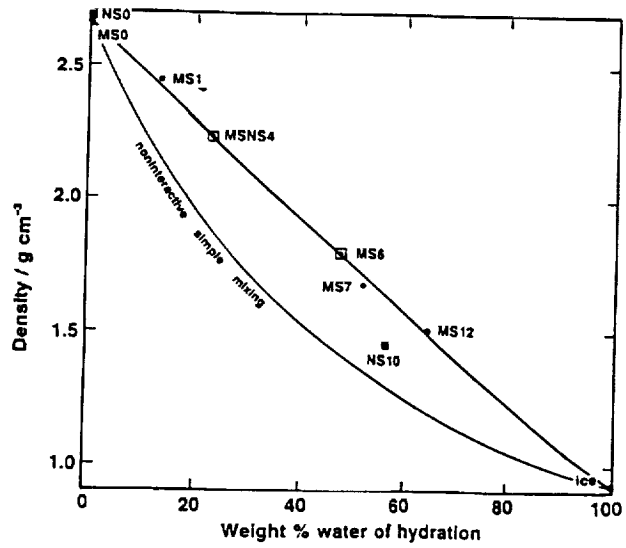

FIG. 5. Densities of solids in the systems H_2O–$MgSO_4$ and H_2O–Na_2SO_4 as functions of hydrated water content. Sources in text.

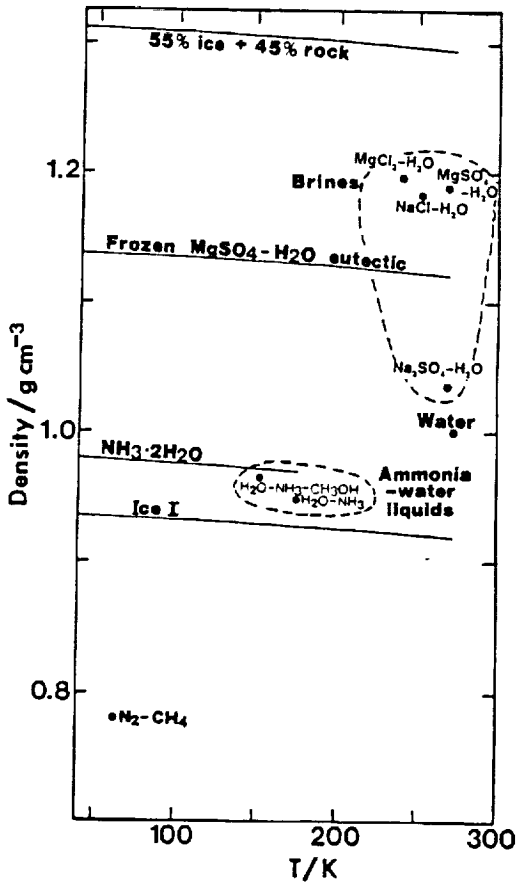

FIG. 6. Densities of selected solids and liquids of volcanological interest. After Kargel (1990).

salt–water volcanism may frequently have yielded to later plutonism. Under certain circumstances plutonism might generate surface tectonic features such as domical uplifts or patterns of parallel, radial, or concentric fractures or dike swarms.

Despite the apparent "buoyancy crisis," morphologic evidence exists for widespread late (i.e., post heavy bombardment) volcanism on several icy satellites. One solution to the buoyancy crisis is apparent upon examining Fig. 6. Pure water, dilute brines, and eutectic sodium sulfate solutions are less dense than a frozen ternary eutectic assemblage; hence, these less saline solutions could readily extrude. Section 5.1 presents several models where early crust-forming ternary eutectic melting events exhaust the supply of magnesium sulfate in the region of partial melting, yielding to later production of binary eutectic sodium sulfate solution or nearly pure water. Thus, while some situations might favor an early permanent transition from hypersaline volcanism to plutonism, other plausible conditions would allow a late-stage resumption of volcanism by extrusions of water or sodic brine.

Viscosities. The viscosity of magma is encountered in every problem of magma migration and lava flowage. Kargel *et al.* (1991), in an experimental study of ammonia–water liquids and crystal–liquid slurries, highlighted the important effects of partial crystallization on rheology. The relative differences in lava rheologies are well indicated by comparisons of liquid viscosities at their respective freezing points in the crystal-free state. These data should not be directly utilized in rheological modeling of lava flows since they do not take into account the important effects of partial crystallization. Rather, these data are useful for determining geologically familiar rheological analogs (e.g., silicate lavas). The undaunted physical modeler might choose to utilize these data after applying an empirical factor accounting for crystallization (Greenberg *et al.* 1991, Schenk 1990), or by employing an empirical function relating the relative viscosity and degree of crystallinity (Kargel *et al.* 1991).

Available viscosity data with appropriate extrapolations are shown in Fig. 7 for aqueous magnesium sulfate. The eutectic H_2O–$MgSO_4$ liquid has a viscosity ~ 0.06 P. The eutectic liquid in the system H_2O–$MgSO_4$–Na_2SO_4 has a viscosity ~0.10 P. Aqueous eutectic NaCl, $MgCl_2$,

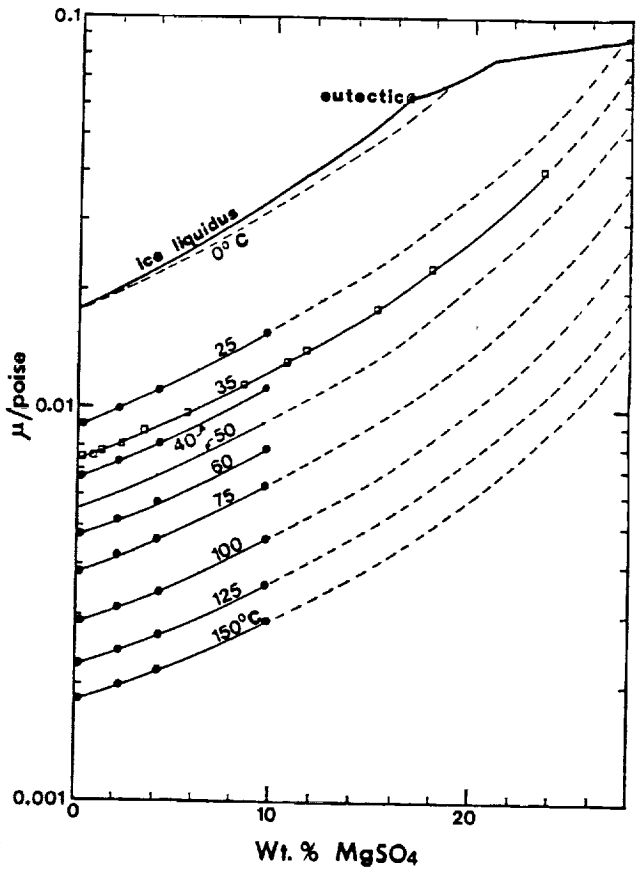

FIG. 7. Viscosities of magnesium sulfate solutions. Sources: Korosi and Fabuss (1968) (solid circles), Novikova (1957) (open squares). Dashed sections where extrapolated. From Kargel (1990).

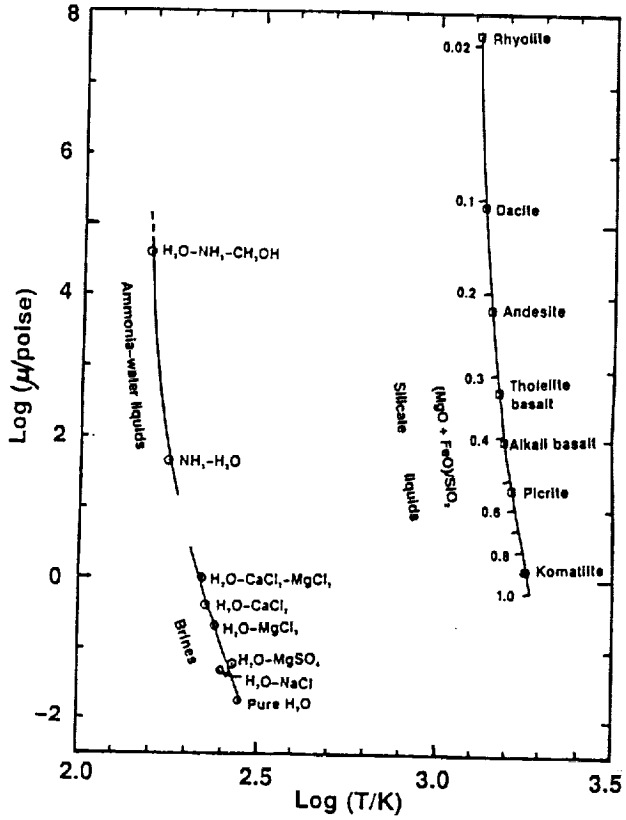

FIG. 8. Viscosities of volcanologically interesting liquids at their respective freezing points. Aqueous substances represent eutectic compositions, the viscosities of which are from Kargel *et al.* (1991) and sources referenced in the text. Silicate data are based on published viscometry of natural and synthetic silicate liquids (Shaw 1969, Urbain *et al.* 1982, McBirney and Murase 1984, Murase *et al.* 1985, Tauber and Arndt 1986, Ryerson *et al.* 1986, Hummel and Arndt 1985, Scarfe *et al.* 1983). The melting points of silicates are based on experimental phase equilibria (dry) from Cox *et al.* 1979 and Morse 1985. The quantity $(MgO + FeO)/SiO_2$, in weight percent, is a measure of the degree of differentiation of silicate liquids. Strongly silica-undersaturated alkaline liquids do not lie on the curve.

and $CaCl_2$ indicate viscosities of, respectively, 0.05, 0.2, and 0.4 P. Multicomponent aqueous chlorides may have somewhat higher viscosities, but probably not over 1 P.

Figure 8 summarizes the crystal-free viscosities of cryovolcanic and silicate liquids at their respective freezing points. The aqueous mixtures span a range of viscosities comparable to the range exhibited by silicate lavas. Salt–water eutectic mixtures are one to two orders of magnitude more viscous than water, but are two to three orders of magnitude less viscous than basalt and ammonia–water eutectic liquid. This physical contrast probably would be reflected in important differences, along compositional lines, in volcanological behavior.

The low viscosities of salt brines would encourage melt segregation from residual crystalline matrices at very low melt fractions (McKenzie 1985), favoring fractional partial melting over equilibrium batch melting, and fractional crystallization in preference to equilibrium crystallization. Fractional melting involves removal of liquid in small increments as melting proceeds, and may be approximated as continuous removal of ideal eutectic compositions interrupted when one or another solid phase is exhausted in the solid residue. Melting resumes when the next eutectic temperature is attained in the simpler system lacking the exhausted phase. In equilibrium batch melting the liquid is extracted in one or a few large increments, typically allowing the liquid composition to migrate up a cotectic after a solid phase is exhausted (see Cox *et al.* 1979).

5. APPLICATIONS

5.1. Structural Models

Construction. This section examines possible internal chemical structures resulting from the differentiation of a series of generic satellites and asteroids in the system H_2O–$MgSO_4$–$NaSO_4$, plus inert rock (Fig. 3a). The supply and transfer of heat is not considered, but rather is assumed to be sufficient to induce complete differentiation. The deep internal pressures in large asteroids, in icy satellites the size of Tethys, and in the icy crust of Europa are on the order of a kilobar. This is a sufficiently low pressure that Fig. 3a and satellite structural models based on Fig. 3a, even though strictly valid for 1 atm, are probably suitable approximations. However, the interior pressures in Ganymede and other large icy satellites attain up to 50 kbars, and qualitatively important effects on phase equilibria are expected. Even so, the models presented here are useful in advertising the probable importance of salts, particularly sulfates, in the low-temperature differentiation and geologic evolution of these large objects. But high-pressure phase equilibria in relevant systems are sorely needed for more accurate modeling and reliable insights into the histories of the larger objects (Hogenboom *et al.* 1991 and in preparation).

Structural models in Fig. 9 were constructed for five initial rock fractions varying from 1.0 (pure chondritic rock) to 0.4 by mass. The percentage of sulfates in the rock component was calculated using the average S abundance in Orgueil, 6.25 mass% (Anders and Grevesse 1989), and the average fraction of this S occurring as sulfates, 0.40 (Fredriksson and Kerridge 1988, Table 1); these two values yield the fraction of sulfate sulfur (S^{-6}) in Orgueil: 2.50% by mass. This amount of oxidized S was apportioned among the elements Ca, Mg, and Na in the ratios measured by Fredriksson and Kerridge (1988, Table 2), with the minor approximation that $NiSO_4$ and $MnSO_4$ in Orgueil were summed along with $MgSO_4$, and K_2SO_4 was summed with Na_2SO_4. The mass fractions of sulfates in the chondritic rock component, calculated on an anhydrous basis, are $MgSO_4$ 6.05%, Na_2SO_4 2.07%, and $CaSO_4$ 1.79%. Only the first two components are highly water-

soluble, giving a total of 8.12% highly soluble salts. The calculated mass percentages of hydrated salts are epsomite ($MgSO_4 \cdot 7H_2O$) 8.80%, bloedite ($MgSO_4 \cdot Na_2SO_4 \cdot 4H_2O$) 4.87%, and gypsum ($CaSO_4 \cdot 2H_2O$) 2.27%. The quantity of water associated with the two highly soluble phases, epsomite and bloedite, sums to 5.55%.

The exact meaning of "rock : ice ratio" is unclear when dealing with systems containing hydrated silicates and salts. Furthermore, the quantity of rock differs before and after leaching. A more precise term is needed,

$$R_i = m_{r,i}/(m_{r,i} + m_w),$$

where R_i is the initial mass fraction of chondritic rock (including salts and water of hydration), $m_{r,i}$ is the initial mass of chondritic rock, and m_w is the mass of water added to the chondritic rock. The total fraction of water in an ice–chondrite mixture is greater than $1 - R_i$ since the rock itself contains water. R_i would correspond to the true rock fraction only if chondritic rock and ice are mixed without reequilibration or differentiation. Reequilibration without differentiation actually would yield more rock and less ice than indicated by R_i since epsomite and bloedite would take up water as they transformed to mirabilite and magnesium sulfate dodecahydrate. Low-temperature differentiation and leaching of soluble salts from the rock would result in less rock than R_i. The final mass fraction of rock, R_f, after differentiation is

$$R_f = (1 - 0.1367)R_i = 0.8633\ R_i.$$

Melting and crystallization sequences can be followed in Fig. 3a after calculating the fractions of H_2O, $MgSO_4$, and Na_2SO_4. Fig. 2a (system H_2O–$MgSO_4$) considerably assists the interpretation of petrologic evolution in the ternary system (Fig. 3a). The amount of water in each model satellite is calculated as the amount of water of hydration of epsomite and bloedite in the initial rock (5.55% of initial rock mass) plus the amount of added water. Phyllosilicate water is assumed to be stably bound to the rock. The amounts of the ternary components are resummed to 100%. Chondrite–water mixtures are shown in Fig. 3a as the straight line running from the composition of Orgueil to the water apex.

Differentiation was assumed to progress by continuous fractional melting, resulting in a perfectly gravitationally stably stratified structure. Figure 9 shows the internal structures of the five differentiated model objects. The idealized evolution of each model is briefly described below.

Model A. Figure 9a, with $R_i = 1.0$, shows the differentiated structure of an object initially composed of pure chondritic rock with no added water. Epsomite and bloedite melt incongruently, yielding the peritectic liquid P2 (Fig. 3a), containing over 30% $MgSO_4$ and 4% Na_2SO4. Liquid P2 is less dense than the rocky residue, so the liquid is readily erupted, forming a volcanic crust. Each successive volcanic flow would have an identical composition until either epsomite or bloedite is exhausted in the object's interior. P2 flows could solidify by fractional crystallization (where crystals gravitationally settle and segregate from the liquid almost as rapidly as they form) or by equilibrium crystallization (where crystals remain in contact and continuously reequilibrate with the cooling liquid). Solidification of most silicate flows approximates equilibrium crystallization. If liquid P2 volcanic flows cool analogously, the final homogenous crystalline mixture would be composed of 84% $MgSO_4 \cdot 12H_2O$ + 11% $Na_2SO_4 \cdot 10H_2O$ + 5% ice. However, as discussed in Section 4, the low viscosity of the hypersaline P2 brine might favor fractional crystallization. In this case each flow would consist of several layers of different compositions: the top and last layer to solidify would have the composition of ternary eutectic E.

In the next stage of melting, the residue left by formation of liquid P2 melts incongruently at peritectic P3 (Fig. 3a). Liquid P3, not shown in Fig. 3a (but consult the binary approximation in Fig. 2a), is denser than the volcanic crust of composition P2, and probably would be unable to ascend to the surface. Rather, liquid P3 would pool near or intrude the base of the crust, eventually forming the upper mantle layer of the asteroid.

The residue left from the second stage of melting then suffers a third stage of incongruent melting, yielding a small amount of liquid and a final solid residue composed of anhydrous sulfates. This stage of melting also yields a liquid substantially denser than the upper mantle, thus resulting in the formation of a lower mantle layer. The anhydrous sulfates probably would remain in the rocky core until water was released from the dehydration of gypsum and phyllosilicates.

The average density of this object after differentiation is 2.69 g cm^{-3}, representing ~2.8% volume expansion over the undifferentiated initial chondrite. Much of this expansion takes place after formation of the peritectic P_2 crust. Since all liquids generated subsequently would tend to intrude beneath this early-formed crust, one expects extensional strains of ~1%, sufficient to cause significant crustal rifting.

Model B. Figure 9b shows the structure of a satellite with $R_i = 0.7$. This object contains enough water that epsomite and bloedite contained in the initial chondritic rock would react with added water to form magnesium sulfate dodecahydrate and mirabilite, leaving excess water to form ice. This mixture first melts at the ternary eutectic E resulting in the formation of a thick volcanic layer (later to become the upper mantle). If each successive volcanic flow cooled by equilibrium crystalliza-

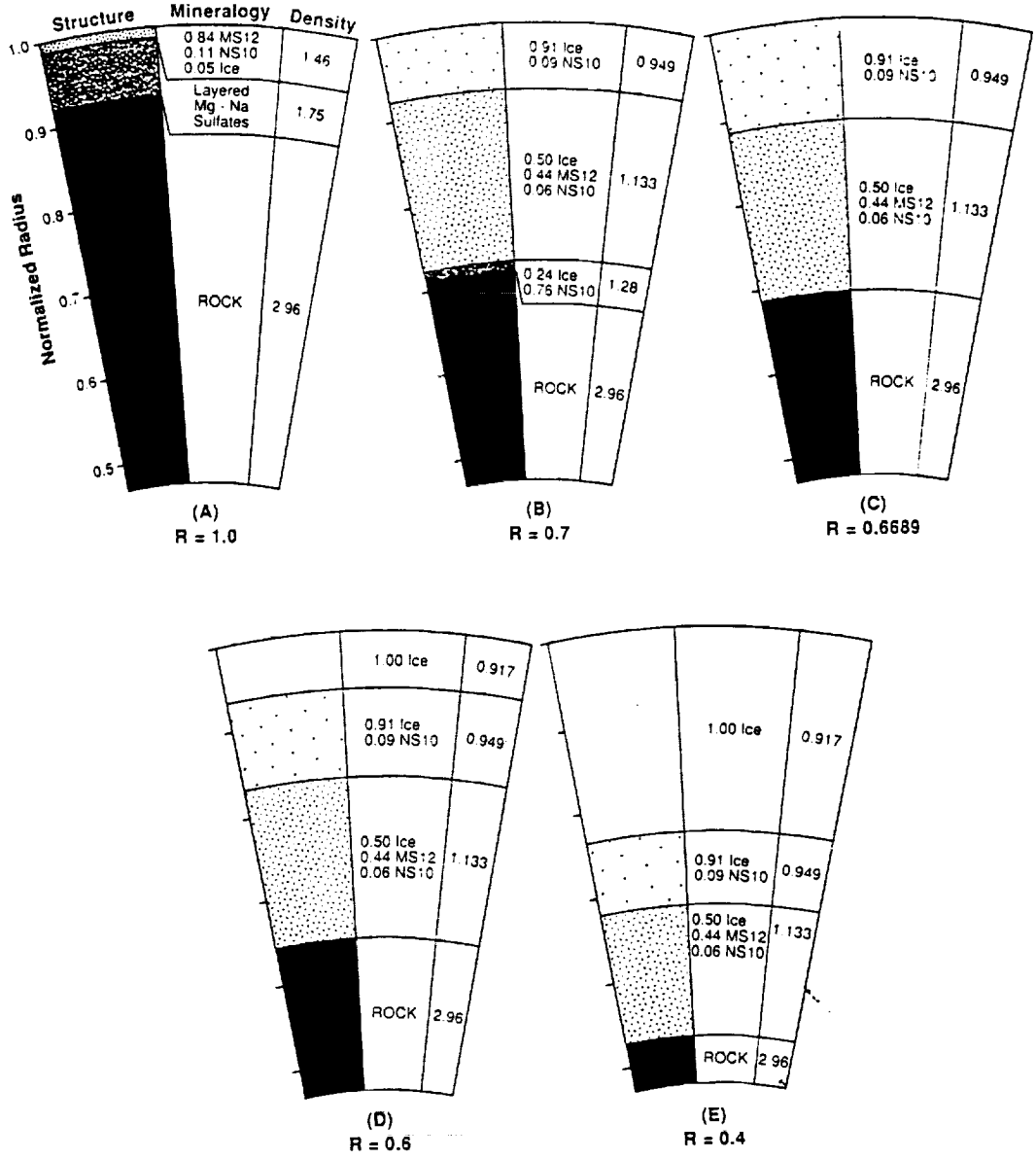

FIG. 9. Structural models of differentiated objects having various initial rock fractions ranging from 1.0 to 0.4. Left-hand column of each diagram gives the structures. The middle column gives the mineralogies of each layer (MS12, $MgSO_4 \cdot 12H_2O$; NS10. $Na_2SO_4 \cdot 10H_2O$; ROCK. the composition of Orgueil minus leachable Mg and Na sulfates and these phases' apportionments of hydrated water). The right-hand column gives the densities of each frozen layer.

tion this layer would be composed of 50% ice + 44% $MgSO_4 \cdot 12H_2O$ + 6% $Na_2SO_4 \cdot 10H_2O$; its density is 1.133 g cm^{-3} (at 1 atm pressure).

Fractional eutectic melting and extraction of liquid E (in Fig. 3a) from the interior would drive the solid residue toward the binary join H_2O–Na_2SO_4. The subsequent evolution of this residue, composed of ice and mirabilite (plus rock), is best visualized in the binary H_2O–Na_2SO_4 phase diagram (Fig. 2b). A second stage of melting could occur at the binary eutectic, producing a liquid containing 4% Na_2SO_4 and no $MgSO_4$. This liquid has a density of about 1.05 g cm^{-3}, substantially less than the density of the frozen ternary eutectic layer (1.13 g cm^{-3}). Therefore, this binary liquid could easily ascend to the surface, forming a crust composed of 91% ice + 9% mirabilite, and leaving a residue in the rocky core composed of mirabilite. Mirabilite may then melt incongruently at 32.5°C, forming an anhydrous residue of thenardite and a liquid containing 34% Na_2SO_4. The dense binary peritectic liquid would intrude at the base of the mantle, forming a frozen lower

mantle composed of 76% mirabilite – 24% ice. The average density of this satellite is 1.76 g cm^{-3}.

Model C. The initial rock fraction, R_i = 0.6689, has been chosen so that ternary eutectic melting leaves a residue of ice and mirabilite in precisely the ratio of the binary eutectic; thus, ternary eutectic melting is followed by binary eutectic melting in the system H_2O–Na_2SO_4, without leaving a residue of either salt or ice. R_i is also very similar to Ganymede's; Mueller and McKinnon (1988) calculated R_i = 0.64 to 0.65 when the rock was assumed to have a C1 chondrite composition and Ganymede was assumed to be differentiated. The differentiation of this object is qualitatively the same as in model B except that there is no mirabilite residue and, thus, no Na_2SO_4-rich lower mantle layers. The average density of this satellite is 1.68 g cm^{-3}.

Model D. This model is again similar to models B and C except that water ice is left in the residual rocky core after mirabilite is exhausted during the binary phase of melting in the system H_2O–Na_2SO_4. The excess water ice melts at 273 K, yielding pure water with a density less than the ternary eutectic mantle, but greater than the density of the binary sodium sulfate-rich layer; hence, water may tend to intrude between these two salt-rich layers. However, when it freezes, water ice is less dense than the overlying layer composed of ice and mirabilite, so the intruding ice may tend to work its way to the surface over time. In any case, the assumption that the final differentiated structures are gravitationally stably stratified means that the final structure indeed exhibits an ice crust. Exactly what really would happen is not obvious. Ice might ascend slowly in small diapirs, rather like terrestrial salt domes, or overturn could be catastrophic. Alternatively, this water could dissolve substantial quantities of salt, becoming gravitationally stable at depth or mixing with the crust or mantle.

The average density of this object is 1.54 g cm^{-3}. With R_i = 0.6, this mixture is similar to Callisto's composition as calculated by Mueller and McKinnon (1988) (although obviously the structure calculated here is different from that calculated by Mueller and McKinnon).

Model E. This is qualitatively the same as model D, but the amount of water is greater, resulting in a thicker ice crust. The average density is 1.26 g cm^{-3}, similar to the least dense, iciest satellites in the Solar System.

Importance of Na#. *Na* is defined as $Na_2SO_4/(Na_2SO_4 + MgSO_4)$. The models in Fig. 9 assume that the initial rock has the composition of Orgueil, with Na# = 0.255. However, Na# differs among various chondrites, and even varies considerably within Orgueil itself, so Na# should really be considered a free parameter.

The models in Fig. 9 have Na# = 0.255, compared to Na# = 0.15 for the ternary eutectic liquid. Any line drawn from eutectic E through any of the ice-bearing mixtures (models B, C, D, and E) necessarily intersects the joint H_2O–Na_2SO_4 (see Fig. 3a). Simply, but significantly, this means that ternary eutectic melting of any mixture of ice and Orgueil-like rock will leave a residue containing H_2O and Na_2SO_4, and not retaining $MgSO_4$. Hence, $MgSO_4$ is always the first component to be exhausted in models B through E in Fig. 9, with the consequence that the differentiated structures always have a mirabilite–ice binary eutectic layer overlying a ternary $MgSO_4$-rich layer. If, however, Na# < 0.15 in the initial rock component then the ternary eutectic liquid has Na# greater than the initial rock: then ternary eutectic melting would leave a residue composed of H_2O and $MgSO_4$ and depleted in Na_2SO_4. Therefore, the petrologic evolution of objects having Na# < 0.15, and their resulting differentiated structures and geologic histories, would be very different from those depicted in Fig. 9.

Fate and significance of minor components. Figure 9 does not consider the possible petrologic roles of minor soluble and abundant but weakly soluble components. Consideration of petrologically evolved silicate planets such as the Earth and Moon, where minor mantle components often become major crustal constituents, is sufficient reason to briefly consider minor salts in the evolution of icy satellites and asteroids.

Phase equilibria shown in Fig. 3 indicate that Ni is compatible while Mn and K can be considered incompatible with respect to Mg-rich sulfates. Therefore, early-generated liquids will be Ni-poor and K- and Mn-rich compared to the initial salts, thus enriching the solid residuum in Ni and depleting it in K and Mn. Continued melting will yield liquids progressively more enriched in Ni and depleted in K and Mn. Complex evolutionary scenarios could involve remelting prior melts. This could yield liquids so enriched in K and Mn that they become major components, and could grossly deplete Ni. It is not known whether any icy satellites or asteroids have such complicated geological histories, but a brief look at Europa and Ganymede suffices to allow this possibility. Magmatic redistribution of ^{40}K-carrying salts such as K_2SO_4 could be an important factor affecting the subsequent thermal structures and evolution of differentiated asteroids and icy satellites.

K and Rb salts could eventually be useful in automated, *in situ* isotopic dating of cryovolcanic flows (Kargel 1989). K and Rb salts have yielded correct ages for terrestrial evaporites, although groundwater flow and subtle heating often disturbs parent–daughter systems (Brookins *et al.* 1980, 1985). The frequent problems encountered in dating terrestrial evaporites would not be expected in deep-frozen cryovolcanic flows.

$CaSO_4$ is expected to be a minor component under all

circumstances because of its low solubility. Its abundance, though low, is very sensitive to the abundances of major salts and to the mode of petrogenesis of the liquid. For instance, the abundance of $CaSO_4$ is very different in waters formed by melting ice (in the presence of gypsum), by dehydrating gypsum, or by dehydrating phyllosilicates (in the presence of anhydrite).

In sum, minor salts could be very useful in chemical and isotopic probing of the evolution and internal structures of icy satellites and asteroids, provided that *in situ* analyses become feasible.

High-temperature dehydration. The models in Fig. 9 consider only low-temperature melting events, ignoring the potential of gypsum and phyllosilicates to contribute water to the crust and mantle through comparatively high-temperature dehydration. Indeed, the residual rock cores shown in Fig. 9 still contain about 14.6% water of hydration. This water could be released beginning near 40°C with the dehydration of gypsum (Posnjak 1938), and continuing in steps to 500°C with the dehydration of clays. If low-temperature leaching does not release chlorine, then it would surely be liberated during the dehydration of phyllosilicates. A brief consideration of elemental and water abundances suggests that these hydrothermal fluids would contain an average of ~1% chloride salts. Anhydrous sulfates left from prior melting events would also dissolve in the fluid.

Implications of a possible high-temperature origin of sulfates. Oxidation of reduced sulfur to form the sulfates observed in carbonaceous chondrites requires, of course, a source of oxygen. This source remains a topic of continuing speculation. Oxidizing agents may have included HOOH formed by ultraviolet hydrolysis reactions in protoplanetary atmospheres, or O_2 generated in satellite and asteroid interiors by γ and β hydrolysis of water (J.S. Lewis, private communication). These mechanisms may yield sulfate by reactions at low temperatures. The fact that terrestrial oxidation of sulfides such as pyrite occurs rapidly in sedimentary environments clearly indicates that, given a suitably oxidizing aqueous environment, low-temperature kinetics are no hindrance to efficient sulfate formation. However, M. Zolensky (private communication) suggests that a comparatively high-temperature (>100°C) event may have been responsible for oxidation and aqueous alteration in C1 chondrites.

This high-temperature scenario could have important implications for this work. High temperatures might not permit large amounts of water to be retained; ice could melt and the water might be extruded before sulfur oxidations occurs, or, if temperatures never exceed the melting point of ice, sulfates might never be formed. Either way, aqueous sulfate magmatism as described in this work might not occur. On the other hand, high-temperature formation of sulfates might be followed by higher-temperature dehydration of phyllosilicates; such an event might yield hypersaline sulfate brines, but brine magmatism would follow a radically different scenario than outlined in the models above. Alternatively, pressures >24 kbars in the deep interiors of large icy satellites might allow sulfate-forming reactions in high-pressure ice-bearing assemblages. As an additional or alternative phenomenon, impact shock heating may result in local high-temperature conditions favoring formation of sulfates, while colder regolith more distant from the impact site could retain ice and perhaps cold-trap ice melted by the impact. Sulfate- and ice-rich compositions could also be produced by heterogeneous accretion of separate ice-rich and sulfate-rich planetesimals. These complex scenarios are presented as a reminder that sulfate magmatism is neither bound to follow simple scenarios, nor is sulfate brine magmatism the inevitable consequence of melting cosmic ice–rock mixtures.

5.2 Carbonaceous Chondrites

Origin of salt veins. Carbonaceous chondrites provide fascinating insights into processes of aqueous alteration and low-temperature partial melting in chondritic asteroids and icy satellites. The aqueous parent fluids from which chondrite salts precipitated may have been hydrothermal fluids released by dehydration of silicates, impact melts of icy targets, or liquids formed by anatexis of ice–rock mixtures (DuFresne and Anders 1962, Bostrom and Fredriksson 1964, Nagy and Anderson 1964, Lewis 1967, Lewis and Krouse 1969, Richardson 1978, Kerridge *et al.* 1979, Bunch and Chang 1980, Clayton and Mayeda 1984, Barber 1985, Tomeoka and Buseck 1985, Zolensky 1984, Fredriksson and Kerridge 1988, Zolensky and McSween 1988, Zolensky *et al.* 1989, Grimm and McSween 1989, Keller and Buseck 1990).

It is frequently noted that aqueous alteration and chemical precipitation in the chondrites apparently occurred largely *in situ*, and that redistribution of soluble matter was restricted to the scales of individual salt veinlets and nodules (mm–cm scales). Large-scale redistribution would certainly have caused bulk samples of these meteorites to deviate strongly from chondritic (solar) composition, which is not observed (significant but small departures are observed, on small spatial scales). This means that the salt veins are probably not igneous dikes or cryovolcanic conduits in the usual sense in that relatively little transfer of aqueous brine took place along these fractures. Figure 9a, a model representation of a generic differentiated chondritic asteroid, does not represent the evolution of the carbonaceous chondrites, which are essentially undifferentiated.

Ice may have been involved in the genesis of some

chondrite brines and salts (Grimm and McSween 1989, Jones *et al.* 1988). This is an important issue toward which the compositions of sulfates contribute considerable insight. The origin of sulfate ion has been linked to the oxidation of reduced sulfur (Lewis 1967, Lewis and Krouse 1969), since native S and sulfates (among other alteration products) are observed with reaction relationships with corroded sulfides, especially pyrrhotite (Bostrom and Fredriksson 1964, Bass 1970).

Richardson (1978) inferred that three successive generations of salt veins precipitated in several different CI chondrites. these generations being dominated first by Ca–Mg–Fe-carbonates, then by Ca–sulfate (gypsum), and last by Mg–Ni–Na–sulfate. This sequence is in order of increasing degree of oxidation and increasing solubility in water. The collective set of observations, including petrographic relations discussed by many other workers suggests that the CI chondrites were derived from an asteroidal impact regolith. The aqueous environment of the salt veins evolved from relatively acidic, moderately reducing, low salinity conditions during precipitation of carbonates, to basic, oxidizing, hypersaline conditions during precipitation of Mg-rich sulfates. The increase in salinity may have involved one or more of three factors: progressive silicate alteration by the brine, or either evaporative or freezing concentration of salts. However, the third series of salt veins described by Richardson (1978) can also be explained by a very late event involving dehydration and recrystallization of sulfates due to solar heating after the meteoroid entered an Earth-crossing orbit, or even after landing on Earth.

Saturation in magnesium sulfate requires a hypersaline brine equal to or more saline than the H_2O–$MgSO_4$ eutectic (17% $MgSO_4$), roughly five times saltier than sea water. It is productive to examine published meteorite sulfate compositions in the context of aqueous sulfate equilibria.

Chondrite sulfates: The Ni problem. Several salt veins from two different meteorites contain large but widely variable amounts of $NiSO_4$, while other veins in the same meteorites contain almost none (Fredriksson and Kerridge 1988), implying gross macroscopic chemical disequilibrium. As shown in Fig. 3e and discussed in Part 3, the partitioning behavior of Mg and Ni between liquids and solids in the aqueous Mg–Ni–sulfate system is of order unity, and complete solid solution exists between the two sulfate end-members. Thus, severe fractionation of Ni from Mg to the degree observed cannot be accomplished by normal igneous processes. But the fact that severe fractionation did occur is all the more remarkable since aqueous processes are believed to have occurred largely *in situ*, with little opportunity for multistaged igneous fractionation. Two explanations for this are offered below, the first one involving the pH of the solution, the second involving progressive oxidation.

Large variations in the abundance of $NiSO_4$ could occur if the solution pH shifted between slightly acidic values where Ni could have existed as dissolved $NiSO_4$, and slightly basic values where Ni existed stably as $Ni(OH)_2$ or some other nearly insoluble solid. For Ni activities ~0.01 the critical pH for this equilibrium is ~6.5 (Brookins 1988). This is sufficiently basic that Fe should reside in stable solid oxides or hydroxides, consistent with the lack of a major $FeSO_4$ component in chondrite salt veins. It is also sufficiently acidic that Mg would remain as soluble $MgSO_4$ rather than solid $Mg(OH)_2$. Solution pH could rise above 6.5, triggering precipitation of $Ni(OH)_2$, by progressive hydrolysis of silicates or by freezing or evaporative concentration of minor alkali sulfates in an initially acidic solution. Subsequent magnesium sulfate precipitates would be sharply depleted in Ni. Alternatively, or additionally, the extremely variable Ni abundances in chondrite sulfates could be related to a trend of progressive oxidation that can be inferred on independent grounds. Partial oxidation of (Fe, Ni)S results in the residual sulfide becoming more Ni-rich than it was initially, since NiS is oxidized with greater difficulty than FeS. Late-stage oxidation of Ni-rich sulfides would produce Ni-rich sulfate veins.

Mg–Na sulfate compositions of chondrite veins. The ternary compositions of chondrite sulfates provide useful constraints on the origin of the veins. As discussed in Part 3, phase equilibria among highly soluble salts in C1 and C2 chondrites can be described accurately in the three-component system H_2O–$MgSO_4$–Na_2SO_4 (Fig. 3a) if minor components are summed with chemically similar major ones. Very importantly, recall that we do not reliably know the original amount of hydrated water in these salts. The ternary compositions of these salts provide reliable information only on their Na/Mg ratios. It is useful to define an expression for this ratio: Na# = "Na_2SO_4" : ("Na_2SO_4" + "$MgSO_4$"), where "$MgSO_4$" includes $NiSO_4$ and $MnSO_4$ calculated as the molar equivalent mass of $MgSO_4$, and "Na_2SO_4" includes K_2SO_4 calculated as the molar equivalent mass of Na_2SO_4.

Analyses of four individual sulfate veins and two bulk soluble extracts of sulfates from two meteorites have been reported in the literature (Bostrom and Fredriksson 1964, Fredriksson and Kerridge 1988). More recent analyses of sulfates from 10 carbonaceous chondrites yielded semi-quantitative estimates of sodium and magnesium sulfate contents (Burgess *et al.* 1991), but the analytical techniques utilized were very crude and the breakdown of total sulfates into metal sulfate components was by rather indirect and uncertain inference. Thus, the data of Burgess *et al.* do not significantly assist in this particular exercise.

Two bulk soluble extracts of Orgueil sulfates give

Na# = 0.255 and 0.083, clearly indicating that this meteorite is grossly heterogeneous with respect to its sulfate vein compositions. Expressed as molar fractions these numbers are, respectively, 0.226 and 0.071. Despite first appearances, this heterogenity does not indicate fluid transport and salt/fluid fractionation on the spatial scale of Orgueil (decimeters). This is because each portion of Orgueil contains both veins and matrix, and what is present in the local veins is absent in the matrix so that each bulk sample of Orgueil (including veins and matrix) remains more or less solar in composition.

Four individual vein analyses give Na#'s of 0.338 (Orgueil vein #7), 0.336 (Orgueil vein #6), 0.335 (Ivuna vein #20), and 0.143 (Ivuna vein #19) (from Fredriksson and Kerridge 1988). In molar fractions these numbers are, respectively, 0.302, 0.301, 0.300, and 0.124. Of these vein analyses, three (from two different meteorites) are virtually identical in Na#, although Ni/Mg varies considerably. The other vein is similar to any of three eutectics, including the eutectic in equilibrium with ice, mirabilite, and epsomite (Fig. 3a).

The three clustered Na#'s do not correspond to any known eutectic liquid in the aqueous Mg–Na sulfate system, nor do they correspond to any of the mixed Mg–Na sulfates known to occur. Fredriksson and Kerridge (1988) suggested a compositional similarity to nickel bloedite ($MgSO_4 \cdot Na_2SO_4 \cdot 4H_2O$), but the stoichiometry is incorrect for this or any other known sulfate. If bloedite is a major mineral then a consistent fraction of epsomite or another pure magnesium sulfate must be intermixed in these veins. The clustering of these three sulfates seems real, however. Since it is unlikely that three veins from two meteorites just happen to have the same composition, this clustering argues for the existence either of a previously unknown mixed salt with the approximate stoichiometry $(Mg, Ni)_2Na_2(SO_4)_3 \cdot xH_2O$, or of a previously unknown eutectic occurring near this composition. Kinetic factors may have been responsible for precipitation of an unknown metastable mixed Mg–Na–sulfate compound (which may subsequently have reverted to bloedite and epsomite). Alternatively, it is possible that the pressure variable is responsible; perhaps at the modest pressures deep in the interiors of chondrite parent bodies an unknown high-pressure mixed sulfate precipitates with the stoichiometry inferred above, or perhaps high pressures result in a different invariant melting composition corresponding to the clustered vein compositions. The Ivuna #19 sulfate composition, corresponding closely to known eutectics, may represent melting or precipitation at lower pressures where phase equilibria are similar to the 1-atm case. In any event, an experimental study of polybaric phase relations in this system would be a valued endeavor, as would the acquisition of additional high-quality chondrite sulfate compositions. Unless the method of Burgess *et al.* (1991) can be significantly improved this author does not recommend the heating–oxidation technique.

Chemical data reported by Fredriksson and Kerridge (1988) indicate that in one Mg–Na–Ni sulfate vein, apparently the vein Ivuna #19, Na and Ni are concentrated together on one side of the vein. Such zoning probably indicates chemical evolution of the brine from which this vein precipitated; hence, the liquid composition was not precisely that of a eutectic, at least not at the time the vein precipitated (the parent solution could be a high-pressure eutectic, however). Figure 3e tells us that any sulfates precipitated early would tend to have slightly higher Ni contents than the liquid, and precipitation would force the liquid to migrate in the direction of Ni depletion. The early liquidus phase assemblage was both Na- and Ni-rich. Candidate sodic phases are mirabilite and bloedite. However, even the most sodic portions of this vein contain more Mg than either of these phases, so the brine must have been precipitating along a cotectic involving coprecipitation of a magnesium sulfate in addition to a sodic phase. In the region of Fig. 3e there are few choices. Given also the Na# of this vein, 0.143, it seems quite probable that the early evolution of this brine involved cooling and precipitation along the cotectic between mirabilite and epsomite. If cooling continued these solid phases would react with the residual liquid at the peritectic, forming magnesium sulfate dodecahydrate: perhaps eventually the liquid would attain the eutectic involving precipitation of water ice. This evolution would result in just the sort of chemical trends observed, since Na and Ni would be depleted in the late-forming crystal assemblage. It also indicates that the brine was not in equilibrium with ice when the highly sodic portion of the vein was precipitated. This conclusion is consistent with the calculations of Zolensky *et al.* (1989), who concluded that CI (C1) chondrites were probably altered from CM (C2) or CV3 (C3) chondrite material at temperatures ~50 to 150°C, while CM (C2) chondrites were altered near 0°C.

5.3. *Europa*

Europa has one of the youngest, smoothest, brightest, and geologically most active surfaces in the Solar System (Smith *et al.* 1979). Europa's average albedo, 0.7 (Buratti and Veverka 1983), is exceeded in the Solar System only by the surfaces of Enceladus and Triton, both of which also have had geologically dynamic histories. Water ice reflectivity and absorption features in the visible and near infrared spectrum of Europa require water ice to be the dominant component of the visible surface (Clark 1980, Clark *et al.* 1986). Other, more subtle spectral features and albedo variations, however, indicate minor impurities including sulfur dioxide (Ockert *et al.* 1987). Europa ap-

parently suffered global volcanic resurfacing comparatively recently. Indeed, Squyres *et al.* (1983) suggested that active and very widespread resurfacing may be occurring by frost deposition associated with water volcanism. Europa's mean density, 3.04 g cm^{-3}, is intermediate between the densities of aqueously differentiated C1 chondrites (2.69 g cm^{-3}; model A, above) and Io (3.53 g cm^{-3}) and is just slightly greater than the density of C2 chondrites. Squyres *et al* (1983) suggested that Europa contains a dense, mainly anhydrous rocky core and a water ice crust ~100 km thick formed by dehydration of hydrous silicates.

Model A (Fig. 9a), though strictly applicable for the aqueous differentiation of C1 chondrites, qualitatively suggests a different structure and evolutionary history than modeled by Squyres *et al.* (1983). Europa originally may have resembled C2 chondrites, roughly approximated here as a mixture of one part C1 and two parts C3 chondrites supplying 6% water (Squyres *et al.* 1983). Thus, Europa contained one-third as much water, but also one-third as much salt as C1 chondrites. Differentiation may be approximated within the ternary system H_2O–$MgSO_4$–Na_2SO_4 (Fig. 3a). The initial stages of igneous evolution should be identical to that described in model A, except that the volumes of each differentiated layer would be one-third that shown in model A.

Europa shows clear indications of a prolonged and continuing igneous evolution, which must require a more complex scenario than outlined in model A. Indeed, Europa is nearly as large as Earth's Moon, where extensive igneous silicate differentiation occurred. It seems inescapable that radiogenic heating plus tidal deformational heating would have elevated internal temperatures in Europa to the point where gypsum and hydrous silicates would have dehydrated (Lewis 1971, Squyres *et al.* 1983). Thus, the remainder of Europa's water associated with hydrated silicates should also be in its crust. After this later addition of water, Europa's crust, ~110 km thick, would constitute ~8.8% of the satellite's mass (6.0% H_2O; 2.0% $MgSO_4$; 0.69% Na_2SO_4; minor sulfates of K, Mn, and Ni; 0.09% chlorides—probably mainly $MgCl_2$; 0.01% $CaSO_4$; and negligible Ca–Mg carbonates assuming slightly acidic to basic pH). Resumming the three major components to 100%, the bulk composition of Europa's crust would be H_2O 69%, $MgSO_4$ 23%, and Na_2SO_4 8%.

Continued heating of Europa's crust by tidal dissipation would result in further differentiation of the crust. The road to complete differentiation would have been very complex, but once complete, Europa's crust would be composed of a thin lower crust ~15 km thick composed of anhydrous magnesium and sodium sulfates, and a thick (~95 km) ternary eutectic upper crust composed of ~50% water ice, 44% $MgSO_4 \cdot 12H_2O$, and 6% $Na_2SO_4 \cdot 10H_2O$. Any further heat input would result in repetitive congruent melting of the eutectic crustal layer. While trace and minor components could fractionate during repeated melting, the major components would maintain the same eutectic composition in the liquid phase and solid residues, irrespective of the extent of melting. The eutectic liquid is more dense than its coexiting solid assemblage, so eruptive activity would tend to be inhibited. Instead, the liquid would pool between the overlying frozen eutectic saline crust and the anhydrous lower crust, forming magma chambers or a saline magma ocean.

Complete freezing of lower crustal brine would be more difficult than in the salt-free case since solutes would depress the freezing points. While sulfates would mostly freeze out between 260 and 269 K, the aqueous eutectic chloride fraction of the brine would not completely freeze until about 221 K (for 1 atm; pressures of ~1 kilobar 95 km deep would depress the freezing point of the chloride solution to about 212 K). This could greatly reduce the rigidity of the upper crust, thus allowing prodigious rates of tidal dissipative heating and vigorous geologic activity to be maintained into the present epoch (Cassen *et al.* 1980, Squyres *et al.* 1983).

Crystallization of brines in the lower crust would result in volume expansion and possibly tensile fracturing of the upper crust. Lower crustal brines could be forcibly extruded under pressure during progressive freezing. Fractional crystallization seems likely, given the low viscosity of the brine and the high density differences between the brine and all solid phases. Complex vertical mineralogical zonation of the crystallizing magma could occur. Remelting of these layers would produce liquids of many compositions, some less dense and others more dense than the overlying ternary eutectic crust. Extrusive activity would selectively involve the least dense, least saline brines, e.g., aqueous sodium sulfate eutectic liquid formed by melting ice plus mirabilite.

Brine eruptions, whether or not resembling the model outlined above, should have left physical evidence on the Europan surface. The low relief of Europa's volcanic plains (compared, say, to Triton's) is consistent with the low viscosities of brines (Kargel *et al.* 1991). It is somewhat surprising that spectral evidence of salts has not been reported, as it seems difficult to avoid melting any part of Europa, at any stage in its evolution, without involving substantial quantities of salts. However, water evaporated from erupted brines would tend to recondense widely on the cold surface of Europa (Squyres *et al.* 1983) and might tend to hide the spectral signature of the expected magnesium and/or sodium sulfates and other salts. The ultraporous microstructure of Europa's surface as inferred from photometry (Domingue *et al.* 1991) is consistent with such frost deposition. Furthermore, cryovolcanic salts would be hydrated and mixed with water ice, so the strong spectral signature of intimately mixed ice

and chemically bound water may mask the spectral signature of salts.

5.3. Ganymede

Geology and composition. Ganymede's average density, 1.93 g cm^{-3}, is much lower than those of Io (3.55) and Europa (3.01) (Schubert *et al.* 1986). Ganymede's density falls between the densities of compressed (nonporous) C1 chondrites (2.6–2.8), and compressed water ice (ranging from 0.92 to 1.4 for various relevant polymorphs), indicating that Ganymede, like the other icy satellites, contains substantial fractions of both rock and ice (Lupo and Lewis 1979, Schubert *et al.* 1986, Mueller and McKinnon 1988). This simple but important fact supports well-based theoretical predictions that ice should be an abundant low-temperature condensate in the outer Solar System and specifically in Ganymede (Lewis 1971, 1972). Telescopic observations confirm that ice is the major constituent of Ganymede's surface, although there is also an important rocky component (e.g., Clark *et al.* 1986).

The estimation of the ice and rock fractions in icy satellites has been an important objective of many workers. Schubert *et al.* (1986) and Mueller and McKinnon (1988) clearly showed that without tighter constraints on the composition of the rock and on Ganymede's state of differentiation, one cannot derive a unique rock fraction. This important parameter may be as low as 0.49 to as high as 0.65. However, the geology of Ganymede's surface requires at least some degree of internal differentiation. Extensive if not complete differentiation seems probable. Modeling the case of extensive differentiation, Mueller and McKinnon (1988) calculated rock fractions ranging from 0.54 to 0.59 depending on the type of rock composing Ganymede's core. However, the authors pointed out that regardless of the core's present composition it very likely evolved from an initial rock component resembling C1 chondrites. If the rock fraction is expressed in terms of the initial fraction of C1 chondrite rock, a differentiated Ganymede would have contained 64 to 65% of its mass as rock, the remainder being ice. The latter set of rock fractions, 0.64 to 0.65, corresponds to R_i in the models shown in Fig. 9. The quoted range of 0.54 to 0.59 would roughly correspond to R_f, the final rock fraction after soluble salt extraction; however, this correspondence is not exact, since the models of Mueller and McKinnon (1988) leave the anhydrous salts in the rock while extracting only their water content.

Pre-Voyager theoretical models showed the likelihood that Ganymede would be differentiated (Consolmagno and Lewis 1978). This prediction is confirmed even in low-resolution full-disc images showing bright and dark terrains on Ganymede's surface. Higher resolution images reveal terrains with considerably varied crater densities and intensely fractured and volcanically flooded terrains, indicating a complex history of differentiation (Smith *et al.* 1979, Head *et al.* 1981, Woronow *et al.* 1982, Squyres 1982, Parmentier *et al.* 1982, Casacchia and Strom 1984, Croft 1985 and 1986, McKinnon and Parmentier 1986, Schenk and McKinnon 1987, Croft and Goudreau 1987, Golombek and Banerdt 1986, Allison and Clifford 1987, Murchie and Head 1988, Mueller and McKinnon 1988, Tittemore 1990). Bright terrain typically intrudes older dark terrain (Parmentier *et al.* 1982, Squyres 1982), and usually the light terrain is heavily deformed by one or more sets of extensional and probably also transtensional tectonic features (Murchie and Head 1988).

Volcanism and extensional tectonism are closely interrelated on Ganymede as they are on Earth. Fracture zones are frequently the sources, and tectonic depressions are commonly the containment basins for erupted plains-forming liquids (Head *et al.* 1981, Parmentier *et al.* 1982, Allison and Clifford 1987). In many areas tectonic grooving was followed by cryovolcanic flooding, in turn sometimes followed by reactivation of grooving and reflooding. Thus, near the end of a period of heavy impacting, Ganymede seems to have suffered late episodes of intense tectonic and cryovolcanic surface modification (Woronow *et al.* 1982).

An absence of obvious flow margins in the best Voyager images of Ganymede's smooth plains indicates that flow thicknesses must be <100 m. Hence, the erupted liquids possessed low viscosities and yield strengths relative to much thicker flows on the satellites of Uranus and Neptune. After considering the 1/7g surface gravity, the erupted substances may have been rheologically comparable to any substance as "thin" as or "thinner" than andesite (Kargel 1990). Of course, silicate lavas are disallowed in Ganymede's situation, so rheologically compatible and compositionally likely substances would include water, salt brines, or ammonia–water liquids, the latter only as long as there are low contents of additional components and suspended crystals (Kargel *et al.* 1991). Since substantial quantities of ammonia are unlikely to have condensed in the relatively warm Jovian nebula, water or salt brines are more likely than ammonia–water liquid.

The freezing-point depression caused by salts also may assist in melting in a satellite that may convectively regulate its internal temperatures below the melting point of pure ice. Magnesium sulfate alone would only lower the melting point by 4 K, but certain other salts, particularly the chlorides, are more effective freezing point depressants. Once volcanism initiates the fraction of rock in the solid residual core increases, causing the viscosity of the core to increase, resulting in higher convective temperatures or even a complete failure of

the convective mechanism, thereby promoting further melting.

Internal structure of a differentiated salty Ganymede. Figures 9C and 9D bracket Ganymede's composition. Of course, these models do not consider the important effects of elevated pressures in Ganymede's interior, nor of qualitatively different scenarios involving possible fractional crystallization of magma oceans. Despite this outrageous neglect, it sems probable that Ganymede would have some type of compositionally layered structure; based on these models the structure would include a $MgSO_4$-rich mantle ~500 to 600 km thick, containing ~15–20% by mass $MgSO_4$ and Na_2SO_4, plus minor quantities of other salts. This layer would be overlain by less salt-rich icy upper mantle and crustal layers an additional several hundred kilometers thick.

Pressures near the core/mantle boundary would be ~12–13 kbars, so the mantle and crust also would be layered with respect to ice polymorphs, including phases up to ice VI near the base of the mantle. The effects of pressures on sulfate phase stability are uncertain, although sparse and conflicting experimental data suggest a phase change in epsomite near 5 kbars and perhaps another at pressures over 10 kbars (Bridgman 1948a,b, Livshits *et al.* 1963). Mantle and crustal compositions reflect phase equilibria during partial melting which would have occurred under pressures ranging as high as 50 kbars near the center of Ganymede. Such high pressures would certainly impact subsolidus and solid–liquid phase equilibria in ways that are difficult to predict. Therefore, Fig. 9 is not at all a reliable guide to Ganymede's interior structure, but is a valid indication of the probable importance of salts in Ganymede's and other icy satellite's histories and interior structures.

Taking Figs. 9c and 9d literally, Ganymede's surface would be composed of volcanic flows of water or sodium sulfate–water solutions. However, in reality it would be difficult to extrude these liquids through the magnesium sulfate-rich mantle without substantial contamination by magnesium sulfate. Also, if Ganymede's Na# < 0.15 then sodium sulfate would be exhausted before magnesium sulfate, causing a different petrologic evolution of late-stage liquids. Coupled with the unknown pressure-related effects on phase equilibria, it is not yet possible to predict with any certainty what Ganymede's surface composition should be. Even so, it seems a priori highly probable that salts, particularly magnesium and/or sodium sulfates, would be significant components.

6. SUMMARY

Brine volcanism may explain resurfacing observed on some icy satellites, particularly Europa and Ganymede, and is expected to have been important in the evolution of chondritic asteroids. Carbonaceous chondrite mineralogies, cosmic elemental abundances, and salt solubilities suggest that $MgSO_4$ and Na_2SO_4 are the most important solutes. Internal chemical structural models of icy satellites and asteroids suggest a wide range of possible evolutionary scenarios, some involving the formation of thick salt-rich crusts and mantles.

Salt–water eutectic brines have densities lower than typical ice–rock mixtures, and therefore are buoyant and can be extruded onto the surfaces of icy satellites during early stages of differentiation. The ternary $MgSO_4$–Na_2SO_4–H_2O eutectic liquid has a density of ~1.19 g cm^{-3}, compared to 1.13 g cm^{-3} for the equivalent frozen eutectic mixture; therefore, a solid eutectic crust would float on its own liquid. $MgSO_4$-rich aqueous volcanism would become increasingly difficult as a eutectic-composition crust became thicker. Early eutectic volcanism may generally yield to later plutonism or even formation of stable brine magma oceans. Late-stage water or Na_2SO_4–H_2O eutectic volcanism would be favored, since these liquids are less dense than the $MgSO_4$-rich eutectic crust. Such late-stage water-rich volcanism could occur if ice and mirabilite are left in excess amounts in the core after exhaustion of magnesium sulfate.

Hypersaline brines have much lower viscosities than familiar silicate lavas, although they are more viscous than pure water. Aqueous sulfate flows may produce extensive flows on the order of a meter thick, constructing vast volcanic plains of low relief such as observed on Ganymede and Europa. Chloride brines are generally more viscous than sulfate brines. Under low-*g* conditions on icy satellites and asteroids chloride brines would probably behave fluid dynamically much as basalt behaves on Earth, producing characteristic flow thicknesses of ~2–20 m. Chemical as well as geomorphic evidence should exist on the surfaces of objects affected by brine volcanism, and might be discernable in observations planned for Galileo.

ACKNOWLEDGMENTS

This work was supported by NASA Grant NHGW-340. The author acknowledges constructive reviews by Michael Zolensky and Ray Reynolds, and extensive discussions over the years with Steve Croft.

REFERENCES

ALLISON, M. L., AND S. M. CLIFFORD 1987. Ice-covered water volcanism on Ganymede. *J. Geophys. Res.* **92**, 7865–7876.

ANDERS, E., AND N. GREVESSE 1989. Abundances of the elements: Meteoritic and solar. *Geochim. Cosmochim. Acta* **53**, 197–214.

ARCHIBALD, E. H., AND W. A. GALE 1924. The system magnesium sulfate–sodium sulfate–water and a method for the separation of the salts. *J. Am. Chem. Soc.* **46**, 1760–1771.

BARBER, D. J. 1985. Phyllosilicates and other layer-structured materials in stony meteorites. *Clay Miner.* **20**, 415–454.

BASS, M. N. 1970. Textural relations of sulfide, sulfate, and sulfur in Orgueil Meteorite. *Meteoritics* **5**, 180–181. [Abstract]

BENRATH, A., AND E. NEUMANN 1939. Uber Mischkristalle in der Vitriolreihe. V. *Z. anorg. allgem. Chemie* **242**, 70–78.

BLASDALE, W. C. 1927. *Equilibria in Saturated Salt Solutions*, American Chemical Society Monograph Series, p. 79. Chem. Catalog Co., New York.

BODALEVA, N. V., AND I. N. LEPESHKOV 1956. A study of solubility in the system K_2SO_4–$MgSO_4$–$CaSO_4$–H_2O at 55°. *Zh. Neorgan. Khim.* **1**, 995–1007.

BOSTROM, K., AND K. FREDRIKSSON 1964. Surface conditions of the Orgueil Meteorite parent body as indicated by mineral associations. *Smithsonian Misc. Coll.* **151**.

BRAITSCH, O. 1971. *Salt Deposits: Their Origin and Composition*. Springer-Verlag, New York. [Translated by P.J. Burek and A. E. M. Nairn].

BRIDGMAN, P. W. 1948a. The linear compression of various single crystals to 30,000 kg/cm^2. *Proc. Amer. Acad. Arts Sci.* **76**, 89–99.

BRIDGMAN, P. W. 1948b. Rough compressions of 177 substances to 40,000 kg/cm^2. *Proc. Amer. Acad. Arts Sci.* **76**, 71–87.

BROOKINS, D. G. 1988. *Eh–pH Diagrams for Geochemistry*. Springer-Verlag, New York.

BROOKINS, D. G., J. K. REGISTER, JR., AND H. W. KRUEGER 1980. Potassium–argon dating of polyhalite in southeastern New Mexico. *Geochim. et Cosmochim. Acta* **44**, 635–637.

BROOKINS, D. G., H. W. KRUEGER, AND T. M. BILLS 1985. Rb–Sr and K–Ar analyses of evaporite minerals from southeastern New Mexico. *Isochron/West* **43**, 11–12.

BUNCH, T. E., AND S. CHANG 1980. Carbonaceous chondrites. II. Carbonaceous chondrite phyllosilicates and light element geochemistry as indicators of parent body processes and surface conditions. *Geochim. Cosmochim. Acta* **44**, 1543–1577.

BURATTI, B., AND J. VEVERKA 1983. Voyager photometry of Europa. *Icarus* **55**, 93–110.

BURGESS, R., I. P. WRIGHT, AND P. T. PILLINGER 1991. Determinations of sulphur-bearing components in C1 and C2 carbonaceous chondrites by stepped combustion. *Meteoritics* **26**, 55–64.

CAMERON, F. K., AND J. M. BELL. 1905. The solubility of gypsum in magnesium sulfate solutions. *J. Phys. Chem.* **10**, 210–215.

CAMERON, A. G. W. 1978. Physics of the primitive solar accretion disk. *Moon Planets* **18**, 5–40.

CASACCHIA, R., AND R. G. STROM 1984. Geologic evolution of Galileo Regio, Ganymede. *Proc. Lunar Planet. Sci. Conf. 14, part 2, J. Geophys. Res.* **89**(Suppl), B419–B428.

CASSEN, P., S. J. PEALE, AND R. T. REYNOLDS 1980. Tidal dissipation in Europa: A correction. *Geophys. Res. Lett.* **7**, 987–988.

CHEN, C. T. A., J. H. CHEN, AND F. J. MILLERO 1980. Densities of NaCl, MgCl2, Na2SO4, and MgSO4 aqueous solutions at 1 atm from 0 to 50°C and from 0.001 to 1.5 m. *J. Chem. Eng. Data* **25**, 307–310.

CLARK, R. N. 1980. Ganymede, Europa, Callisto, and Saturn's rings: Compositional analysis from reflectance spectroscopy. *Icarus* **44**, 388–409.

CLARK, R. N., F. P. FANALE, AND M. J. GAFFEY 1986. Surface composition of natural satellites. In *Satellites* (J. A. Burns and M. S. Matthews, Eds.), pp. 437–491. Univ. Arizona Press, Tucson.

CLAYTON, R. N., AND T. K. MAYEDA 1984. The oxygen isotope record in Murchison and other carbonaceous chondrites. *Earth Planet. Sci. Lett.* **67**, 151–161.

CONSOLMAGNO, G. J., AND J. S. LEWIS 1978. The evolution of icy satellite interiors and surfaces. *Icarus* **34**, 280–293.

COX, K. G., J. D. BELL, AND R. J. PANKHURST 1979. *The Interpretation of Igneous Rocks*. Allen & Unwin, Boston.

CROFT, S. K. 1985. A new scenario for differentiation of Ganymede and Callisto. *Lunar Planet. Sci. XVI*, 152–153.

CROFT, S. K. 1986. Ganymede and Callisto: Toward a new synthesis. In *Rep. Planet. Geol. Geophys. Prog.-1985*, NASA TM 88383, pp. 57–59.

CROFT, S. AND B. GOUDREAU 1987. Tectonism and volcanism in Ganymede's dark terrain. *Lunar Planet. Sci. XVIII*, 209–210. [Abstract]

CROFT, S. K., J. I. LUNINE, AND J. S. KARGEL 1988. Equation of state of ammonia–water liquid: Derivation and planetological application. *Icarus* **73**, 279–292.

DODD, R. T. 1981. *Meteorites: A Petrologic–Chemical Synthesis*. Cambridge Univ. Press, Cambridge.

DOMINIGUE, D. L., B. W. HAPKE, G. W. LOCKWOOD, AND D. T. THOMPSON 1991. Europa's phase curve: Implications for surface structure. *Icarus* **90**, 30–42.

DUFRESNE, E. R., AND E. ANDERS 1962. On the chemical evolution of the carbonaceous chondrites. *Geochim. Cosmochim. Acta* **26**, 1085–1114.

ETARD, M. 1894. Recherches experimentales sur les solutions saturees. *Annales de Chimie, 7th Ser.* **2**, 503–574.

EUGSTER, H. P. 1980. Geochemistry of Evaporitic Lacustrine Deposits. *Annu. Rev. Earth Planet. Sci.* **8**, 35–63.

FABUSS, M., A. KOROSI, AND A. K. M. SHAMSUL HUQ 1966. Densities of binary and ternary aqueous solutions of NaCl, NaSO4, and MgSO4, of sea waters, and sea water concentrates. *J. Chem. Eng. Data.* **11**, 325–330.

FOLAND, K. A., C. M. B. HENDERSON, AND J. GLEASON 1985. Petrogenesis of the magmatic complex at Mount Ascutney, Vermont, U.S.A. I. Assimilation of the magmas based on Sr and O isotopic and major element relationships. *Contrib. Mineral. Petrol.* **90**, 331–345.

FREDRIKSSON, K., AND J. F. KERRIDGE 1988. Carbonates and sulfates in CI chondrites: Formation by aqueous activity on the parent body. *Meteoritics* **23**, 35–44.

GOLOMBEK, M. P., AND W. B. BANERDT. 1986. Early thermal profiles and lithospheric strength of ganymede from extensional tectonic features. *Icarus* **68**, 252–265.

GREENBERG, R., S. K. CROFT, D. M. JANES, J. S. KARGEL, L. A. LEBOFSKY, J. I. LUNINE, R. L. MARCIALIS, H. J. MELOSH, G. W. OJAKANGAS, AND R. G. STROM 1991. Miranda. In *Uranus* (J. T. Bergstralh, E. D. Miner, and M. S. Matthews, Eds.). Univ. Arizona Press, Tucson, pp. 693–738.

GRIMM, R. E., AND H. Y. MCSWEEN, JR. 1989. Water and the thermal evolution of carbonaceous chondrite parent bodies. *Icarus* **82**, 244–280.

HARKINS, W. D., AND H. M. PAINE 1919. Intermediate and complex ions. V. The solubility product and activity of the ions in bi-valent salts. *J. Am. Chem. Soc.* **41**, 1155–1168.

HEAD, J. W., M. L. ALLISON, E. M. PARMENTIER, AND S. W. SQUYRES 1981. High-albedo terrain on Ganymede: Origin as flooded graben. *Lunar Planet. Sci. XII*, 418–420.

HOGENBOOM, D. L., J. S. KARGEL, J. P. GANASAN, AND J. S. LEWIS 1991. The magnesium sulfate–water system at pressues to 4 kilobars. *Lunar Planet. Sci. XXII*, 581–582.

HUMMEL, W., AND J. ARNDT 1985. Variation of viscosity with temperature and composition in the plagioclase system. *Contrib. Mineral. Petrol.*, **90**, 83–92.

JONES, T. D., L. A. LEBOFSKY, AND J. S. LEWIS 1988. The 3-micron

hydrated silicate signature on C class asteroids: Implications for origins of outer belt objects *Lunar Planet. Sci. XIX*, 567–568. [Abstract]

KARGEL, J. S. 1986. *The Geochemistry of Basalts and Mantle Inclusions from the Lunar Crater Volcanic Field, Nevada: Petrogenetic and Geodynamic Implications*, M. S. Thesis. Department of Geology and Mineralogy, The Ohio State University. Columbus, Ohio.

KARGEL, J. S. 1989. Can we radiometrically date cryovolcanic flows on icy satellites? *Lunar Planet. Sci. XX*, 498–499. [Abstract]

KARGEL, J. S. 1990. *Cryomagmatism in the Outer Solar System*. Ph.D. Dissertation, University of Arizona, Tucson.

KARGEL, J. S., S. K. CROFT, J. I. LUNINE, AND J. S. LEWIS 1991. Rheological properties of ammonia–water liquids and crystal–liquid slurries: Planetological applications. *Icarus* **89**, 93–112.

KEIL, L. P., AND P. R. BUSECK 1990. Aqueous alteration in the Kaba CV3 carbonaceous chondrite. *Geochim. Cosmochim. Acta* **54**, 2113–2120.

KERRIDGE, J. F., A. L. MACKAY, AND W. V. BOYNTON 1979. Magnetite in CI carbonaceous meteorites: Origin by aqueous activity on a planetesimal surface. *Science* **205**, 395–396.

KOROSI, A. AND B. M. FABUSS 1968. Viscosities of binary aqueous solutions of NaCl, KCl, Na2SO4, and MgSO4 at concentrations and temperatures of interest in desalinization processes. *J. Chem. Eng. Data* **13**, 548–552.

LEWIS, J. S. 1967. A possible origin for sulfates and sulfur in meteorites. *Earth Planet. Sci. Lett.* **2**, 29–32.

LEWIS, J. S. 1971. Satellites of the outer planets: Their physical and chemical nature. *Icarus* **15**, 174–185.

LEWIS, J. S. 1972. Low temperature condensation from the solar nebula. *Icarus* **16**, 241–252.

LEWIS, J. S. 1974. The temperature gradient in the solar nebula. *Science* **186**, 440–442.

LEWIS, J. S., AND H. R. KROUSE 1969. Isotopic composition of sulfur and sulfate produced by oxidation of FeS. *Earth Planet Sci. Lett.* **5**, 425–428.

LEWIS, J. S. AND R. G. PRINN 1980. Kinetic inhibition of CO and N2 reduction in the solar nebula. *Astrophys. J.* **238**, 357–364.

LIVINGSTONE, D. A. 1963. Chemical composition of rivers and lakes. in *Data of Geochemistry* (M. Fleischer, Ed.), *6th ed. USGS Prof. Pap.* 440-G.

LIVSHITS, L. D. YU. S. GENSHAFT, AND YU. N. RYABININ 1963. Equilibrium diagram of the crystal hydrates of $MgSO_4$ at high pressures. *Russ. J. Inorg. Chem.* **8**, 676–678.

LOEWEL, M. H., 1855. Observations sur la Sursaturation des Dissolutions Salines. *Ann. Chim. Phys. Ser. 3* **43**, 405–420.

LUCCHITTA, B. K. 1980. Grooved terrain on Ganymede. *Icarus* **44**, 481–501.

LUPO, M. J. AND J. S. LEWIS 1979. Mass–radius relationships in icy satellites. *Icarus* **40**, 157–170.

MCBIRNEY, A. R., AND T. MURASE 1984. Rheological properties of magmas, *Annu. Rev. Earth Planet. Sci.*, 337–357.

MCKENZIE D. 1985. The extraction of magma from the crust and mantle. *Earth Planet. Sci. Lett.* **74**, 81–91.

MCKINNON, W. B., AND E. M. PARMENTIER, 1986. Ganymede and Callisto. In *Satellites* (J. A. Burns and M. S. Matthews, Eds.). pp. 718–763. Univ. Arizona Press, Tucson.

MORSE, S. A. *Basalts and Phase Diagrams*, Springer-Verlag, New York.

MUELLER, S., AND W. B. MCKINNON, 1988. Three-layered models of ganymede and callisto: Compositions, structures, and aspects of evolution. *Icarus* **76**, 437–464.

MURASE, T., A. R. MCBIRNEY, AND W. G. MELSON 1985. Viscosity of the dome of Mount St. Helens. *J. Volcanol. Geotherm. Res.* **24**, 193–204.

MURCHIE, S. L., AND J. W. HEAD 1988. Possible breakup of dark terrain on Ganymede by large-scale shear faulting. *J. Geophys. Res.* **93**, 8795–8824.

NAGY, B., AND C. A. ANDERSEN 1964. Electron probe microanalysis of some carbonate, sulfate and phosphate minerals in the Orgueil Meteorite. *Am. Mineral.* **49**, 1730–1736.

NOVIKOVA, L. V. 1957. A study of solubility for the system CaSO4–MgSO4–H20 at 35° by the method of tracer atoms. *Zh. Neorgan. Khim.* **2**, 662–668.

OCKERT, M. E., R. M. NELSON, A. L. LANE, AND D. L. MATSON 1987. Europa's ultraviolet absorption band (260 to 320 nm): Temporal and spatial evidence from ICE. *Icarus* **70**, 499–505.

PERMENTIER, E. M., AND J. W. HEAD 1979. Internal processes affecting surfaces of low-density satellites: Ganymede and Callisto. *J. Geophys. Res.* **84**, 6263–6276.

PARMENTIER, E. M., S. W. SQUYRES, J. W. HEAD, AND M. L. ALLISON 1982. The tectonics of Ganymede. *Nature* **295**, 290–293.

PATCHETT, P. J. 1980. Thermal effects of basalt on continental crust and crustal contamination of magmas. *Nature* **283**, 559–561.

POSNJAK, E., 1938. The system CaSO4–H2O. *Am. J. Sci. Ser. 5*, **35-A**, 247–272.

PRINN, R. G., AND B. FEGLEY, JR. 1981. Kinetic inhibition of CO and N2 reduction in circumplanetary nebulae: Implications for satellite composition. *Astrophys. J.* **249**, 308–317.

PRINN, R. G., AND B. FEGLEY, JR., 1988. Solar nebula chemistry: Origin of planetary, satellite, and cometary volatiles. In *Planetary and Satellite Atmospheres: Origin and Evolution*. Univ. of Arizona Press, Tucson.

PURDON, F. F., AND V. W. SLATER, 1946. *Aqueous Solution and the Phase Diagram*. Arnold. London.

REITMEIJER, F. J. M. 1990. Salts in two chondritic porous interplanetary dust particles. *Meteoritics* **25**, 209–213.

RICHARDSON, S. M. 1978. Vein formation in the C1 carbonaceous chondrites. *Meteoritics* **13**, 141–159.

ROBSON, H. L. 1927. The system MgSO4–H2O from 68 to 2400. *J. Amer. Chem. Soc.* **49**, 2772–2783.

ROHMER, A. R. 1939. Contribution A l'etude du Sulfate de Nickel et du Sulfate de Colbalt. *Ann. Chimie Ser. 11*, **11**, 611–633.

ROOZEBOOM, M. H. W. B. 1889. Etude experimentale et theorique sur les conditions de l'equilibre entre les combinaisones solides et liquides de l'eau avec des sels, particulierement avec le chlorure de calcium. *Rec. Trav. Chim. Pays-Bas* **8**, 1–146.

RYERSON, F. J., H. C. WEED, AND A. J. PIWINSKII 1988. Rheology of subliquidus magmas 1. Picritic compositions. *J. Geophys. Res.* **93**, 3421–3436.

SCARFE, C. M., D. J. CRONIN, J. T. WENZEL, AND D. A. KAUFFMAN 1983. Viscosity–temperature relationships at 1 atm in the system diopside–anorthite. *Am. Mineral.* **68**, 1083–1088.

SCHENK, P. M. 1991. Fluid volcanism on Miranda and Ariel: Flow morphology and composition. *J. Geophys. Res.* **96**, 1887–1906.

SCHENK, P., AND W. MCKINNON 1987. Ring geometry on Ganymede and Callisto. *Icarus* **72**, 209–234.

SCHUBERT, G., T. SPOHN, AND R. T. REYNOLDS 1986. Thermal histories, compositions and internal structures of the moons of the Solar System. In *Satellites* (J. A. Burns and M. S. Matthews, Eds.), pp. 224–292. Univ. of Arizona Press, Tucson.

SHAW, H. R. 1969. Rheology of basalt in the melting range. *J. Petrol.* **10**, 510–535.

SMITH, B. A. AND 21 other authors 1979. The Jupiter System Through the Eyes of Voyager 1. *Science* **204,** 951–971.

SOBOLEVA, O. S. 1960. Equilibrium polytherm of the system MgSO4–NiSO4–H2O. *Akad. Nauk SSSR Proc. Chem. Sec.*, 1231–1233.

SQUYRES, S. W. 1982. The evolution of tectonic features on Ganymede. *Icarus* **52,** 545–559.

SQUYRES, S. W., R. T. REYNOLDS, P. M. CASSEN, AND S. J. PEALE 1983. Liquid water and active resurfacing on Europa. *Nature* **301,** 225–226.

TANTZOV, N. V. 1924. Solubility of the crystalline hydrates of Ni sulfate. *J. Russ. Phys.-Chem. Soc.* **55,** 335–341.

TAUBER, P., AND J. ARNDT 1986. Viscosity–temperature relationship of liquid diopside. *Phys. Earth Planet. Inter.* **43,** 97–103.

TAYLOR, S. R. AND S. M. MCLENNAN 1985. *The Continental Crust: Its Composition and Evolution.* Blackwell Scientific, Boston.

TITTEMORE, W. C., 1990. Chaotic motion of Europa and Ganymede: Fracturing, resurfacing, and the Ganymede–Callisto dichotomy. Submitted for publication.

TOMEOKA, K., AND P. R. BUSECK 1985. Indicators of aqueous alteration in CM carbonaceous chondrites: Microtextures of a layered mineral containing Fe, S, O, and Ni. *Geochim. Cosmochim. Acta* **49,** 2149–2163.

URBAIN, G., Y. BOTTINGA, AND P. RICHET, 1982. Viscosity of liquid silica, silicates, and alumino-silicates. *Geochim. Cosmochim. Acta* **46,** 1061–1072.

VAN KLOOSTER, H. S. 1917. Saturated solutions of potassium and magnesium sulphates at 250 C. *J. Phys. Chem.* **21,** 513–518.

WATSON, B. E. 1982. Basalt contamination by continental crust: Some experiments and models. *Contrib. Mineral. Petrol.* **80,** 73–87.

WORONOW, A., R. G. STROM, AND M. GURNIS 1982. Interpreting the cratering record: Mercury to Ganymede and Callisto. In *Satellites of Jupiter* (D. Morrison and M. S. Matthews, Eds. 237–276. Univ. of Arizona Press, Tucson.

ZOLENSKY, M. E. 1984. Hydrothermal alteration of CM carbonaceous chondrites: Implications of the identification of tochilinite as one type of meteoritic PCP. *Meteoritics* **19,** 346–347. [Abstract]

ZOLENSKY, M. AND H. Y. MCSWEEN, JR. 1988. Aqueous alterations. In *Meteorites and the Early Solar System* (J. F. Kerridge and M. S. Matthews, Eds.), pp. 114–143. Univ. of Arizona Press, Tucson.

ZOLENSKY, M. E., W. L. BOURCIER, AND J. L. GOODING 1989. Aqueous alteration on the hydrous asteroids: Results of EQ3/6 computer simulations. *Icarus* **78,** 411–425.